**INSTITUTO TECNOLÓGICO Y DE ESTUDIOS SUPERIORES DE MONTERREY**

**CAMPUS MONTERREY**

**DIVISIÓN DE INGENIERÍA Y ARQUITECTURA**
**PROGRAMA DE GRADUADOS EN INGENIERÍA**



# EVALUATION OF HYDROGEL MATERIALS FOR INSULIN DELIVERY IN CLOSED LOOP TREATMENT OF DIABETES MELLITUS

**TESIS**

**PRESENTADA COMO REQUISITO PARCIAL PARA OBTENER EL GRADO ACADÉMICO DE:**

**DOCTORA EN CIENCIAS DE LA INGENIERÍA**
**ESPECIALIDAD EN MECATRÓNICA**

**POR:**

**IRMA YOLANDA SÁNCHEZ CHÁVEZ**

**MONTERREY, N.L.**                    **ENERO DE 2008**

**INSTITUTO TECNOLÓGICO Y DE ESTUDIOS SUPERIORES DE MONTERREY**

**CAMPUS MONTERREY**

**DIVISIÓN DE INGENIERÍA Y ARQUITECTURA**
**PROGRAMA DE GRADUADOS EN INGENIERÍA**

Los miembros del comité de tesis recomendamos que el presente proyecto de tesis presentado por Irma Yolanda Sánchez Chávez sea aceptado como requisito parcial para obtener el grado académico de:

**Doctora en Ciencias de la Ingeniería**
**Especialidad en Mecatrónica**

Comité de Tesis:

_____
Dr. Sergio Omar Martínez Chapa
Departamento de Ingeniería Eléctrica y
 Computacional
ITESM, Campus Monterrey
Supervisor

_____
Dr. Nicholas A. Peppas
Departments of Biomedical and
 Chemical Engineering
The University of Texas at Austin
Supervisor

_____
Dr. Hugo Alberto Barrera Saldaña
Departamento de Bioquímica y Medicina Molecular
Facultad de Medicina de la UANL
Sinodal

_____
Dr. Blanca Hazalia Lapizco Encinas
Departamento de Biotecnología e
 Ingeniería de Alimentos
ITESM, Campus Monterrey
Sinodal

_____
Dr. Rubén Morales Menéndez
Centro de Innovación en Diseño y
 Tecnología
Departamento de Mecatrónica y
 Automatización
ITESM, Campus Monterrey
Sinodal

Aprobado:

_____
Dr. Francisco Ángel Bello
Director del Programa de Graduados en Ingeniería
Enero, 2008

A Dios,

        por las personas que viven con diabetes, quienes son ejemplo ante la adversidad,

        por mi esposo, Fernando, quien ha sido una muestra especial y generosa de amor divino en mi vida, y

        por mi patria, México, para que sea un mejor lugar para los míos.

**Acknowledgements**

I want to express my gratitude to Dr. Sergio Martínez for his advice and friendship during my doctoral studies. I recognize his support as leader of the BioMEMS group and committed professor at my university. I am also thankful to Dr. Nicholas Peppas for receiving me in his laboratory group, which he considers an extended family. I share with all his students the appreciation of his guidance and example.

I thank Dr. Hugo Barrera, Dr. Blanca Lapizco and Dr. Rubén Morales for their interest and constructive comments in the evaluation of the present dissertation. I appreciate the collaboration of Dr. Rubén Morales for the Monte Carlo simulation tests included in this work.

I am thankful for the opportunity to do my doctoral studies and continue my teaching labor at Tecnológico de Monterrey. I acknowledge the economic support from Tecnológico de Monterrey and Schlumberger Faculty for the Future Program during my doctoral formation.

I thank family, professors, workmates, classmates, labmates, students and friends who have given me company, encouragement, understanding and inspiration in this part of my life.

IRMA YOLANDA SÁNCHEZ CHÁVEZ

Tecnológico de Monterrey
January 2008

# Abstract

The recovery of diminished or lost regulatory functions of physiological systems drives important research efforts in biomaterials and modeling and control engineering. Special interest is paid to diabetes mellitus because of its epidemic dimensions. Hydrogels provide the multifunctionality of smart materials and the applicability to medical regulatory systems, which is evaluated in this dissertation. The polymeric matrix of a hydrogel experiences reversible changes in volume in response to the pH of the environment, which depends on the presence of key metabolites in a physiological medium. The hydrogel swells due to internal repulsive electrostatic forces opening the matrix and releasing a preloaded drug. The contracted state of the hydrogel hinders the diffusion of the drug out of the polymer.

In this work, poly(methacrylic acid-graft-ethylene glycol), P(MAA-g-EG), hydrogel membranes that incorporate glucose oxidase are used for insulin delivery. These glucose sensitive membranes are characterized and modeled for the closed loop treatment of type I diabetes mellitus. A physiological compartmental model is extended to represent the treatment system of a diabetic patient. Physical parameters of the P(MAA-g-EG) hydrogel material are obtained from experimental characterization and used as a basis to describe anionic and cationic hydrogels. The performance of the system closed by a hydrogel-based device is explored and compared to the dynamic behavior of a conventional scheme with an explicit controller element.

A control algorithm for optimal insulin delivery in a type I diabetic patient is presented based on the linear quadratic control problem theory. The glucose-insulin dynamics is first represented by a linear model whose state variables are the glucose and the insulin concentrations in the blood. These variables allow the formulation of an appropriate cost function for a diabetes treatment in terms of the deviation from the normal glucose level and the dosage of exogenous insulin. The optimal control law is computed from this cost function under the servocontrol and regulatory approaches. Superior robustness of the regulatory control design is shown before random variations of the parameters of the linear physiological model. Further evaluation of the regulatory controller is realized with a high order nonlinear human glucose-insulin model. The control system performance can be improved by adjusting the weighting factors of the optimization problem according to the patients needs. The optimal controller produces a versatile insulin release profile in response to the variations of blood glucose concentration.

Simulations demonstrate limitations in the range of swelling and contraction of hydrogels in a physiological environment due to factors such as the continuous presence of glucose in blood composition, the buffer characteristics of physiological fluids and the Donnan equilibrium effect. Results show that insulin loading efficiency is critical for the long term service of a hydrogel-based device, while delivery by a diffusion mechanism is convenient since it allows a basal insulin supply. The evaluation of hydrogel macrosystems prompts the consideration of the detected pros and contras in hydrogel microsystems, as well as in composite systems that may combine different materials and structures.

x

**General Index**

**Index of Figures**

**Index of Tables**

## 1. Introduction

In Mexico, diabetes mellitus has gained importance during the transformation of the epidemiologic profile of the country in the last decades. Infectious diseases have decreased due to improvements in sanitation and hygiene. On the other hand, non-infectious illnesses are more noticeable as consequence of socio-demographic factors that include the aging of the population and unhealthy practices regarding exercise and nutrition. The prevalence and the evolution of the diabetes mellitus, characterized by the inability of the body to produce or to use insulin, are aggravated by such factors. Currently, diabetes mellitus is considered as the main non-transmissible illness. Diabetes mellitus passed from the eighth to the first cause of death in less than 20 years. National statistics show that 9% of adults were diabetic in 2005 and the morbidity for this cause increased at a rate of 3% per year from 2001 to 2005 [1].

The situation of diabetes mellitus in Mexico is a manifestation of a worldwide health problem. The International Diabetes Federation (IDF) reports 246 millions of adults (between 20 and 79 years old) with diabetes in 2007, corresponding to 6% of the adult population and 3.7% of the total population in the world. For the year 2025, the number of diabetic adults is estimated in 380 millions, which represents 7.3% and 4.8% of the expected adult and total population, respectively [2]. Nowadays, the United States, Europe and the Western Pacific region have the highest numbers of diabetes cases, while Arab countries have the highest proportion of the population with diabetes. The foreseen spread rate of the disease at 3% per year in adults will affect mainly the young and productive urban populations in developing countries. This tendency is explained by the transformation of the lifestyle with technological progress.

Latin American and Caribbean countries have serious deficiencies regarding prevention, diagnostics and treatment of diabetes, which are the basic strategies to control this epidemic. The access to the information about diabetes is limited. More than one-third of diabetics are undiagnosed, and 50% of the new cases detected present already advanced complications due to the lack of glycemic control. The quality of diabetes care is low as indicated indirectly by the statistics of diabetic patients who attend medical consultations to check their eye, heart, kidneys or feet health [3].

Diabetes mellitus, being a lifelong disease that requires continuous medical attention, has important economical effects on the patient and the society. The complications of the disease, treatment expenses and incomes lowered because of unfavorable health conditions to work affect the quality of life of the families. The costs of the disease are classified as direct and indirect (Table 1.1). Direct costs are related to drugs, consultation and hospitalization. Indirect costs quantify the loss of productivity due to temporary and permanent disability and premature mortality. For Latin America and the Caribbean in the year 2000, the World Health Organization (WHO) estimates a total indirect cost of 14 million years of productive life and US$ 55 billion, and a total direct cost of US$ 11 billion [4]. The American Diabetes Association (ADA) reports a total direct cost of US$ 92 billion and a total indirect cost of US$ 40 billion for USA in the year 2002 [5]. From the world total expenditure on diabetes direct costs, 80% is spent in the economically wealthiest countries and this percentage tends to increase [2].

Diabetic mellitus cases are classified as insulin dependent or type 1 and insulin independent or type 2, regardless of the age of the patient. Other types of diabetes are related to different genetic syndromes, hormonal or receptor abnormalities and pancreatic diseases. The statistics mentioned above refer to the number of proportion of the population with any type of diabetes mellitus. Type 2 diabetes represents approximately the 90% of diabetes cases in developed countries [2] and a higher percentage in developing countries (97.5% in Latin America and Caribbean, for instance, in the year 2000 [4]).

Insulin therapy can transform diabetes from a fast mortal disease to a condition of life with all its possibilities in length and activities. Although the treatment of type 2 diabetes focuses on exercise and diet, the external infusion of insulin can be advantageous in approximately 5% of type 2 patients [4]. On the other hand, type 1 diabetes treatment is based on the supply of exogeneous insulin.

Diabetes treatment has evolved with technological and scientific advances. Traditional treatment is based in medical prescription of insulin injections based on glucose measurements performed manually with a certain low frequency. The development of glucose sensors and insulin delivery devices has helped to approach a more continuous and opportune insulin administration [6, 7]. Automatic continuous control systems offer the possibility of a precise blood glucose regulation in a diabetic patient [8].

Desirable portability, reliability and comfortability of closed loop systems impose implementation challenges. Different insulin delivery routes [9] and control algorithms [10] have been proposed for the closed loop treatment of diabetes. Practical implementation of some of these systems has been done in hospital installations [11], due to the volume, complexity and supervision requirements of the instrumentation involved. Integration of the functional elements of a control system in a single device is necessary for an efficient closed loop treatment.

Smart materials can be designed to perform different functions for a particular application. Hydrogels are ionic polymers that expand or contract in response to the pH of the medium. The hydrophilicity of the polymer allows for the absorption of drugs in solution. The change of intra and intermolecular spaces affect the diffusion resistance of the hydrogel, which modulates the drug release. Hydrogels have been evaluated as a competitive alternative for open loop treatment of diabetes mellitus [12]. This work analyzes systems to provide insulin to diabetic patients based on two approaches: 1) the use of separate controller, actuator and sensor units, and 2) the use of glucose sensitive hydrogels as smart materials that integrate the functions of the previously mentioned units in a single device (Figure 1.1).

The general objective of this investigation is to evaluate the potential of hydrogel materials for feedback treatment systems. For this purpose, a particular glucose sensitive hydrogel was synthesized and characterized. The information generated from experimentation was used to model and simulate hydrogel materials and their application in closed loop diabetes treatment. An optimal controller was used to set a reference frame

for the performance of hydrogel-based system. Hydrogels were analyzed from a functional and dynamic point of view, parting form their biocompatibility and stable biochemical components: enzymes and imbibed drug.

This document includes background information regarding the biological basis of diabetes mellitus, its therapeutic avenues and treatment technology in Chapter 2. The research objectives are stated in Chapter 3. The synthesis of poly(methacrylic acid-grafted-ethylene glycol) hydrogel membranes is reported in Chapter 4. The characterization of the synthesized material is presented in Chapter 5 and Chapter 6 from static and dynamic experiments, respectively. In Chapter 7, the mechanochemical compliance is studied through swelling and tensile experiments for the description and simulation of the fundamental pH responsive viscoelastic behavior of hydrogels. Chapter 8 presents the model of a hydrogel-based system as a glucose sensitive insulin delivery element for the treatment of diabetes mellitus. An optimal linear quadratic controller is designed in Chapter 9. The use of the mathematical controller is discussed considering the non-linearity of the physiological glucose-insulin process, measurement noise and estimation of unmeasured variables. In Chapter 10, simulation of the two types of closed loop diabetes treatments of a patient with a specific diet is used for the evaluation of the performance of the hydrogel-based feedback glucose regulation system. Final reflections and possible directions of future work are discussed in Chapter 11.

**Table 1.1.  Quantifiable Costs of Diabetes Mellitus.**  Direct and indirect costs reflect a combined effect of number of cases and quality of attention or treatment of the disease.

|  | *Mexico (2000) [4]* | *Latin America and Caribbean (2000) [4]* | *United States of America (2002) [5]* |
|---|---|---|---|
| *Direct costs (billions of US dollars)* | | | |
| Medication | 0.77 | 4.7 | |
| Consultation | 0.34 | 2.5 | |
| Hospitalization | 0.23 | 1 | |
| Care of complications | 0.64 | 2.5 | 24.6 |
| Total | 1.97 | 10.7 | 92 |
| *Indirect costs ((billions of US dollars)* | | | |
| Mortality | 0.6 | 3 | |
| Temporary disability | 0.2 | 0.8 | |
| Permanent disability | 12 | 50 | |
| Total | 13 | 54 | 40 |
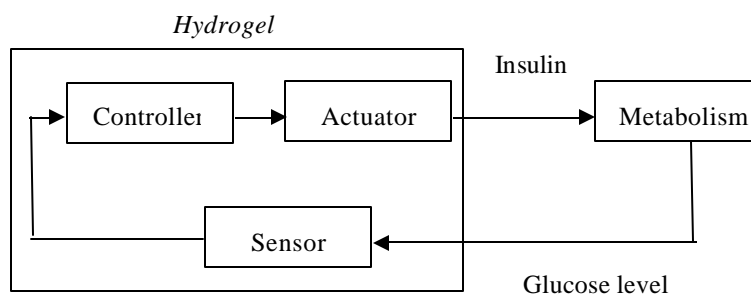


**Figure 1.1. Closed Loop Approaches for Diabetes Mellitus Treatment.**  Separate controller, actuator and sensor elements can be proposed to close the glucose feedback control system.  Alternatively, a multifunctional hydrogel based system can be used for the closed loop treatment of diabetes.

**References**

1.  Salud: México 2001-2005.  http://evaluacion.salud.gob.mx/saludmex2005/sm2005.htm (as seen on June 18, 2007).

2.  Diabetes Atlas, third edition ©International Diabetes Federation 2006.

3.  Barceló A, Vovides Y. The Pan American Health Organization and World Diabetes Day.  Pan Am J Public Health. 2001;10(5):297-298.

4.  Barceló A, Aedo C, Rajpathak S, Robles S. The cost of diabetes in Latin America and the Caribbean. Bulletin of the World Health Organization 2003;81(1):19-27.

5.  American Diabetes Association. http://www.diabetes.org/diabetes-statistics.jsp (as seen on June 18, 2007).

6.  Polla DL. BioMEMS applications in medicine. Proceedings of International Symposium on Micromechatronics and Human Science. 2001:13-15.

7.  Staples M, Daniel K, Cima M, Langer R. Application of micro- and nano-electromechanical devices to drug delivery.  Pharmaceut Res. 2006;23(5):847-863.

8.  Heller A. Integrated medical feedback systems for drug delivery. AIChE J. 2005;51(4):1054-1066.

9.  Peppas NA, Kavimandan NJ. Nanoscale analysis of protein and peptide absorption: Insulin absorption using complexation and pH-sensitive hydrogels as delivery vehicles. Eur J Pharm Sci. 2006;29:183–197.

10. Bequette BW. A critical assessment of algorithms and challenges in the development of closed-loop artificial pancreas. Diabetes Technology & Therapeutics. 2005;7(1):28-47.

11. Chee F, Fernando T,  van Heeden P. Expert PID control system for blood glucose control in critically ill patients.  IEEE T Info Technol B.  2003;7(4):419-425.

12. Peppas NA, Bures P, Leobandung W, Ichikawa H. Hydrogels in pharmaceutical formulations. Eur J Pharm Biopharm. 2000;50:27-46.

## 2. Background

### 2.1. Biological Basis of Diabetes Mellitus

Diabetes mellitus is a chronic disease that affects the ability of the body to produce insulin or to be sensitive to insulin. This results in elevated fasting and postprandial blood glucose levels. The insulin allows the absorption of glucose in the cells to be used as energy source. There are two major types of diabetes mellitus: juvenile-onset diabetes (type 1) and maturity-onset diabetes (type 2). In type 1 diabetes the cells of the pancreas that produce insulin are destroyed, which suggests a treatment based on administration of exogeneous insulin. Type 2 diabetes is usually related to obesity. In type 2 diabetes, tissues are less sensitive to insulin maybe because of insufficiency of insulin receptors on the surface membranes of the cells. Lose of weight may make medicaments unnecessary in adult diabetes. In both types of diabetes, important disabling complications such as retinopathy, nephropathy, neuropathy and lower extremity amputation may develop. Progress in the understanding of the pathophysiology of diabetes has been linked to the proposal of therapeutic avenues.

Carbohydrates are the primary exogenous source of glucose. The body homeostatic mechanisms maintain glucose levels within a narrow range in spite of fasting and food ingestion. Within the pancreas there are small encapsulated clusters of cells called islets of Langerhans. These cells are of three types: alpha, beta and delta [1]. When blood glucose levels are low, alpha cells secrete glucagon, which elevates blood glucose concentration. However, if blood glucose level is too high, beta cells release insulin helping body cells to increase their uptake of glucose. Delta cells produce the hormone somatostatin to inhibit the release of either glucagon or insulin.

Alterations in the carbohydrates metabolic pathways (shown in Figure 2.1) explain diabetes [2]. Ingested carbohydrates break into small compounds, that include glucose, sucrose and fructose, by the action of digestive enzymes ($\alpha$- amylase, maltase and $\alpha$-glucosidase). The produced glucose stimulates beta cells to secrete insulin. Insulin activates the glucose transporter GLUT-4, which is uniquely expressed in skeletal and cardiac muscles and in adipose tissues, to assist glucose utilization. The glucose-insulin metabolism performs as a natural closed loop system where the glucose level is detected and a corrective action is carried out by insulin production to promote glucose utilization.

The balance between glucose promoted insulin release and insulin induced glucose tissue intake is disturbed by excessive glucose levels for long periods, a consequence referred to as glucose toxicity. As a toxic effect of hyperglycemia, reactive oxygen species, ROS, are generated that further alter the function of the beta cells since pancreatic islets have low expression of antioxidant enzymes. This oxidative stress is aggravated by the ROS increased generation of tumor necrosis factor, TNF-$\alpha$. This factor is considered to produce insulin resistance by four mechanisms: the decrement in the autophosphorylation of insulin receptor, the conversion of insulin receptor substrate-1 into an inhibitor of insulin receptor tyrosine kinase, the decrement of GLUT-4 transporter in muscle cells and the

6

accumulation of fat (due to increased fatty acids and triglycerides and decreased high density lipoprotein).

## 2.2. Therapeutic Avenues

Although hyperglycemia is considered as a risk factor for the progress of diabetic complications, these are also related to oxidative stress. Therefore, therapies have evolved to attack a variety of targets (metabolic and gene regulatory) by interfering with different mechanisms, in both types of diabetes. Synthetic medicines have been developed as $\alpha$-glucosidase inhibitors to reduce glucose production from ingested carbohydrates, sulfonilureas and biguanides that influence the activation of glucose and insulin receptors, respectively, and aldose reductase inhibitors to prevent cataract formation and other diabetic complications. Phytochemicals aim at carbohydrate metabolic targets that participate in oxidative alteration mechanisms. The antioxidant and polyphenolic compound content of phytochemicals scavenges free radicals and, therefore, reduces TNF-$\alpha$ expression and oxidative stress. Phytochemicals have also shown therapeutic activity regarding carbohydrate digestion and absorption and insulin release. Transcription factors that intervene in glucose homeostasis represent a class of therapeutic targets. They are more difficult to manage because they are expressed in multiple tissues, they may regulate large number of genes and perform functions, which are not fully known [2].

Although alternative therapies research is leading to different resources for diabetes treatment, insulin continues to be the best way of controlling blood glucose even for type 2 diabetes. Some researchers affirm that the resistance of type 2 diabetic patients and physicians to use insulin is due to the following misconceptions: insulin autoinduced resistance (insulin treatment improves insulin sensitivity), increased cardiovascular risk (associated to insulin resistance, which is not developed by insulin administration), excessive weight gain (modest weight gain as a side effect of insulin use is of approximately 4 kg), severe hypoglycemia (hypoglycemic episodes that require assistance of another person are not common in type 2 diabetic patients) [3].

Diabetes therapy based on administration of insulin is essential for type 1, but also highly effective for type 2. This therapy has been improved by the introduction of insulin analogues (lispro and aspart), which have similar onset and duration of action than human insulin. Insulin therapy can preserve $\beta$-cell function in early stages of the disease and improve lipid metabolism [4]. For these reasons, insulin administration is also benefitial for the treatment of type 2 diabetes. The adverse effects of insulin therapies are hypoglycemia, weight gain and progression of retinopathy (when glycosylated hemoglobin, $HbA_{1c}$, levels are higher than 7%).

Current available insulin products are classified according to the velocity of absorption and duration of action. Rapid acting insulins are mainly used at mealtimes (for prandial or bolus dose) or in insulin pumps. Short acting or regular insulins are injected 20 to 30 minutes before meals; however, its effect is almost immediate when supplied

intravenously. Intermediate acting insulins are used for basal administration, as well as long acting insulins, which are absorbed in crystalline or microprecipitated form (Table 2.1).

The combined use of different types of insulin is challenged by absorption variability. Physiological or intensive insulin regimens try to imitate normal insulin secretion by the proper combination of short or rapid acting insulin, as bolus insulin and suplements, and separate basal intermediate or long acting insulin, with a minimum of 4 to 6 injections per day [4]. Non-physiological treatments with less insulin injections and no separation of prandial and basal doses, can be managed but eliminating flexibility to schedule or skip meals. Physiological therapies reduce costs by decreasing complications with better glucose level control. Adjustments of insulin regimens are necessary according to the activity of the patient.

Treatments with physiological insulin replacement and continuous subcutaneous insulin infusion or pump therapy reached 200 000 type 1 diabetes patients in the year 2002 [5]. Continuous insulin infusion with insulin pump often leads to a reduction of the total amount of insulin dose. A basal dose is programmed in an external insulin pump, and bolus insulin is activated manually by the patient.

Self monitoring of glucose levels is important for a better control in diabetic patients [6] either for the adjustments in a traditional insulin injection treatment or for a continuous insulin administration. The treatment of diabetes nowadays emphasizes the control over $HbA_{1c}$ levels to reduce microvascular complications [4]. HbA1c and glucose levels are correlated, although they have different dynamics because hemoglobin is glycated by exposure to high glucose concentrations for long periods of time. Therefore, glucose measurement is particularly needed for the continuous determination of insulin supply.

Benefits of continuous insulin infusion can be enhanced by closed loop or automatic operation. A closed loop is formed through the feedback of blood glucose levels to a system that can adjust insulin administration accordingly. The essential functional elements of a closed loop treatment includes a glucose sensor to retrieve information from the physiological process, an insulin delivery actuator to modify the state of the physiological process, and a controller that determines how to operate the insulin actuator to achieve the required blood glucose concentration changes to reach normal levels. This scheme resembles the functions of a healthy pancreas more closely than the current insulin pump therapy due to the continuity of sensing, actuation and regulating functions.

Closed loop or feedback systems can be based either on controller algorithms, or on self-regulating devices. The use of a controller algorithm requires a physical implementation to interact with the physical parts of the sensor and the actuator elements. Although microfabrication technology may achieve high levels of integration for a compact presentation of this type of systems, particular physical features have to be incorporated for each element producing a heterogeneous system that implies a more complex interaction with the physiological medium. A self regulating device generally has a simpler and more homogenous configuration due to a natural and high level of integration of sensor, control and actuation functions. The main or even the only component of these systems is a smart

material, that is, an environmental responsive physical element.  In this work hydrogel-based systems are studied for blood glucose control.


## 2.3.  Glucose Sensors

The following summary of glucose sensors technology is based on the review by Peura in 1991 [7] and complemented with literature about posterior significant developments.

The first glucose sensors were developed by Clark and Lyons in 1962. These sensors were based on the oxidation reaction of glucose catalyzed by glucose oxidase detected electrochemically. The first commercial sensor with this technique was manufactured by Yellow Springs Instrument Company and used in the "Biostator" control system fabricated by Thousands Laboratories. The *in vitro* application of the amperometric enzymatic sensors has been successfully used in clinic laboratories and portable personal glucose meters. Nevertheless, its application *in vivo* is not reliable after days from its implantation because they can be encapsulated by tissues or produce calcification [8]. The advantage of the principle of enzymatic oxidation is that glucose concentration can be correlated to different variables: partial pressure of oxygen, pH due to the generated gluconic acid [9], and concentration of produced hydrogen peroxide [10].  However, the main problem of these sensors is their long term stability due to the deterioration of the enzyme.

In the 1980s, electrocatalytic sensors based on the direct oxidation of glucose on a platinum electrode, without the presence of an enzyme, were investigated [11, 12].  This type of sensors takes advantage of the glucose selectivity of the metallic solid electrode. These sensors are more susceptible to interferences, but also more stable than electroenzymatic sensors.

By the time that electrocatalytic sensors were developed, different optical techniques were also applied on glucose detection and measurement. For instance, a pH color indicator exposed to the oxidation of glucose was monitored by light transmission changes between two optical fibers [13].  Detection by molecular affinity was also studied using fluorescent labeled glucose receptors.

The absorption spectroscopy in the infrared region is an important technique for the biological substance identification in aqueous solution. The application of this technique for glucose measurement was reported in reference [14].  Absorption spectroscopy allows for a direct and stable detection. Nevertheless, the glucose measurement in an aqueous solution, like the blood, by conventional methods of spectroscopy of IR absorption has difficulties due to the high background IR absorption of water and low analyte concentrations [63].

The spectroscopy of attenuated total reflection in the multiple infrared (ATR) is not affected strongly by the thickness and optical properties of the medium, unlike conventional IR spectroscopy.  ATR is a potential noninvasive technique since it can be used to detect the infrared spectrum of blood from the skin.  Early applications of ATR for glucose measurement took place in the 1980s and 1990s.  A $CO_2$ laser can be used as

source of excitation and the peak IR absorption can be related to glucose concentration [64].

All the above mentioned technologies are supported by basic principles and have the potential for the fabrication of miniature and implantable sensors. Currently, microsytems technology and nanotechnology research are applied for the solution of issues regarding risk of implantation and comfort, speed and continuity of the measurement, easiness of operation and cost.

Electrochemical biosensors, with glucose oxidase particularly, continue being of interest in the monitoring and treatment of the diabetes because of its simple and economic configuration. At the beginning of the twenty fist century, glucose sensors represented 98% of the commercially available medical enzymatic biosensors [15]. Planar technologies form the electronic industry are based on the deposition, etching and removal of layers on a silicon substrate. These technologies have been modified to manufacture biosensors, by incorporating enzymes and additional layers to protect and enhance the selectivity of their response [16]. Figure 2.2 shows the three-layer configuration of a biosensor. Researchers have suggested microfabricated iridium oxide reference electrodes as an alternative to Ag/AgCl electrodes for continuous glucose monitoring [17]. Electrochemical enzymatic biosensors have also been fabricated based on carbon nanotubes (CNT) achieving a high electrocatalytic effect and a fast response or transfer of electrons [18, 19]. These nanoelectrodes have the potential to work without redox mediator nor membranes (Figure 2.3).

Responsive or smart materials have been used in the development of biosensors. A pH sensor suitable for biomedical applications has been constructed based on a microcantilever patterned with a hydrogel (Figure 2.4). The change in volume of the hydrogel causes a bending response of the microcantilever. The sensor response can be adjusted by modifying the polymeric network structure of the hydrogel [20].

Although implantable biosensors can be perceived as an ideal resource for continuous and precise glucose control, external applications solve other operative requirements. Research on human skin interface for extraction of molecules may solve continuous monitoring needs. Life time of implantable biosensors is limited by consumption of active components unless they can be regenerated *in situ* in the human body. Skin interface based devices have the advantages of minimum invassion, no blood samples required and easy active components supply. The Glucowatch (Cygnus Inc.) is a commercial device approved by the Food and Drug Administration, FDA, to allow diabetics to monitor their glucose levels every 20 minutes over a 12 hour test period using only one finger stick blood test to calibrate the system. Gel pads with glucose oxidase are changed every 12 hours and the sensor is a platinum electrode detecting hydrogen peroxide produced by the reaction of glucose with glucose oxidase. Further developments can be made with a better comprehension of transmission mechanisms such as electroosmosis, diffusion and molecule drift currents with skin models [21].

## 2.4. Insulin Delivery Actuators

A list of commercialized insulin delivery devices and their characteristics is presented by Stewart et al. (2004) [22]. A comparison among different types of insulin delivery devices is also discussed by DeWitt et al. (2003) [4]. These authors give an overview of the still most popular insulin delivery methods in our days. The next paragraphs synthesize information from these sources.

The main insulin delivery devices currently used are syringe, pen and pump (Figure 2.5). The syringe is the traditional and original delivery system from the first insulin administration to a patient in 1922. The concept of the continuous subcutaneous insulin infusion or insulin pump has existed from the 1960s, although it was not recommended by the American Diabetes Association until 1985. Insulin pens were introduced to the United States market in 1987 [22]. Pens and pumps include an insulin reservoir.

Compared to the use of syringes, insulin pens are easier to carry, simpler to operate, more precise and cause less pain. Insulin pens are easier to handle than separate syringe and insulin vial. The dose can be adjusted precisely with a dial that clicks with each increment (0.5, 1 or 2 units), as an additional indication to control the amount of insulin to administer. The use of short needles (5, 6 or 8 mm) with large gauge numbers (from 27 to 31) or smaller bores produce little or no pain during the injection. Insulin cartridges are available for specific insulin types. Insulin for pens is 30% more expensive than bottled insulin [4]. More insulin is wasted in pens because the needle should be previously primed. The patients that use insulin pens should prepare with a backup insulin delivery in case of malfunction.

The insulin pump is a small programmable device with an infusion set that minimizes needle punctures by the selection of a delivery site that is changed every 3 days and avoids the problem of variable injection site adsorption. Only fast acting insulin is used with a pump. Better glycemic control is achieved with insulin pumps thanks to a continuous delivery regimen. The patient requires training to use the insulin pump and should have a backup delivery system [22].

Other insulin administration methods are being investigated or already in the market. Jet injectors are also commercially available but at a very high price. These devices introduce insulin through the skin without needles by using pressure force. Research on implantable insulin pumps, topical insulin patches, artificial pancreas, inhaled insulin and oral insulin try to increase the comfort and efficiency of diabetes treatment [22].

Therapeutic microsystems developed in the last two decades include micropumps, microvalves, microneedles for precision microfluidic dispensing. These devices offer the actuation potential of autonomous care management systems and precision drug delivery systems. Reviews by Grayson et al. [23] and Polla [24], and other sources were consulted to present the following summary of distinctive design principles for drug delivery microsystems.

Immunoisolation devices are polymer or silicon semipermeable capsules to isolate implanted islet cells from the biological environment, while allowing them to remain viable. In diabetes treatment, these cells would secrete insuline. Silicon capsules are produced with two silicon bound membranes with good mechanical strength and reproducible features [23].

Smart materials have also enriched the design of actuator devices. Micropumps and microvalves for microfluidic systems and drug delivery systems have been fabricated with shape memory alloys (SMA) [25, 26], magnetic [27] and piezoelectric [28] elements.

Drug delivery systems may consist of microparticles or microreservoirs that can be ingested or injected. The surface of microparticles can be decorated with biomolecules to target specific cells [29]. An array of silicon microreservoirs covered with individual gold membranes has been proposed. Each membrane is dissolved electrochemically by the application of voltage. Although the drug is released in pulses, these can be combined to control dosage with a different profile. Microreservoirs have also been fabricated with polymer caps to allow for drug release either by diffusion through the polymer membranes or by their degradation [30].

Injectable devices include microneedles and injectable micromodules. Microneedles are made out of silicon, glass or metal. They are used for drug delivery and for sensing applications. Microhypodermic needles have been fabricated as disposable arrays of microneedles and arrays of solid needles. The fist type of arrays can be coupled to a syringe, and the latter is used with patches to increase skin permeability. Injection of microdevices through large-gauge hypodermic needles, would simplify the implantation procedure by eliminating surgery [31].


## 2.5. Mathematical Controllers

Traditional diabetes medical treatment is based on the dosing of exogenous insulin, which is done frequently in a fixed prescribed amount without continuous monitoring or feedback information. A closed loop control system has the potential for a precise blood glucose regulation in a diabetic patient, constituting an artificial pancreas.

Insulin infusion for continuous blood glucose control can be done subcutaneously and intravenously. The subcutaneous route is easier and safer to manage, which is an advantage for closed systems implementation since it is the route used in traditional open loop diabetes treatment. The intravenous route avoids time delays to reach blood stream and to produce body response, which is convenient for continuous closed loop performance. Both insulin delivery types have been considered in closed loop treatment systems [32, 33]. Rapid acting insulins may combine the advantages of both routes because of their fast absorption after subcutaneous injection.

Although insulin directly attacks the typical problem of hyperglycemia in a diabetic patient, the administration of a therapeutic agent to prevent and correct hypoglycemia has not reached consensus from the first control algorithm proposed by Albisser in 1974 [34] to

our days [35]. The study of pharmaceutical preparation and medical application of glucagon [36] is concerned about its side effects, short half life after injection and patient compliance, as debated in scientific reunions such as Diabetes Technology Meeting 2006.

An open loop treatment system may be seen as a partially closed loop system because medical prescription of insulin is based on home glucose monitoring among other information of the patient [32]. Decision support systems have been designed for diabetes management for this kind of therapy systems.

The design of mathematical controllers parts from the model of the process. Empirical models can be obtained from input-output data which are used to derive structure and parameters. The structure of the model can be defined a priori, as in the case of the Ackerman linearized model for glucose-insulin metabolism [37]. On the other hand, compartmental models give a detailed phenomenological description of the process. The number of compartments or level of detail can vary as illustrated by the models of Bergman [38] and Sorensen [39].

Controllers defined with proportional, integral and derivative terms of the difference between the desired and the actual process variable values (PID controllers) have been used for blood glucose control. Early developments such as the "Biostator" by Clemens [40] and algorithms by Steil and coworkers [41], explored PID type controllers. A PID based on a sliding scale approach, tested in patients in intensive care unit, was reported by Chee et al. [42]. A proportional-derivative or PD controller has been derived with a pole assignment strategy and tested in patients [32]. Sorensen [39] worked with the internal model control strategy, which produces PID structures. In this type of controllers, the definition of the integral action of a controller is particularly linked to the risk of hypoglycemia because of the characteristic oscillatory response that the integration of error produces [43].

Advanced control techniques have also been applied. Some researchers have considered the optimization of a performance function defined as the integral of square errors between the actual and the desired glucose levels. Errors are computed based on different sampling intervals [44] and using different insulin delivery techniques like the combination of infusion and injections [45]. The main disadvantage of these schemes was the occurrence of hypoglycemia caused by the manipulation or corrective action determined by the controllers. Additional conditions such as restricted manipulation and model parameter uncertainty have been considered in the application of $H_8$ control for glucose regulation [46] with satisfactory simulation results, that is, with correction of hyperglycemia without induction of hypoglycemia.

Robustness of closed loop systems has been achieved by adaptive and predictive mechanisms to account for sparse glucose measurement [47] and time variations of the glucose-insulin process. The model predictive control algorithm implements a self-tuning controller that has been studied by simulation [48, 49] and tested in vivo [50].

Simulation of control systems allows for preliminary evaluation of closed loop treatments. Control algorithms have been discussed from two types of simulation scenarios: the correction of an initial hyperglycemic state [41, 51] and the recovery of a

normal glucose level before the increment caused by a meal or glucose ingestion [39, 44, 46, 48]. Although practical issues regarding noisy and non-continuous measurements and unmeasured variables have been considered, safety considerations regarding the operation of the sensor and the delivery device have not been incorporated in simulation scenarios.

## 2.6. Hydrogels

Ionic hydrogels are polymers that expand or contract in response to the pH of the medium [52]. The hydrophilicity of the polymer allows for the absorption of drugs in solution. The change of intra and intermolecular spaces affect the diffusion resistance of the hydrogel, which modulates the drug release. Hydrogels have been evaluated as a competitive alternative for open loop treatment of diabetes mellitus [53]. The multifunctionality of hydrogels as smart materials suggests their application for diabetes closed loop treatment.

The pH sensitivity can be coupled to glucose concentration in hydrogel materials by the incorporation of glucose oxidase enzyme [54, 55]. Glucose oxidase catalyzes the oxidation of glucose, which produces gluconic acid altering the pH of the medium. The hydrogel structure serves as an insulin reservoir and delivery device by containing pre-absorbed insulin that is released according to glucose responsive volume or porosity changes.

Catioinic hydrogels exhibit high volume at low pH, while anionic hydrogels contract as pH is reduced (Figure 2.6). The swelling behavior is affected by elastic-retractive forces as well as ionic interactions. In an anionic hydrogen, for example, the acid functional groups of the backbone of the polymer develop negative charges at a pH above the $pK_a$. Electrostatic repulsive forces among the fixed charges cause the hydrogel to swell. Osmotic forces also develop as a result or exchange of free cations through the ionized gel. When the pH decreases, the electrostatic forces disappear and the hydrogel contracts. The volume changes depend on the viscoelasticity of the material.

Ionic polymers can perform as solvent activated delivery systems [56]. In general, polymers are capable of controlled drug release based on diffusion, chemical reaction or solvent activation. Diffusion controlled release takes place in systems that consist of a core of drug surrounded by a membrane or in membranes with a drug content uniformly distributed. Chemical controlled systems allow for drug release as the polymer either degrades or erodes. Solvent activated systems are osmotic-controlled or swelling-controlled.

In this work poly(methacrylic acid-graft-ethylene glycol), P(MAA-g-EG), is used as a reference hydrogel material for characterization and modelation because of its biocompatibility, since an implantable system is desirable for the closed loop diabetes treatment system. The incorporation of poly(ethylene glycol), PEG, grafts enhances the acceptance of the material in the body as well as the activity of biochemical components, such as insulin and glucose oxidase in the studied materials [57].

14

The decoration of the hydrogel material with PEG tethers also affects the swelling behavior through a phenomenon of complexation resultant from the formation of entanglements and hydrogen bonds [58]. The largest volume changes in P(MAA-g-EG) have been observed in gels containing approximately equimolar amounts of methacrylic acid and ethylene glycol and the longest molecular weight PEG grafts [59].

Concerning drug delivery function, solute transport through P(MAA-g-EG) membranes has been shown to be dependent of the swelling using proxyphylline, vitamin $B_{12}$ and FITC-dextran [60]. Oral insulin delivery systems have been proposed based on P(MAA-g-EG); these systems protect the insulin from the acid environment of the stomach and allow insulin release at the neutral pH of the upper part of the small intestine. The retention of this type of systems is achieved by PEG tethers that adhere to the mucosal layer [62]. These systems offer a convenient alternative to traditional insulin injections for open loop treatment. This work explores the potential of glucose sensitive hydrogels for closed loop treatment based.

## 2.7. Conclusions

In this chapter, the carbohydrate metabolism has served as a frame of reference to current and future therapeutic avenues for diabetes mellitus. Closed loop systems, as one of them, face important challenges regarding design and implementation.

Glucose oxidase has been used in different generations of glucose sensors, which can have a double implication. On one side the enzymatic sensing principle is effective and available in different structures. On the other hand, it can be a reference for the evaluation of new detection methods and devices. The continuous measurement remains as the main difficulty for a glucose biosensor due to the degradation of the enzyme.

The development of the insulin pump has solved the requirement of a continuous and versatile action of the dosifier for a feedback system for pancreatic functions replacement. However, the disadvantage of the insulin pump is the uncomfortable insertion of a needle, whose site must be changed every three weeks to prevent infection and excessive fibrosis with the consequent reduced absorption capability. As a matter of fact, this problem is present in the other two commercially available options, syringe and insulin pen.

In addition to the difficulties to achieve a targeted interaction of implants, there are other challenges for their therapeutic use. The main issues regarding implantable devices are the possible negative effects over the body (toxicity) as well as the fouling caused by body reactions (calcification or tissue encapsulation). Moreover, operation requirements such as replenishment of active components (drug in a delivery system or enzymes in a biosensor) may require invasive procedures.

The main aspect for the application of feedback control systems in the medical field is security. This essential requirement can be approached by several means as in other application areas: stability, detection of faults, redundant systems. The basic guarantee of a

closed loop treatment system must be a stable operation. Robustness has been emphasized by some authors [46]. Although advanced control strategies have produced good results, and computational power and speed are each time less restrictive, a robustness analysis and a cost-benefit balance would often lead to moderate levels of complexity.

The biocompatibility and the potential of high level of integration of hydrogel systems make them an attractive option for glucose regulation with important advantages over closed loop control systems with explicit controller, actuator and sensor elements (implemented as individual devices).
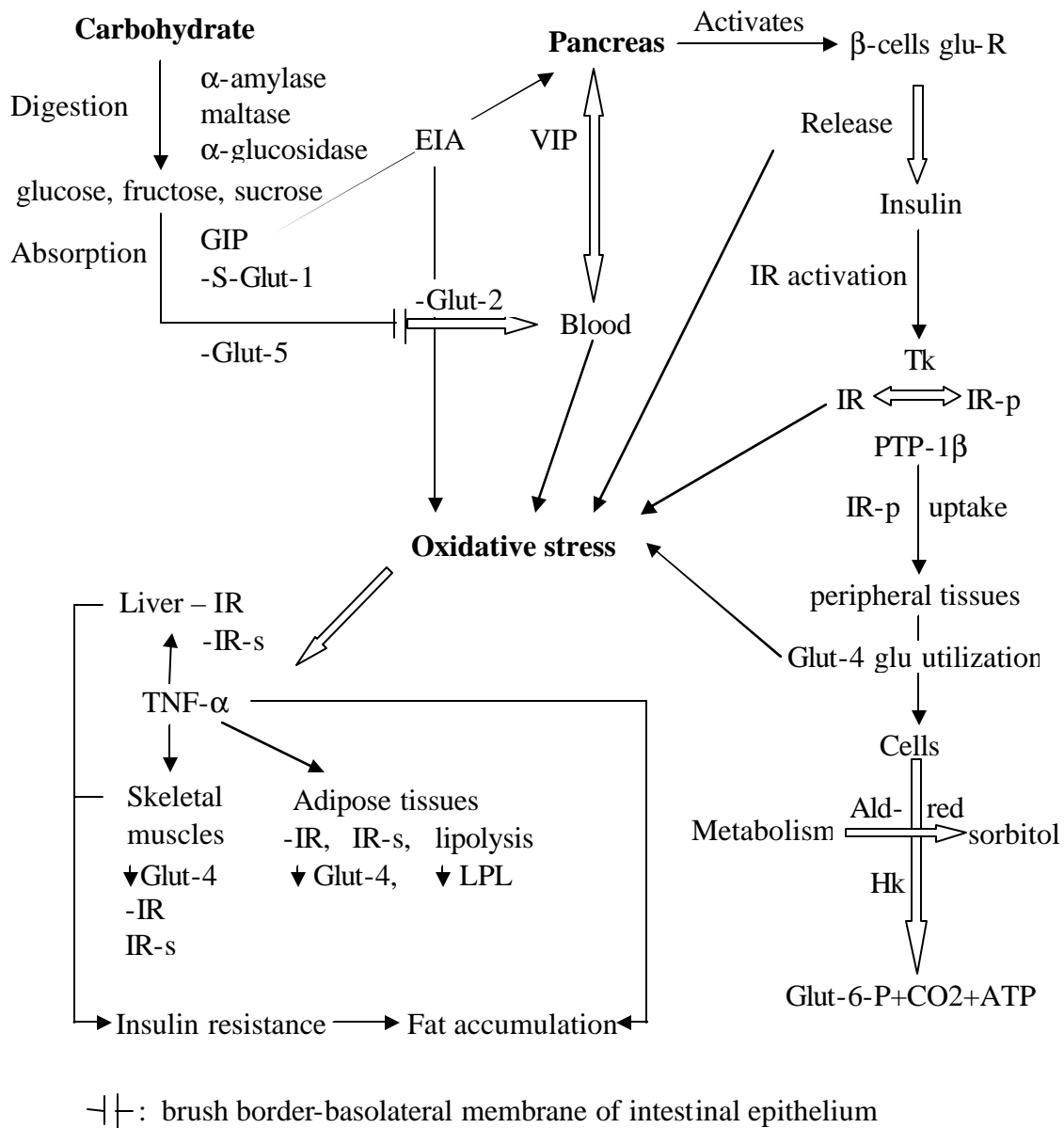
**Figure 2.1. Carbohydrate metabolic pathways.** S-Glut-1: sodium-glucose cotransporter (glucose transport across the intestine); GIP: gastrointestinal peptide; VIP: vasoactive intestinal peptide; EIA: entero-insular axis; glu R: glucose receptor; IR: insulin receptor; IR-s: insulin receptor substrate; Tk: tyrosine kinase enzyme; PTP: protein phosphotyrosin phosphatase; TNF: tumor necrosis factor; Ald-red: aldose reductase (catalysis of reduction of glucose into sorbitol); Hk: hexokinase; LPL: lipoprotein lipase. Adapted from [2].

**Table 2.1. Insulin Products.** Different action characteristics (assuming 0.1-0.2 U/kg per injection) fit specific needs for a physiological therapy. Abbreviations: L, Lente; NPH, neutral protamine Hagedorn; NPL: neutral protamine lispro. Adapted from [4].

| Insulin | Onset | Peak | Duration, h |
|---------|-------|------|-------------|
| Rapid acting<br>  Lispro (Humalog)<br>  Aspart (NovoLog) | 5-15 min | 30-90 min | 5 |
| Short acting<br>  Regular U100<br>  Regular U500<br>  Buffered regular (Velosulin) | 30-60 min | 2-3 h | 5-8 |
| Intermediate acting | | | |
|   Isophane insulin<br>  (NPH, Humulin N/Novolin N) | 2-4 h | 4-10 h | 10-16 |
|   Insulin zinc<br>  (Lente, Humulin L/Novolin L) | 2-4 h | 4-12 h | 12-18 |
| Long acting | | | |
|   Insulin zinc extended<br>  (Ultralente, Humulin U) | 6-10 h | 10-16 h | 18-24 |
|   Glargine (Lantus) | 2-4 h | No peak | 20-24 |
| Premixed | | | |
|   70% NPH/30% regular<br>  (Humulin 70/30) | 30-60 min | Dual | 10-16 |
|   50% NPH/50% regular<br>  (Humulin 50/50) | 30-60 min | Dual | 10-16 |
|   75% NPL/25% Lispro<br>  (Humulin Mix 75/25) | 5-15 min | Dual | 10-16 |
|   70% NP/30% aspart<br>  (NovoLog Mix) | 5-15 min | Dual | 10-16 |
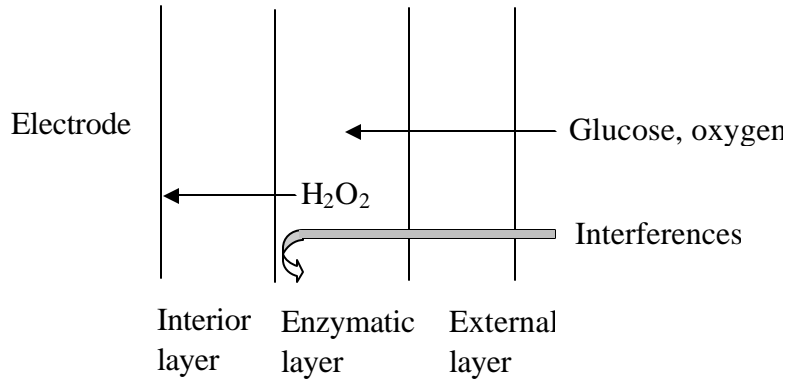
**Figure 2.2. Membranes on a biosensor electrode.** Microfabrication or planar technologies can produce layers to enhance the selectivity of the sensor. Adapted from [16].
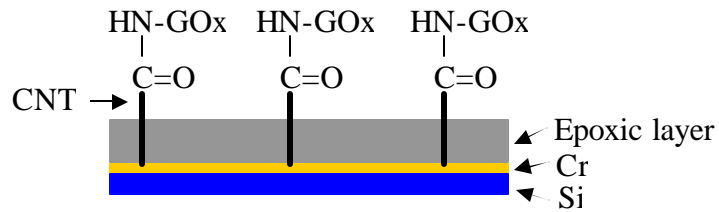


**Figure 2.3. Enzymatic nanoelectrodes.** Carbon nano tubes (CNT) are functionalized to attach glucose oxidase (GOx) molecules covalently [18].
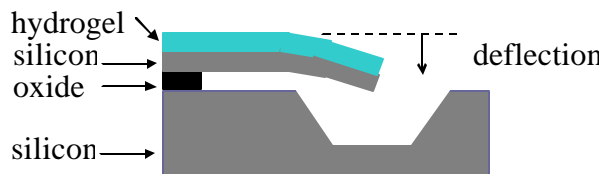


**Figure 2.4. Microcantilever sensor.** Volume changes of the hydrogel layer induce a displacement of the free end of the cantilever. Adapted from [20].
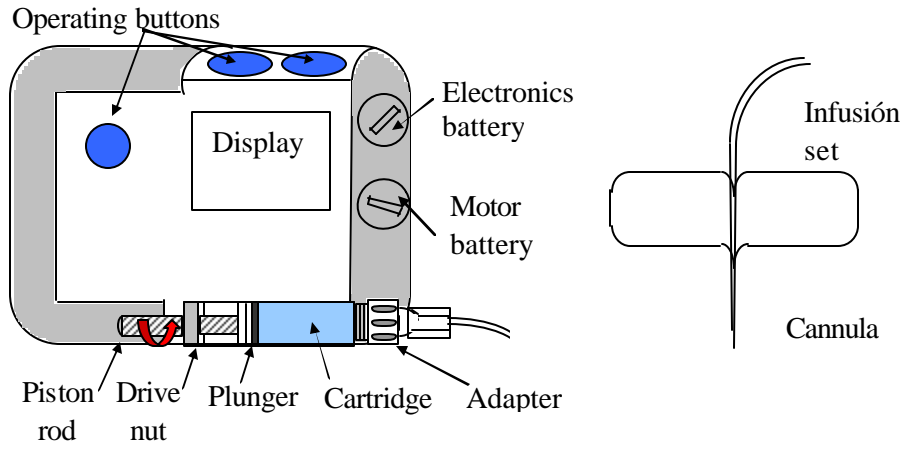
(a)
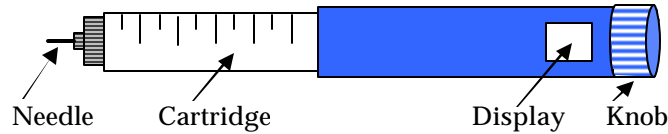


(b)

**Figure 2.5. Commercial Insulin Delivery Devices.** (a) Insulin pump (H-TRONplus by Disetronic (adapted from [62]). (b) Insulin pen.
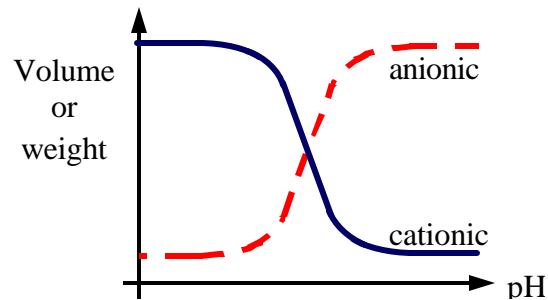


**Figure 2.6. Ionic Hydrogels.** The anionic hydrogel swells and the cationic hydrogel contracts as pH increases.

## References

1.  Seely RR, Stephens TD, Tate P. Anatomy & physiology. St Louis: 1995. Seeley, R.R, Stephens, T.D., and Tate, P. (1995) Anatomy & physiology (3rd edition). St Louis: Mosby-Year Book, Inc.

2.  Tiwari AK, Rao JM. Diabetes mellitus and multiple therapeutic approaches of phytochemicals: present status and future prospects. Current Science. 2002;83(1):30-38.

3.  White JR, Campbell RK. Insulin in the treatment of type 2 diabetes mellitus. Am J Health-Syst Pharm. 2003;60:1145-1152.

4.  DeWitt DE, Hirsch IB. Outpatient Insulin Therapy in Type 1 and Type 2 Diabetes Mellitus. JAMA. 2003;289(17):2254-2264.

5.  Bode BW, Sabbah HT, Gross TM, Fredrickson LP, Davidson PC. Diabetes management in the new millennium using insulin pump therapy. Diabetes Metab Res Rev. 2002;18(1):14-20.

6.  Franciosi M, Pellegrini F, De Berardis G. The impact of blood glucose self-monitoring on metabolic control and quality of life in type 2 diabetic patients. Diabetes Care. 2001;24:1870-1877.

7.  Peura RA. Blood glucose biosensors - A review. IEEE Cast Studies in Medical Instrument Design. 1991:51 – 64.

8.  Moussy, F. Implantable glucose sensor: progress and problems. Proceedings of IEEE Sensors. 2002;1:12-14.

9.  Pereira C, Oliveira J, Silva R, Silva F. Amperometric glucose biosensor based on assited ion transfer through gel-supported microinterfaces. Anal. Chem. 2004;76:5547-5551.

10. Madou M, Morrison SR. Chemical Sensing with Solid State Devices. Academic Press, Inc. 1988.

11. Lewandowsky JJ. Amperometric glucose sensor: short-term, in-vivo test, Diabetes Care. 1982;5(3):238-244.

12. Yao SJ, Li VWT, Dokko Y, Krupper MA, Wolfson Jr SK. Electrochemical detection of glucose at low potentials. Proceeding IEEE/NSF Symposium on Biosensors. 1984:75-77.

13. Peterson JI. A miniature pH sensor potentially suitable for glucose measurements. Diabetes Care. 1982;5(3):272-274.

14. Zeller H, Novak P, Landgraf R. Blood glucose Measurement by IR spectroscopy. Interntional Journal of Artificial Organs. 1989;12(2):129-134.

15. Harsanyi T, Santha H. Polytronics for biotronics: unique possibilities of polymers in biosensors and bioMEMS? Polymers and Adhesives in Microelectronics and Photonics. 2nd International IEEE Conference. 2002:211-215.

16. Gregory CM. Fabrication methods for integrated biosensors. IEE Colloquium on Advances in Sensors. 1995:10/1-10/5.

17. Yang H, Kang SK, Shin DH, Kim H, Kim YT. Microfabricated iridium oxide reference electrode for continuous glucose monitoring sensor. Transducers, Solid-State Sensors, Actuators and Microsystems. 12th Innational Conference. 2003;1:103–106.

18. Lin Y, Lu F, Tu Y, Ren Z. Glucose biosensors based on carbon nanotube nanoelectrode ensembles. Nano Letters. 2004;4(2):191-195.

19. Tu Y, Lin Y, Ren ZF. Nanoelectrode arrays based on low density aligned carbon nanotubes. Nano Letters. 2003;3(1):107-109.

20. Hilt JZ, Gupta AK, Bashir R, Peppas NA. A bioMEMS sensor platform based on a cantilever with a precisely patterned environmentally sensitive hydrogel. EMBS/BMES Conference Proceedings. 2002;2:1650–1651.

21. Connolly P, Cotton C, Morin F. Opportunities at the skin interface for continuous patient monitoring: a development model based on lactate and glucose. Proceedings of the IEEE-EMBS Special Topic Conference on Molecular, Cellular and Tissue Engineering. 2002:50 – 51.

22. Stewart KM, Wilson MF, Rider JM. Insulin delivery devices. J Pharm Pract. 2004;17(1):20-28.

23. Grayson ACR, Shawgo RS, Johnson AM, Flynn NT, Yawen LI, Cima MJ, Langer R. A BioMEMS review: MEMS technology for physiologically integrated devices. Proceedings of the IEEE. 2004;92(1):6-21.

24. Polla DL. BioMEMS applications in medicine. Proceedings of International Symposium on Micromechatronics and Human Science. 2001:13-15.

25. Reynaerts D, Peirs J, Van Brussel H. Design of a SMA-actuated implantable drug delivery system. Proceedings of the Sixth International Symposium on Micro Machine and Human Science. 1995:111.

26. Benard WL, Kahn H, Heuer AH, Huff MA. A titanium-nickel shape-memory alloy actuated micropump. Internacional Conference on Transducers, Solid-State Sensors, Actuators and Microsystems. 1997;1:361-364.

27. Khoo M, Liu C. A novel micromachined magnetic membrane microfluid pump. Proceedings of the 22nd Annual Internacional Conference on the IEEE Engineering in Medicine and Biology Society. 2000;3:2394-2397.

28. Maillefer D, Van Lintel H, Rey-Mermet G, Hirschi R. A high-performance silicon micropump for an implantable drug delivery system. IEEE International Conference on Micro Electro Mechanical Systems. 1999: 541-546.

29. Ahmed A, Bonner C, Desai TA. Bioadhesive microdevices for drug delivery: a feasibility study. Microdev. 2001;3:89-95.

30. Santini JT, Cima MJ, Langer R. A controlled-release microchip. Nature 1999;397:335-338.

31. Henry S, McAllister DV, Allen MG, Prausnitz MR. Microfabricated microneedles: a novel approach to transdermal drug delivery. J. Pharm. Sci. 1998;87:922–925.

32. Bellazi R, Nucci G, Cobelli C. The subcutaneous route to insulin-dependent diabetes therapy. IEEE Eng Med Biol. 2001;20(1):54-64.

33. Parker R, Doyle III F, Peppas NA. The intravenous route to blood glucose control. IEEE Eng Med Biol. 2001;20(1):65-73.

34. Albisser AM, Leibel BS, Ewart TG, Davidovac Z, Botz CK, Zingg W. An Artificial endocrine pancreas. Diabetes. 1974;23:389-396.

35. Damiano E. Closed-loop blood-glucose control using dual subcutaneous infusion of insulin and glucagons in vivo. Diabetes Technology Meeting 2006, Atlanta, Georgia: S12.

36. Donsmark M. Physiological Aspects and Pharmacology of Commercial Glucagon preparations. Diabetes Technology Meeting 2006, Atlanta, Georgia: S14.

37. Ackerman E, Gatewood LC, Rosevear JW, Molnar GD. Model studies of blood-glucose regulation. Bull Math Biophys. 1965;27:21-37.

38. Bergman RN, Phillips LS, Cobelli C. Physiologic evaluation of factors controlling glucose tolerance in man. J Clin Invest. 1981;68:1456-1467.

39. Sorensen J. A physiologic model of glucose metabolism in man and its use to design and assess improved insulin therapies for diabetes. PhD thesis. Dept. of Chemical Engineering, MIT, 1985.

40. Clemens AH. Feedback control dynamics for glucose controlled insulin infusion systems. Med. Prog. Technol. 1979;6:91-98.

41. Steil GM, Panteleon AE, Rebrin K. Closed-loop insulin delivery—the path to physiological glucose control. Adv. Drug Deliver Rev., 2004;56:125-144.

42. Chee F, Fernando T, Van Heeden P. Expert PID control system for blood glucose control in critically ill patients. IEEE Trans. Info. Tech. in Biomed. 2003;7(4):419-425.

43. Bequette BW. A critical assessment of algorithms and challenges in the development of a closed-loop artificial pancreas. Diabetes Technology and Therapeutics. 2005;**7:**28-47.

44. Ollerton, RL. Application of optimal control theory to diabetes mellitus. Int J Control. 1989;50:2503-2522.

45. Fisher ME. A semiclosed-loop algorithm for the control of blood glucose levels in diabetics. IEEE Trans. Biomed. Eng. 1991;38:57-61.

46. Parker RS, Doyle FJ III, Ward JH, Peppas NA. Robust $H_8$ glucose control in diabetes using a physiological model. AIChE J. 2000;46:2537-2549.

47. Woodruff, E., Gulaya, S. & Northrop, R. (1988). The Closed-Loop Regulation of Blood Glucose in Diabetes. Proc. of the 14th Annual Northeast Bioengineering Conference, pp. 54-57.

48. Parker RS, Doyle FJ III, Peppas NA. A model-based algorithm for blood glucose control in type I diabetic patients. IEEE Trans. Biomed. Eng. 1999;46:148-157.

49. Lynch SM, Bequette BW. Estimation-based model predictive control of blood glucose in type I diabetics: a simulation study. Proceedings of the IEEE 27th Annual Northeastern Bioengineering Conference, Storrs, CT. 2001:79-80.

50. Dudde R, Vering T. Advanced insulin infusion using a control loop (ADICOL) concept and realization of a control-loop application for the automated delivery of insulin. 4th International IEEE EMBS Special Topic Conf. on Info. Tech. App. in Biomed. 2003:280-282.

51. Furler SM, Kraegen EW, Smallwood RH, Chisolm DJ. Blood glucose control by intermittent loop closure in the basal mode: computer simulation studies with a diabetic model. Diabetes Care. 1985;8:553-561.

52. Peppas NA, Hydrogels. In Biomaterials Science. Ratner, BD, Hoffman AS, Schoen FJ, Lemons JE, Eds. Academic Press, NY. 2004:100-107.

53. Peppas NA, Bures P, Leobandung W, Ichikawa H. Hydrogels in pharmaceutical formulations. Eur J Pharm Biopharm. 2000;50:27-46.

54. Albin GW, Horbett TA, Miller SR, Ricker NL. Theoretical and experimental studies of glucose sensitive membranes. J. Control. Release. 1987;6:267-291.

55. Podual K, Doyle FJ III, Peppas NA. Preparation and dynamic response of cationic copolymer hydrogels containing glucose oxidase. Polymer. 2000;41:3975-3983.

56. Brannon-Peppas L. Biomaterials-Polymers in Controlled Drug Delivery. Polymers in Controlled Drug Delivery (MPB archive, Nov 97). http://www.devicelink.com/mpb/archive/97/11/003.html.

57. Peppas NA, Keys KB, Torres-Lugo M, Lowman A. Poly(ethylene glycol)-containing hydrogels in drug delivery. Journal of Controlled Release. 1999;62:81–87.

58. Kima B, Peppas NA. Analysis of molecular interactions in poly(methacrylic acid-g-ethylene glycol) hydrogels. Polymer. 2003;44: 3701–3707.

59. Lowman AM, Peppas NA. Analysis of the complexation/decomplexation phenomena in graft copolymer networks. Macromolecules. 1997;30:4959-4965.

60. Lowman AM, Peppas NA. Solute transport analysis in pH-responsive, complexing hydrogels of poly(methacrylic acid-g-ethylene glycol). J Biomater Sci Polymer Edn. 1999;10(9):999-1009.

61. Peppas NA, Wood KM, Blanchette J. Hydrogels for oral delivery of therapeutic proteins. Expert Opin Biol Ther. 2004;4(6):881-887.

62. Accu Chek. http://www.accu-chek.es/es_ES/image/insulin_pump_sensor_system.gif as seen on 12/13/07.

63. Bhandare P, Stohr E, Mendelson Y, Perua RA. IR spectrophotometric measurement of glucose in phosphate buffered saline solutions: effects of temperature and pH. Proceedings of the 1992 Eighteenth IEEE Annual Northeast Bioengineering Conference. 1992:103-104.

64. Kaiser N. Laser absorption spectroscopy with an ATRprism-noninvasive in vivo determination of glucose. In: Hepp KD. Feedback-controlled and preprogrammed insulin infusion in diabetes mellitus. New York: Thieme Verlag, 1979:30-33.

## 3. Objectives

The use of biocompatible smart materials is a promising strategy for the development of highly integrated feedback control systems for maintaining normal glucose levels in diabetic patients. Such integration produces a characteristic dynamic behavior that depends on the conditions of the physiological medium and, at the same time, produces a control effect over the physiological process.

In the Biomaterials Laboratory lead by Professor Peppas at the University of Texas at Austin, poly(methacrylic acid-graft-ethylene glycol), P(MAA-g-EG), has been studied as drug carriers and delivery systems under a primary focus on open loop treatments [1-5]. This previous work validates P(MAA-g-EG) as an adequate material for medical applications and is used in this investigation as a general reference for the study of ionic hydrogels. Insulin release from glucose sensitive materials based on the cationic poly(diethylamionethyl methacylate-graft-ethylene glycol), P(DEAEM-g-EG), hydrogel has also been studied *in vitro* within the same research group [6]. In this thesis, membranes out of both anionic and cationic hydrogels are considered for the modelation of ionic hydrogels and their evaluation in the specific context of closed loop treatment of diabetes.

The hypothesis of this work is that hydrogel based systems with glucose sensitivity for insulin delivery can be modeled and evaluated by applying bio-chemical and mechanical principles, and implement an implicit controller closed loop system for the treatment of a diabetic patient.

The specific objectives of this thesis are the following:

1) Synthesize glucose sensitive as well as only pH sensitive hydrogels membranes based on P(MAA-g-EG).

2) Analyze the kinetic influence of synthesis parameters such as solvent content, type and length of crosslinking agent and inclusion of enzymes on the polymeric mesh size.

3) Characterize the equilibrium response of the fabricated hydrogels in solution at different pH and glucose concentration as well as the porosity in dry state.

4) Perform dynamic experiments to determine the swelling sensitivity and time constants.

5) Define a three dimensional mechanochemical compliance from swelling experiments.

6) Diagnose the formation of macropores by the sudden contraction of the fabricated anionic hydrogels.

7) Characterize a global kinetic constant for the enzymatic system incorporated in glucose sensitive hydrogels.

8) Calculate diffusivities of the solutes of interest (insulin, glucose, and hydrogen ions) through the synthesized hydrogel membranes.

9) Analize release profiles from insulin preloaded hydrogels before different initial glucose concentrations in a continuous dissolution system.

10) Determine the mechanical modulus of P(MAA-g-EG) hydrogel by tensile mechanical tests.

11) Extend the time-temperature superposition technique for the calculation of the one-dimensional mechanical compliance of hydrogels from swelling experiments, and perform specific calculations for P(MAA-g-EG) membranes.

12) Apply the one-dimensional and the three-dimensional mechanochemical compliances in the prediction of volume swelling ratio as a function of time.

13) Model the interaction of a glucose sensitive hydrogel with the diabetic physiological process by extending the multi-compartment model by Sorensen [7].

14) Simulate anionic and cationic hydrogels based on the experimental characterization of a reference material.

15) Explore optimal control design approaches to obtain an explicit robust controller using a single-compartment physiological model.

16) Apply the linear quadratic optimal theory using a linearized approximation of a high order non-linear physiological process [7], for the design of a controller that satisfies the essential double condition of achieving normoglycemia with the minimum amount of exogenous insulin to resemble a healthy pancreas.

17) Compare hydrogel and controller closed loop systems before a dietary regimen of three daily meals to conclude about the potential of the first type of systems.

**References**

1.  Peppas NA, Klier J. Controlled release by using poly(methacrylic acid-g-ethylene glycol) hydrogels. J Controlled Release. 1991;(16):203-214.

2.  Lowman AM, Peppas NA. Analysis of the complexation/decomplexation phenomena in graft copolymer networks. Macromolecules. 1997;30:4959-4965.

3.  Lowman AM and Peppas NA, Solute transport analysis in pH-responsive, complexing hydrogels of poly(methacrylic acid-g-ethylene glycol). J Biomater Sci, Polym Ed. 1999;10:999-1009.

4.  Lowman AM, Morishita M, Kajita M, Nagai T, Peppas NA. Oral delivery of insulin using pH-responsive complexation gels. J Pharm Sci. 1999;88:933-937.

5.  Peppas NA, Wood,KM, Blanchette JO. Hydrogels for oral delivery of therapeutic proteins. Expert Opinion On Biological Therapy. 2004;4(6):881–887.

6.  Podual K, Dolye FJ III, Peppas NA. Insulin release from pH sensitve cationic hydrogels. Proceed. Intern. Symp. Control. Rel. Biact. Mater. 1998;25:56-57.

7.  Sorensen J. A physiologic model of glucose metabolism in man and its use to design and assess improved insulin therapies for diabetes. PhD thesis. Dept. of Chemical Engineering, MIT, 1985.

## 4. Structure and Synthesis of Hydrogel-Based Systems

The hydrogel-based systems under study are membranes of poly(methacrylic acid-grafted-ethylene glycol) or poly(MAA-g-EG). Two types of membranes are fabricated: pH sensitive films and glucose and pH responsive films. The former systems serve as controls for the analysis of the behavior of the latter. The kinetics of the synthesis process determines the structural characteristics of the material, which are related to the mesh size of the polymeric matrix. The polymerization process for the elaboration of poly(MAA-g-EG) hydrogel membranes is explained here.

### 4.1. Reagents

The reagents used for the synthesis and the characterization of poly(MAA-g-EG) hydrogels are shown in Appendix A4.1. The monomer used was methacrylic acid (MAA) (Sigma-Aldrich, Milwaukee, WI). Poly(ethylene glycol) monomethylether monomethacrylate (PEGMMA, molecular weight 1000 g/mol) (Polysciences, Warrington, PA) gave stealth properties to the material and acts as stabilizer when enzymes are included. Two options were considered for use as crosslinking agent: tetraethyleneglycol-dimethacrylate (TEGDMA) (Sigma-Aldrich) and poly(ethylene glycol)-dimethacrylate (PEGDMA, molecular weight 1000 g/mol) (Polysciences, Warrington, PA). The chain length of the crosslinking agent determines the internal stress and affects the physical integrity of the hydrogel. Irgacure 186® (Sigma-Aldrich) was used as a photoinitiator for the free radical polymerization process.

The solvent for the reactants consisted of ethanol and water or ethanol and an enzyme solution; in both cases, the polar nature of the solvent allowed for the miscibility of the monomer, stabilizer, crosslinking agent and initiator. Hydrochloric acid 1 N (Fischer Scientific, Fair Lawn, NJ) was used to lower the pH of the reactive mixture to a value between 2 and 3. For a glucose sensitive hydrogel, glucose oxidase (Sigma-Aldrich) and catalase (Sigma-Aldrich) were mixed with a 50 mM sodium acetate buffer, and functionalized by the reaction with acryloyl chloride, as proposed in previous hydrogel preparations with these enzymes [1]. Phosphate and dimethyl glutaric acid biological buffers were used to study the behavior of the hydrogels.

### 4.2. Equipment

The experimental work was performed at the Laboratory of Biomaterials of the Department of Chemical Engineering at the University of Texas at Austin. The equipment required for the synthesis and the study of hydrogel-based systems serve purposes of fabrication, storage and analysis. The equipment for analysis is described in the chapters of experimental characterization.

The monomers were stored at 4°C in a refrigerator, and enzymes like glucose oxidase were stored at -20°C in a freezer. The reactants were carefully measured using an analytical balance with a resolution of $10^{-5}$ grams, and pipettes with resolution of 1

microliter and different ranges between 0 and 1 milliliter. A vortex system and a sonicator provided proper mixing of the reagents. A glove box allowed for a leak-tight environment for work in absence of oxygen. A UV lamp inside the glove box was installed to carry on photopolymerization. UV light intensity was verified with a radiometer-photometer in preparation for polymerization. Deionized water was produced with a Millipore system. A vacuum oven was used to dry the films. All these apparatus were operated in a laboratory equipped with glassware, water, air and vacuum lines, nitrogen tanks, fume hoods, special cabinets for flammables, showers, etc. under safety norms defined by the Occupational and Safety Health Administration (OSHA).

## 4.3. Procedures

The poly(MAA-g-EG) gel, henceforth designated as P(MAA-g-EG) hydrogel, was prepared from MAA and PEGMA-1000 with a 1:1 feed molar ratio of monomer repeating units, which corresponds to 23 methacrylic acid repeating units per graft of PEGMA-1000. TEGDMA or PEGDMA-1000 can be used as a crosslinking agent in 1 mol % of total monomer mixture. PEGDMA-1000 can reduce the stress in the molecular structure by giving more space between chains that are crosslinked. Irgacure 184 ® was added in 1 weight % of total monomer mixture to initiate photopolymerization. Equal volumes of ethanol and water were used as the solvent, and kept a 1:1 volume ratio with respect to the monomer mixture. The reactive mixture was purged with nitrogen and poured in a mold formed with glass slides separated by Teflon® spacers. UV light was applied in absence of oxygen for 30 min. The film formed was washed in deionized water for 7 days, and then cut into small discs for its characterization. The discs were dried at room temperature for 24 hours and then inside a vacuum oven at 60°C for 3 hours. The dried discs were stored in a desiccator for later use.

A glucose sensitive hydrogel was synthesized by substituting water by an enzyme solution of 380 units of glucose oxidase/mL in the previous preparation. The specification of 27000 glucose oxidase units per unit of MAA allowed for working with approximately the same volume proportions for the solvent than in the preparation without enzymes. Glucose oxidase (GOx) and catalase were used in a 1:6.39 units ratio (a unit of glucose oxidase oxidizes 1 $\mu$mol of $\beta$-D glucose to D-gluconolactone and hydrogen peroxide per minute at pH 5.1 at 35°C, and a unit of catalase corresponds to the amount of enzyme which decomposes 1 $\mu$mol of hydrogen peroxide per minute at pH 7 and 25°C). Catalase breaks the peroxide molecules, providing oxygen for the regeneration of glucose oxidase. The excess of catalase was intended to assure oxygen availability. The enzymes were dissolved in a pH 5.1 sodium acetate buffer, and acryl oil chloride was added for the functionalization reaction in an ice-water bath with continuous mixing. The functionalization of the enzyme adds double bonds ($CH_2=CH_2$-glucose oxidase) that allow a covalent attachment to the polymer structure (multiple double bonds may convert the enzyme in a type of crosslinking agent during the synthesis process). The enzyme solution could be stored in a refrigerator for a short period of time. Appendix A4.2 shows typical formulations of hydrogels. Appendix A4.3 lists the preparation steps for the polymer synthesis.

## 4.4. Polymerization Kinetics

The polymerization process consisted of a photoinitiated free radical chain mechanism. The theory of this mechanism explained by Odian in [2] is used to explain the particular reaction kinetics for the synthesized hydrogels. Adsorbed UV radiation decomposes the photosensitizer or initiator $I$ into two primary radicals $R$:

$$I \rightarrow 2R^{\cdot} \tag{1}$$

In the case of Irgacure 186®, the radicals may be produced by fragmentation and hydrogen abstraction [2]. A possible fragmentation of the Irgacure 184® ketone is described by:



$$\tag{2}$$
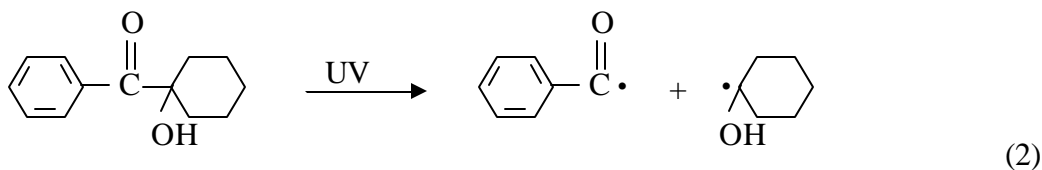
The ethanol present in the reaction solution can be a hydrogen donor for the hydrogen abstraction process:



$$\tag{3}$$
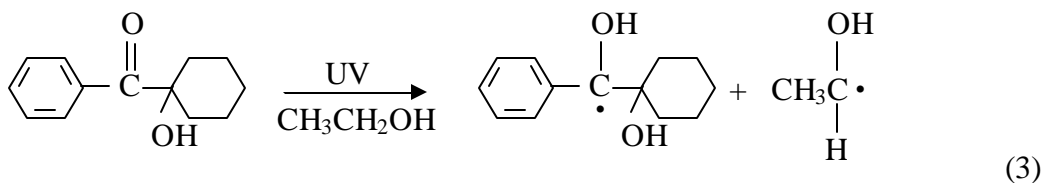
In both cases, the two radicals produced are different although equally represented by $R$.

The initialization includes the relatively fast addition of each primary radical to the first monomer unit M, according to the reaction [2]:

$$R^{\cdot} + M \rightarrow M_1^{\cdot} \tag{4}$$

The most probable structure of the initial propagating radical is formed by the attachment of the primary radical to carbon 2 of a 1-1 disubstituted monomer [2], such as methacrylic acid, for steric reasons:



$$\tag{5}$$
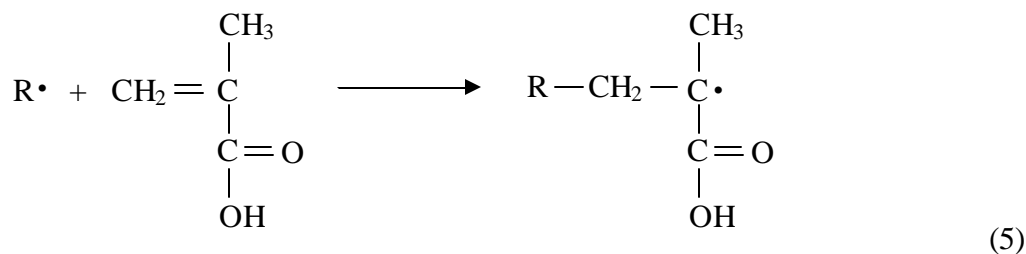
The active UV radiation that causes reaction (1) or absorbed radiation $I_{abs}$ is calculated by:

$$I_{abs} = \varepsilon I_0 [I] \frac{\lambda}{Nhc} 1000 \qquad (6)$$

where $I_{abs}$ is expressed in moles of photons per liter per second, $\varepsilon$ is the molar absorption coefficient (molar absorptivity) of the monomer in L/mol-cm, $I_0$ is the incident light intensity in W/cm$^2$, [I] is the concentration of the initiator or photosensitizer in mol/L, h is Planck's constant ($6.626 \times 10^{-34}$ J-s per photon), c is the light velocity (299.7925 m/s), $\lambda$ is the wavelength in m (365 nm), hc/$\lambda$ is the energy of a single photon, N is the Avogadro number ($6.022 \times 10^{23}$ photons/mol of photons) and the factor of 1000 converts cubic centimeters to liters [2].

The rate of initiation is determined by the dominant reaction (1). Assuming that both radicals initiate polymerization, the rate of initiation, $R_i$, is given by the rate of production of primary radicals:

$$R_i = \frac{d[M_1^{\bullet}]}{dt} = 2\left(-\frac{d[I]}{dt}\right) = 2 f I_{abs} \qquad (7)$$

where 2 is the stoichiometric coefficient that indicates that each mol of initiator contributes with two radicals, f is the quantum yield for initiation or number of pairs of chain radicals generated per mol of photons (quantum or Einstein of light) [2].

In the propagation stage of the polymerization process, chain radicals increase their size through successive monomer additions. A monomer is added by the formation of a bond with one electron from the double bond of the monomer and the odd electron of the radical. The unpaired electron in the place of the previous double bond is shifted to the end of the chain for the free radical attack of the next monomer unit [2]:

$$M_1^{\bullet} + M \rightarrow M_2^{\bullet}, \qquad (8a)$$

$$M_2^{\bullet} + M \rightarrow M_3^{\bullet}, ..., \qquad (8b)$$

$$M_{n-1}^{\bullet} + M \rightarrow M_n^{\bullet}. \qquad (8c)$$
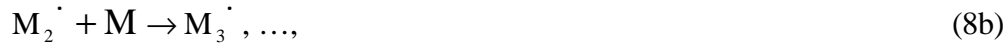
Successive additions of methacrylic acid units through the mechanism shown in equation (5), result in a head-to-tail structure for the propagating chains [2]. The chain radical with k+1 monomer units (where k is even) would be:

$$R \left[ CH_2 - \underset{\underset{OH}{\overset{|}{\underset{C=O}{\overset{|}{C}}}}}{\overset{CH_3}{\overset{|}{C}}} \underset{}{\overset{tail}{-}} CH_2 - \underset{\underset{OH}{\overset{|}{\underset{C=O}{\overset{|}{C}}}}}{\overset{CH_3}{\overset{|}{C}}} \right]_{k/2} CH_2 - \underset{\underset{OH}{\overset{|}{\underset{C=O}{\overset{|}{C}}}}}{\overset{CH_3}{\overset{|}{C}}} \cdot \qquad (9)$$
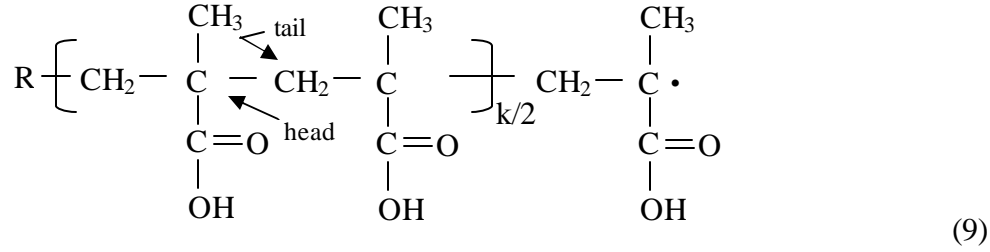
The rate of propagation is the sum of the rate of decrement of monomer concentration in all propagation reactions taking place simultaneously. Under the assumptions of a single propagation constant and equal reactivity for all the chain radicals regardless of their size, the rate of propagation also designated as the rate of polymerization *Rp* is [2]:

$$R_p = k_p [M_1^{\bullet}][M] + k_p [M_2^{\bullet}][M] + ... + k_p [M_{n-1}^{\bullet}][M], \qquad (10a)$$

$$R_p = k_p \left( [M_1^{\bullet}] + [M_2^{\bullet}] + ... + [M_{n-1}^{\bullet}] \right)[M], \qquad (10b)$$

$$R_p = k_p [M^{\bullet}][M], \qquad (10c)$$

where $[M^{\bullet}]$ is the total chain radical concentration.

The process is terminated either by combination of two chain radicals in a single polymer molecule or by disproportionation or transfer of a hydrogen atom resulting in two polymer molecules, one saturated and one unsaturated [2]:

$$M_n^{\bullet} + M_m^{\bullet} \xrightarrow{k_{tc}} M_{n+m}, \qquad (11a)$$

$$M_n^{\bullet} + M_m^{\bullet} \xrightarrow{k_{td}} M_n + M_m, \qquad (11b)$$

where $k_{tc}$ and $k_{td}$ are the termination rate constants for the combination and the disproportionation processes respectively.

The termination reaction has a second order dynamics, regardless of the mechanism [2]:

$$R_{tc} = -\frac{d[M^{\bullet}]}{dt}\bigg|_{tc} = 2\frac{d[M_{n+m}]}{dt} = 2k_{tc}[M^{\bullet}]^2, \qquad (12a)$$

$$R_{td} = -\frac{d[M^{\bullet}]}{dt}\bigg|_{td} = 2\frac{d[M_n]}{dt} = 2\frac{d[M_m]}{dt} = 2k_{td}[M^{\bullet}]^2, \qquad (12b)$$

$$R_t = R_{tc} + R_{td} = 2(k_{tc} + k_{td})[M^{\bullet}]^2 = 2k_t[M^{\bullet}]^2, \qquad (12c)$$

where the factor 2 accounts for the elimination of two chain radicals per termination event.

In order to express the rate of polymerization in terms of concentration of stable species, the steady-state assumption is made by writing [2]:

$$R_t = R_i, \tag{13a}$$

$$[M\cdot] = \left(\frac{f\,I_{abs}}{k_t}\right)^{1/2}, \tag{13b}$$

$$R_p = k_p[M]\left(\frac{f\,I_{abs}}{k_t}\right)^{1/2}. \tag{13c}$$

From the propagation rate and the termination rate (or initiation rate because of equation 13a), the kinetic chain length or average number of monomer units per radical, $\nu$, can be determined [2]:

$$\upsilon = \frac{R_p}{R_i} = \frac{k_p[M]}{2(fk_t\,I_{abs})^{1/2}}. \tag{14}$$

The average number of monomer units in a polymer molecule or number average degree of polymerization when the growth of the chains stops by combination is two times the kinetic chain length [2]. Termination by combination for the polymerization of methacrylic acid would produce the following macromolecule by overcoming hindering steric conditions:



(15)
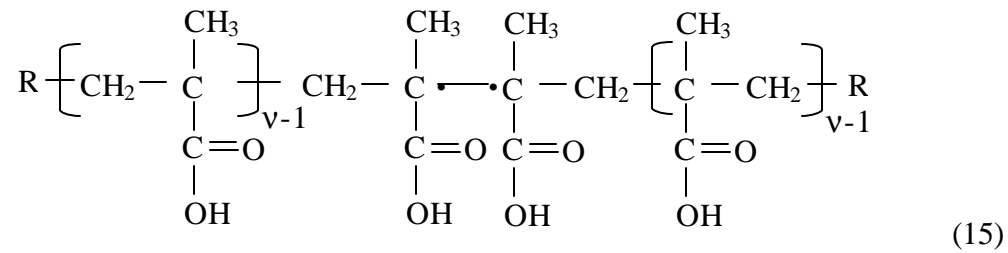
Even when the combination mechanism is more frequent than disproportionation, the latter may account for a significant number of termination events, specially at high temperatures, as more hydrogens (in the beta position with respect to the radical center) for transfer are available and there is a greater steric hindrance for the combination of two radical chains. Disproportionation produces the two poly(methacrylic acid) molecules [2] as indicated by the following equation:

$$(16)$$
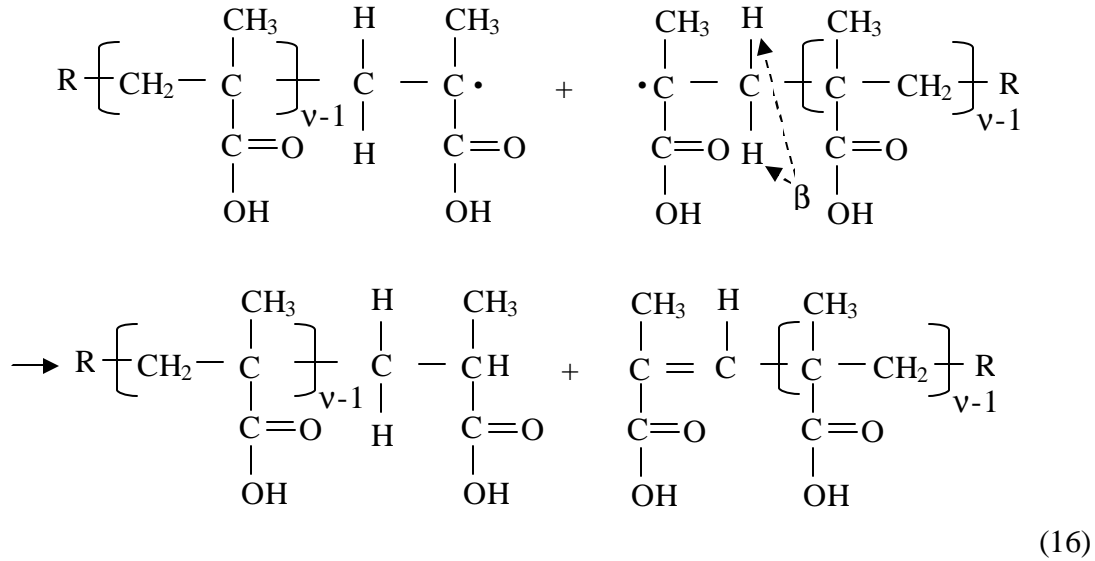
The conditions of the particular polymerization system under study make disproportionation a possible mechanism and maybe the main termination process. However, the number average degree of polymerization is estimated considering both termination processes as equally probable:

$$\overline{X}_n = \frac{1}{2}(\upsilon + 2\upsilon) = \frac{0.75 k_p [M]}{(f k_t I_{abs})^{1/2}}. \qquad (17)$$

The average molecular weight $\overline{M}_n$ of the uncrosslinked polymer can be calculated as:

$$\overline{M}_n = M_0 \overline{X}_n, \qquad (18)$$

where $M_0$ is the molecular weight of the monomer.

The polymerization carried out with a crosslinking agent, such as tetraethylene glycol dimethacrylate, produces a molecular mesh structure. Additionally, the presence of poly(ethylene glycol) (1000) monomethyl ether monomethacrylate produces grafts that produce entanglements through hydrogen bonds and give stealth properties to the material [3]. Figure 4.1 shows the structure of a P(MAA-g-EG) hydrogel.

The molecular weight between crosslinks can be estimated with the Peppas-Merril equation [4]:

$$\frac{1}{\overline{M}_c} = \frac{2}{\overline{M}_n} - \frac{\frac{V}{V_1}\left[ln\left(1-\upsilon_{2,s}\right)+\upsilon_{2,s}+\chi_1\upsilon_{2,s}^2\right]}{\upsilon_{2,r}\left[\left(\frac{\upsilon_{2,s}}{\upsilon_{2,r}}\right)^{1/3}-0.5\left(\frac{\upsilon_{2,s}}{\upsilon_{2,r}}\right)\right]}, \tag{19}$$

where $\overline{M}_c$ is the average molecular weight between crosslinks, $V$ is the specific volume of the polymer, $V_1$ is the molar volume of the swelling agent, $\upsilon_{2,s}$ is the volume fraction of the polymer in the swollen state, $\upsilon_{2,r}$ is the volume fraction of the polymer in the relaxed state after synthesis, and $\chi_1$ is the Flory polymer-solvent interaction parameter.

The polymer volume fractions for the Peppas-Merrill equation are calculated as the inverse of the volume swelling ratio or the volume of the pure polymer over the volume of the swollen polymer which results from the absorption of solvent either in the synthesis process (relaxed state) or in a different medium (swollen state), typically after a preparatory drying for storage.

The average length between crosslinks or mesh size, $\xi$, is calculated by:

$$\xi = l\left(\upsilon_{2,s}\right)^{-1/3}\sqrt{\frac{2\overline{M}_c C_n}{M_0}}, \tag{20}$$

where $l$ is the bond length along the polymer chain (1.54Å for carbon-carbon bonds) and $C_n$ is the characteristic ratio of the polymer [4]. Although the reaction really consists of a copolymerization process due to the presence of the crosslinking agent, the consideration of the polymerization kinetics may be appropriate since the concentration of the crosslinking agent is generally low. The grafts of poly(ethylene glycol) affect the properties of the material, therefore the $C_n$ and $\chi_1$ parameters of the hydrogel are assigned the mean values of those for poly(ethylene glycol) and poly(methacrylic acid). Table 4.1 contains the parameters used for mesh size calculations.

## 4.5. Results

Synthesis procedures were modified with the type of crosslinking agent, the excess of solvent and the presence of enzymes. The mesh size is determined for each synthesis variation. Table 4.2 lists the calculated values for the mesh size of the membranes synthesized under different conditions.

The excess of solvent is considered with respect to the water absorbed at equilibrium at the pH of the reaction mixture. The procedure to obtain excess of solvent consisted in the correction of the pH of the reaction mixture without modifying the amount of solvent (water, ethanol or enzyme solution). According the hydrogel formulations (Appendix A4.2), the volume fraction of the solvent in the reaction mixture is around 0.5.

The pH was adjusted to an approximate value of 3; under this pH, the P(MAA-g-EG) hydrogel contracts and, therefore, the volume fraction of the solution absorbed reduces significantly below 0.5. Therefore, the addition of microliters of hydrochloric acid achieved the excess of solvent without diluting the reaction mixture. Precise excess of solvent is evaluated after equilibrium experiments with the synthesized hydrogel materials (Section 5.1).

Volume fractions of the swollen polymer are obtained from equilibrium swelling experiments from Section 5.1. The volume fractions used in mesh size calculations are considered at 37°C and two different pH values: 3.2 and 7. These pH values define the range of interest, from an acid pH that can be produced by the enzymatic oxidation of glucose to the neutral pH of physiological fluids that would interact with an implanted hydrogel-based system.

## 4.6. Discussion

The longer crosslinking agent and the excess of solvent content of the reaction mixture are expected to increase the water absorption capability of the hydrogel by producing a higher mesh size. Calculations for synthesis 1 and 2 (Table 4.2) give a bigger mesh size for samples at pH of 7, when the pH of the reactive mixture is corrected to produce excess of solvent. Comparison of synthesis 2 and 4 do not give a significant evidence of the effect of the length of the crosslinking agent, possibly because its molar concentration was the same in both cases and the distribution of crosslinking points along linear polymerization chains may not have been affected. A bigger mesh size might result from a lower crosslinking agent concentration. However, the crosslinking agent was added in small amounts, and a lower concentration may have failed to produce the hydrogel film. Although no hydrochloric acid was added in synthesis 3, the pH of the reaction mixture may have been lower than in synthesis 4, because of the acidity of the enzyme solution, which can explain the higher mesh size estimation.

The equilibrium mesh size at a pH of 3.2 describes the openings of the polymeric network after synthesis. At a pH of 7, the mesh opening is characterized under close physiological conditions. At the pH chosen to load a hydrogel sample with insulin, the equilibrium mesh opening is useful for the comparison with the hydrodynamic diameter of insulin, in order to verify if a diffusion loading process is possible (the insulin loading procedure is discussed in Section 6.5.1). For instance, the mesh size of a P(MAA-g-EG) hydrogel sample produced according to the synthesis procedure 1 (127 Å) at a pH of 5 is 8 times the hydrodynamic radius of insulin (16 Å), just below the pH-volume transition point. At a pH of 3.2, the mesh size is 0.4 times the hydrodynamic radius of insulin, which would prevent insulin diffusion, while at a pH of 7 the mesh size is 24 times the hydrodynamic radius of insulin, which would favor insulin transport sterically (from the electrostatic point of view, insulin release would be promoted, but no insulin loading; see discussion of isoelectric point of insulin effect in loading process in Section 6.5.1).

## 4.7. Conclusions

Synthesis conditions produce hydrogel materials with different mesh sizes. Particularly, the solvent volume fraction in the relaxed state is used to affect the opening size of the crosslinked polymer. The analysis of the resultant mesh size provides a reference to determine if a certain species can be transported across the hydrogel membrane.

The synthesis proceeds with an excess of solvent when the volume fraction of solvent in the reactive mixture is higher than the solvent volume fraction at equilibrium, at the pH of the reactive mixture. The excess of solvent is caused by lowering the pH of the reactive mixture instead of increasing the amount of solvent in the formulation of the hydrogel.

The synthesis procedures of P(MAA-g-EG) lead to a molecular structure that can open and close the space for insulin transport as pH is changed from 3.2 to 7. Higher excess of solvent in the reaction mixture produces a more open polymeric mesh. Other synthesis specifications can relate to the mesh size by the polymerization kinetics model and the Peppas-Merrill equation. The Peppas-Merrill equation considers also the operation conditions, by the solvent volume fraction in the swollen state, for the estimation of the mesh size.

**Figure 4.1. Polymerization Reaction for the Production of P(MAA-g-EG) Hydrogel.**
The reactants include Irgacure 184® photoinitiator, methacrylic acid monomer (MAA), tetraethylene glycol dimethacrylate (TEGDMA) crosslinking agent and poly(ethylene glycol) (1000) monomethyl ether monomethacrylate (PEGMMA). The resultant structure shows crosslinking segments, grafts and entanglements.

**Table 4.1. Parameters for the Estimation of the Mesh Size of Poly(MAA-g-EG) Hydrogel Network.**

| Parameter | Value |
|---|---|
| Molar volume of swelling agent, $V_1$, [5] | 18 mL/mol |
| Density of water, $\rho$(water), [5] | 1 g/mL |
| Density of ethanol, $\rho$(ethanol), [5] | 0.789 g/mL |
| Density of PMAA, $\rho$(PMAA), [6] | 1.0153 g/mL |
| Density of PEG, $\rho$(PEG), [6] | 1.1135 g/mL |
| Density of heptane, $\rho(C_7H_{16})$, [5] | 0.6837 g/mL |
| PMAA-solvent interaction parameter, $\chi_1$(PMAA), [7] | 0.5987 |
| PEG-solvent interaction parameter, $\chi_1$(PEG), [7] | 0.55 |
| Characteristic ratio of PMAA, Cn(PMAA), [6] | 14.6 |
| Characteristic ratio of PEG, Cn(PEG), [6] | 3.8 |
| Molecular weight of MAA repeating unit, $M_0$, [6] | 86 g/mol |
| Concentration of monomer, [M] | 3.574 mol/L |
| Concentration of Irgacure 184 photosensitizer, [I] | 0.0257 mol/L |
| Initiator efficiency, f | 0.5 |
| Molar absorption coefficient of Irgacure 184 at 365 nm, $\varepsilon$, [8] | 10 L/mol·cm |
| Propagation rate constant of MAA chain radicals, $k_p$, [7] | 670 L/mol·s |
| Termination rate constant of MAA polymerization, $k_t$, [7] | $2.1\times10^6$ L/mol·s |

**Table 4.2. Mesh Size of Hydrogel Membranes Synthesized with Procedure Variations.** The solvent may consist of a mixture of ethanol and water (no enzymes incorporated) or ethanol and enzyme solution. The pH of the reaction mixture can be adjusted to a value of 3 to create excess of solvent with respect to the solution imbibed of the hydrogel material at the same pH. TEGDMA and PEGDMA-1000 are used as crosslinking agents.

| Synthesis procedure | Description | pH | Mesh size (Å) |
|---|---|---|---|
| Synthesis 1 | No enzymes incorporated, no pH correction, TEGDMA crosslinking agent. | 3.2 | 6 |
| | | 7 | 393 |
| Synthesis 2 | No enzymes incorporated, pH correction, TEGDMA crosslinking agent. | 3.2 | 3 |
| | | 7 | 450 |
| Synthesis 3 | Enzymes incorporated, no pH correction, PEGDMA-1000 crosslinking agent. | 3.2 | 4 |
| | | 7 | 524 |
| Synthesis 4 | No enzymes incorporated, pH correction, PEGDMA-1000 crosslinking agent. | 3.2 | 5 |
| | | 7 | 459 |

## References

1. Podual K, Doyle III FJ, Peppas NA. Preparation and dynamic response of cationic copolymer hydrogels containing glucose oxidase. Polymer. 2000;41:3975–3983.

2. Odian G. Principles of polymerization (3rd edition). New York: John Wiley and Sons, Inc., 2004.

3. Hoffman AS. Applications of smart polymers as biomaterials. In: Ratner BD, Hoffman AS, Schoen FJ, Lemons JE. Biomaterials Science (2nd edition). California: Elsevier Academic Press, 2004:107-115.

4. Peppas NA, Barr-Howell BD. Characterization of crosslinked structure of hydrogels. In: Peppas NA. Hydrogels in medicine and pharmacy. Boca Raton: CRC Press, 1986;1:28-55.

5. Perry RH, Green DW, Maloney JO. Perry's Chemical Engineers' Handbook (6th edition). New York: McGraw Hill, 1984.

6. Brandrup J, Immergut EH. Polymer handbook (3rd edition). New York: John Wiley & Sons, Inc., 1989.

7. Barton AFM. CRC handbook of polymer-solvent interaction parameters (1st edition). Ann Arbor, MI: CRC Press, 1990.

8. Bryant SJ, Nuttelman CR, Anseth KS. Cytocompatibility of UV and visible light photoinitiating systems on cultured NIH/3T3 fibroblasts. J Biomat Sci.-Polym E. 2000;11:439-457.

**Appendix A4.1. Reagents for Synthesis and Characterization of Hydrogel-Based Systems.**

| Reagent | Chemical name | Chemical formula | CAS number | Molecular weight | Density g/cm$^3$ | NFPA 704 |
|---|---|---|---|---|---|---|
| Methacrylic acid (Sigma-Aldrich, Milwaukee, WI) | 2-methyl-2-propenoic acid | CH3C=CH2COOH | 79-41-4 | 86.06 | 1.015 | (red 2, blue 3, yellow 2) |
| PEGMMA 1000 (Polysciences, Warrington, PA) | Poly(ethylene glycol) (1000) monomethyl ether monomethacrylate | $CH_3C=CH_2CO-(OCH_2CH_2)_nOCH_3$, n=23 | 26915-72-0 | (44)1000+100 | 1.1135 | |
| TEGDMA (Sigma-Aldrich, Milwaukee, WI) | Tetraethylene glycol-dimethacrylate | $O[CH_2CH_2OCH_2CH_2OCOC(CH_3)=CH_2]_2$ | 109-17-1 | 330.37 | 1.082 | |
| PEGDMA 1000 | Poly(ethylene glycol) dimethacrylate | $CH_2=CCH_3CO(OCH_2CH_2)nOCOCH_3C=CH2$ | 25852-47-5 | | | |
| Irgacure 184 (Sigma-Aldrich, Milwaukee, WI) | 1-hydroxycyclohexyl phenyl ketone | $HOC_6H_{10}COC_6H_5$ | 947-19-3 | 204.26 | 1.1 | |
| Ethanol (Fischer Scientific, Fair Lawn, NJ ) | Ethyl alcohol | $CH_3CH_2OH$ | 64-17-5 | 46.07 | 0.789 | (red 3, blue 0, yellow 0) |
| Water | Hydrogen hydroxyde | $H_2O$ | | 18.02 | 1 | |
| Chlorhydric acid | | HCl | | | | |
| Glucose oxidase from Aspergillus niger (Sigma-Aldrich, Milwaukee, WI) | β-D-glucose:oxygen 1-oxidoreductase | | 9001-37-0 EC 1.1.3.4 | 160 kDa or kg/mol | | |

**Appendix A4.1. Reagents for Synthesis and Characterization of Hydrogel-Based Systems. Continuation.**

| Reagent | Chemical name | Chemical formula | CAS number | Molecular weight | Density g/cm$^3$ | NFPA 704 |
|---|---|---|---|---|---|---|
| Catalase from Aspergillus niger (Sigma-Aldrich, Milwaukee, WI) | hydrogen-peroxide:hydrogen-peroxide oxidoreductase | | 9001-05-2<br><br>EC 1.11.1.6 | 385 kDa or kg/mol | | |
| Acryloyl chloride | 2-propenoyl chloride | CH2=CHCOCl | 814-68-6 | 90.51 | 1.119 | |
| Sodium acetate, trihydrate (Sigma-Aldrich, Milwaukee, WI) | Acetic acid sodium salt, trihydrate | $CH_3COONa \cdot 3H_2O$ | 6131-90-4 | 136.08 | | |
| ββ–dimethylglutaric acid (Flucka, Sigma-Aldrich, Milwaukee, WI) | Glutaric acid dimethyl ester<br><br>Dimethyl glutarate | $CH_3OCO(CH_2)_3COOCH_3$ | 1119-40-0 | 160.17 | | |
| Sodium hydroxide 1N (Fischer Scientific, Fair Lawn, NJ ) | | 1N NaOH | 1310-73-2 | | | |
| Sodium chloride (Fischer Scientific, Fair Lawn, NJ ) | Sodium chloride | NaCl | 7647-14-5 | 58.43 | | |
| Dextrose (Sigma-Aldrich, Milwaukee, WI) | 6-(hydroxymethyl)oxane-2,3,4,5-tetrol<br><br>D-glucose | $C_6H_{12}O_6$ | 50-99-7 | 180.16 | | |
| Insulin from bovine pancreas (Sigma-Aldrich, Milwaukee, WI) | | | | 5808 | | |

Note. The table includes basic data of the chemicals like the common name for the localization of the corresponding material safety data sheet (MSDS), the Chemical Abstracts Service (CAS) register number that identifies the compound, and the fire diamond according to the standard 704 by the US National Fire Protection Agency (NFPA). The NFPA 704 indicates the level of health hazard (blue), flammability (red), reactivity (yellow) and particular risks (white) of the chemicals in the scale from 0 (no risk or normal) to 4 (severe risk).

## Appendix A4.2.  Polymer Formulations

Solvent volume fraction in all formulations is 50% approximately.

### Formulation 1.  Tetraethylene glycol dimethacrylate as crosslinking agent

| Reagent | Amount |
|---|---|
| MAA | 0.971g |
| PEGMMA-1000 | 0.54 g |
| TEGDMA | 0.039 g |
| Irgacure 184 ® | 0.015 g |
| Water | 0.756 g |
| Ethanol | 0.958 g |
| HCl 1N | 10 to 20 µL, to adjust pH 2.5 |

### Formulation 2.  Tetraethylene glycol dimethacrylate as crosslinking agent and incorporation of enzymes

| Reagent | Amount |
|---|---|
| MAA | 0.971 g |
| PEGMMA-1000 | 0.54 g |
| TEGDMA | 0.039 g |
| Irgacure 184 ® | 0.015 g |
| Enzyme solution | 0.805 g |
| Ethanol | 0.706 g |
| HCl 1N | 10 to 20 µL to adjust pH 2.5 |

Enzyme solution

| Reagent | Amount |
|---|---|
| 50mM sodium acetate buffer , pH 5.1 | 5 mL |
| Glucose oxidase 146000 units/gram | 0.013 g |
| Catalase | 175 µL |
| Acryloyl chloride | 3  µL |

### Formulation 3.  Poly(ethylene glycol) dimethacrylate as crosslinking agent

| Reagent | Amount |
|---|---|
| MAA | 0.971 g |
| PEGMMA-1000 | 0.54 g |
| PEGDMA-1000 | 0.136 g |
| Irgacure 184 ® | 0.015 g |
| Water | 0.787 g |
| Ethanol | 0.992 g |
| HCl 1N | 10 to 20 µL to adjust pH 2.5 |

**Formulation 4.** **Poly(ethylene glycol) dimethacrylate as crosslinking agent and incorporation of enzymes**

| Reagent | Amount |
|---|---|
| MAA | 0.971 g |
| PEGMMA-1000 | 0.54 g |
| PEGDMA-1000 | 0.136 g |
| Irgacure 184 ® | 0.015 g |
| Enzyme solution | 0.805  g |
| Ethanol | 0.964 g |
| HCl 1N | 10 to 20 μL to adjust pH 2.5 |

## Appendix A4.3.  Protocol for Synthesis of P(MAA-g-EG) Films

1.  Remove hydroquinone (HQ) inhibitor from MAA using a 9×0.8 in prepacked column (Sigma-Aldrich, Milwaukee, WI).

    Prepare the set up shown in the figure inside a fume hood.  Turn the lamps off inside the hood to protect the monomer from the light.

    Pour the received monomer through a packed colum and colect the purified monomer with the ambar bottle in the ice bath.

    Store the purified MAA in the refrigerator.
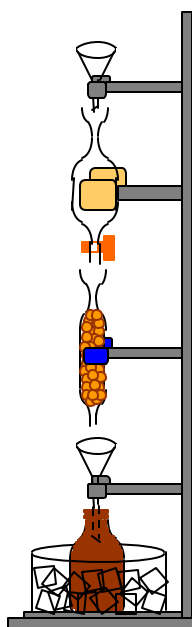


**Figure A4.3.1. Inhibitor removal from MAA using a packed column.**

2.  Prepare enzyme solution to elaborate glucose sensitive  hydrogel.

    Set up an ice bath on a stirrer plate inside the hood (light off).  Place a conical flask with 50 mM acetate buffer and a magnetic stir bar inside the ice bath.

    Add the glucose oxidase to the conical flask.

    Use argon or nitrogen to purge the bottle of the catalase, and pull the enzyme with a syringe.  Remove the purge from the bottle and cover the mouth of the bottle with wrapping film. Add the catalase to the conical flask (push and pull the syringe several times with the solution to wash away the catalase from the syringe and make sure that all the catalase is discharged to the flask).

    Add acryloyl chloride and let the mixture react for 1 hour.

Store the enzyme solution in the refrigerator for later use (in the next 24 hours).
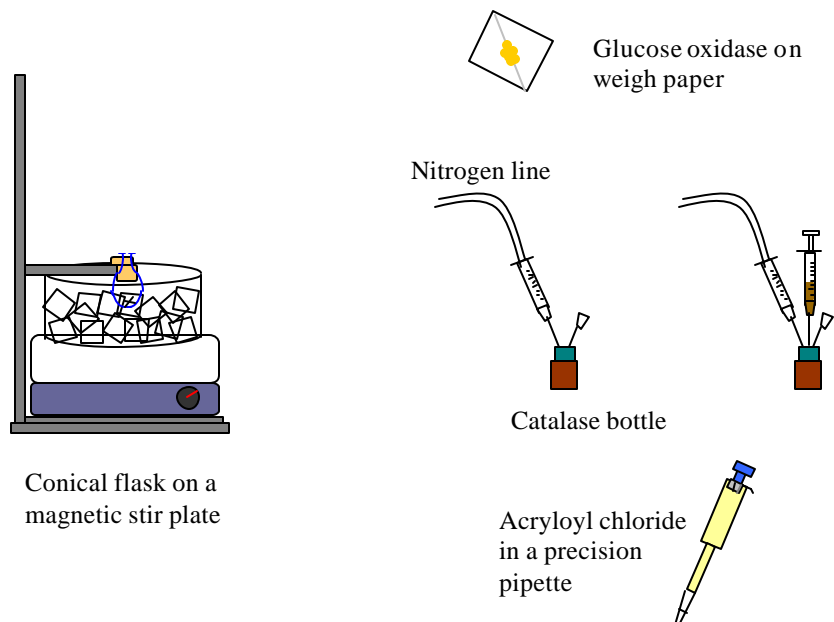


**Figure A4.3.2. Preparation of enzyme solution.** Ice bath (left) and handling of main components (right).

3.  Add components of polymerization solution in a small amber bottle. Add water or the enzyme solution and ethanol first, monomers next (MAA, PEGMMA-1000 and crosslinker), and initiator last.

4.  Cover mouth of the amber bottle with wrapping film and mix the mixture for 15 minutes with a sonicator (make sure to dissolve solid components).

5.  Prepare glass slides for casting the film. Wash the glass slides with water and soap, ethanol and acetone, (rinse with water after applying each solvent). Sigmacote ® (Sigma-Aldrich, Saint Louis, MI) can be used to ease the separation of the film. Apply a few drops of Sigmacote ® on one side of the glass slides and distribute the liquid by sliding one wet glass surface over the other, let them dry and rub them with a tissue. Place a 0.7 mm Teflon spacer between the two slides (the interior surfaces may be pretreated with Sigmacote ®) to form a "pocket" to hold the mixture. Secure the glass slides and spacer in position with binder clips.

6.  Prepare the glove box for UV polymerization.

    Turn on the UV lamp inside the glove box, measure and adjust the UV light intensity between 16 and 17 mW/cm$^2$.

Verify the output of the glove box to be directed to the hood. Attach a glass Pasteur pipette to the nitrogen line inside the glove box for purging the solution.

Introduce the glass assembly and two glass Pasteur pipettes with dropper bulbs. Fix the bottle with the reactive mixture and stick the pipette for purging.

7.  Close the glove box, open the nitrogen tank and adjust a pressure of 15 psi to purge the glove box for 45 minutes.

8.  Open the valve to purge the solution and let nitrogen bubble vigorously to remove dissolved oxygen for 20 minutes.

9.  Use the gloves to remove the purge pipette from the bottle. Use one of the pipettes with bulbs to drop the solution between the glass slides.

10.  Place the glass assembly with the solution below the UV lamp and apply UV light for 30 minutes.

11. Close the nitrogen tank and remove the glass slides from the glove box. Peel the film from the glass slides and put it into 1 L jar of deionized water. If the film contains enzymes, store the jar in the refrigerator. Change the water two or three times daily to remove unreacted components.
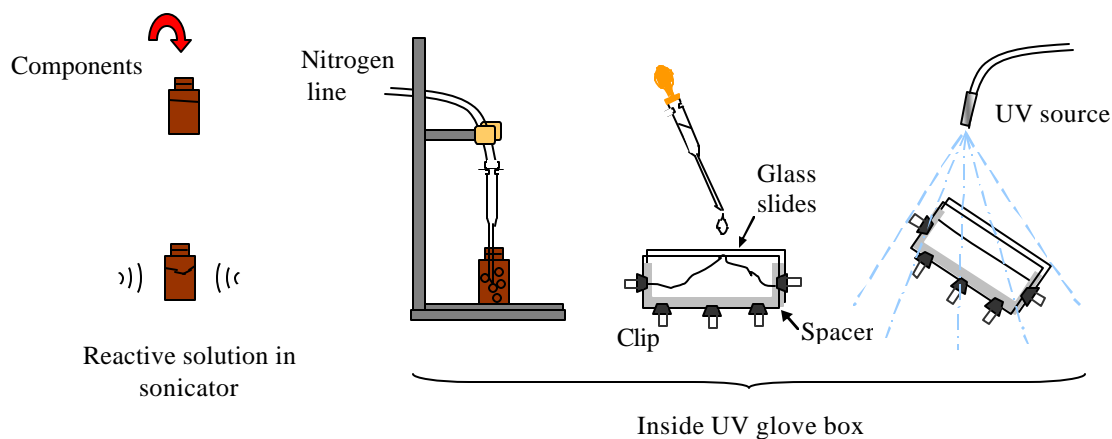


**Figure A4.3.3.  UV polymerization.**  A homogeneous mixture of reactive components is prepared (left).  Inside a glove box (right), the oxygen is displaced from the environment and from the solution by nitrogen, the solution is cast in a glass assembly and the UV polymerization reaction takes place.

## 5. Static Characterization

Steady state response of P(MAA-g-EG) hydrogels was determined under different environmental conditions. The fundamental pH sensitivity was tested by determining the final volume of samples immersed in different pH buffers. The porosity of the dry samples is analyzed to corroborate the effect of specific synthesis parameters. Solutions with different glucose concentration were used to inspect glucose sensitivity of hydrogels containing a reactive enzymatic system.

In addition to the modification of the testing environment of the hydrogel samples, the synthesis of the materials was varied by the use of excess solvent or adjustment of the pH of the reactive mixture, the length of the crosslinking agent and the presence of enzymes. All these parameters were studied and compared with equilibrium swelling experiments at different pH and porosimetry studies of dry samples. Equilibrium glucose response was obtained from samples with the same particular formulation.

## 5.1. Equilibrium pH Responsive Swelling

## 5.1.1. Fundamentals

Ionic hydrogel materials essentially respond to pH changes of the environment. In order to determine the maximum degree of swelling of the hydrogel at different pH values, equilibrium must be achieved chemically and mechanically. Chemical species are distributed according to their permeability through the hydrogel-solution interface. Internal stress forces must also stabilize to achieve the final deformation of the sample.

Two quantities are defined to describe the size change of a hydrogel under a particular environmental condition: volume swelling ration, Q, and weight swelling ratio, q, given by:

$$Q = \frac{V_s}{V_d}, \tag{1}$$

$$q = \frac{W_s}{W_d}, \tag{2}$$

where V and W are the volume and the weight of the sample, and the suffixes s and d denote the swollen and the dry state, respectively [1].

The volume swelling ratio, Q, is preferred for theoretical calculations of diffusivity coefficients and mesh size [1]. For such calculations, it is useful to express the volume fraction of the solvent, $\upsilon_1$, which can be derived from Q in the following way:

$$\upsilon_1 = 1 - \frac{1}{Q}. \tag{3}$$

By comparing the swelling ratio, either in terms of volume, weight or volume fraction of solvent, it is possible to determine a critical pH for the material, which

corresponds to a characteristic value for the transition between low and high degrees of swelling.

Analytically, the equilibrium behavior of swelling ratio with respect to pH is described by a hyperbolic tangential function with constant parameters a, b, c and d:

$$Q = a + b\,tanh\big(c(pH) + d\big), \tag{4}$$

and the critical pH can be calculated as the inflection point of the curve.

### 5.1.2. Experimental Procedure

The use of analytical balance may be the most convenient way to determine the size of a hydrogel disc sample (in comparison with measuring length dimensions) because the manipulation of the sample is minimum and the measurement is direct and highly differentiated due to the resolution of the instrument. The weight swelling ration is then the most practical parameter to obtain experimentally. However, the volume swelling ration can also be calculated from analytical balance measurements.

In the Laboratory of Biomaterials, a balance with an appropriate set up (Appendix A5.1) to apply Archimedes principle was used to determine volumes and volume swelling ratios. Through the determination of the weight of the sample in air, $W_a$, and in heptanes, $W_h$, the volume of the sample, V, is calculated as:

$$V = \frac{1}{\rho_h}(W_a - W_h), \tag{5}$$

where $\rho_h$ is the densitiy of heptane. The volume swelling ratio is obtained from the measurements in the swollen (suffix s) and dry state (suffix d):

$$Q = \frac{W_{a,s} - W_{h,s}}{W_{a,d} - W_{h,d}}. \tag{6}$$

Basic physiological conditions were reproduced to perform the experiments such as ionic concentration and temperature. Dimethyl glutaric acid buffers were prepared for different pH values with a molar strength of 0.1 M [2]. These solutions are standards for biological systems in a wide pH range and their preparation is indicated in Appendix A5.2. The closed flasks containing the hydrogel sample in solution were placed in a water bath where the temperature was kept constant at the body temperature of 37°C.

The experimental procedure to obtain the equilibrium response of the hydrogel consisted in identifying the samples to expose at each pH, weighing the dry samples (both in air and in heptane), introducing the samples into 50 mL of buffer solutions with different pH values, and weighing the swollen samples after 24 hours of immersion at 37°C. The swollen samples were handled with blunt forceps to avoid a fracture, blotted with a delicate task tissue to eliminate excess of solution, and weighed immediately after blotting to reduce evaporation (Appendix 5.3). An alternative experiment was performed by subjecting a single hydrogel sample to a sequence of pH changes (this experiment is described in detail

in Chapter 6). The steady state volume-pH points generated equilibrium information influenced by the history of the material.

### 5.1.3. Results and Discussion

Equilibrium experiments performed for hydrogels synthesized with variations in the proportion of solvent, length of crosslinking agent and content of enzymes are presented in Figures 5.1 and 5.2. The solvent in the synthesis of the hydrogel was in excess when the reactive mixture contained a higher proportion of solvent than the swollen material at equilibrium. A correction of the pH of the reactive mixture is a better practice to produce an excess of solvent than increasing the amount of solvent in the formulation. The crosslinking agents differed in the number of ethylene glycol units (4 in TEGDMA or 23 in PEGMMA-1000). The synthesis of the gels was done with and without enzymes in the solvent. Tables 5.1 and 5.2 summarize synthesis conditions, parameters of the swelling ratio function and critical pH values.

The hydrogel samples in the collapsed state had a volume swelling ratio of 1.5. At high pH, the samples reached a volume swelling ration between 15 and 25 (Figure 1). In synthesis 3, the use of the enzyme solution itself decreased slightly the pH of the reactive mixture resulting in a high proportion of solvent, but only similar to the volume fraction at equilibrium (Table 5.1). When the hydrogel was synthesized with TEGDMA as a crosslinking agent and excess of solvent, the material showed less swelling at high pH, as noticed from curves for synthesis 1 and 2. The solvent may participate in the polymerization reaction either growing or terminating chains [3]. The excess of solvent may have hindered the crosslinking of the monomer allowing for more space between equally charged groups (in a loose network) and decreasing the stretching electrostatic repulsive forces that caused the volume change of the sample [4, 5]. The opposite occurred when PEGDMA 1000 was used in synthesis 3 and 4, possible because the greater length of the crosslinking agent may have acted as a higher resistance against the action of repulsive forces, and been dominant over the latter.

During the experimental work, samples equilibrated at a relatively high pH fractured. Although the differences in these pH values are small (Table 5.1), they distinguish the integrity of the films: the lower the pH of fracture, the more fragile the material. The use of solvent in excess and a short crosslinking agent seems to make the hydrogel discs more difficult to fracture and easier to handle.

It can be observed that at low pH, the volume swelling ratio was the same for the four synthesis cases, but not the solvent volume fraction (Figure 5.2). When solvent was used in excess in the synthesis by decreasing the pH, the solvent volume fraction was higher at low pH, as derived from the comparisons of the pair of curves 1 and 2 and the pair of curves 3 and 4. Contrarily, the solvent volume fraction at high pH approximated to 95% in all the cases.

The critical pH at which the sharp volume transition occurred was not affected significantly by the considered variations in the synthesis. The average value for the critical pH of P(MAA-g-EG) materials is 5.6 as obtained from the inflexion points of the

hyperbolic tangent functions that fit the behavior or the volume swelling ratio in the four cases.

The experiment where the pH input was changed incrementally and then decrementally (presented in Section 6.1) gave distinctive equilibrium curves for each trajectory shown in Figure 5.1.3. These results reveal a hysteresis effect in the swelling action of the hydrogel material as a result of residual stresses or wearing out of the material.
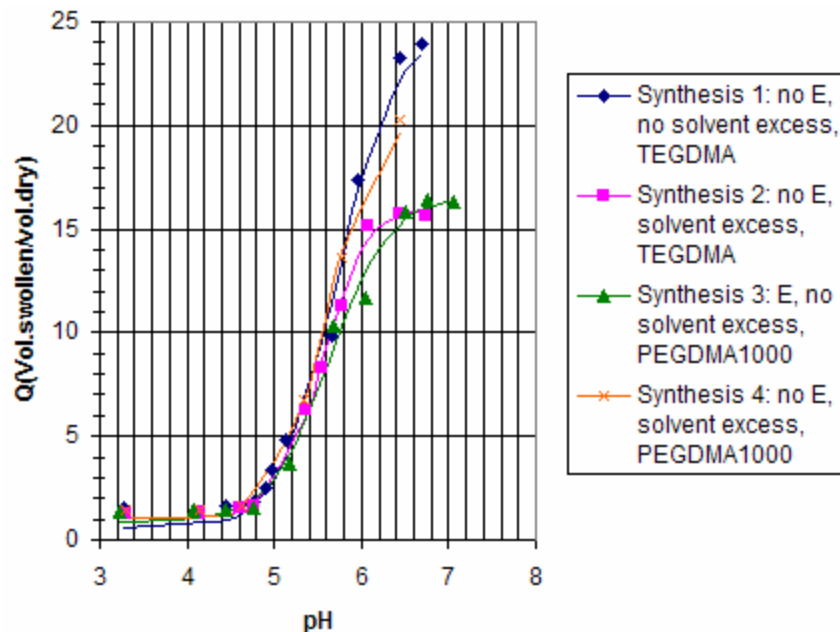
**Figure 5.1.1. Equilibrium Volume Swelling Ratio.** The equilibrium volume swelling ratio Q is plotted as a function of pH. The experimental data are represented by the marks and the fitted hyperbolic tangential functions (table 5.2) are plotted with the continuous lines. Samples were equilibrated in dimethyl glutaric acid solutions at 37°C. The synthesis description indicates if enzymes (E) were used, if the solvent was in excess in the synthesis by adjusting the pH of the reactive mixture to 2.5 – 3 with hydrochloric acid solution, and the crosslinking agent (TEGDMA or PEGDMA).
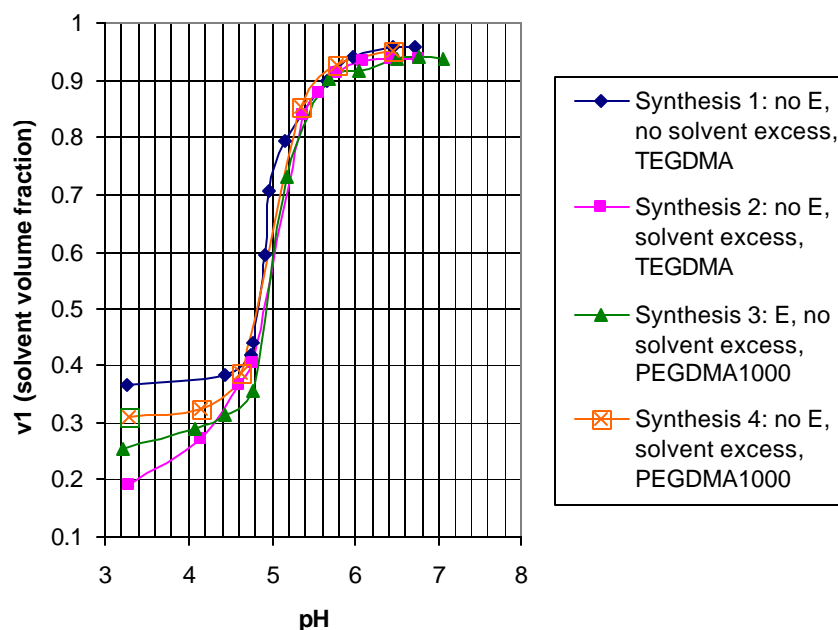
**Figure 5.1.2. Equilibrium Solvent Volume Fraction.** The equilibrium solvent volume fraction $\upsilon_1$ is shown as a function of pH. Samples were equilibrated in dimethyl glutaric acid solutions at 37°C. The synthesis description indicates if enzymes (E) were used, if the solvent was in excess in the synthesis by adjusting the pH of the reactive mixture to 2.5 – 3 with hydrochloric acid solution, and the crosslinking agent used (TEGDMA or PEGDMA 1000).

**Table 5.1.1. Synthesis Conditions of Materials Submitted to Equilibrium Tests.** P(MAA-g-EG) hydrogels were synthesized with variations in crosslinking agent, pH of reactive mixture and enzyme content. Only synthesis 3 incorporates glucose oxidase and catalase. The pH was lowered with HCl solution in synthesis 2 and 4. The volume percentage of solvent in the reactive mixture and at equilibrium can be compared at the pH of the synthesis to determine the excess of solvent in the preparation. Regarding the integrity of the synthesized films, a fracture was observed in samples equilibrated at certain pH value (fracture pH).

| Synthesis No. | Reactive mixture | | | Equilibrium solvent v% at approx. pH of reactive mixture | Fracture pH |
|---|---|---|---|---|---|
| | Crosslinking agent | pH | Solvent v% | | |
| 1 | TEGDMA | 6 | 54 | 95 | 5.66 |
| 2 | TEGDMA | 3 | 54 | 20 | 6.85 |
| 3 | PEGDMA | 5 | 50 | 60 | 5.68 |
| 4 | PEGDMA | 3 | 54 | 30 | 5.78 |

**Table 5.1.2. Results of Equilibrium Swelling Experiments.** The equilibrium volume swelling ratio Q data are fitted by a hyperbolic tangent function with $R^2$ above 0.99 in all cases. The critical pH is reported as the abscissa of the inflexion point of the function. The curves of these analytical functions are shown in Figure 5.1. The program CurveExpert was used to fit the data [6].

| Synthesis No. | $Q = a + b\,tanh\,(c(pH)+d)$, x is pH of the medium | | | | Critical pH |
|---|---|---|---|---|---|
| | a | b | c | D | |
| 1 | 12.5529 | 11.9906 | 1.5497 | -8.8588 | 5.7165 |
| 2 | 8.5094 | 7.4761 | 2.0496 | -11.3714 | 5.5482 |
| 3 | 8.7427 | 7.8454 | 1.4927 | -8.4124 | 5.6356 |
| 4 | 10.8627 | 9.7866 | 1.8038 | -10.1010 | 5.5998 |
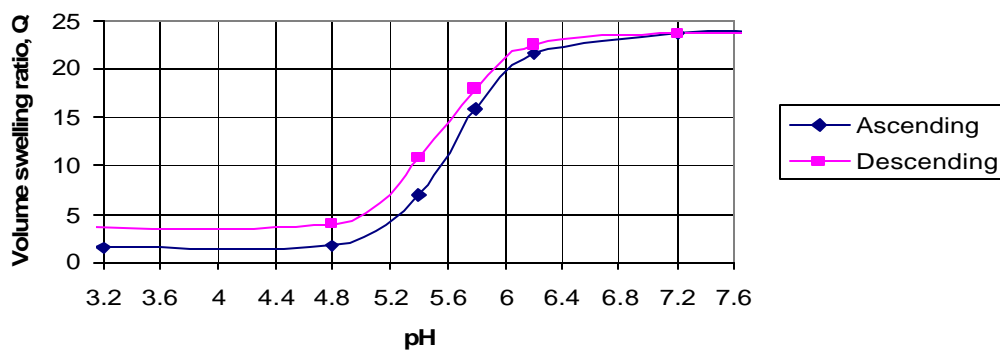


**Figure 5.1.3. Hysteresis of Volume Swelling Ratio.** A P(MAA-g-EG) hydrogel disc (synthesis 3, with excess of solvent, PEGDMA and enzymes) subjected to a sequence of pH step experiments show different equilibrium trajectories for ascending and descending directions of pH changes.

## 5.2. Porosimetry

### 5.2.1. Fundamentals

The porosity of hydrogel materials is analyzed through the intrusion of mercury under controlled pressures. Mercury does not penetrate spontaneously small pores, because it is a non-wetting liquid for most surfaces. Therefore, external pressures must be applied to inject the mercury into the pores.

The Washburn equation establishes an inverse relation between the diameter of the pores, d, and the pressure, $\Delta P$, required for the mercury to penetrate them:

$$d = \left( \frac{1}{\Delta P} \right) 4\gamma \cos\theta, \tag{7}$$

where $\gamma$ is the surface tension of mercury, $\theta$ is the contact angle between the mercury and the sample and the pores are supposed to have a cylindrical geometry. The average contact angle of mercury 140°C and the surface tension of mercury at 20°C under vacuum is 480 mN/m [7].

In a porosimetric analysis, the pressure is increased, the pore diameter is calculated at each pressure value, and the cumulative volume of mercury introduced into the sample is measured. As a result, the porosity and mean diameter are determined, and the cumulative and the incremental intrusion volume profiles with respect to the pore diameter can be obtained.

The porosity is the ratio of the volume of the pores over the total bulk volume of the sample. The volume of the pores is given by the total volume of intruded mercury. The median diameter is calculated from the pressure value where 50% of the total intrusion volume is reached [7].

The area below the cumulative mercury intrusion volume curves is higher for more porous samples. The height of the peaks of the incremental mercury intrusion volume indicates the distribution of pore sizes in the sample: the higher the incremental value, the more pores of the corresponding diameter in the sample [7].

### 5.2.2. Experimental Procedure

The Autopore III system [8] was used to characterize the porosity of the hydrogel materials. This equipment performs low and high pressure analysis in the ranges of 0-30 psia and 30-50 psia, respectively (Figures 5.2.1, 5.2.2 and 5.2.3). The porosimeter can report intrusion volumes with respect to a reference. When the reference is the analysis of the empty penetrometer, compensation is made for the compressibility of the penetrometer and the mercury. Moreover, the reference may be the raw data from the study of a non-porous material. This reference is used to estimate the pore size more precisely eliminating

the compressibility effect of the non-porous material, the penetrometer and the mercury. Appendix 5.4 presents the configuration details for the porosimetry tests.

The samples to analyze in the mercury porosimeter were representative of limited solvent, equilibrium absorbed solvent and more than equilibrium solvent used in the synthesis of the polymer (synthesis 1, 2 and 3 of Table 5.1.1). The samples must be dry to be tested in the porosimeter. Therefore, the porosity of the swollen hydrogel was not considered. The protocol for the mercury porosimetry tests is described in Appendix 5.5.

## 5.2.3. Results and Discussion

The pressure range for the mercury porosimeter from 0 to 50 psi of the Autopore III is not enough to inquire pores of the expected diameter in the order of tens of Angstroms. However, the resulting graphs corroborate the effect of the excess of solvent of the reactive mixture in the synthesis of hydrogels. The higher the excess of solvent, the bigger the pores of the material.

The results of the mercury penetration analysis are shown in Figures 5.2.4, 5.2.5 and 5.2.7. The cumulative intrusion volume curves differentiate better at smaller diameter or higher pressure values. In this region, the polymer synthesized with more solvent content reaches a higher cumulative intrusion volume. The curves of differential intrusion volume with respect to pore size indicate the distribution of pore diameters (Figures 5.2.6 and 5.2.8). These curves show at least a tendency of a more presence of submicron diameter pores, since the increment in intrusion volume is higher when the mercury reaches smaller pores.
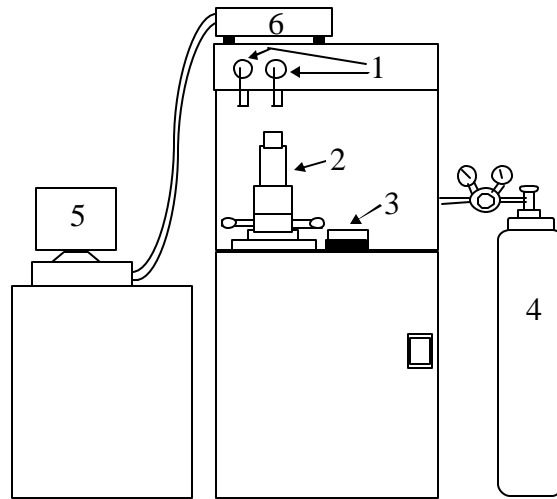
**Figure 5.2.1. Scheme of the AutoPore III System.** The equipment has two low pressure ports (1) and one high pressure chamber (2). Mercury level can be observed by a small window (3). A nitrogen tank (4) is required for the operation of the system. A computer (5) is connected to the analysis unit of the system (6).
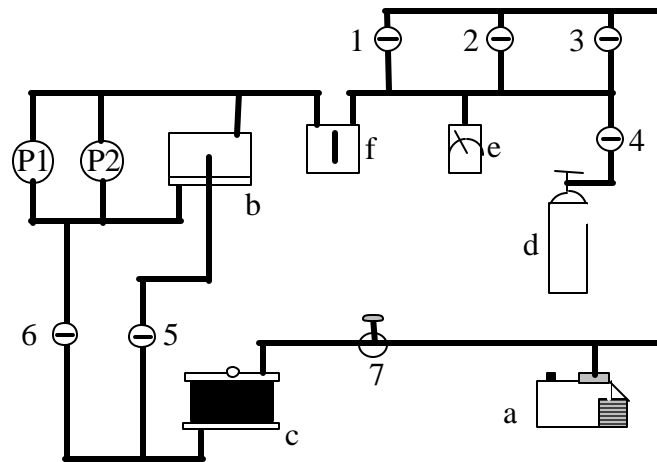


**Figure 5.2.2. Low-Pressure Subsystem of Micromeritics Autopore III.** The main equipment for the low pressure tests are the following: ports (P1, P2), vacuum pump (a), mercury container (b), main mercury reservoir (c), nitrogen supply (d), pressure transmitter (e), mercury trap (f), valves to regulate mercury input to the ports (1, 2, 3), valve for nitrogen flow to displace mercury (4), drain valves (5, 6, 7).
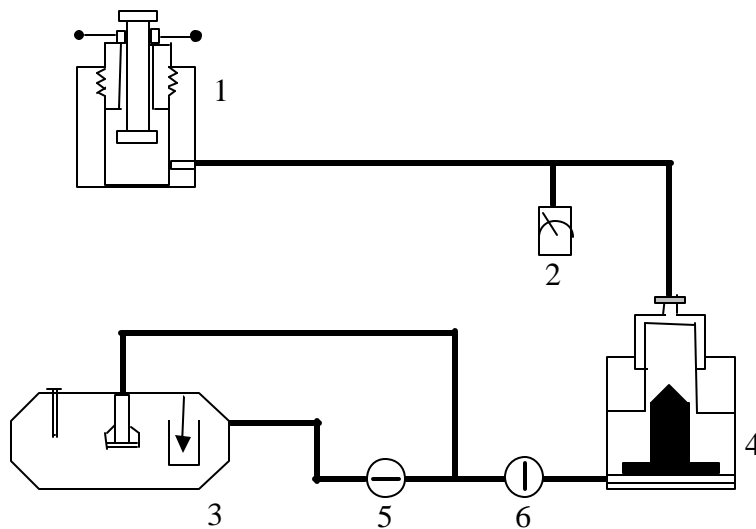
**Figure 5.2.3. High Pressure Subsystem of Micromeritics Autopore III.** The following elements are shown: high pressure chamber (1), pressure transmitter (2), hydraulic pump (3), pressure regulator (4), valves (5, 6).
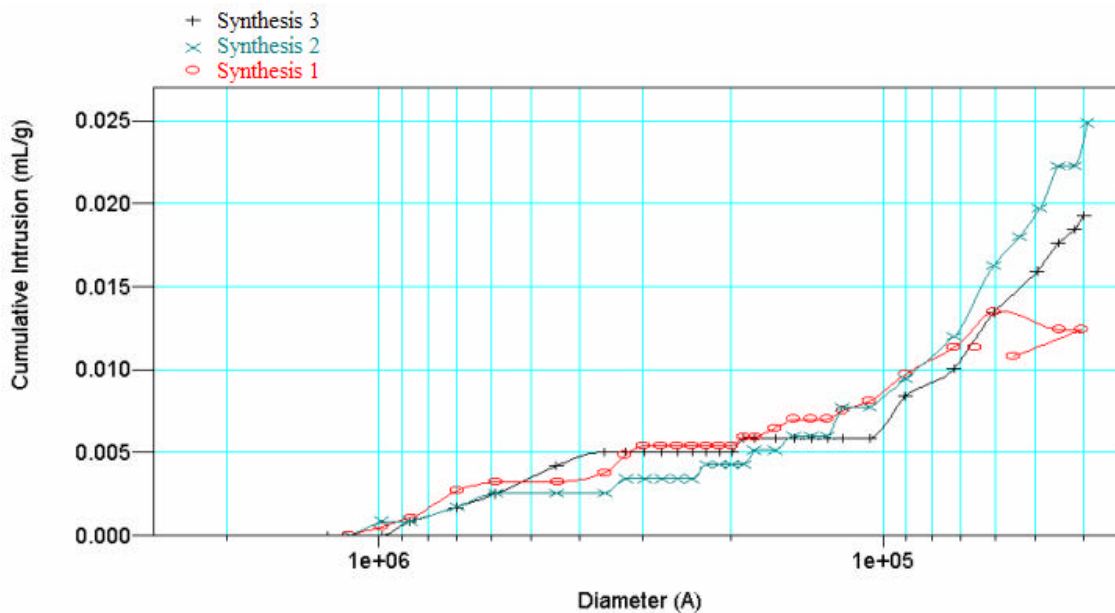


**Figure 5.2.4. Cumulative Intrusion with Respect to Diameter.** Cumulative intrusion as a function of diameter in Angstroms, in samples synthesized with limited solvent (synthesis 1), with excess of solvent with respect to equilibrium (synthesis 2) and with an amount of solvent equal to solvent content at equilibrium (synthesis 3). No compressibility correction is made.
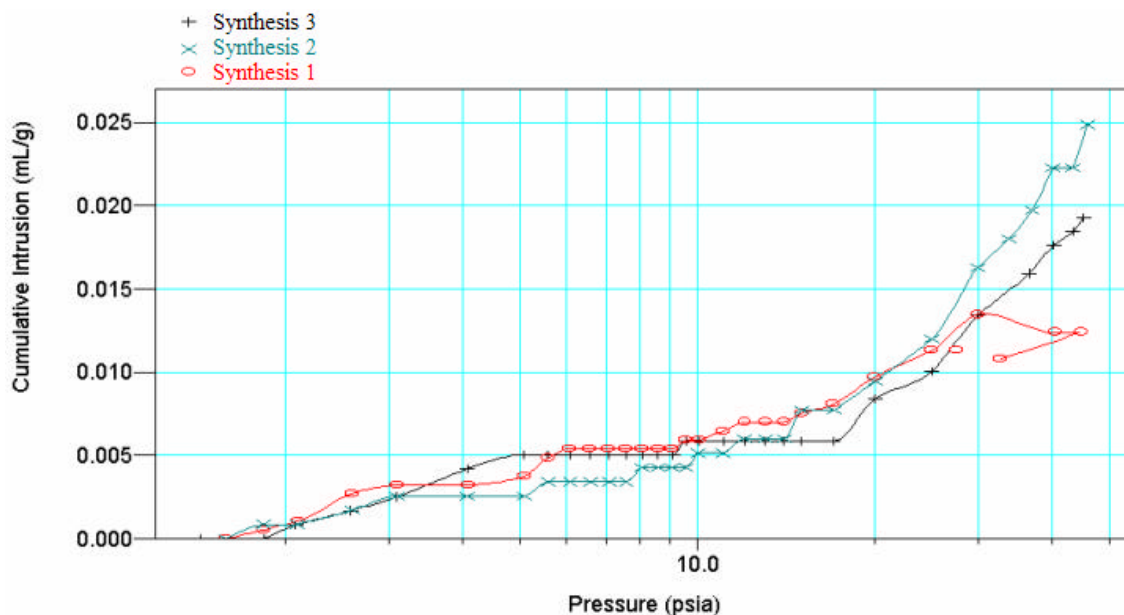
**Figure 5.2.5. Cumulative Intrusion with Respect to Pressure.** Cumulative intrusion as function of pressure, in samples synthesized with limited solvent (synthesis 1), with excess of solvent with respect to equilibrium (synthesis 2) and with an amount of solvent equal to solvent content at equilibrium (synthesis 3). No compressibility correction is made.
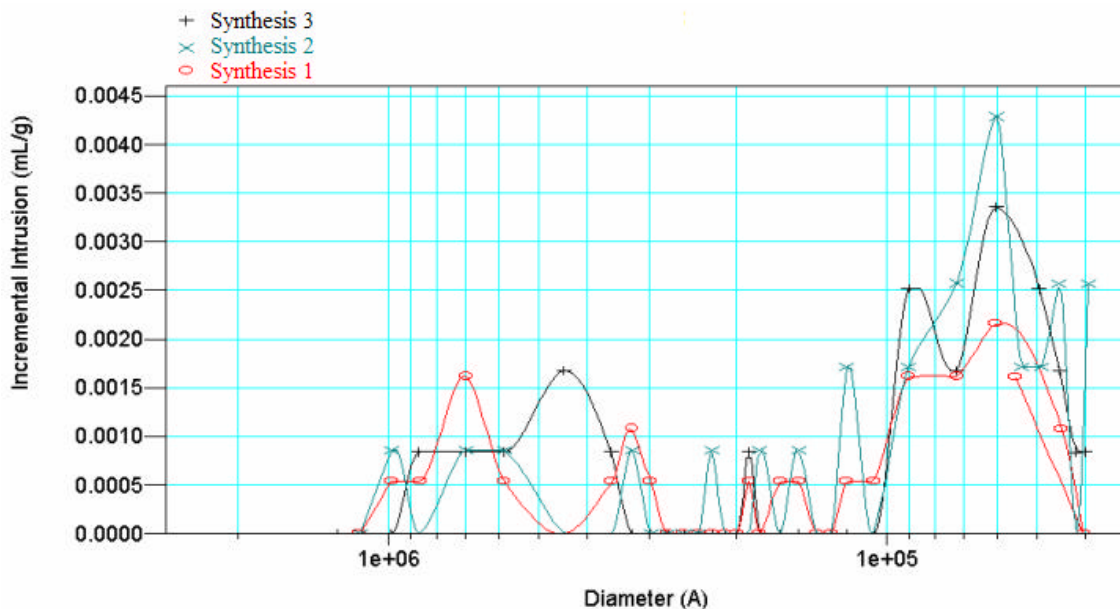


**Figure 5.2.6. Incremental Intrusion with Respect to Diameter.** Incremental intrusion as function of diameter in Angstroms, in samples synthesized with limited solvent (synthesis 1), with excess of solvent with respect to equilibrium (synthesis 2) and with an amount of solvent equal to solvent content at equilibrium (synthesis 3). No compressibility correction is made.

61
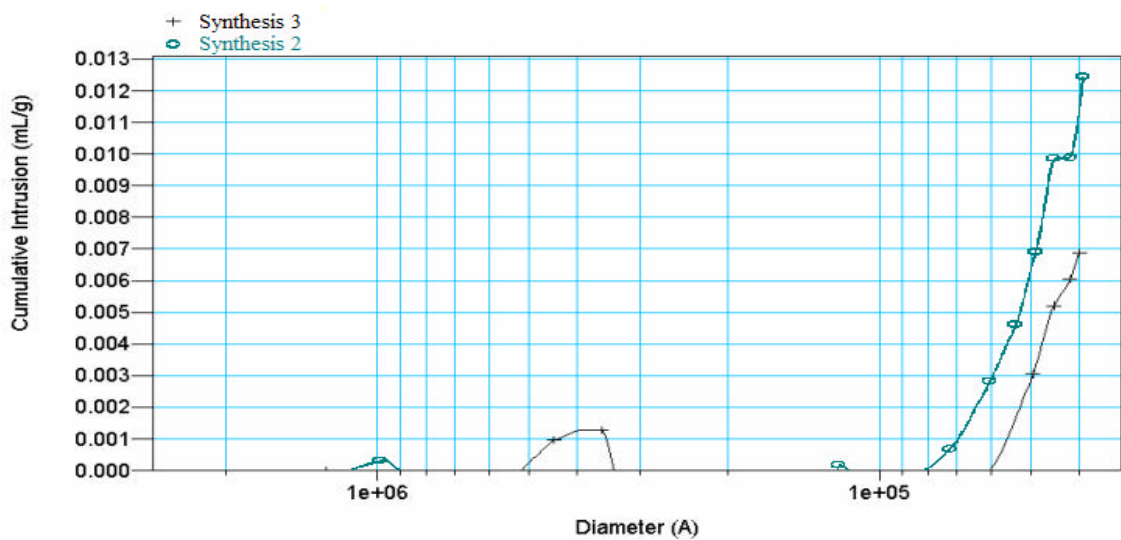
**Figure 5.2.7. Cumulative Intrusion with Compensation of Compressibility of the Material.** Mercury intrusion in synthesis 1 sample with less solvent than equilibrium is used as a reference to calculate the cumulative intrusion in samples synthesized with excess of solvent with respect to equilibrium (synthesis 2) and with an amount of solvent equal to solvent content at equilibrium (synthesis 3).
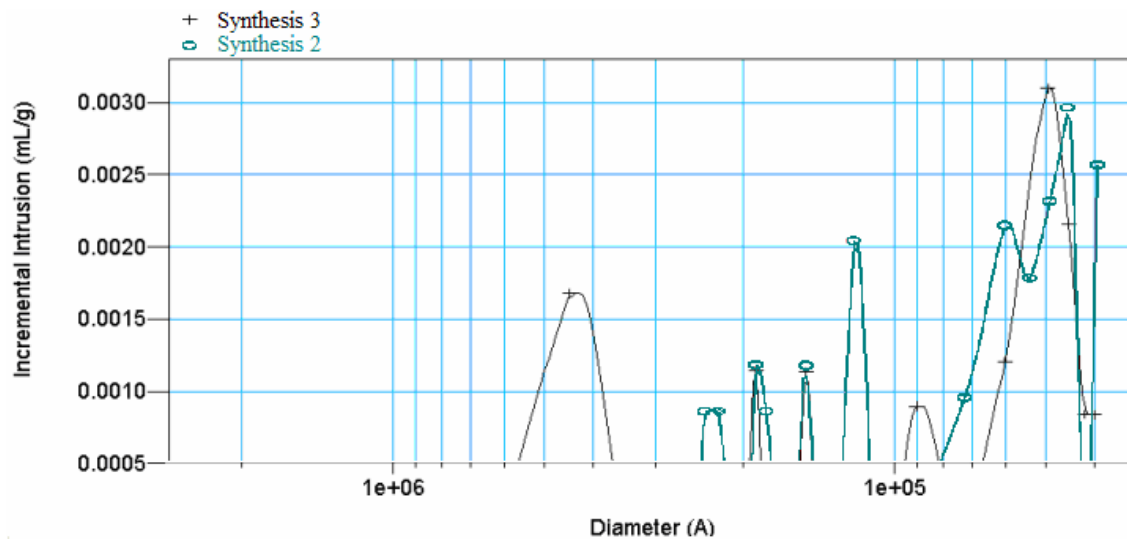


**Figure 5.2.8. Incremental Intrusion with Compensation of Compressibility of the Material.** Mercury intrusion in synthesis 1 sample with less solvent than equilibrium is used as a reference to calculate the incremental intrusion in samples synthesized with excess of solvent with respect to equilibrium (synthesis 2) and with an amount of solvent equal to solvent content at equilibrium (synthesis 3).

62

## 5.3. Equilibrium Glucose Responsive Swelling

### 5.3.1. Fundamentals

Glucose responsiveness of the hydrogel is achieved by the pH changes caused by the oxidation of glucose in presence of glucose oxidase. Oxygen is required to reactivate the glucose oxidase enzyme. The oxygen for this regeneration process is recovered by the chemical dissociation of the hydrogen peroxide product by the action of catalase enzyme incorporated in the system. The gluconic acid, produced by the oxidation of glucose, dissociates affecting the hydrogen ion concentration or pH of the medium.

#### 5.3.1.1. Enzymatic reactions

An enzymatic reaction can be explained by the following sequence where ES and EP represent the enzyme-substrate and the enzyme-product complexes, respectively, and the superscript $^?$ indicates a transition state [9]:

$$E + S \longleftrightarrow ES \longleftrightarrow ES^{\neq} \longleftrightarrow EP \longleftrightarrow EP^{\neq} \longleftrightarrow E + P \qquad (8)$$
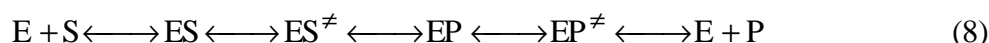
Figure 5.3.1 shows the changes in free energy for each stage of the previous sequence. The catalytic action of the enzyme reduces the energy barrier for the transformation of the substrate into the product. Besides the chemical transformation of the reaction medium, physical changes may also take place, for example, the final difference of the free energy of the substrate and the product may produce a significant temperature change.

The velocity of the enzymatic reactions is characterized by the Michaelis-Menten constant [9], which represents the concentration of the substrate for an initial velocity equal to half the maximum velocity (Appendix 5.6). The Michaelis-Menten constant for the glucose oxidase reaction with glucose in solution at 25°C is 20 mM or 360.32 mg/dL [10]. This value is representative of high glucose concentrations in the blood; therefore, the reaction is in principle appropriate for the *ex-vivo* detection of physiological glucose levels. However, the Michaelis-Menten constant depends on the reaction medium and its conditions.

#### 5.3.1.2. Reaction mechanism for enzymatic oxidation of glucose

The basis for the detection of glucose with the hydrogel-based system is the high glucose affinity of the enzyme glucose oxidase. Glucose oxidase is a flavoprotein (Figure 5.3.2), i.e., its activity depends on two flavin molecules (FAD). These molecules are oxidative agents strongly attached to the enzyme. Reduced flavins ($FADH_2$) can reoxidize in presence of oxygen. This reoxidizing capability is fundamental for the function of the glucose oxidase enzyme.

The glucose oxidase enzyme, E, catalyzes the conversion of glucose into gluconic acid:

$$C_6H_{12}O_6 + O_2 \xrightarrow{\quad E \quad} C_6H_{10}O_6 + H_2O_2 . \tag{9}$$
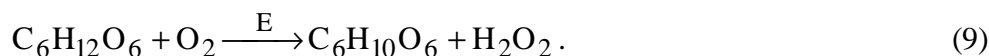
The mechanism of this reaction can be proposed according to the following equations:

$$
\begin{aligned}
C_6\,H_{12}\,O_6 &\rightarrow C_6\,H_{10}\,O_6 + 2H^+ + 2e^- \\
E - FAD + 2H^+ + 2e^- &\rightarrow E - FADH_2 \\
E - FADH_2 + O_2 &\rightarrow H_2O_2 + E - FAD
\end{aligned}
\tag{10}
$$
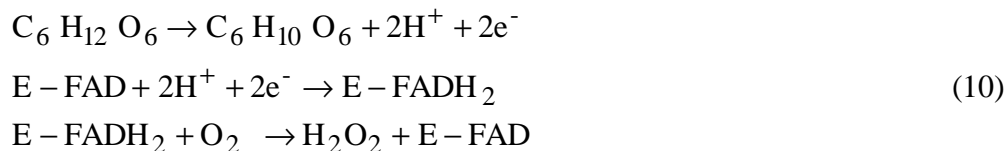
The details of this mechanism have been explained in [10] and summarized in Appendix 5.7.

In the hydrogel system, oxygen is replenished by the catalase breakdown reaction of hydrogen peroxide. The activity of the catalase enzyme depends on four heme groups [11, 12, 13]. The catalytic action is based on reversible binding between iron centers of the heme groups and oxygen atoms from the substrate. The structure of catalase is shown in Figure 5.3.3.

Although the catalyzed mechanism of hydrogen peroxide decomposition is not well known, the following steps are proposed [11, 14]:

$$
\begin{aligned}
H_2O_2 + Fe(III)\text{-}E \;?\;\; &H_2O + O{=}Fe(IV)\text{-}E \\
H_2O_2 + O{=}Fe(IV)\text{-}E?\;\; &H_2O + O_2 + Fe(III)\text{-}E
\end{aligned}
\tag{11}
$$
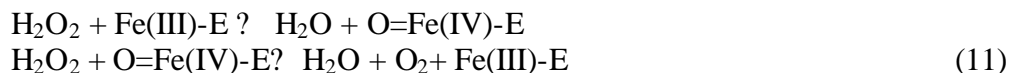
where Fe-E represents the iron atom of the heme group attached to the rest of the catalase enzyme; the oxidation number of the iron is indicated in parenthesis. In this case, contrary to the glucose oxidase reaction, the hydrogen peroxide substrate itself regenerates the catalase enzyme. Appendix 5.8 gives details of this mechanism.

### 5.3.2. Experimental Work

Equilibrium experiments were proposed to verify the discrimination of different physiological glucose concentrations by the degree of swelling of the hydrogel material. After washing, the samples were weighed and set into 100, 150 and 200 mg/dL glucose solutions at 37°C for 24 hours. The samples at the new equilibrium were weighed in air and heptane. Finally the samples were dried and weighed to calculate volume swelling ratios. The detailed protocol of these experiments is given in Appendix 5.9.

The underlying assumption of these experiments is that a higher glucose concentration would produce higher conversion to gluconic acid, a lower pH and, finally, a lower volume swelling ratio of the hydrogel sample.

### 5.3.3. Results and Discussion

Equilibrium experiments in Figure 5.3.4 gave practically the same weight and volume change for all the samples immersed in different glucose concentration solutions. This observation suggests a saturation of the material in such a way that no more glucose can be oxidized, the pH stops changing and no significant or congruent size variations can be noticed among the samples (the experiment at 150 mg/dL glucose concentration would have been expected to give a weight ratio between the ones obtained for the other two experiments at 100 and 200 mg/dL). The expected behavior of decreasing tendency in size with an increasing glucose concentration is not supported by the small range of the response variables (weight ratio or volume ratio).

### 5.4. Conclusions

Hydrogels exhibit a non-linear sensitivity before pH changes in the environment. A sharp transition in the equilibrium volume behavior is observed around a specific pH value. Such critical pH value is not altered significantly by the variation of synthesis parameters such as pH of reactive solution, type of crosslinking agent and presence of enzymes, since these do not affect the concentration of acid groups in the polymer structure. The excess of solvent in synthesis with respect to absorbed solvent in equilibrium does not imply concentration changes for the monomer, since the total volume of the reactive mixture was practically constant.

The use of a short crosslinking agent and the adjustment of a low pH in the reactive mixture produced better results for the integrity of the hydrogel material. However, due to the big difference in the length of the two crosslinking agents used (of 4 and 23 ethylene glycol units), a possible improvement with the use of an intermediate length cannot be discarded because of the reduction of internal residual stresses with respect to a short crosslinking agent. That is, an excessive length of crosslinking molecule may undesirably increase residual stresses due to the weight of sections that may not be able to extend when the material tends to swell.

Porosimetry studies verified the relation of a higher excess of synthesis solvent with bigger pores in the dry material. These studies do not describe the porous behavior in solution operation conditions. However, the knowledge of a high porosity in the dry state can suggest the possibility of syneresis pore formation, which affects the transport properties of the material.

Equilibrium glucose swelling experiments did not prove glucose sensitivity of the hydrogel samples. Apart from the preservation of the activity of the enzymes, the saturation of the system explains the obtained results. This observation leads to the consideration of dynamic glucose swelling experiments, where the response of the hydrogel before it is saturated with glucose may show differences.

Regardless of the saturation effect, the equilibrium or net Gibbs energy change in the enzymatic glucose reaction may produce a change in temperature that suggests the use of temperature sensitive hydrogel-based systems as another possibility to explore.
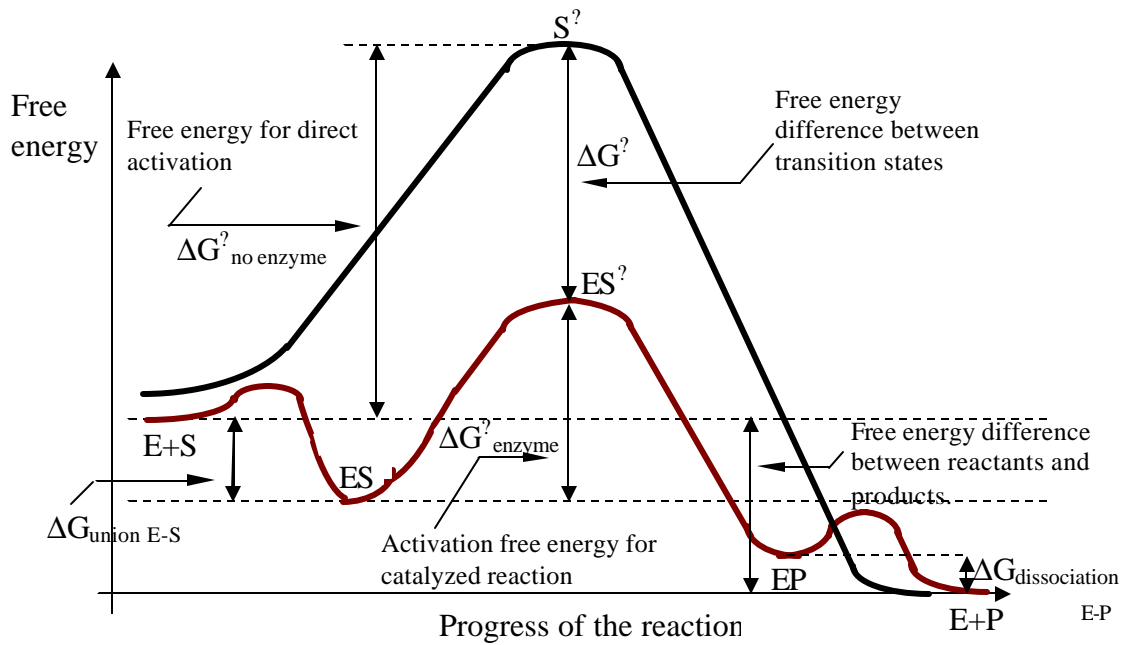
**Figure 5.3.1. Energy Diagram for Enzymatic Reaction.** The black line represents the energy states of a non-catalyzed reaction. The red line describes the free energy in the course of an enzymatic reaction. G is free energy, S is substrate and P is product. Adapted from [9].

(a) General topology


(b) FAD molecules (coenzyme)


(c)  Active site


(d)  Two subunits


(e) Disulfide bridge in subunit


(f) Two domains in subunit
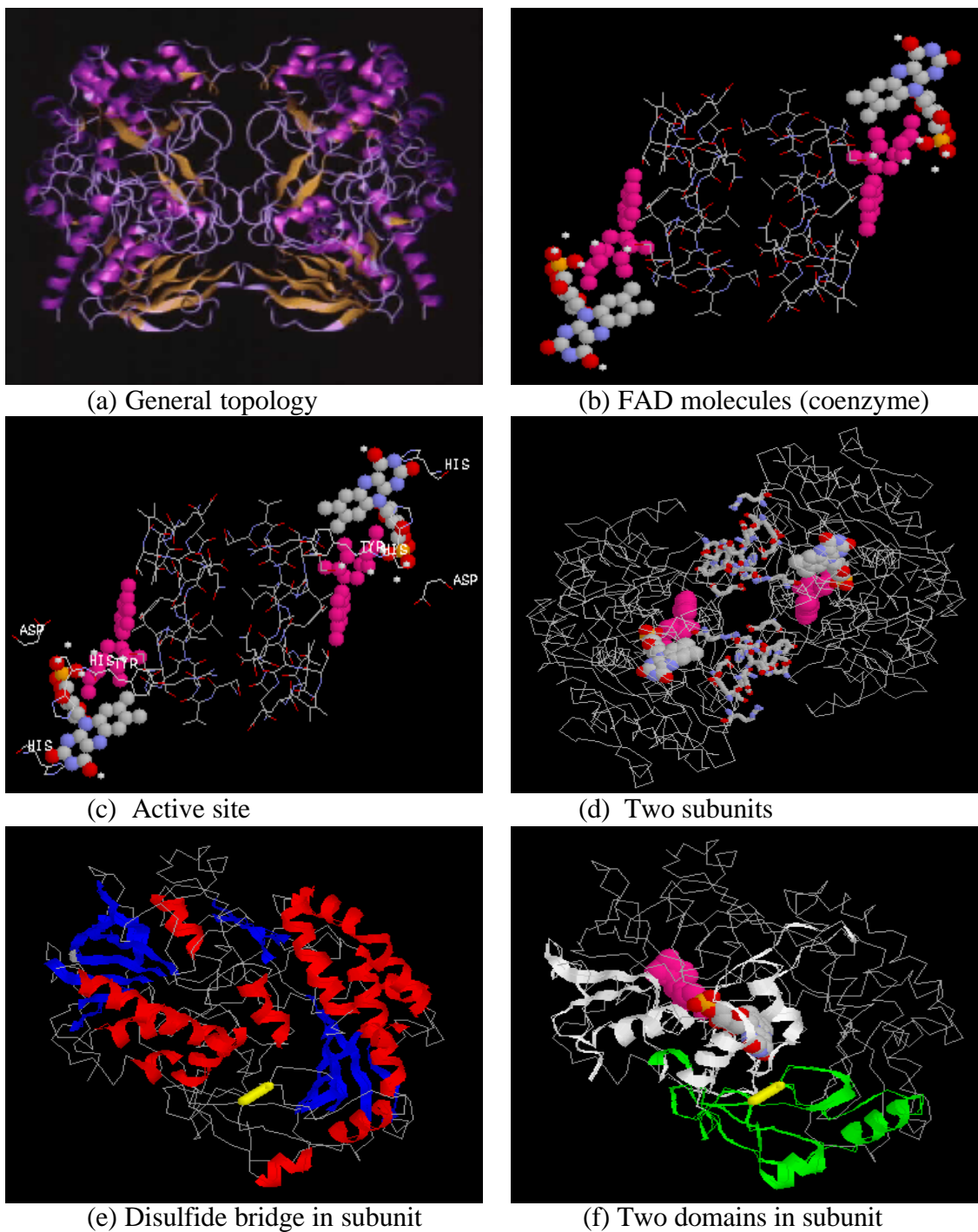
**Figure 5.3.2. Structure of Glucose Oxidase.** This enzyme is an ellipsoidal dimmer with dimensions 70 Å x 55 Å x 80 Å (a).   Residues 75 to 98 join the flavin or FAD molecules (b).  The active site (c) is formed by the following residues: Tyr 515 (tirosin), His 559 (histidin), His 516 and Asp 548 (aspartic acid).  The two subunits that form the molecule of glucose oxidase are linked by a different set of residues (d).  A subunit contains a disulfur union (yellow), α helices (red) and β sheets (blue) (e), two domains (domain 1 in white, domain 2 in green) and a molecule of FAD (f) [10].
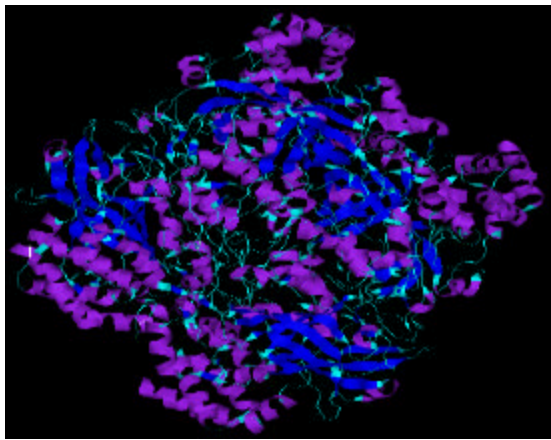
(a) General topology
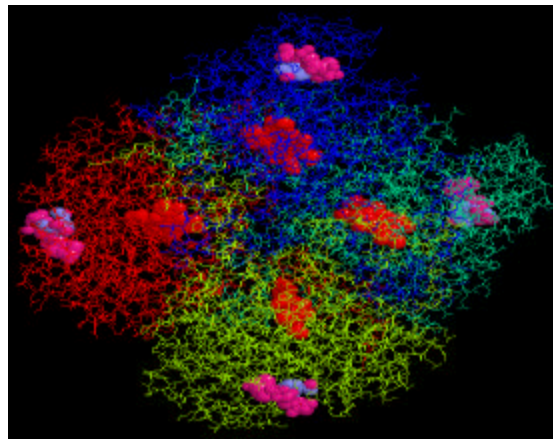

(b) Four subunits
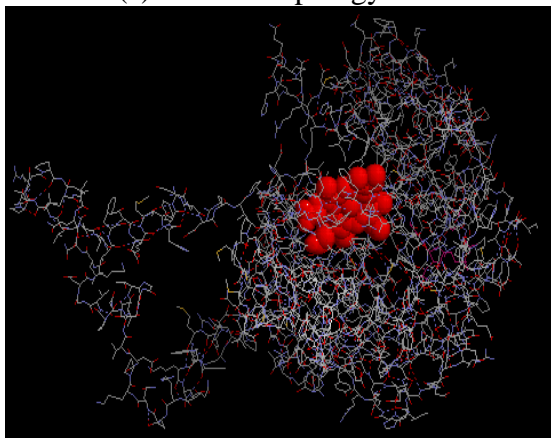

(c) Heme prosthetic group in a subunit
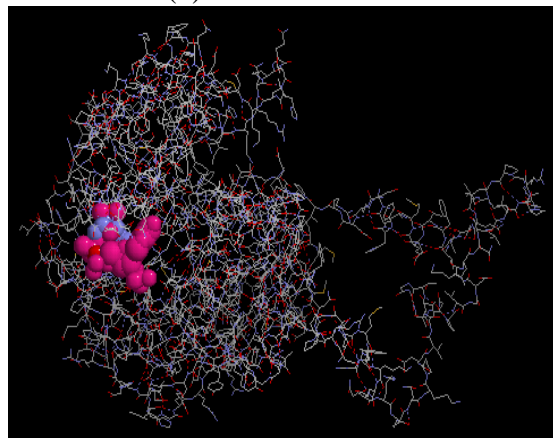

(d) NADP in a subunit
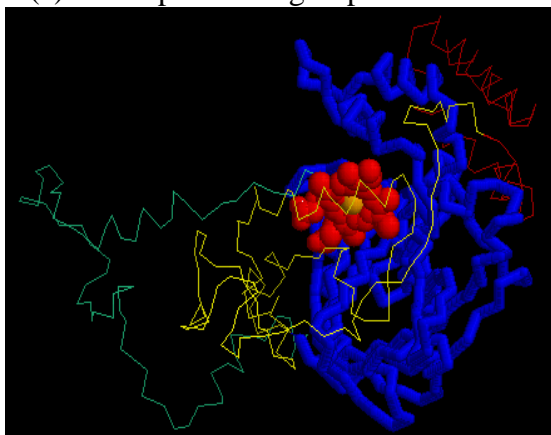

(e) Four domains in a subunit
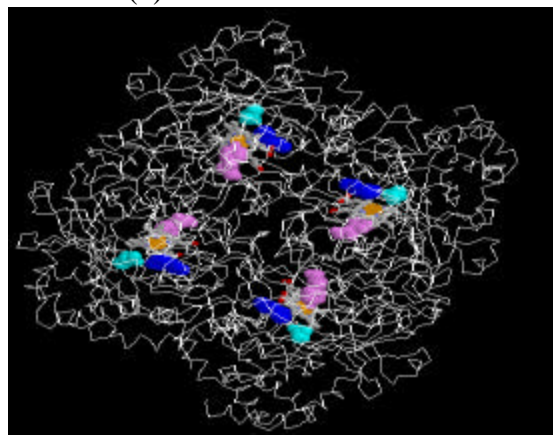

(f) Active sites

**Figure 5.3.3. Structure of Catalase.** The catalase enzyme has a molecular weight between 220 000 and 350 000 kD (a). This enzyme is a tetramer with subunits of approximately 500 amino acids (b). The catalytic center of each catalase monomer or subunit contains a heme prosthetic group (c). A nicotinamide adenine dinucleotide phosphate (NADP) may be present to protect the enzyme from oxidation by its substrate (d), as in the case of beef liver catalase. Each subunit is formed by four domains (e). Each of the four active sites of a catalase tetramer is formed by His[74] (blue), Asn[147] (cyan), Tyr[357] (violet) and a heme group (grey)and interacts with a $H_2O_2$ molecule (orange) (f).

68
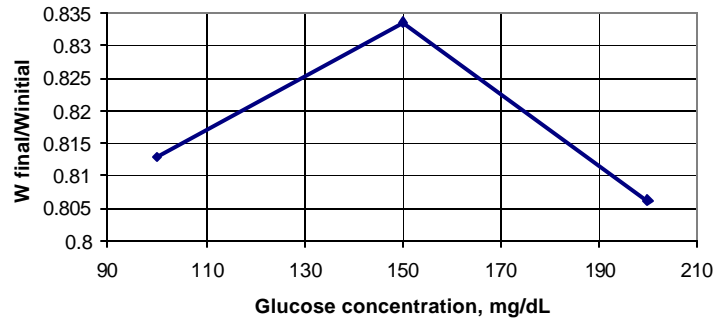
(a)
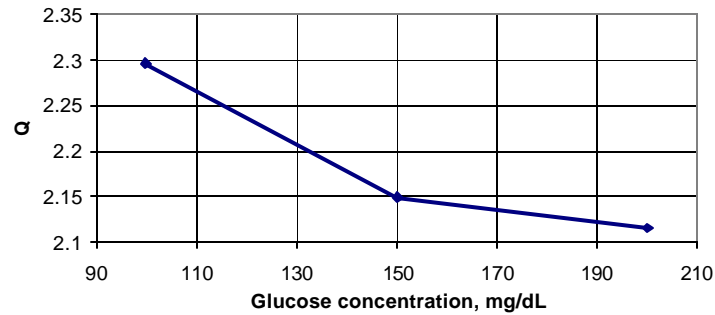


(b)

**Figure 5.3.4. Equilibrium Experiments in Glucose Solutions.** Samples are set into 100, 150 and 200 mg/dL glucose solutions at 37°C. Graph a shows the final weight ratio with respect to the initial equilibrium weight in deionized water. Graph b shows the volume swelling ratio with respect to the dry weight obtained after the experiment. Although the range of both ratios is very narrow, the expected descending tendency is clearer in graph b. The peak in graph a and the narrow range of both graphs do not support a meaningful variation.

**References**

1. Lowman AM, Dziubla TD, Bures P, Peppas NA. Structural and dynamic response of neutral and intelligent networks in biomedical environments. In: Peppas NA, Sefton MV. Molecular and Cellular Foundations of Biomaterials. New York: Elsevier Academic Press, 2004;29:75-130.

2. Lentner C (editor). Geigy scientific tables (8th, rev. and enl. ed.). Basle, Switzerland: Ciba-Geigy. 1981;278-283.

3. Odian G. Principles of polymerization (3rd edition). New York: John Wiley and Sons, Inc., 2004.

4. Hilt JZ, Gupta AK, Bashir R, Peppas NA. Ultrasensitive BioMEMS sensors based on microcantilevers patterned with environmentally responsive hydrogels. Biomed Microdev. 2003;5(3):177-184.

5. Peppas NA. Is there a future in glucose-sensitive, responsive insulin delivery systems? J. Drug Del. Sci. Tech. 2004;14(4):247-256.

6. Hyams D. CurveExpert Version 1.37 Copyright C 1995-2001.

7. Lane AM. Interpretation of Mercury Porosimetry Data (catalysis, morphology, pores). University of Massachusetts Amherst, 1984.

8. AutoPore III 9420 Analyzer Operator's Manual v1.01. Micromeritics, Inc. 1996.

9. Lehninger A Biochemistry: the molecular basis of cell structure and function. New York: Worth Publishers, Inc., 1975.

10. Cardosi, M. http://www-biol.paisley.ac.uk/ (Chemscape Chime plug in by MDL Information Systems, Inc.)

11. Boon EM, Downs A, Marcey D. Catalase Structural Tutorial Text. http://www.callutheran.edu/Academic_Programs/Departments/BioDev/omm/catalase/cat1.htm (as seen on November 14, 2007).

12. Vainshtein. Three-dimensional structure of the enzyme catalase. Nature. 1981;293:411-412.

13. O'Malley J, Weaver J. Subunit structure of glucose oxidase from aspergillus niger. Biochem. 1972;11:3527

14. Jones P, Suggett A. The cata-ase-hydrogen peroxide system. A theoretical appraisal of the mechanism of catalase action. Biochem J. 1968:110(4):621-629.

**Appendix 5.1. Volume Measurement of Hydrogel Samples**

According to the Archimedes principle, the volume of a hydrogel sample immersed in a non-solvent and non-absorbable liquid such as heptane is equal to the volume of displaced liquid, and the weight of the displaced liquid equals the magnitude of the buoyant force. The weight of the sample in heptane to measure is equal to the weight in air minus the buoyant force. In order to account for the buoyant force, the sample must be suspended in a fixed position in such a way that it is surrounded completely by the fluid. Since the density of the hydrogel is higher than the density of heptane, a perforated basket is used to set the sample and prevent it from sinking. The next figure shows the elements to weigh a sample in heptane.
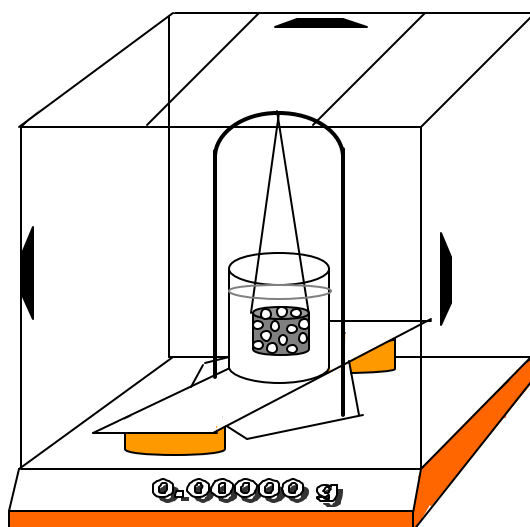


**Figure a5.1.1.   Set Up for Weight Measurements in Liquid Environments.** Analytical balance with a set up to weigh hydrogel samples in a non-absorbable liquid.

The glass is set on a base supported at the extremes to avoid contact with the sensing plate located at the center. The perforated basket is suspended from the arc structure which is fixed to the sensing plate. Heptane is poured in the glass until the basket is completely covered. The balance is reset. When the sample is deposited in the basket, the net force sensed and displayed will be equal to the weight in heptane. The buoyant force is equal to the weight in air minus the weight in heptane, and is proportional to the volume of the sample.

**Appendix 5.2. Dimethyl glutaric Acid Buffers Preparation**

       The dimethyl glutaric acid buffers are prepared according to Geigy Tables. Two stock solutions are used: ββ-dimethyl glutaric acid 0.1 M (16.02 g/L) and sodium hydroxide 0.2 N.

       Mix 100 mL of ββ-dimethyl glutaric acid stock solution, X mL of sodium hydroxide stock solution and 5.844 g of sodium chloride and complete a volume of 1000 mL for an ionic strength of 0.1 M.

| pH | X (mL) |
|-----|--------|
| 3.2 | 14.4 |
| 3.4 | 20.9 |
| 3.6 | 26.8 |
| 3.8 | 32.4 |
| 4.0 | 36.6 |
| 4.2 | 40.3 |
| 4.4 | 43.1 |
| 4.6 | 45.7 |
| 4.8 | 48.3 |
| 5.0 | 51.5 |
| 5.2 | 53.6 |
| 5.4 | 58.2 |
| 5.6 | 63.6 |
| 5.8 | 68.7 |
| 6.0 | 73.6 |
| 6.2 | 78.5 |
| 6.4 | 83.3 |
| 6.6 | 87.4 |
| 6.8 | 91.0 |
| 7.0 | 93.2 |
| 7.2 | 94.9 |
| 7.4 | 95.8 |
| 7.6 | 96.8 |

**Appendix 5.3.  Equilibrium Experiment Protocol**

The equilibrium experiment consists in the measurement of the steady state volume swelling ratio at different pH values at 37°C.

1. The pH values of interest are selected and buffer solutions are elaborated.

2. Flasks are filled with 50 mL of either the low or high pH buffer solution.

3. A dry disc sample is set in each flask with a particular pH buffer.

4. The flasks are placed in a water bath at 37°C.  The volume of the hydrogel sample is allowed to reach equilibrium during a lapse of 24 hours.

5. The hydrogel samples at equilibrium are weighed in air and in heptane.  Each sample is handled with blunt forceps, the excess of water in the surface is removed with a tissue, and the weight in air is measured. Immediately after this measurement, the sample is weighed in heptane.  This procedure is done quickly and carefully to reduce drying and cooling and avoid breaking the hydrogel disc.

## Appendix 5.4. Parameters for Porosimetry Analysis

Analysis of the sample synthesized with approximately the same proportion of solvent than in equilibrium (synthesis 3).

```
                        Micromeritics Instrument Corp

WIN9400 Series                 Unit 192            Port 1/1              Page  1
V2.00

                Sample:  Sample with GOx and with no pH correction
              Operator:  IS
             Submitter:
                  File:  C:\WIN9420\PARAMS\SEP28.SMP

      LP Analysis Time:  09/28/06 12:55:12            Sample Weight:  0.023 g
Penetrometer:            0619- (07)  5 Bulb, 0.392 Stem, Solid

Pen. Constant:          11.007 µL/pF     Adv. Contact Angle:     130.000 degrees
Pen. Weight:            63.6083 g        Rec. Contact Angle:     130.000 degrees
Stem Volume:            0.3920 mL        Hg Surface Tension:     485.000 dynes/cm
Max. Head Pressure:     4.4500 psia      Hg Density:             13.5335 g/mL
Pen. Volume:            5.9639 mL        Sample Weight:           0.0230 g
                                         Assembly Weight:       144.1297 g

Low Pressure:
       Evacuation Pressure:         500.000 µmHg
       Evacuation Time:                   5 mins
       Mercury Filling Pressure:       1.43 psia
       Equilibration Time:               10 secs

High Pressure:
       Equilibration Time:               10 secs

Blank Correction Sample:   C:\WIN9420\PARAMS\P07SEP11.SMP
Blank Correction ID:       Sample file to calibrate penetrometer 070619

                        Intrusion Data Summary

            Total Intrusion Volume =       0.0050 mL/g
                   Total Pore Area =        0.002 m²/g
       Median Pore Diameter (Volume) =     507064 A
         Median Pore Diameter (Area) =      41720 A
       Average Pore Diameter (4V/A) =      115212 A
                      Bulk Density =       1.4543 g/mL
          Apparent (skeletal) Density =   1.4649 g/mL
                          Porosity =       0.7288 %
```

Penetrometer calibration (analysis of penetrometer without sample).

```
                        Micromeritics Instrument Corp

WIN9400 Series                  Unit 192            Port 1/1              Page  1
V2.00

               Sample:  Sample file to calibrate penetrometer 070619
             Operator:  IS
            Submitter:
                 File:  C:\WIN9420\PARAMS\P07SEP11.SMP

     LP Analysis Time:  09/11/06 16:50:18           Sample Weight:  0 g
Penetrometer:          0619- (07)  5 Bulb, 0.392 Stem, Solid

Pen. Constant:         11.007 µL/pF    Adv. Contact Angle:    130.000 degrees
Pen. Weight:           63.6083 g       Rec. Contact Angle:    130.000 degrees
Stem Volume:           0.3920 mL       Hg Surface Tension:    485.000 dynes/cm
Max. Head Pressure:    4.4500 psia     Hg Density:            13.5335 g/mL
Pen. Volume:           5.9639 mL       Sample Weight:         0.0000 g
                                       Assembly Weight:       1.0000 g

Low Pressure:
        Evacuation Pressure:          500.000 µmHg
        Evacuation Time:                5 mins
        Mercury Filling Pressure:      1.43 psia
        Equilibration Time:            10 secs

High Pressure:
        Equilibration Time:            10 secs

No Blank Correction

                         Intrusion Data Summary

            Total Intrusion Volume =       0.0004 mL/g
                   Total Pore Area =        0.000 m²/g
     Median Pore Diameter (Volume) =       9.7718 µm
       Median Pore Diameter (Area) =       7.5609 µm
       Average Pore Diameter (4V/A) =     10.4581 µm
                      Bulk Density =       0.0000 g/mL
       Apparent (skeletal) Density =       0.0000 g/mL
                          Porosity =       1.0000 %
                 Stem Volume Used =           0 % ****
```

75

**Appendix 5.5.  Porosimetry Tests Protocol**

The following protocol is based on the operation manual of the AutoPore III system of Micromeritics.   The software of the systems allows the capture of sample and penetrometer data, the configuration and the execution of the low and high pressure tests, and the analysis of the results.

1. A penetrometer with a bulb of 5 $cm^3$ and a stem of 0.392 $cm^3$ is selected for testing hydrogel discs of 7 mm of diameter and 0.7 mm of thickness approximately.   The penetrometer is washed with soap and water, rinsed with isopropyl alcohol and dried with high pressure air.  High vacuum grease is applied on the tip of the stem and on the lip of the bulb for perfect sealing during the tests.

2. The selected penetrometer is calibrated to compensate for the compressibility of the penetrometer and the mercury.  A blank file or calibration file is generated after performing the low and high pressure tests without sample.

3.  The dry hydrogel sample is weighed. The penetrometer must be prepared as described in step 1 for the next analysis.

4. The dry hydrogel is set inside the penetrometer.  The greased penetrometer is closed with a seal and a threaded cap.  The penetrometer with the sample is weighed.  The penetromer includes the weight of the grease and is calculated by subtracting the weight of the sample from the weight of the penetrometer with the sample.

5. The penetrometer containing the sample is loaded into the low pressure chamber and the automatic test is started from the computer.

6. The low pressure run starts by evacuating the penetrometer to a pressure of less than 50 µm of mercury.  The porosimeter is filled with mercury at a pressure of 1.5 psia covering the sample but practically not penetrating it.  From the value of 1.5 psia, the pressure is increased, using nitrogen as a displacement medium, and the intrusion volume is measured.

7.  Mercury volumes are measured at each constant pressure value, when the intrusion rate drops below 0.001 µL/g-s.  The cumulative intrusion volume is recorded at each pressure point.

8.  When the pressure of 30 psia is reached, the system returns to atmospheric pressure to allow removing the penetrometer from the low pressure chamber. The assembly formed by the mercury filled penetrometer with the sample is weighed (the assembly weight is required for the calculations performed by the analysis software).

9. The assembly is inserted into the high-pressure chamber, where mineral oil is used as displacement medium.  The test is automatically continued with increasing pressures from 30 psia and measurement of equilibrium mercury intrusion volumes.

10. When the high pressure test ends, the atmospheric pressure is recovered and the assembly is removed for proper disposal of the contained mercury and sample and the cleaning of the penetrometer.

## Appendix 5.6. Michealis-Menten Constant

The derivation of the Michaelis-Menten constant presented by Leningher in [9] is extended here with a detailed explanation and mathematical development. Enzymatic reactions present a mixed kinetics and a saturation phenomenon. At low substrate concentrations, the velocity of the reaction is of first order and at high concentrations, the kinetics becomes zero order (Figure A5.6.1).
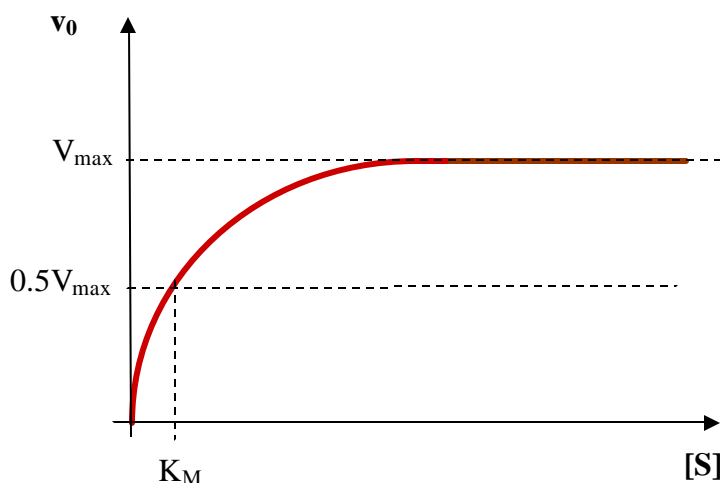


**Figure a5.6.1.  Initial velocity of reaction**

The following assumptions are made to analyze the initial velocity of reaction: only one substrate, S, is considered; the total concentration of the enzyme E, is given by $[E_T]=[E]+[ES]$; the concentration of the substrate is much higher than the concentration of the enzyme $[S]>>[E]$, and the mechanism of reaction is described by:

$$E + S \xleftrightarrow{\quad k_{+1},k_{-1}\quad} ES$$
$$ES \xleftrightarrow{\quad k_{+2},k_{-2}\quad} E + P$$

(a5.6.1)

where the velocity constants, k, for the direct and inverse reactions have a negative and a positive subindex, respectively.

The initial velocity, $v_0$, of the enzymatic reaction can be expressed in terms of the second step of the mechanism as:

$$v_0 = k_{+2}[ES]$$

(a5.6.2)

The quantities $k_{+2}$ and [ES] cannot be measured directly and, for this reason, an alternative equation is needed.

The initial velocity of the reaction can be stated in terms of the production of the complex ES in the first step of the mechanism:

$$\frac{d[ES]}{dt} = k_{+1}([E_T] - [ES])[S] \tag{a5.6.3}$$

Even when the complex ES can also be formed from E and P by the reverse reaction in the second step of the mechanism, this contribution is neglected because in the beginning of the reaction the concentration of the substrate is very high and the concentration of the product is very low.

The initial velocity of the reaction can also be expressed in terms of the consumption of the complex ES in the reverse reaction of the first step and the direct or forward reaction in the second step.

$$-\frac{d[ES]}{dt} = k_{-1}[ES] + k_{+2}[ES] \tag{a5.6.4}$$

At equilibrium, the formation velocity and dissociation velocity of the complex ES are equal. From this equilibrium condition, the Michaelis-Menten constant, $K_M$, can be obtained:

$$k_{+1}([E_T] - [ES])[S] = k_{-1}[ES] + k_{+2}[ES] \tag{a5.6.5}$$

$$\frac{([E_T] - [ES])[S]}{[ES]} = \frac{k_{-1} + k_{+2}}{k_{+1}} = K_M \tag{a5.6.6}$$

Equation a1.6 can be solved for the concentration of the complex ES. In this way, the concentration [ES] is expressed as a function of the total concentration of the enzyme, the concentration of the substrate and the Michaelis-Menten constant:

$$[ES] = \frac{[E_T][S]}{K_M + [S]} \tag{a5.6.7}$$

Combination of equations a1.2 and a1.7 gives:

$$v_0 = k_{+2} \frac{[E_T][S]}{K_M + [S]} \tag{a5.6.8}$$

Since the concentration of the substrate is relatively high, the enzyme may saturate, that is, the entire enzyme is found in the form of the complex ES. When this happens the maximum velocity is attained:

$$v_{max} = k_{+2}[E_T] \tag{a5.6.9}$$

Therefore, the initial velocity can be expressed as a function of measurable quantities (without the constant $k_{+2}$):

$$v_0 = \frac{V_{max}[S]}{K_M + [S]} \qquad\qquad\qquad (a5.6.10)$$

This is the Michaelis-Menten equation [9]. It can be observed from equation a1.10 that the Michaelis-Menten constant is equal to the concentration of the substrate when the initial velocity is half the maximum velocity.

## Appendix 5.7. Mechanism of Glucose Enzymatic Oxidation

The reaction mechanism proposed by Cardosi [10] is shown in figure a5.7.1. The reaction cycle starts with glucose oxidase, GOx, in its oxidized form (structure I). The first result of the interaction with the glucose substrate is the formation of the enzyme-substrate complex (structure II). Next, a transfer of hydrogen ions and electrons produces the reduction of the cofactor FAD to $FADH_2$, and the oxidation of glucose to gluconolactone, that is transformed instantaneously into gluconic acid. The just reduced enzyme (structure III) cannot react with oxygen. The glucose substrate itself activates the reduced enzyme for reoxidation. In this step the glucose substrate is not modified, it only causes a conformational change of the enzyme. The active reduced enzyme (structure IV) reacts very fast with molecular oxygen producing a group addition to carbon 4a of FAD (structure V). The same group is released as hydrogen peroxide from the enzyme structure and the enzyme returns to the active oxidized state. The structural changes of the coenzyme FAD are summarized in Figure a5.7.2.
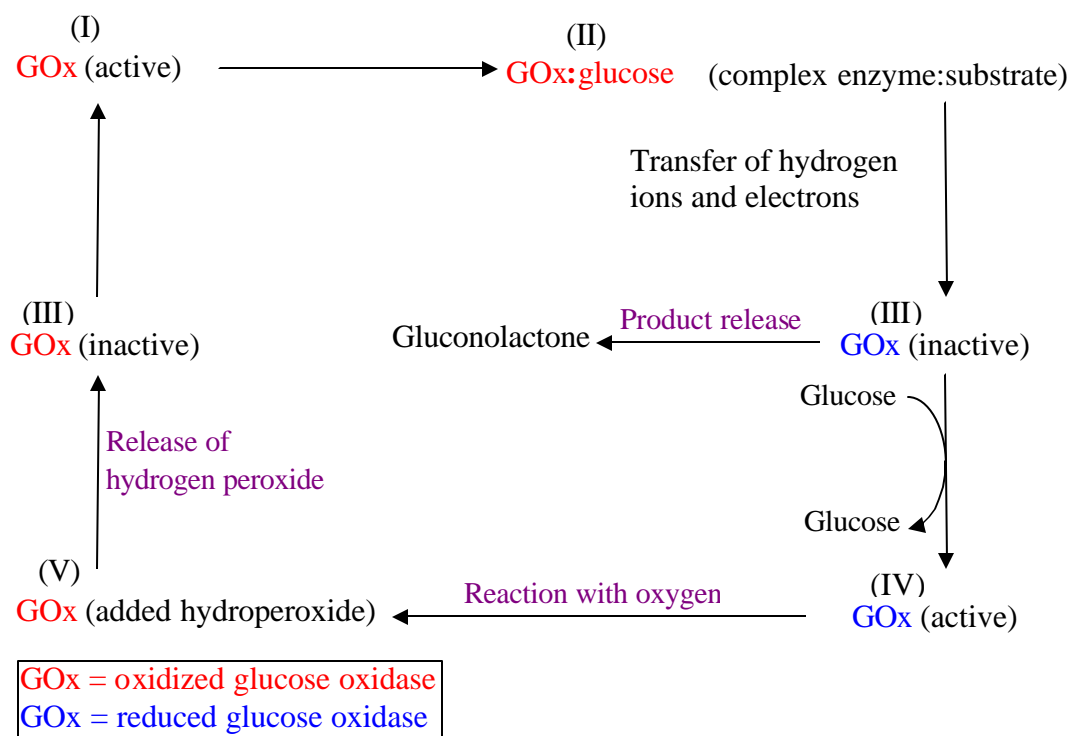


**Figure a5.7.1. Glucose Oxidation Mechanism in Presence of Glucose Oxidase and Oxygen.** Adapted from [10].

81
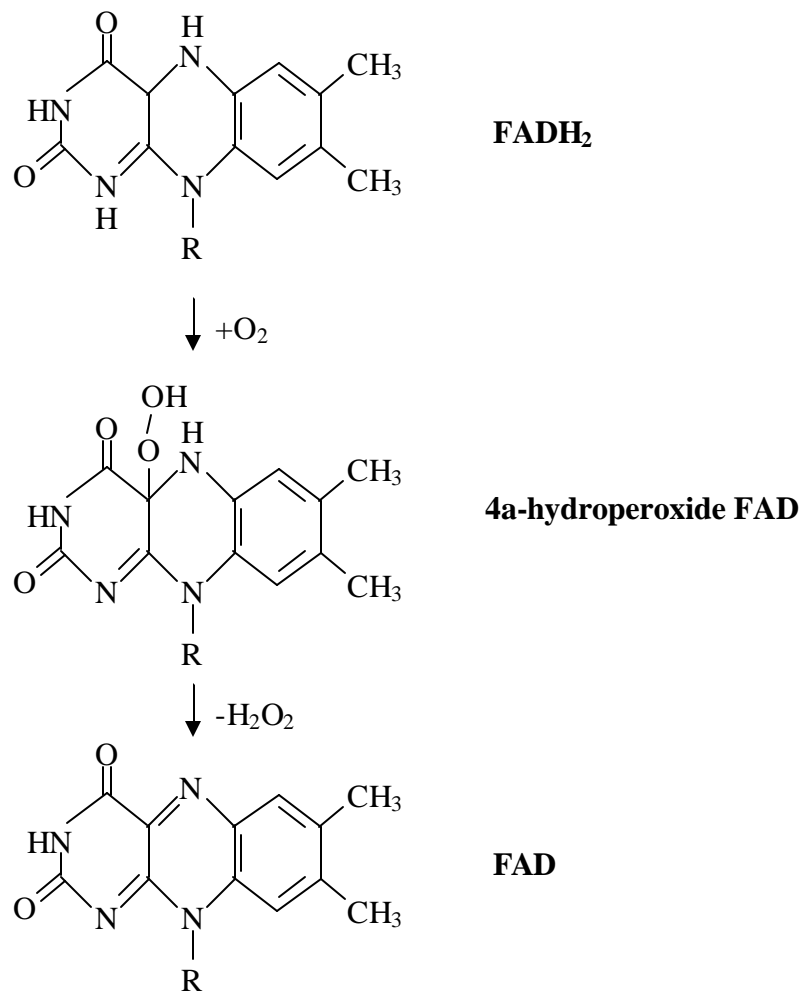
**Figure a5.7.2. Structural Changes of FAD during Glucose Oxidation.** Adapted from [10].

**Appendix 5.8.  Mechanism of Enzymatic Decomposition of Hydrogen Peroxide**

The heme group of a catalase monomer consists of a protoporphyrin ring (four pyrrole rings linked by methane bridges), a central iron atom, two vinyl groups and two propionate side chains as shown in figure a5.8.1.

Hydrogen peroxide molecules reach the embedded heme groups through funnel-shaped channels.  The residues forming these channels as well as the heme cavities or pockets are hydrophobic, except for some that are thought to participate in the substrate binding and scission.  In a heme cavity, the hydrogen peroxide may interact with His[74] (histidine residue with amino basic group) and Asn[147] (asparagine residue with amide group).  These residues perform as mediators for the transfer of protons.  First, the mentioned residues allow for the elongation of the oxygen-oxygen bond in a hydrogen peroxide molecule, which breaks as a proton is transferred from one oxygen to the other, and the deprotonated oxygen atom is coordinated with the iron center.  A second hydrogen peroxide reacts similarly, but the fracture of the oxygen-oxygen bond this time recovers the original state of the iron center of the enzyme.  This mechanism is shown in the scheme of Figure a5.8.2.  The Tyr[357] residue (tyrosine with a hydroxyl group) may aid in the oxidation of the iron ion and the fast stabilization of the inherent heme radical (by elimination of the radical electron).  Figure a5.8.3 emphasizes the active components in the catalase reaction.
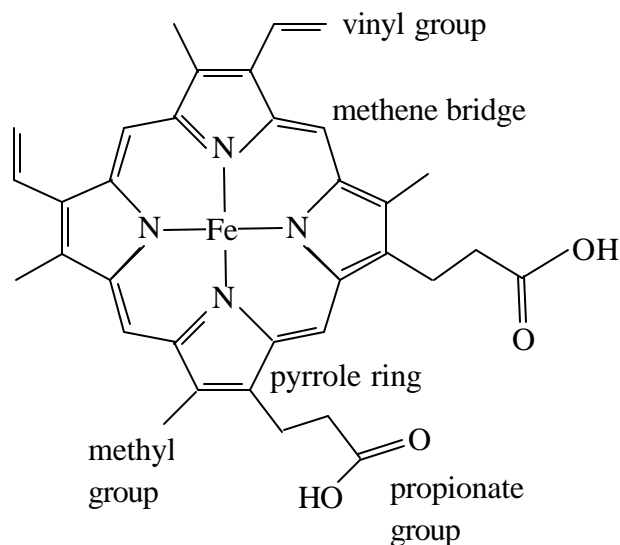


**Figure a5.8.1. Heme prosthetic group of catalase.**
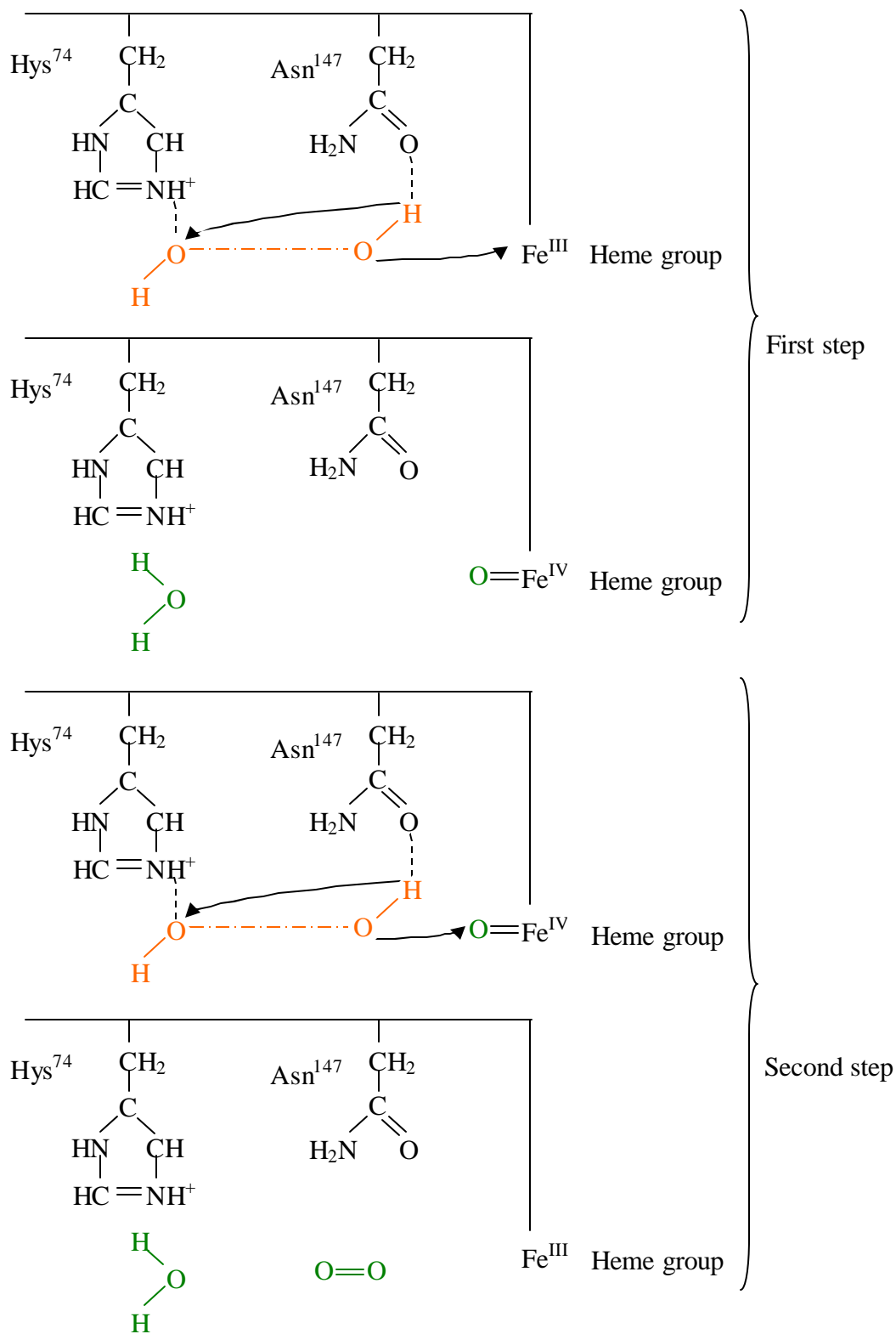
**Figure a5.8.2. Mechanism of Hydrogen Peroxide Decomposition in Presence of Catalase.** The scheme shows that the interaction with the hydrogen peroxide promotes iron oxidation followed by iron reduction.

84
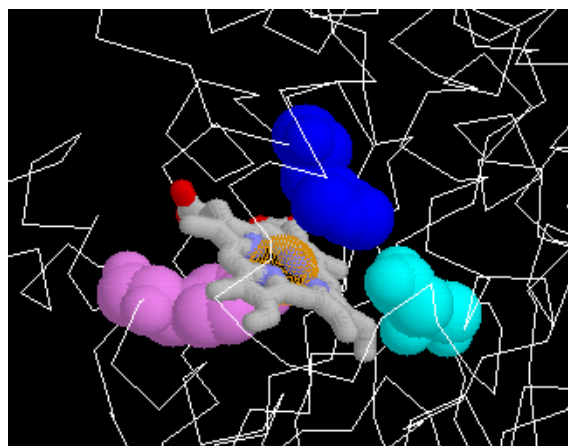
**Figure a5.8.3. Interaction of catalase active site with $H_2O_2$ substrate.** $His^{74}$ (blue), $Asn^{147}$ (cyan), $Tyr^{357}$ (violet), heme group (grey), $H_2O_2$ (orange).

**Appendix 5.9.  Glucose Responsiveness Equilibrium Experiments Protocol**

*Equilibrium under different glucose concentrations*

1. Glucose solutions of 100, 150 and 200 mg/dL are prepared using deionized water and D-glucose (Aldrich).

2.  Three disc samples cut from a recently washed film under refrigeration are weighed in air.

 3.  Each hydrogel sample is set in a solution of different glucose concentration (100, 150 and 200 mg/dL) in a water bath at 37°C.  In all cases, solution volumes of 6 mL are managed for a consistent base of comparison with other glucose responsiveness experiments.

4. The equilibrium weight of the samples is measured in air after 24 hours of exposure to glucose containing solutions.

5. The samples are dried at room temperature to get the dry weight.

6. Hydrogel volume values are obtained from experimental correlations of weights in air and in heptane.

## 6. Dynamic Characterization

The transient response of the P(MAA-g-EG) hydrogel before chemical changes in the environment was explored. This chapter presents the dynamic characterization of hydrogel membranes in terms of sensitivities and time constants, syneresis pore formation, reaction rate constant for the enzymatic reaction system, diffusivities for the solutes of interest (glucose, hydrogen ions and insulin), and insulin release studies.

## 6.1. Dynamic Swelling Experiments

### 6.1.1. Fundamentals

Hydrogels are considered as ***single input - single output*** systems for their dynamic analysis. The input variable is defined as an external variable that can be manipulated to produce a change in the system. The output variable signs the effected change or response of the system to the input. The input and output variables are chosen according to type of system and the objective of the study. For different hydrogel systems and purposes the *input* may be *temperature, concentration, stress or strain*, and the *output* could be *volume, weight, solvent fraction, strain or stress*. In this section, the input of the P(MAA-g-EG) is the pH and the output is the volume swelling ratio.

The response of the hydrogels as dynamic systems can be tested by oscillatory and step experiments. The oscillatory experiment consists in the application of pH changes in the form of pulses with constant amplitude and duration and alternating direction. In a step experiment, the hydrogel has an initial constant swelling ratio, the pH is changed in an instant and the output is allowed to reach a new steady state. Both experiments serve for a comparison of the swelling and contraction response.

The time response of the hydrogels before pH changes is characterized through two parameters: gain or sensitivity and time constant or relaxation time. These parameters are calculated from the transitory swelling response of the hydrogel to a pH step input. In a small pH range, the dynamic behavior can be represented by a linear first order ordinary differential equation [1]:

$$\tau \frac{dQ(t)}{dt} + Q(t) = K \, pH(t), \tag{1}$$

where $\tau$ is the time constant and K is the gain or sensitivity.

When an abrupt change of I units of pH is applied at t=0, the solution of Equation (1) is:

$$\overline{Q}(t) = K \, I \left[ 1 - \exp\left( -\frac{t}{\tau} \right) \right], \tag{2}$$

where $\overline{Q}$ is the change of the swelling ratio with respect to the initial state.

The gain parameter can be calculated as the final change of the swelling ratio over the magnitude of the pH input [1], as can be derived from Equation (2) when time tends to infinite:

$$K = \frac{\overline{Q}(t \to \infty)}{I} = \frac{Q(t \to \infty) - Q(t = 0)}{I} .$$  (3)

From the rearrangement of Equation (2), the inverse of the time constant is the magnitude of the slope of the curve of the natural logarithm of 1 minus the fraction of swelling ratio change with respect to time:

$$ln\left(1 - \frac{\overline{Q}(t)}{KI}\right) = -\frac{t}{\tau} .$$  (4)

The slope of the function (4) can be evaluated at initial times, but the swelling ratio at of the end of experiment is necessary [1].

The time constant can also be determined as the time when the swelling ratio has reached the 63% of the total change [1], as suggested by the evaluation of Equation (1) in t=τ:

$$\overline{Q}(t = \tau) = 0.632K\,I .$$  (5)

The time constant can be also referred as a relaxation time of the hydrogel, since it indicates how fast the material relaxes adopting a new volume when the pH of the environment varies. The gain or sensitivity may be interpreted as a three-dimensional mechanochemical compliance to relate the volume change (expressed in terms of the volume swelling ratio, Q), not a theoretical characteristic length, to a pH change.

### 6.1.2. Experimental Work

For the oscillatory experiment, a hydrogel sample was previously immersed in a pH 3.2 buffer solution for a minimum of 24 hours at 37°C to determine the initial volume swelling ratio at equilibrium. The pH pulses were applied from 3.2 to 7 with 45 minutes of duration at the same temperature. At time zero, the sample was changed to a pH 7 buffer solution. After 45 minutes, the sample was set in a pH 3.2 buffer solution to complete a cycle of 90 minutes. The sample was weighed in air and heptane every 5 minutes. This cycle was repeated two more times with the same sample. The complete 270 minute experiment was performed with three different disc samples. Appendix A6.1 details the protocol for an oscillatory experiment.

Step inputs were proposed in the same pH range of the oscillatory tests. A step experiment requires the sample to have a steady volume before the pH change is applied.

The weight of the sample in air and in heptane was monitored constantly during the first 8 hours to capture two thirds of the transitory response approximately. The final measurements were done 24 hours from the start of the experiment to determine the new steady sate volume swelling ratio, which corresponded to the initial condition for the next step. The magnitude of the steps was small (compared to the magnitude of the pH pulses in the oscillatory experiment) to support the linearity assumption of Equation (1). The data in the last third part of the time response, except for the final steady condition, is not necessary to evaluate the initial slope of the linear fit proposed by Equation (4). The procedure of the step experiment is documented in Appendix A6.2.

## 6.1.3. Results and Discussion

The behavior of the hydrogel material in the oscillatory experiment is shown in Figure 6.1.1. The volume swelling ratio of the hydrogel did not oscillate around a constant mean value, that is, the response was biased in the direction of the change induced by the pH different from the initial equilibrium condition. In this case, the equilibrium was disturbed by an increment in pH that caused an augment in the disc volume, and the oscillation of the response had an ascending tendency. The duration of the pulse was not enough to stabilize the response or to observe a hysteresis effect. However, the experiment gave evidence of non-linearity and velocities of expansion and contraction of the hydrogel. The swelling process showed a constant slope in the corresponding half cycles or positive pulses. The magnitude of the slope of swelling was smaller than the magnitude of the initial contraction slope. The contraction or syneresis process produced slope variations of an exponential trajectory in time during the negative pulse. Although the inertia of the volume change was manifested in the bias of the response, a dead time effect was not detected when the pH variable changed direction. The mesh size of the polymer was calculated during the oscillatory experiments and showed gradual but significant changes from the initial equilibrium value.

The sequence of step experiments in the range from 3.2 to 7 is presented in Figure 6.1.2. The steady states in the ascending subsequence of steps were not repeated in the descending subsequence, which indicates hysteresis in the response of the material. The non-linear behavior is also denoted by the different dynamic parameters obtained from each experiment in a specific operation range. The gain and time constant parameters can be compared in Table 6.1.1.

The critical pH or transition pH is also detected from the sequence of step experiments by distinctive features of the response summarized in Table 6.1.1. For the case of the anionic gel under experimentation, the critical pH is 5.6. The hydrogel showed the highest sensitivity when the pH was close to this value. Around the critical pH, the contraction response was faster than the swelling response, while the opposite occurred in other operations zones.
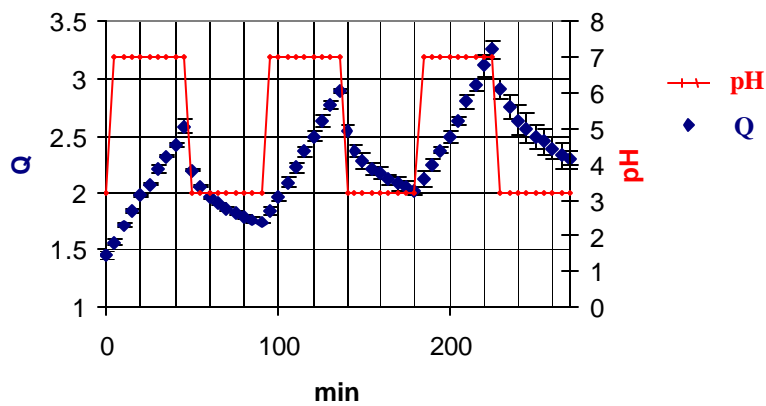
(a)
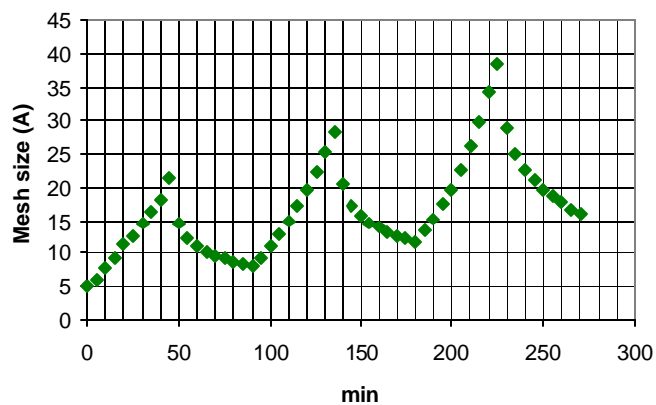


(b)

**Figure 6.1.1. Oscillatory Experiment.** (a) Volume swelling ratio. (b) Mesh size calculations. Hydrogel samples from a film prepared according to synthesis 1 (using TEGDMA and no excess of solvent).
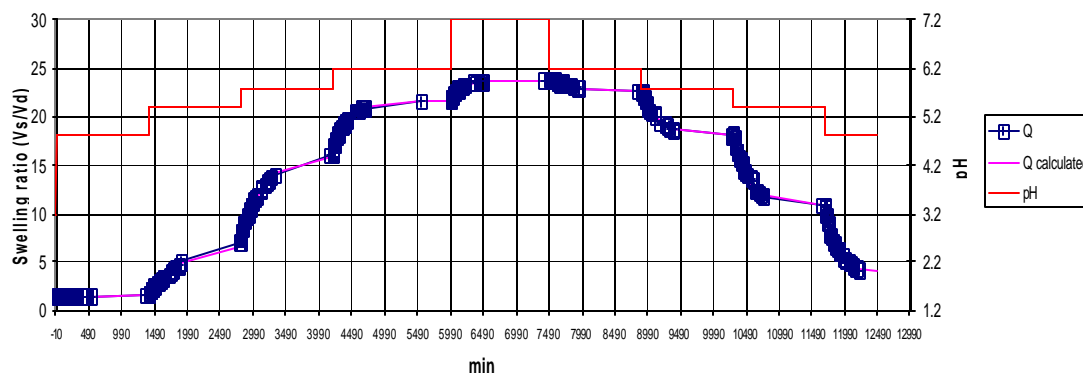
**Figure 6.1.2. Step Experiments.** A P(MAA-g-EG) hydrogel disc (synthesis 3, with excess of solvent, PEGDMA and enzymes) subjected to a sequence of pH step experiments show differences in the volume response.

**Table 6.1.1. Parameters for Swelling Behavior Model of P(MAA-g-EG) Hydrogel.** The parameters are obtained from experiments shown in Figure 6.1.2.

| pH range and change direction | 3D Mechanochemical Compliance | Relaxation Time (min) |
|---|---|---|
| 3.2 to 4.8 | 0.15 | 625 |
| 4.8 to 5.4 | 8.96 | 588 |
| 5.4 to 4.8 | 11.46 | 170 |
| 5.4 to 5.8 | 22.46 | 333 |
| 5.8 to 5.4 | 17.75 | 238 |
| 5.8 to 6.2 | 13.92 | 222 |
| 6.2 to 5.8 | 11.63 | 256 |
| 6.2 to 7.2 | 2.12 | 167 |
| 7.2 to 6.2 | 1.32 | 357 |

## 6.2. Syneresis Pore Formation

### 6.2.1. Fundamentals

Non-uniform contraction of a material may cause the formation of pores. This phenomenon is observed clearly in the cracking caused by the drying process in ceramic and gel materials [2]. The loss of liquid volume during drying can produce an unequal loss of the total volume of the sample. This happens when part of the lost liquid is not expelled due to the shrinkage but for evaporation leaving an empty volume. A similar effect may take place when a hydrogel shrinks in response to a pH change.

A fast contraction of a hydrogel can produce the lack of uniformity in volume change that leads to residual stress forces and formation of macropores (Figure 6.2.1). Such macropores would ease the release of a preloaded drug in the material. In this way, the anionic glucose sensitive hydrogel would effectively deliver insulin upon contraction caused by the oxidation of glucose at a high concentration in the medium.

Visible volume decrements in hydrogel membranes are evidence of the loss of water by shrinkage, however, macropores may also be formed. In order to determine if pore formation takes place in the fabricated materials, the analysis proposed by Chakrabarti et al [2] is applied. The parameter $\alpha$ is defined as a function of the change of total volume of the sample, $V$, with respect to the change of volume fraction of the absorbed solvent, $\upsilon_1$:

$$\alpha = \frac{1}{V}\frac{dV}{d\upsilon_1},\tag{6}$$

where

$$d\upsilon_1 = \begin{cases} (1/V)(1-\upsilon_1)dV, & \text{when } dV = dV_L \\ dV_L/V, & \text{when } dV = 0 \end{cases},\tag{7}$$

and $V_L$ is the volume of the solvent inside the gel. For the case of water loss exclusively by shrinkage ($dV=dV_L$):

$$\frac{1}{V}\frac{dV}{d\upsilon_1} = \frac{d\ln V}{d\upsilon_1} = \frac{1}{1-\upsilon_1} = \frac{-d\ln(1-\upsilon_1)}{d\upsilon_1}.\tag{8}$$

Integration of (8) gives:

$$-\ln\left(\frac{V}{V_0}\right) = \ln\left(\frac{1-\upsilon_1}{1-\upsilon_{1,0}}\right)\tag{9}$$

where $V_0$ and $\upsilon_{1,0}$ are the total volume and the solvent volume fraction before contraction. The plot of $-\ln(V/V_0)$ with respect to $\ln((1-\upsilon_1)/(1-\upsilon_{1,0}))$ has a slope of unity if no macropores are formed in the contraction process.

### 6.2.2. Experimental Work

The previously presented dynamic swelling experiment consisting in a series of pH steps provides information of the shrinking process when pH is decreased. The volume of a dry P(MAA-g-EG) membrane was determined before the sequence of step experiments. In each descending pH step, the membrane initially at equilibrium in a high pH solution was changed to a low pH solution until the new equilibrium state was reached. The transitory volume response was obtained from weight measurements.

The total volume of the sample, V, was calculated based on the displacement of a non-solvent liquid like heptane (as explained in Section 5.1):

$$V = \frac{1}{\rho_h}(W_a - W_h),\tag{10}$$

where $W_a$ is the weight of the sample in air, $W_h$ is the weight in heptane and $\rho_h$ is the density of heptane.

The volume of the solvent, $V_L$, was determined with:

$$V_L = \frac{1}{\rho_w}(W_{a,s} - W_{a,d}),\tag{11}$$

where $W_{a,s}$ is the weight of the swollen membrane in air, $W_{a,d}$ is the weight of the dry membrane in air, and $\rho_w$ is the density of the solvent considered approximately equal to the density of water.

Finally, the volume fraction of the solvent, resultant from evaluation of (11) over evaluation of (10), and the total volume data are fitted with Equation (9).

### 6.2.3. Results and Discussion

From the series of step pH inputs applied to a hydrogel membrane (Figure 6.1.2), those close to the critical pH correspond to a fast contraction or syneresis process (Table 6.1.1). The plots of $-\ln(V/V_0)$ with respect to $\ln((1-\upsilon_1)/(1-\upsilon_{1,0}))$ for the contraction in the pH ranges of 5.8 to 5.4 and 5.4 to 4.8 result in lines with a slope very close to unity (Figure 6.2.1). Therefore, the fabricated P(MAA-g-EG) membranes experience a uniform contraction without the formation of macropores.

The obtained results are not unexpected. Even when the selected operation zones of the membranes correspond to the fastest contraction processes observed, the velocity of the hydrogel response is characterized by large relaxation times. The significant lower relaxation times of a micro P(MAA-g-EG) hydrogel system would favor the production of pores, however the small volume would prevent the non-uniform contraction that causes it.

**(a)**  **(b)**
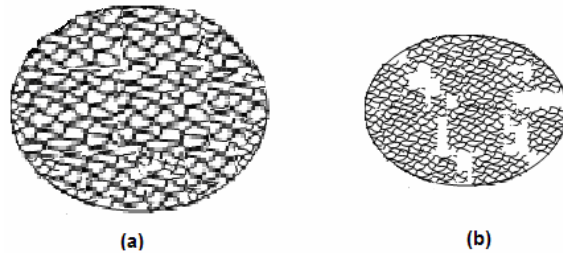
**Figure 6.2.1.   Pore Formation by the Syneresis of the Hydrogel**.    Non-uniform contraction may produce pores that would reduce the transport resistance through the gel. Two states of a hydrogel sample are represented: (a) swollen state, (b) contracted state with the formation of macropores which may interconnect.



**pH change: 5.8 to 5.4**          **pH change: 5.4 to 4.8**

$y = 1.0135x$
$R^2 = 1$

$y = 1.0069x$
$R^2 = 1$
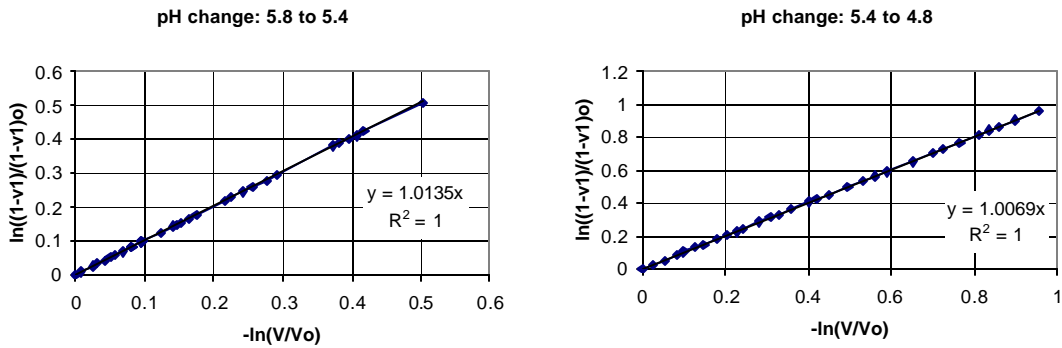
**Figure 6.2.2. Tests for Pore Formation in Different pH Ranges during Fast Contraction.**  Macropore formation by syneresis is negative for the fabricated P(MAA-g-EG) as indicated by the approximately unity slopes of the fitted lines.  Experimental points in the graphs are obtained from the response of the indicated pH steps presented in Figure (6.1.2).

## 6.3. Diffusion Coefficient Experiment

### 6.3.1. Fundamentals

The diffusion through the gel of different species of interest, like glucose, insulin and hydrogen ions, depends on the hydrodynamic radius, r, of the solute as well as on the degree of swelling of the membrane, Q. Diffusion coefficients, D, can be estimated as a fraction of the diffusion coefficient of the solute in pure water, $D_0$. Such fraction depends on the relative size of the solute with respect to the mesh size of the polymeric network and the relation of the volume of dry polymer with respect to the volume of solvent absorbed, as expressed in [3]:

$$D = D_0 \left(1 - \frac{r}{\xi}\right) e^{-\frac{1}{Q-1}}$$

(12)

where the argument of the exponential function can also be expressed in terms of volume fractions for the pure polymer ($\upsilon_2$) and the absorbed solvent ($\upsilon_1$) as: $-\upsilon_2/\upsilon_1$.

The Stokes-Einstein equation gives the hydrodynamic radius of a solute [3]:

$$r = \frac{k_B T}{6\pi\eta D_0}$$

(13)

where $k_B$ is the Boltzmann constant, T is the absolute physiological temperature and $\eta$ is the viscosity of the water at this temperature $(6.92 \times 10^{-4}$ Pa·s at 37°C, for example).

Alternatively, the diffusion coefficient can be determined experimentally using a diffusion cell [4]. A diffusion cell consists of two jacketed reservoirs with upper and lateral ports (Figure 6.3.1). The reservoirs are connected by their lateral ports placing a membrane between them. The reservoir designated as the donor is loaded through its upper port with a specific solute concentration solution. Similarly, the receptor reservoir is fed with a low solute concentration or solute free solution, in order to create a concentration gradient through the permeable membrane. Temperature can be controlled by circulating water through the jackets. Samples of the receptor solution can be extracted from the upper port of the corresponding compartment for analysis. The concentration data are fitted to the following equation to calculate the permeability of the solute [4]:

$$ln\left(1 - \frac{2c_t}{c_0}\right) = -\frac{2A}{V}Pt$$

(14)

where $c_t$ is the concentration of the solute in the receptor reservoir at time t, $c_0$ is the initial concentration on the donor side, V is the volume of a half cell, A is the transfer area, and P is the permeability coefficient that can be estimated from the slope of the logarithmic

function with respect to time. The partition coefficient of the solute is necessary to relate the permeability with the diffusion coefficient. A partition experiment consists on immersing a membrane in a solution with a certain initial concentration, $c_i$, of the solute. The final steady state concentration $c_f$, in the solution is determined to do the following calculation [4]:

$$K_d = \left( \frac{V_{sol}(c_i - c_f)}{V_m} \right) \left( \frac{1}{c_f} \right),$$

(15)

where $V_m$ is the volume of the membrane, $V_{sol}$ is the volume of the solution, the first factor constitutes the concentration of the solute in the membrane, and the partition coefficient $k_d$ is the ratio of the concentration of the solute in the membrane over the concentration in the solution. The diffusion coefficient, D, is:

$$D = \frac{P}{k_d} b,$$

(16)

where b is the thickness of the membrane [4].

### 6.3.2. Experimental Work

Mass transport studies were carried out in a diffusion cell. The experimental set up for the diffusion experiment is shown in Figure 6.3.1. The donor and receptor compartments were interfaced by a hydrogel membrane. The membrane was a disc cut with 10 mm in diameter from a 1.3 mm thick film pre-equilibrated at pH 7. The gel was synthesized with excess of solvent, TEGDMA as a crosslinking agent (synthesis 2 in Table 5.1.1) and without enzymes.

The membrane was exposed to an insulin concentration gradient in the diffusion cell at 37°C. The donor cell was loaded with a pH 7, 50 mg/mL insulin solution, and the receptor cell was charged with pH 7 insulin free PBS buffer. In the preparation of the donor solution, 0.1 N HCl was added to a PBS in order to dissolve the insulin; after insulin dissolution, the pH was recovered by neutralizing the acid with 0.1 N NaOH. A peristaltic pump was used to pump water at 37°C from a temperature controlled water bath to the circulation system of the cell. The pH and the temperature conditions of the experiment aimed to reproduce the basic physiological environment for an implanted hydrogel device.

The diffusion coefficient of insulin through the hydrogel film required monitoring the concentration of the receptor cell along time and also at equilibrium. Standard solutions were prepared by dilutions of the pH 7, 50 mg/mL insulin solution initially loaded in the donor cell. The collected 0.2 mL samples from the experiment and the standard solutions were analyzed in a HPLC (High Pressure Liquid Chromatography) system, to determine the insulin concentration in the receptor cell. Appendix A6.3 shows the protocol for the diffusion experiment.

### 6.3.3. Results and Discussion

At a pH of 7 and 37°C, the diffusion coefficient for insulin through a film synthesized with TEGDMA and excess of solvent (synthesis 2) was determined in a diffusion cell experiment as $1 \times 10^{-10}$ m$^2$/s (experimental data are shown in Figure 6.3.2). Insulin has a diffusion coefficient in water of $2 \times 10^{-10}$ m$^2$/s [5]. The hydrogel film under the mentioned pH and temperature conditions had an equilibrium volume swelling ratio of 23.93 and a mesh size of 416 Å, which gives a Stokes ratio of 16.4 Å and a theoretical diffusion coefficient of $1.86 \times 10^{-10}$ m$^2$/s. Therefore, the calculations of diffusivities with Equation (12) show agreement with those that can be obtain from a diffusion experiment and Equation (16), in spite of experimental errors.

The approximation between both calculations supports the decision to use Stocks law in combination with the experimental volume swelling ratio as a more flexible and practical method for the estimation of diffusion coefficients. In contrast with insulin, glucose and hydrogen ion diffusion coefficients are more difficult to obtain more directly by the diffusion cell experiment and the use of analytical measurements because of solute size differences. The alternative use of Equation (12), on the other hand, avoids these difficulties by considering the experimental volume swelling ratio of the gel and the theoretical hydrodynamic radius of the solute of interest. Equation (12) is conveniently used for the determination of diffusion coefficients for smaller species such as glucose and hydrogen ions (Table 6.3.1 shows parameters to estimate the diffusion coefficient through the gel with Equation (12); diffusivity coefficients in water reported in [6] are used in this work).
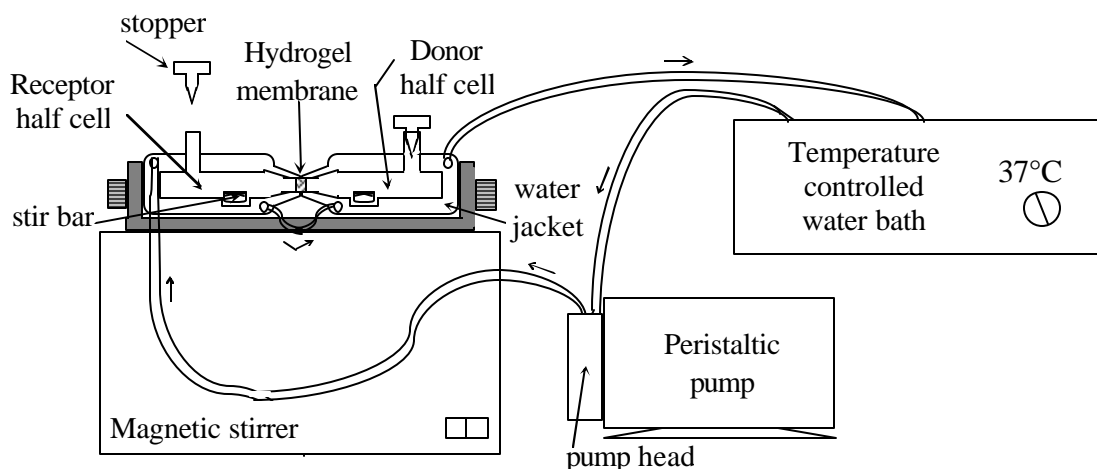
**Figure 6.3.1. Set Up of Diffusion Experiment.** A closed circuit of heating water maintains the temperature of the experiment at 37°C. Continuous mixing allows for homogeneous concentration in each side of the cell. Stoppers prevent evaporation. Samples are collected on the receptor side for quantification of the solute of interest.
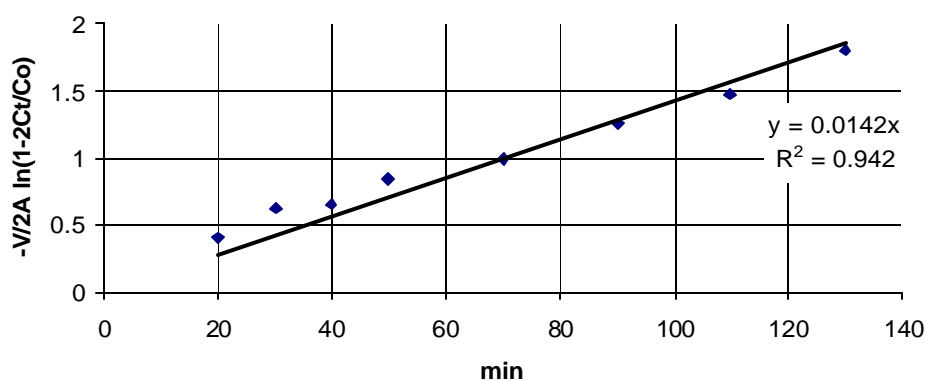


**Figure 6.3.2. Permeability and Diffusion Coefficient of Insulin through a P(MAA-g-EG) Membrane.** The slope of the shown curve from a diffusion cell experiment is the permeability, from which the diffusion coefficient is calculated.

**Table 6.3.1. Diffusion Coefficients in Water and Hydrodynamic Radius of Glucose, Hydrogen Ions and Insulin.** Diffusivities in water are taken from different sources and the hydrodynamic radii are calculated with the Stocks law at 37°C.

| Solute | Diffusivity in water, $D_0$, m$^2$/s | Hydrodynamic radius, r, Å |
|---|---|---|
| Hydrogen ion | $5.85 \times 10^{-9}$, [6] | 0.551 |
| | $5 \times 10^{-10}$, [7] | 6.56 |
| Glucose | $6.9 \times 10^{-10}$, [6] | 4.76 |
| | $9.1 \times 10^{-10}$, [5] | 3.61 |
| Insulin | $1.47 \times 10^{-11}$, [6] | 223 |
| | $2 \times 10^{-10}$, [5] | 16.4 |

98

## 6.4. Glucose Responsive Swelling

### 6.4.1. Fundamentals

Glucose responsiveness is coupled to the pH sensitivity of the hydrogel. Hydrogen concentration in the gel is affected by the ionic dissociation of gluconic acid, which results from the oxidation of glucose by the enzymatic reaction system. The set of reactions that leads to a glucose responsive swelling is presented in Figure 6.4.1. Transitory hydrogel volume changes during the course of the reactions are studied to determine the glucose sensitivity of the system.

The glucose oxidase selectively oxidizes β-D-glucose according to the following reaction [10]:

$$C_6H_{12}O_6 + O_2 \xrightarrow{\text{glucose oxidase}} C_6H_{10}O_6 + H_2O_2 \qquad (17)$$
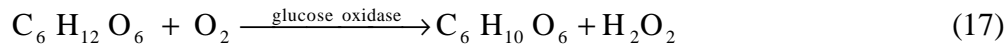
The velocity of reaction (17) depends on the pH. The reaction in solution is very slow at a pH of 3 and relatively faster at pH 8 with a half life of 10 minutes [8]. While the glucose substrate is oxidized, the enzyme cofactor is reduced. Therefore, the glucose oxidase needs to be reactivated by the reoxidation of its cofactor through oxygen or an electron shuttle. The latter is normally toxic.

The D-glucono-1,5-lactone hydrolyzes spontaneously to form gluconic acid [10]:

$$C_6H_{10}O_6 + H_2O \rightarrow C_6H_{12}O_7 \qquad (18)$$

The gluconic acid dissociates affecting the pH of the medium:

$$CH_2(OH)[CH(OH)]_4C(O)OH \xleftarrow{K_a} H^+ + CH_2(OH)[CH(OH)]_4C(O)O^-, \quad (19)$$
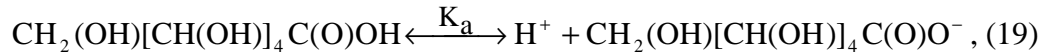
where $K_a$ is the dissociation constant, often expressed as $pK_a$ or the base-10 logarithm of the inverse of $K_a$, that correlates the equilibrium concentrations:

$$K_a = \frac{[H^+][C_5H_{11}O_5COO^-]}{[C_6H_{12}O_7]}. \qquad (20)$$

The catalase breaks the hydrogen peroxide recovering oxygen for the regeneration of glucose oxidase (Section 5.3):

$$2\,H_2O_2 \ ? \ \ 2\,H_2O + O_2 \qquad (21)$$

From the set of reactions previously described, the oxidation of glucose is considered as the dominant step. Assuming a first order dynamics, where the limiting reactant is glucose, the rate of reaction can be expressed as:

$$\frac{d[G]}{dt} = -k[G], \tag{22}$$

where [G] is the concentration of glucose and k is the reaction rate constant. Indirect quantification of glucose consumption by pH measurements in time can be used to estimate the kinetic constant k.

### 6.4.2. Experimental Work

Hydrogel disc samples were cut from a film synthesized with glucose oxidase and catalase enzymes, PEGDMA-1000 and excess of solvent. The samples were washed and stored in deionized water inside a refrigerator. The response before glucose was tested within 48 hours after the synthesis to count with active enzymes.

The glucose responsive swelling experiments were carried out in the absence of NaCl, since strong ions may slow the response of the material [9]. Glucose test solutions were prepared with deionized water, instead of a buffer, in order to observe the pH changes due to the gluconic acid production. For the same reason, small volumes of glucose solutions were used and monitored with a pH meter with a thin electrode. Each sample was dried at the end of the experiment to obtain the reference volume or volume of the dry sample for the calculation of swelling ratios.

An oscillatory experiment at 37°C was proposed to test glucose responsiveness. The sample was changed from deionized water to a 200 mg/dL glucose solution, where it stayed for 45 minutes. Then the sample was put into a 100 mg/dL glucose solution for other 45 minutes. The glucose solutions were alternated other three times after periods of 45 minutes. After the last pulse at 200 mg/dL, at time 225 min, the sample was immersed in deionized water for the last 45 min of the experiment (Figure 6.4.2). The weight was measured each 5 minutes.

The response of the hydrogel was also examined with step inputs in glucose concentration. The weight of the sample was chosen as the output for one step experiment at 37°C (Figure 6.4.4). For a second step input applied at room temperature, the output was the pH of the medium of the hydrogel (Figure 6.4.5). The data from the latter experiments was helpful to determine a reaction rate constant for the enzymatic process taking place inside the material. Appendix 6.4 contains the protocol for oscillatory and step glucose responsive experiments.

### 6.4.3. Results and Discussion

In the oscillatory experiment (Figure 6.4.2), the change from deionized water to 200 mg/dL glucose solution caused the volume of the hydrogel to decrease from the steady equilibrium value. This was the expected behavior since the produced gluconic acid decreases the pH of the environment of the hydrogel. However, the tendency of the size of

the hydrogel was not reversed in spite of the decrement of 100 mg/dL in glucose concentration in the medium.  The volume of the hydrogel kept decreasing at the same rate approximately during the next three pulses.  After 30 min from the last change, from 200 mg/dL glucose solution to deionized water, the gel started increasing its size.

The observation of a continued contraction of the gel when the glucose concentration changed from 200 to 100 mg/dL, indicates that the glucose was still present in enough quantity to continue the enzymatic reaction at the same rate.  Therefore, the gel sample was not sensitive to the magnitude and duration of this pulse.  Contrarily, when the glucose concentration was lowered from 200 to 0 mg/dL (deionized water), the diffusion of glucose inside the gel stopped and the pH increased, causing the volume of the sample to augment.  However, the initial volume and weight were no recovered after more than 15 hours from the return to deionized water, which indicates that some gluconic acid may have remained trapped and given an internal pH different from the external pH.

The Donnan equilibrium effect can also explain the continued contraction of the hydrogel in spite of the reduction of the glucose concentration to which the sample was exposed.   The hydrogel-environment interface can be considered as a semipermeable membrane.  The impermeable species would be the fixed anionic functional groups in the backbone of the polymer, and the hydrogen and gluconate ions would be the permeable species.  The charge of the anionic carboxylic pending groups determine the distribution of hydrogen counterions forming an electric double layer and the repulsion of permeable gluconate co-ions.  In this way the concentration of hydrogen ions inside the gel tends to be higher than the exterior hydrogen concentration, which promotes a relatively low local pH regardless of the glucose concentration in the environment (Figure 6.4.3).

The step experiment of Figure 6.4.4 shows the response to a single change in glucose concentration from 0 (deionized water) to 200 mg/dL.  The weight of the sample decreased monotonically in this case.  The total decrement in volume swelling ratio with respect to the initial value was 20%, while in the previous oscillatory experiment was 24%.  The renewal of the solution each 45 minutes removed produced gluconic acid and may in this way have promoted more effectively the internal reaction achieving a bigger volume reduction with a more pronounced initial slope compared to the step response.

Another glucose step was applied to observe the pH of the environment of the hydrogel sample.  The sample initially at equilibrium in deionized water was changed to a 6 mL, 200 mg/dL glucose solution at room temperature. The pH showed an exponential decrease (Figure 6.4.5) as expected.   The pH of the surrounding solution experimented a total change of 12% or the initial value.

The pH of the environment of the hydrogel sample in response to a glucose concentration step change in the previous experiment (Figure 6.4.5), provided information to determine a reaction rate constant for the enzymatic reaction under the conditions of the hydrogel system.  The hydrogen ion concentration in the local environment of the gel was due to the chemical dissociation of water and part of the produced gluconic acid.  The excess of proton concentration at the initial pH of 6.6 quantifies the dissociated gluconic acid, which is equivalent to the hydrogen and gluconate ions produced:

$$[\text{Gluconc acid}]_{\text{dissociated}} = [H^+]^{\text{from}}_{\substack{\text{gluconic}\\\text{acid}}} = [\text{Gluconate}^-] = 10^{-pH} - 10^{-6.6}. \qquad (23)$$

The $pK_a$ of gluconic acid (3.7) is used to determine the molar concentration of undissociated gluconic acid during the reaction:

$$[\text{Gluconc acid}]_{\text{undissociated}} = \frac{[H^+]^{\text{from}}_{\substack{\text{gluconic}\\\text{acid}}}[\text{Gluconate}^-]}{K_a}. \qquad (24)$$

The sum of dissociated and undissociated gluconic acid gives the total reacted glucose (Figure 6.4.6), since there is a 1 to 1 stoichiometric relation of glucose to gluconic acid in the enzymatic reaction, assuming that the D-glucono-1,5-lactone is completely and instantaneously hydrolyzed to gluconic acid:

$$[\text{Glucose}]_{\text{consumed}} = [\text{Gluconic acid}]_{\text{dissociated}} + [\text{Gluconic acid}]_{\text{undissociated}}. \qquad (25)$$

The rate of glucose reaction (Figure 6.4.7) is obtained by the time derivation of the consumed glucose:

$$V = \frac{d[\text{Glucose}]_{\text{consumed}}}{dt}. \qquad (26)$$

The inflection point that can be noticed in the curve of Figure 6.4.6, leads to a velocity profile with an early maximum shown in Figure 6.4.7, that is, the initial velocity is not the highest in spite of the highest glucose concentration in solution due to the delay of the diffusion process through the membrane.  Finally, the glucose concentration during the reaction is determined by subtracting the reacted glucose from the total glucose:

$$[\text{Glucose}] = [\text{Glucose}]_{\text{initial}} - [\text{Glucose}]_{\text{consumed}}. \qquad (27)$$

A plot of velocity of reaction with respect to the concentration of the glucose substrate (Figure 6.4.8), disregarding the initial raise of velocity, allows for the determination of an average reaction rate constant k of 0.008 min$^{-1}$.  This constant is specific for the enzymatic reaction system in the hydrogel and differs from the constant of the glucose oxidase reaction in solution [9].
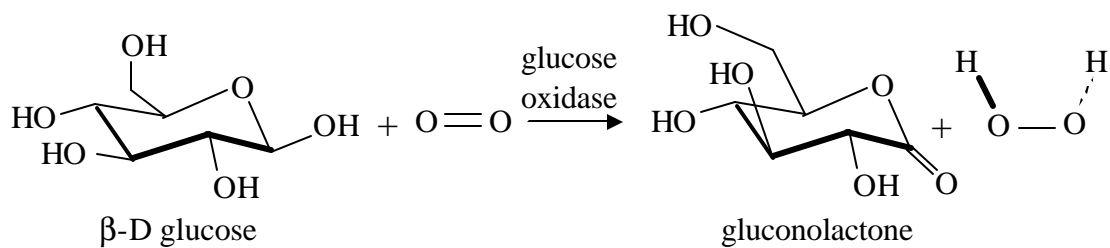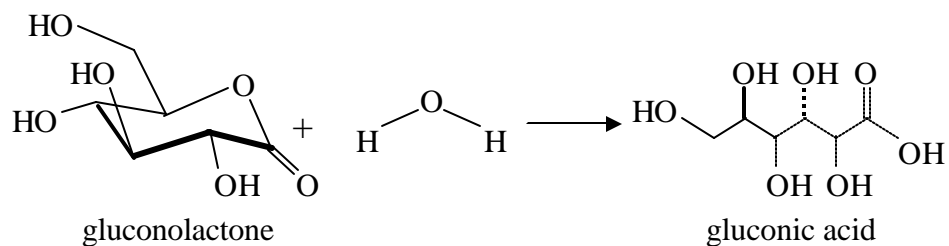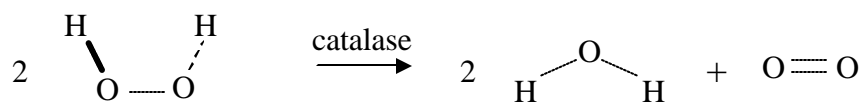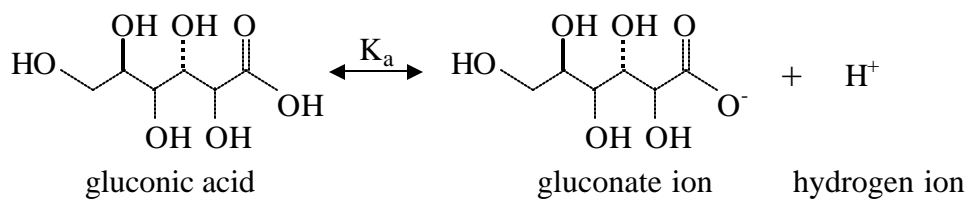
**Figure 6.4.1. Set of Reactions Inside the Glucose Sensitive Hydrogel.** Glucose oxidation (a), hydrolysis of gluconic acid (b), breakdown of hydrogen peroxide (c), gluconic acid dissociation (d).
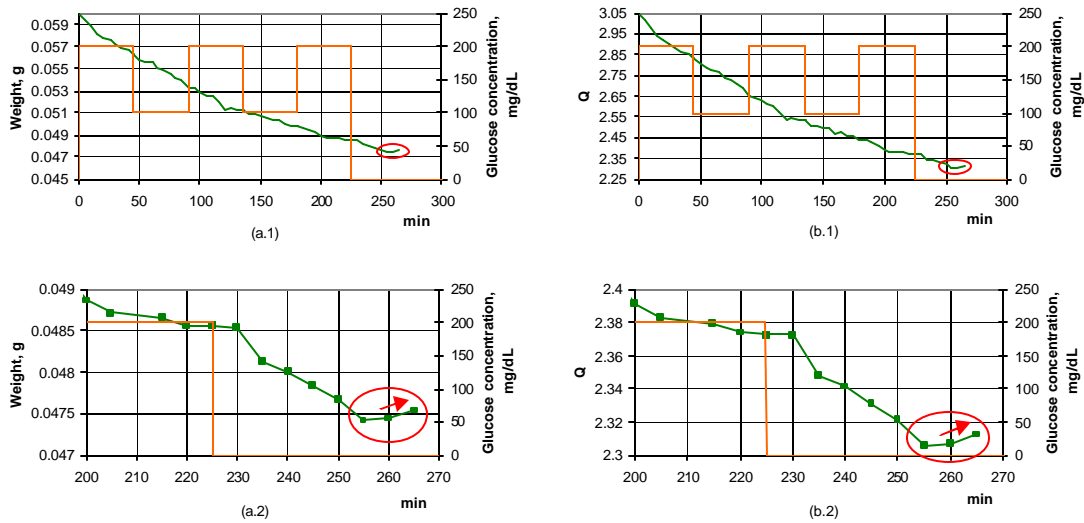
**Figure 6.4.2.  Glucose Oscillatory Experiment.**  The experiment was executed at 37°C. Solutions of 100 and 200 mg/dL of glucose in deionized water were used to immerse a hydrogel sample according to the sequence shown in a.1 and b.1 (in orange). The sample was previously at equilibrium in deionized water. After the oscillatory input sequence, the sample returned to deionized water and recovered some size as marked specially in the zoom graphs a.2 and b.2.
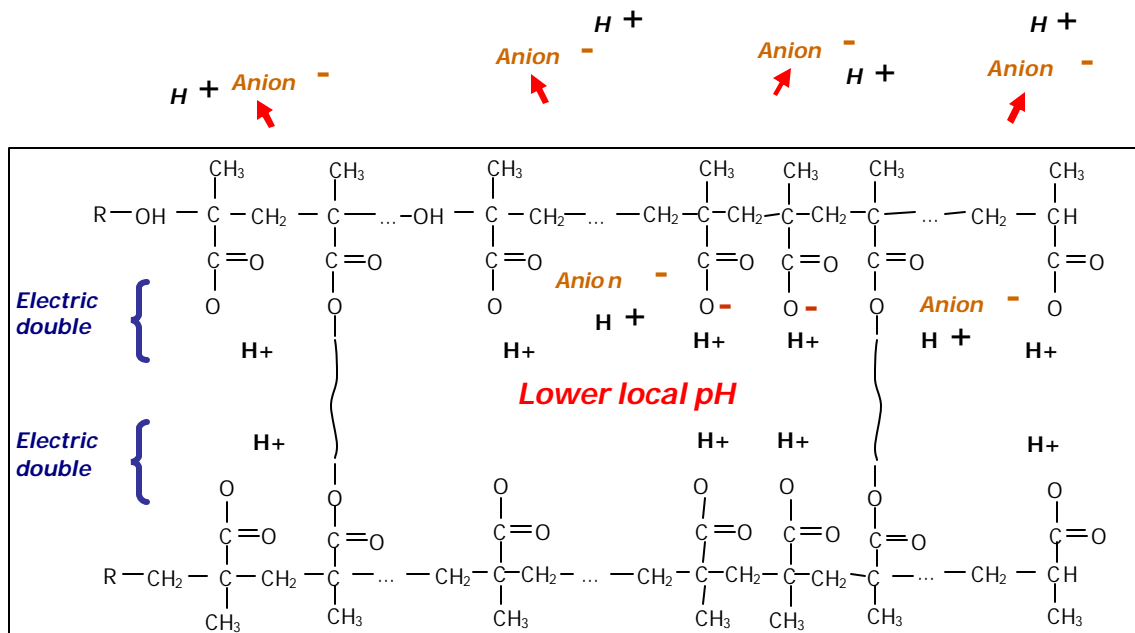


**Figure 6.4.3. Donnan Equilibrium Effect.** The hydrogel membrane is represented by the rectangle.  The tendency to form an electric double layer determines an interior higher concentration of hydrogen ions or lower pH with respect to the surroundings.

104
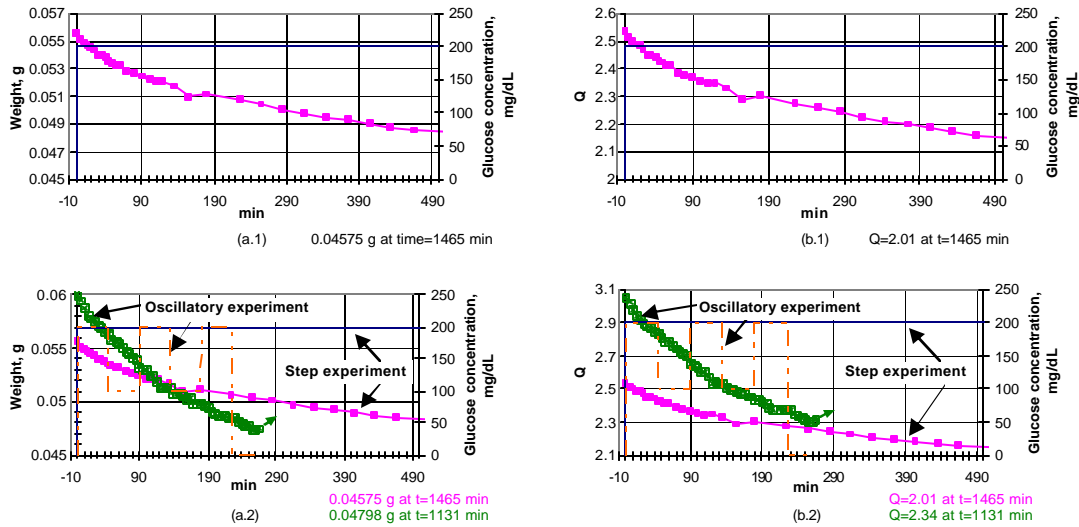
**Figure 6.4.4. Glucose Step and Oscillatory Experiments.** The step experiment was executed at 37°C. A sample previously at equilibrium in deionized water was changed to a 200 mg/dL glucose solution in the step experiment shown in a.1 and b.1. The response to the step and the oscillatory experiment can be compared in a.2 and b.2. The total decrement of the step response with respect to the initial value was 17.86% in weight and 20.24% in volume swelling ratio (Q), while in the oscillatory experiment was 20.03% in weight and 23.53% in Q.



pH=6.07 at t=1358 min
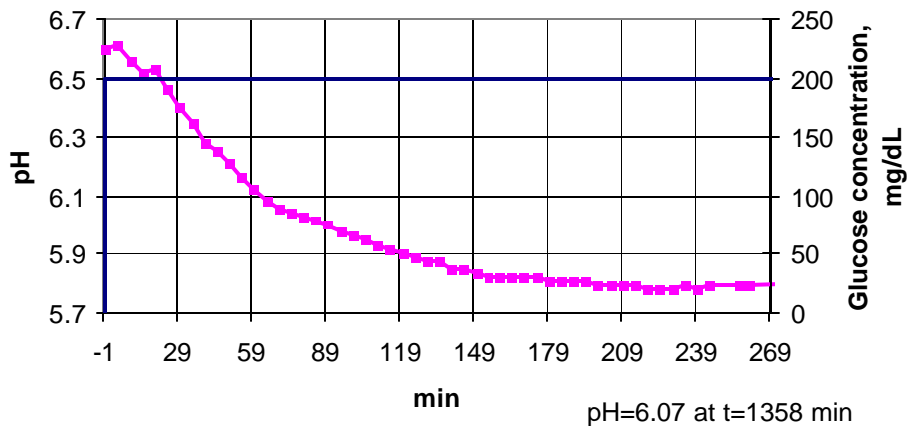
**Figure 6.4.5. pH Response to a Glucose Step Input.** A sample previously at equilibrium in deionized water is changed to a 200 mg/dL glucose solution in the step experiment at room temperature. The pH is monitored as glucose is converted to gluconic acid.
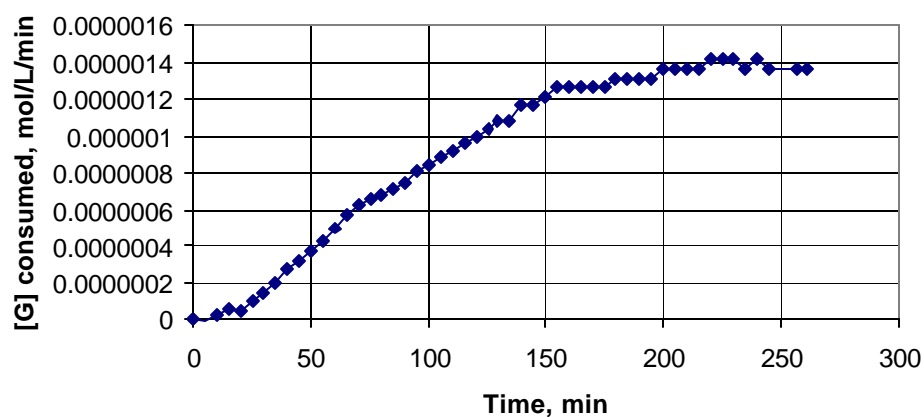
**Figure 6.4.6.  Consumption of Glucose in the Hydrogel System.**  The catalase reaction also took place in the hydrogel and influenced glucose consumption. The curve shows an inflexion point that corresponds to a peak in the velocity of the reaction after relatively small initial speeds.
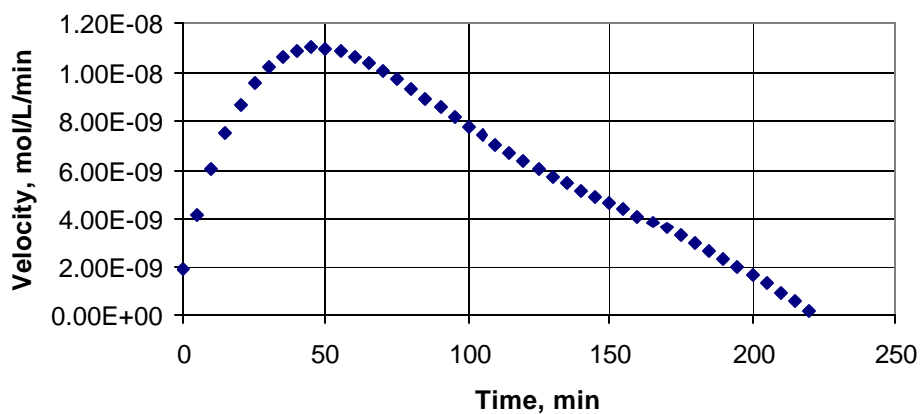


**Figure 6.4.7.  Velocity of Glucose Oxidation Reaction in a Hydrogel System.**  The glucose oxidase reaction and the catalase reaction occurred simultaneously in the gel.
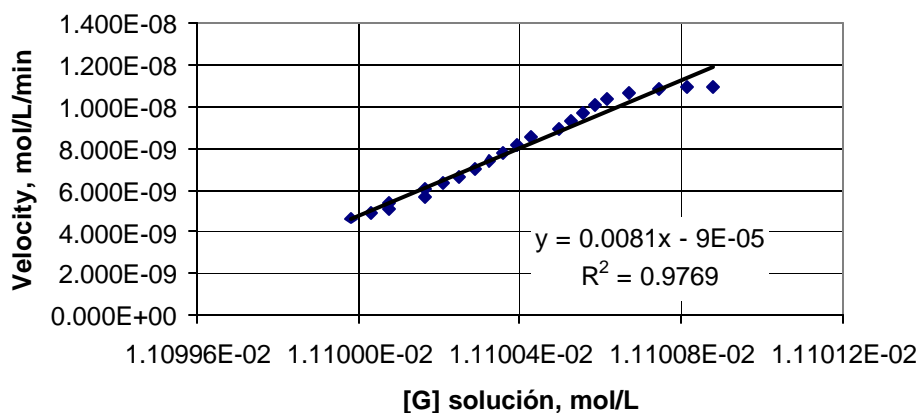
**Figure 6.4.8. Velocity of Glucose Oxidation with Respect to Glucose Substrate Concentration in the Medium of the Hydrogel System.** The chosen segment is representative of the tendency that prevailed most of the time of the reaction. The slope of the linear fit gives an approximation to a reaction rate constant of 0.0081 min$^{-1}$ in the hydrogel.

## 6.5. Insulin Release

### 6.5.1. Fundamentals

#### 6.5.1.1. Controlled Release Mechanisms

Hydrogel-based delivery systems combine several mechanisms to control the release of therapeutic agents. Diffusion is the fundamental means for drug transport through a polymer film. However, the particular characteristics of hydrogels determine the influence of water penetration and chemical responsiveness in the release process.

Delivery from non-swelling membranes is controlled exclusively by diffusion, as in hydrogels fully swollen at certain pH or even glassy polymers [10]. In the case of hydrogel membranes previously loaded from a medium with dissolved insulin and immediately transferred to the delivery medium at the same pH, the amount delivered is represented by the following Equations (28) and (29) during the early 60% and the late 40% of the total release time, respectively [10, 11]:

$$\frac{M_t}{M_x} = \frac{4D^{1/2}}{\pi^{1/2}b}t^{1/2},$$

(28)

$$\frac{M_t}{M_x} = \frac{8\pi D^2}{b^4}exp\left(\frac{\pi D}{b^2}t\right),$$

(29)

where b is the thickness, D is the diffusion coefficient, $M_t$ is the cumulative amount of released insulin at time t, and $M_x$ is the total amount of insulin loaded in the polymer. These equations are also adequate when the swelling is much slower than diffusion, which implies that there is no significant variation of the polymeric structure during the diffusion process [12]. A Deborah number much greater than 1 describes this situation, given the following definition:

$$De = \frac{\tau}{\theta},$$

(30)

where $\tau$ is the relaxation time of the hydrogel (Section 6.1) and $\theta$ is the characteristic diffusion time calculated as the square of the thickness of the membrane, b, over the diffusion coefficient, D:

$$\theta = \frac{b^2}{D}.$$

(31)

In a swelling hydrogel from the dry or glassy state, water penetration allows the diffusion of the contained insulin by a drastic decrement in transport resistance. In this process the interface between swelling and glassy polymer advances in opposite direction

to the interface between polymer and surrounding solution [10, 13].  As a result, the velocities of relaxation and diffusion could be of the same order of magnitude and give De~1.

During volume increments of a hydrated gel membrane due to the response to the environmental pH, the augment of water penetration eases the diffusion of the drug.  This effect is represented by Equation (12) where the diffusivity is related to the volume fraction of water (or solution) in the hydrogel system.  Although the diffusivity changes with respect to the dry states are expected higher, the variations of diffusion coefficient between different hydration states are important to describe the operation of hydrogel-based systems in implants applications.

### 6.5.1.2. Effect of Drug Isoelectric Point and Hydrogel Critical pH Loading Process

Drugs can be incorporated into the hydrogel by including them in the reactive mixture for polymerization or by a diffusion process.  The first option is avoided because the reaction conditions may degrade the therapeutic agent. In a diffusive loading process, the resistance to the penetration of the drug is determined not only by the mesh size of the polymeric network, but also by the electrostatic interactions with the drug.  For this reason, the isoelectric point (pI) of proteins may set a restriction to the highest swelling level of the hydrogel systems to load.  Above the pI, proteins carry a net negative charge as the charge inside a swollen anionic gel. Therefore, in this work, the P(MAA-g-EG) discs may be loaded with insulin at a pH below its pI and also below (but as close as possible to) the critical pH of the gel to ease the absorption process (Figure 6.5.1).

### 6.5.1.3. Insulin Structure

Insulin molecules have a molecular weight of 5808 Da.  The structure of an insulin monomer is defined by three major elements: A chain, B chain and a connecting C-peptide (the latter is absent in mature insulin).  The A chain is formed by two short helices and 21 amino acids, and the B chain is a single $\alpha$ helix with 30 aminoacids. Chains A and B are linked by two disulfide bonds. A third disulfide bond is found within the A chain. Structural variations of insulin from different species involve few aminoacids, but do not affect the three dimensional conformation.  This allows for insulin from certain species to be bioactive in others [14].

Insulin molecules in solution may stay as separate monomer units or form dimers by hydrogen bonds between B chains.  In the presence of zinc, insulin dimers form hexamers by the interaction of metallic ions with histidine residues from B chains. Pharmaceutical preparations of hexamer insulin suspensions produce a slow absorption in the body, while short-acting insulin analogs have either a monomer configuration or a dimmer configuration that dissolves into monomers after injection [14, 15].  Figure 6.5.2 shows the general structure of insulin [16] and the specific variations of different types of insulin.

## 6.5.2. Experimental Work

Insulin delivery studies involve four major stages: elaboration of insulin loading solution, drug absorption in the hydrogel system, drug release from the hydrogel and analysis of samples of the loading and delivery environments. Preparation of insulin loading solutions requires lowering the pH to 3 in order to dissolve insulin. After insulin is dissolved, the pH can be raised to the desired value. During the loading process, the solution is mixed constantly to keep a uniform concentration in the solution and favor uniform absorption in the hydrogel. Drug release studies are performed in a dissolution apparatus (Figure 6.5.3) that provides temperature control and continuous mixing of the delivery medium. Concentrations of the loading and delivery mediums are analyzed using a HPLC system.

The loading pH is specified according to the characteristics of the drug and the material and its enzymatic components. The isoelectric point of insulin is 5.4 [15] and the critical pH of the P(MAA‑g‑EG) is 5.6. Regarding the enzymes present in the gel, the pI of glucose oxidase is 5.1 and the pI of catalase is 6. At a pH of approximately 5, the glucose oxidize enzyme is neutral but the catalase is charged positively. However, the higher concentration of anionic groups of the hydrogel with respect to the enzymes is supposed to determine the net charge of the system. At this pH, the polymeric mesh is moderately open, that is, the concentration of the net negative charges is relatively low and the still positive insulin molecules do not experience an electrostatic rejection force from the hydrogel system. Repulsive forces against insulin absorption are expected at a higher pH with all the elements of the system having negative charges. The loading process is done at room temperature. Appendix 6.5 contains the protocol to load insulin into the hydrogel discs.

The effect of the electrostatic interactions between the pendant groups of the hydrogel and the drug to be absorbed is demonstrated by the characteristics of insulin release from P(MAA‑g‑EG) samples loaded at pH 5 and 7 (Figure 6.5.4). In these tests, the hydrogel samples were synthesized with no enzymes, TEGDMA as crosslinking agent and excess of solvent.

The influence of the crosslinking agent used in the synthesis of hydrogels on drug release is also explored (Figure 6.5.5). Samples with no enzymes and either TEGDMA or PEGDMA‑1000 as crosslinking agent are loaded with insulin at pH 5. The same release conditions are set for both synthesized materials in order to establish a comparison.

Finally, the drug release process is studied in a delivery medium in the presence of glucose (Figures 6.5.6 and 6.5.7). Samples with glucose oxidase and catalase enzymes and TEGDMA crosslinking agent are loaded at pH 5. Insulin release profiles in different glucose concentration solutions and in a glucose free solution are compared.

All the release studies are done in buffer solutions at physiological pH and temperature. This type of experiment is further described in Appendix 6.5.

### 6.5.3. Results and Discussion

The release profiles obtained from enzyme free samples loaded at different pH values are shown in Figure 6.5.4. Higher insulin concentrations were achieved in the delivery medium of the sample loaded at pH 5. The initial fraction of released insulin with respect to the total delivered insulin indicates the depth of absorption of insulin. The insulin absorbed only superficially with a loading pH of 7, since 90% of the total released insulin was delivered in the first 10 minutes. Consequently, the release curve was flat for this case. Such release profile indicated that insulin absorption was hindered by the electrostatic repulsion between the swollen hydrogel and the insulin, both negatively charged at pH of 7. In contrast, the initial released insulin fraction was 0.7 and the delivery profile was exponential when the sample was loaded at pH 5. Loading of samples with insulin was performed at pH 5 for the rest of the release studies.

Figure 6.5.5 shows the release profiles from samples with different crosslinking agent and no enzymes. The longer PEGDMA-1000 hindered the diffusion of insulin in both the loading and releasing processes, due to the reduction of the available space inside the hydrogel. As a result, a lower concentration profile and an almost horizontal released fraction curve were produced when PEGDMA-1000 was used. The delivery from samples with PEGDMA-1000 was markedly slow.

The effect of glucose in the delivery medium was first explored using glucose free and 200 mg/dL glucose solutions (Figure 6.5.6). The glucose sensitive hydrogel samples were synthesized with TEGDMA and excess of solvent for these tests. The glucose presence caused an initial contraction of the material that gave a lower average released insulin fraction of 0.6 while 0.7 was obtained in the absence of glucose. For the rest of the time, the release curves practically overlapped. This region was not subject to a large variability since most of the insulin was released in the first 10 minutes.

When glucose sensitive hydrogel membranes released insulin in different glucose concentration solutions (Figure 6.5.7), the initial released fraction was lower for the higher glucose content. Therefore, the gels showed sensitivity not only to the presence of glucose but also to the concentration.

From observation of the release experiments, the swelling process of the membrane was slow (relaxation swelling times above pH 5 were around 330 min, according to Table 6.1.1) and the diffusion was fast (80% of insulin was released in 20 minutes, as shown in Figure 6.5.6 and Figure 6.5.7). If the early release Equation (4) is evaluated, the diffusion coefficient of insulin can be estimated under the different glucose content conditions of the delivery medium assuming a constant membrane thickness (diameter changes were more drastic) (Table 6.5.1). Lower insulin diffusivities correspond to higher glucose concentrations. The average insulin diffusion coefficient calculated is close to the experimental values determined in Section 6.3, and the average characteristic diffusion time is 140 min. Therefore, a Deborah number larger than 1 supports the consideration of Fickian diffusion as the insulin delivery mechanism by the fabricated hydrogel films. Additionally, a variable diffusion coefficient is necessary to account for the glucose responsiveness of the delivery process.
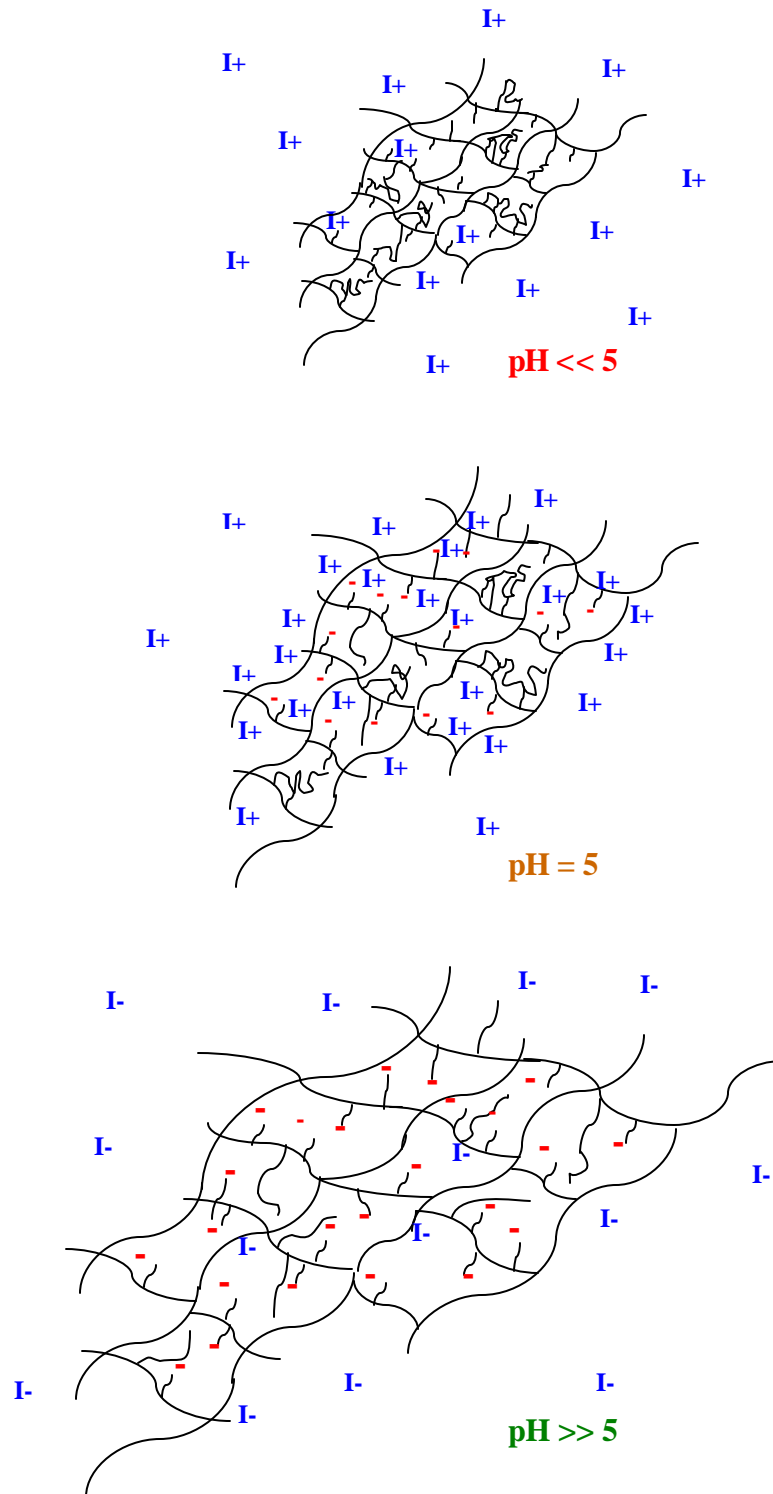
**Figure 6.5.1.  Electrostatic Charges of Anionic Hydrogel System and Insulin at Different pH.**  The electrostatic charge of the functional groups of the anionic polymer is supposed to dominate over the charge of the contained enzymes.  A pH below the isoelectric point of insulin (5.4) but close to the critical pH of the material (5.6) achieves a balance between the diffusion effects of the opening size of the polymer structure and the electrostatic charges of hydrogel and insulin.
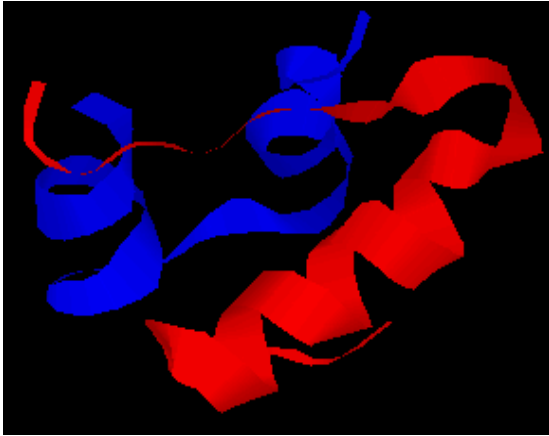
(a) Insulin monomer
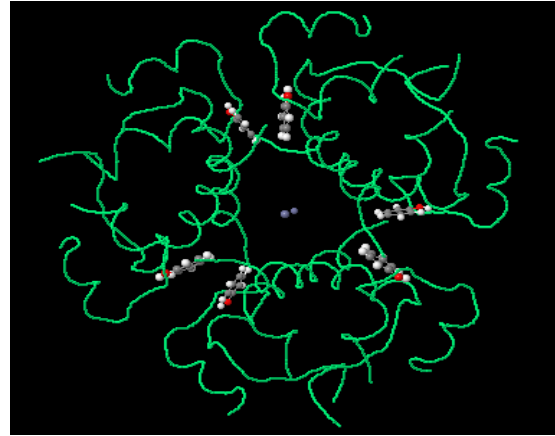


(b) Insulin hexamer
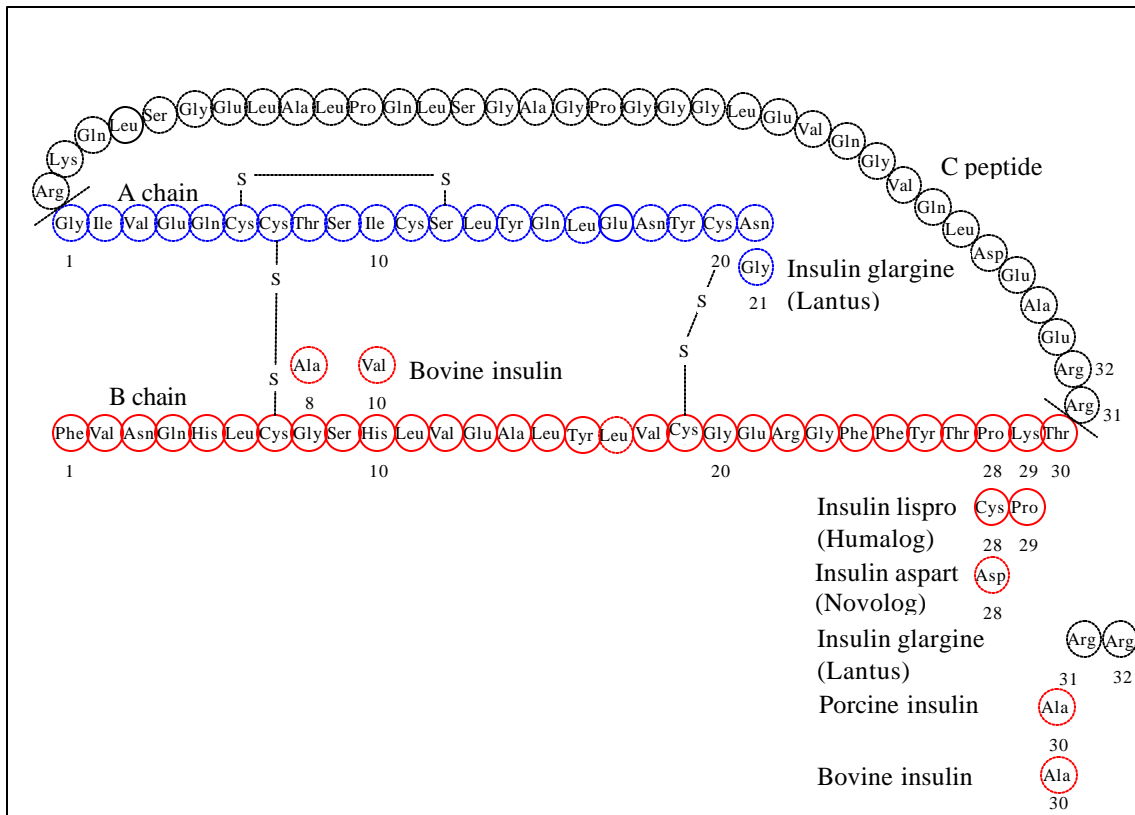


(c) Primary structure of human insulin monomer and residue variations for other types of insulin. Adapted from [14].

**Figure 6.5.2. Insulin Structure.** An insulin monomer (a) is formed by the A chain (blue helices) and the B chain (red helix). The insulin hexamer (b) is formed around two zinc ions through interaction with histidine residues from the subunits [16]. Different types of insulin show few residue changes without three dimensional modifications (c).

113
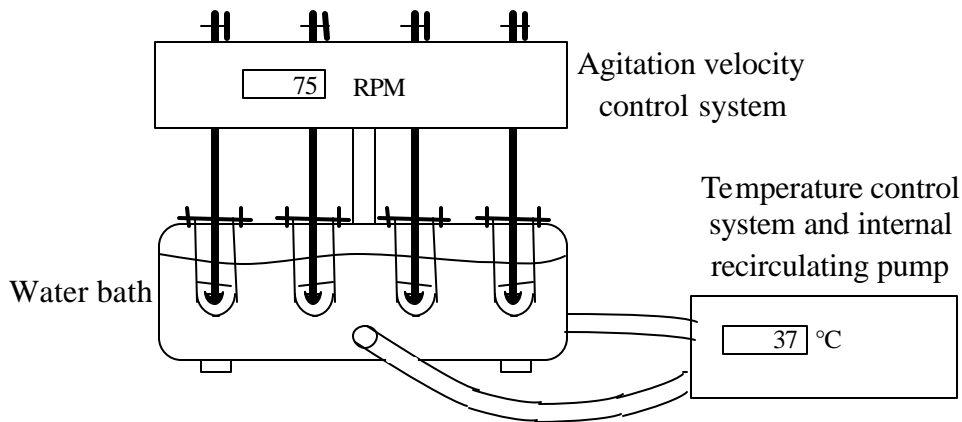
**Figure 6.5.3. Dissolution Apparatus for Insulin Release Experiments.** The system provides continuous stirring and temperature control.
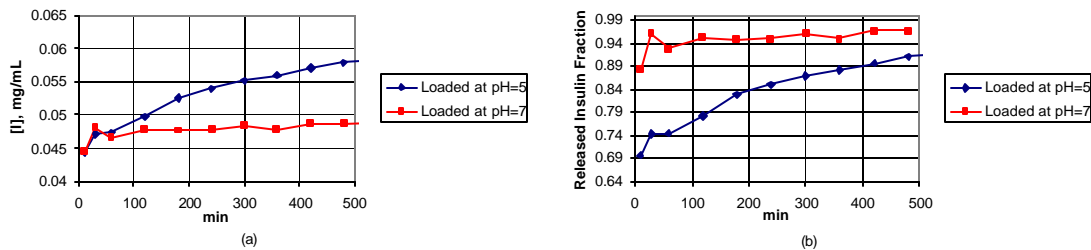


**Figure 6.5.4. Effect of Loading pH.** Samples were previous loaded with insulin at pH 5 and 7. The samples did not contain enzymes. The crosslinking agent was TEGDMA. Insulin concentration in the delivery medium (a) and fraction of released insulin are reported (b).
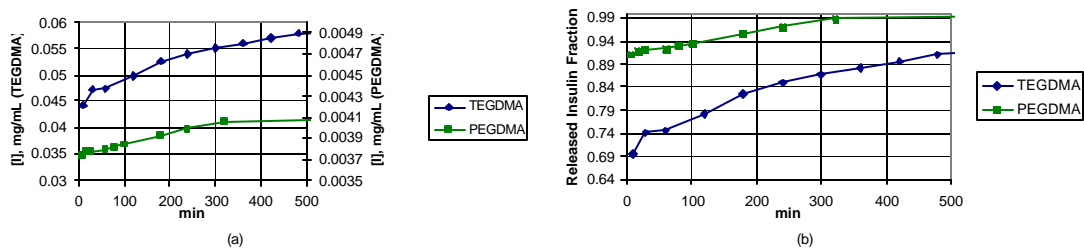


**Figure 6.5.5. Effect of Crosslinking Agent in Drug Delivery.** Samples were previously loaded with insulin at pH 5. The samples did not contain enzymes. The crosslinking agents TEGDMA and PEGDMA have 4 and 23 repeating ethylene glycol units respectively. Insulin concentration in the delivery medium (a) and fraction of released insulin are reported (b).

114
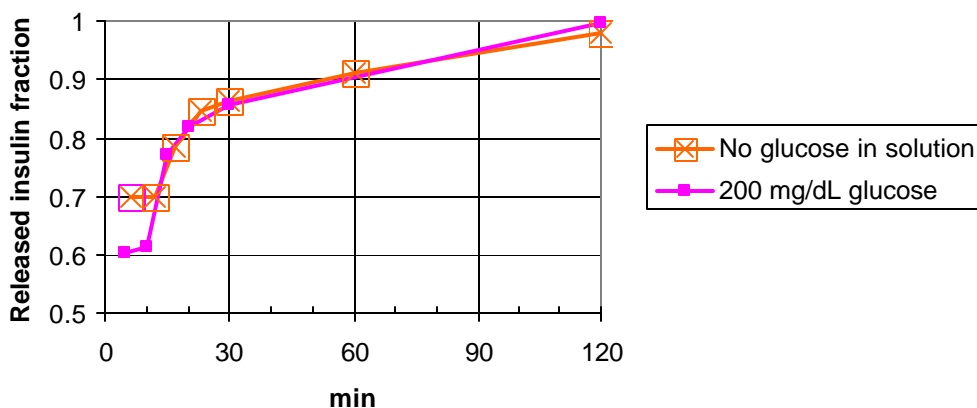
**Figure 6.5.6. Effect of Glucose Presence in Delivery Medium.** Samples were previous loaded with insulin at pH 5. The synthesis of the samples included glucose oxidase and catalase enzymes, TEGDMA and excess of solvent.
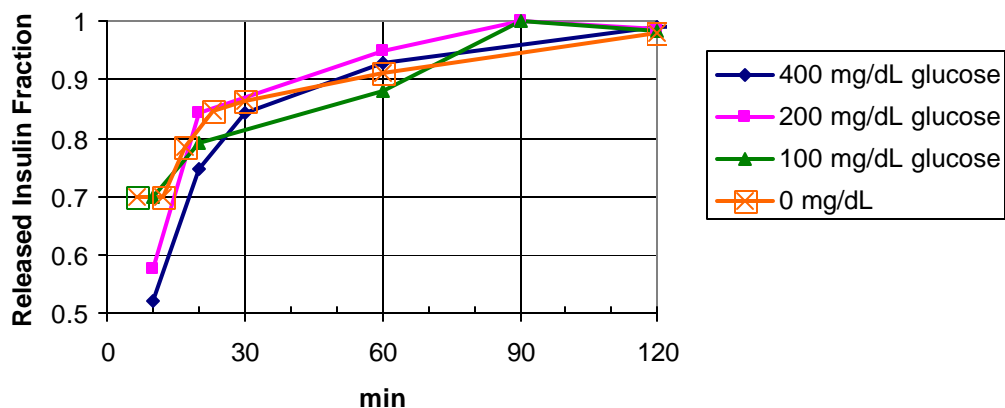


**Figure 6.5.7. Insulin Release in Different Glucose Concentration Solutions.** Samples were previous loaded with insulin at pH 5. The synthesis of the samples included glucose oxidase and catalase enzymes, TEGDMA and excess of solvent. The insulin release response shows glucose sensitivity especially at the beginning of the experiment.

**Table 6.5.1. Estimation of Diffusion Coefficients from Release Experiments.** Volume changes are neglected, a constant thickness of 1.3 mm is considered, initial slope is calculated with earliest available insulin delivery data.

| Glucose concentration in delivery medium, mg/dL | Initial slope of $M_t/M_8$ (released fraction) with respect to $t^{1/2}$, $1/min^{1/2}$ | Estimation of diffusion coefficient, D, $cm^2$/seg | Characteristic diffusion time, $q$, min |
|---|---|---|---|
| 0 | 0.275 | 4.17E-06 | 68 |
| 100 | 0.177 | 1.74E-06 | 162 |
| 200 | 0.181 | 1.82E-06 | 155 |
| 400 | 0.165 | 1.5E-06 | 188 |

115

## 6.6. Conclusions

The dynamic characterization of hydrogels lead to conclusions regarding the drug release mechanism and the potential swelling range of glucose sensitive in physiological conditions.

The pH responsive swelling behavior of the P(MAA-g-EG) hydrogel is characterized by a strong non-linearity determined by different dynamic parameters shown in the distinct operation ranges as well as with the pH change direction (Section 6.1). A higher velocity of contraction with respect to speed of swelling can cause the formation of pores. However, a relative fast syneresis only occurred near the critical pH of the material of 5.6. At a physiological pH, contraction was slower than swelling, which gives a negative indication for the possibility of pore formation and squeezing drug release mechanism.

The drug delivery mechanism for the fabricated P(MAA-g-EG) hydrogel is based on diffusion. A squeezing delivery is discarded from results of Sections 6.2 and 6.5. The excess of solvent in the synthesis of the films was not enough to account for pore formation during contraction, which would favor insulin release before high levels of glucose in the medium. Insulin release studies evidence a diffusion delivery mechanism since initial delivered fraction is smaller at higher glucose concentration that causes lower pH and smaller volume for the hydrogel system.

While the transitory response, particularly the initial insulin release response, shows a correlation with glucose concentration of the environment, the late release profiles are not clearly differentiated (Section 6.5). These results imply that the same swelling behavior is attained in the final part of the experiments. This may be due to the saturation of the enzymatic system regardless of the physiological glucose concentration value. A low saturation level for the hydrogel system can be associated with a low Michaelis-Menten constant with respect to its value in solution (Section 6.4). Moreover, the delivery medium was based on a pH 7 buffer solution, characteristic present in the blood that damped the effect of the gluconic acid production within the hydrogel on the volume changes and the opening of the polymer structure.

The use of a variable diffusion coefficient based on the volume swelling ratio and the mesh size of the hydrogel material may be more convenient than a characteristic constant value under a specific pH condition derived from experiments in a diffusion cell (Section 6.3) or a dissolution apparatus (Section 6.5). The variable diffusion coefficient does not only provide a wider applicability but is also based on simpler and more economical measurement of the volume swelling ratio with respect to the analytical determination of concentrations involved in diffusion and drug release studies. Nevertheless, the consideration of physiological conditions of body fluids discussed above make the constant diffusivities sufficient for the study of hydrogel implants.

The oscillatory glucose responsive experiment (Section 6.4) resembles variations of body glucose levels regardless of the use of deionized water as solvent instead of a neutral buffer. Results show a resistance to reverse the swelling tendency when the hydrogel

samples are changed from a high glucose concentration solution to a low glucose concentration solution.  This can be explained by the saturation of the enzymes, as mentioned above, and by the large time constants of the swelling behavior of the hydrogel. The Donnan equilibrium effect is also a factor that prevents the recovery of high levels of pH when the sample is returned to a low glucose concentration solution.

## References

1. Coughanowr DR. Process systems analysis and control (2nd edition). Boston: McGraw-Hill, 1991.

2. Chakrabarti S,  Sahu J, Biswas A, Acharya HN. Relationship between weight loss and shrinkage during gel drying. J Mater Sci Letters. 1992;11:763-766.

3. Peppas NA, Barr-Howell BD. Characterization of crosslinked structure of hydrogels. In: Peppas NA. Hydrogels in medicine and pharmacy. Boca Raton: CRC Press, 1986;1:28-55.

4. Bell CL, Peppas NA. Water, Solute and Protein Diffusion in Physiologically-Responsive Hydrogels of Poly(methacrylic acid-g-ethylene glycol). Biomaterials. 1996;17:1203-1218.

5. Pillarella MR, Zydney AL. Theoretical analysis of the effect of convective flow on solute transport and insulin release in a hollow fiber bioartificial pancreas. J Biomech Eng-T ASME. 1990;112:220-228.

6. Podual K, Peppas NA. Relaxational behavior and swelling-pH master curves of poly[(diethylaminoethyl methacrylate)-g-(ethylene glycol)] hydrogels. Polym Int. 2005;54:581-593.

7. Barbieri R, Quaglia M, Delfini M, Brosio, E. Investigation of water dynamic behaviour in poly(HEMA) and poly(HEMA-co-DHPMA) hydrogels by proton $T_2$ relaxation time and self-diffusion coefficient n.m.r, measurements. Polymer. 1998;39(5):1059-1066.

8. Cardosi, M.   http://www-biol.paisley.ac.uk/ (Chemscape Chime plug in by MDL Information Systems, Inc.) (as seen on November 16, 2007)

9. Podual K, Doyle III FJ, Peppas NA. Glucose-sensitivity of glucose oxidase-containing cationic copolymer hydrogels having poly(ethylene glycol) grafts. J Control Release. 2000; 67:9-17.

10. Heller J, Hoffman A. Drug delivery Sistems in Chapter 7 Application of Materials in Medicine, Biology and Artificail Organs.  Biomaterials Science, 2nd edition, Ratner B D, Hoffman A S, Schoen F J, Lemons J E, eds. Elsevier Academic Press, San Diego, 2004, 628-648.

11. Baker R W, Lonsdale H K. Controlled release: mechanisms and rates. In Controlled Release of Biologically Active Agents, Tanquary A C, Lacey R E (eds.). Plenum Press, New York,1974,  pp. 15-71.

12. Davidson III R. Peppas N. Solute and penetrant diffusion in swellable polymers. J Controlled Release, 3 (1986) 243-258.

13. Langer R S, Peppas N A. (1983). Chemical and physical structure of polymers as carriers for controlled release of bioactive agents: a review.  Rev. Macromol Chem Phys. C23:61-126.

14. Tofade TS, Liles EA. Intentional Overdose With Insulin Glargine and Insulin Aspart. Pharmacotherapy 2004;24(10):1412-1418.

15. Hasselblatt A, Bruchhausen F, eds. Handbook of experimental pharmacology. Heffler-Heubner New Series XXXII/2 (Altzuler). Springer Verlag New York 1975

16. RCSB Protein Data Bank  http://www.rcsb.org/pdb/home/home.do. (as seen on November 20, 2007) Jmol Viewer.

**Appendix 6.1.  Oscillatory Experiment Protocol**

The oscillatory experiment consists in the periodic change of the pH of the environment of a hydrogel sample at 37°C.

1. Two pH values, 3.2 and 7, are selected for the test and buffer solutions are elaborated.

2. Flasks are filled with 50 mL of either the low or high pH buffer solution.

3. A dry disc sample is set in the flask with 3.2 pH buffer.

4. The flasks are placed in a water bath at 37°C.  The volume of the hydrogel sample is allowed to reach equilibrium during a lapse of 24 hours.

5. The hydrogel sample at equilibrium is weighed in air and in heptane and the time of the experiment is started.  The sample is handled with blunt forceps, the excess of water in the surface is removed with a tissue, and the weight in air is measured. Immediately after this measurement, the sample is weighed in heptane and cleaned to continue the experiment. This procedure is done quickly and carefully to reduce drying and cooling and avoid breaking the hydrogel disc.

6. The sample is changed to the different (7) pH solution already at 37°C.  Each five minutes, the sample is weighed in air and heptane (as described in step 5) during an interval of 45 minutes.

7. The sample is changed to a 3.2 pH solution flask at 37°C, and the weight measurements continue being taken each 5 minutes for the next 45 minutes to complete the fist cycle.

8. Steps 6 and 7 are repeated for two more 90 minutes cycles.

9. Steps 2 to 8 may be repeated with more disc samples.

**Appendix 6.2. Protocol of Step Experiments**

A step experiment consists in a single abrupt change of the pH of the environment of a hydrogel sample at 37°C. Initial and final steady states, as well as the transitory response, are monitored. A series of step experiments is proposed to characterize the material in different change directions and ranges.

1. Buffer solutions are prepared for each pH value to use as an input to the hydrogel system (3.2, 4.8, 5.4, 5.8, 6.2, 7.2). The steps are planned in sequence from the lowest to highest pH and then in the reverse direction.
2. Flasks are filled with 50 mL of a particular buffer solution.
3. A dry disc is stick into the initial (3.2) pH buffer flask. The flask with the sample and the flask with the next (4.8) pH buffer solution are placed in a water bath at 37°C.
4. After 24 hours, the initial equilibrium weight is measured in air and in heptane, the step is applied by changing the sample to the different (4.8) pH solution, already at 37°C, and the time of the experiment is started.
5. Weight measurements are taken each 5 minutes during the first hour, at every 10 minutes in the second and third hours, at each 15 minutes in the fourth hour, and every 30 minutes in the next 4 hours.
6. The next (5.4) buffer solution flask is placed in the water bath in preparation for the subsequent step experiment.
7. After 24 hours, the final steady state weight is measured to conclude one step experiment (from pH of 3.2 to 4.8). This equilibrium measurement also corresponds to the initial steady state of the next step experiment (from 4.8 to 5.4). The sample is changed to the next (5.4) pH buffer solution and the time of the experiment is reset to zero.
8. Steps 5 to 6 are repeated until the sequence is completed.

**Appendix 6.3. Diffusion Experiment Protocol**

1.  A beaker for the preparation of insulin stock solution, four vials and the diffusion cell are pretreated with Sigmacote® (Sigma-Aldrich, Saint Louis, MI) to avoid adhesion of insulin to the glass.

2. A pH 7 PBS buffer can be prepared from two solutions as indicated in the Geigy Tables. Solution A is made with 0.45365 g of $KH_2PO_4$ and 50 mL of deionized water.  Solution B is produced by dissolving 0.7122 g of $Na_2HPO_4 \cdot 2H_2O$ in 60 mL of deionized water. A mixture of 41.3 mL of solution A and 58.7 mL of solution B gives 100 mL of pH 7 PBS buffer solution.

3. An insulin solution is prepared by adding to 56 mL of pH 7 buffer, the following components: 7 mL of 0.1N HCl, 35 mg of bovine insulin (Sigma Aldrich) and 7 mL of 0.1N NaOH, in the order given.  The insulin dissolves at an acidic pH.  The original pH is recovered by adding an equal amount of NaOH at the end. The  final concentration is 50 mg/dL.

4.   Standard solutions are produced by diluting the solution elaborated in step 2.  4 mL standard solutions are prepared and reserved in vials.

| Concentration (mg/dL) | 50 mg/dL solution  (mL) | pH 7 buffer (mL) |
|---|---|---|
| 40 | 3.2 | 0.8 |
| 30 | 2.4 | 1.6 |
| 20 | 1.6 | 2.4 |
| 10 | .8 | 3.2 |

5. Grease is applied on the lips of the diffusion cells to avoid leaks.

6. A disc membrane is cut from a film preequilibrated at pH 7 and set between the diffusion cells.  The membrane is cut with the interior diameter of cell connection surface (9 mm). The membrane may be protected with two pieces of tule with big openings. The membrane is set or inserted in one half cell.  The other half cell is set on the other side of the membrane and the diffusion cell is tightened.

7.  The peristaltic pump is turned on to circulate the heating fluid through the jackets.

8. The donor half cell is filled with 3 mL of the 50 mg/dL insulin stock solution, and 3 mL of pH 7 buffer solution without insulin are put on the receptor side.  The time of the experiment is started.

9.  Every 10 minutes 0.2 mL are taken from the receptor half cell and replaced with 0.2 mL of buffer solution.  The sample is filtered (with a PDVF syringe filter) and collected in a HPLC vial for posterior analysis. Samples are taken during 2.5 hours.

10. A hydrogel disc hydrated at a pH of 7, with 9 mm of diameter and 1.3 mm of thickness, is set in 3 mL of 50 mg/dL insulin solution for at least 5 hours at 37°C. A 0.2 mL sample is taken from the solution to measure the final insulin concentration outside the disc. The equilibrium concentrations of insulin inside and outside the gel are determined to calculate the partition coefficient.

**Appendix 6.4. Glucose Responsiveness Protocols**

*Glucose Oscillatory Input*

1. Glucose solutions of 100 mg/dL and 200 mg/dL are prepared using deionized water and D-glucose (Aldrich).

2. A disc sample cut from a recently washed film under refrigeration is set in deionized water and allowed to stabilize at 37°C in a water bath. Solutions of 100 mg/dL and 200 mg/dL glucose are also set in the water bath. In all cases, liquid volumes of 6 mL are managed for a consistent base of comparison with other glucose responsiveness experiments.

3. The sample is introduced into the solution of 200 mg/dL and the time of the experiment is started.

4. The weight in air of the sample is measured each 5 minutes during 45 minutes. The sample in the glucose solution is returned to the water bath at 37°C after each measurement.

5. The sample is moved to the vial with 100 mg/dL glucose solution, and the weight is measured each 5 minutes for the next 45 minutes.

6. After the first 90 minutes cycle, another complete cycle is carried out in the same way.

7. At time 180 min, a half cycle with 200 mg/dL glucose solution is executed.

8. At time 225 min, the sample is set in a vial with pure deionized water for the next 45 min and weight measurements are continued each 5 minutes.

9. The sample is dried after the experiment to determine the dry weight without concerns about the activity of the enzymes.

10. Hydrogel volume values were estimated by the linear relation between measurements of weights in air and weights in heptane obtained in previous experiments (in which enzymes were not present).

*Glucose step input*

1. A glucose solution of 200 mg/dL is prepared with deionized water and D-glucose (Aldrich). Buffers are not used as solvents to ease the detection of pH changes caused by the enzymatic reaction in the hydrogel.

2. A disc sample cut from a recently washed film under refrigeration is set in deionized water and allowed to stabilize at 37°C in a water bath. Solution of 200 mg/dL glucose is also set in the water bath. Liquid volumes of 6 mL are managed for a clearer detection of pH variations.

3. The sample is introduced into the solution of 200 mg/dL and the time of the experiment is started.

4. The weight in air of the sample is measured each 5 minutes during the first hour, each 10 minutes in the second hour, each 15 minutes in the third hour, each 30 minutes for the next five hours, and a final measurement is taken 24 hours from the start of the experiment. The sample in the glucose solution is returned to the water bath at 37°C after each measurement.

5. The sample is dried after the experiment to determine the dry weight.

6. The volume of the sample is calculated form a correlation of weight in air and weight in heptane previously obtained.

7. A second step experiment is prepared as in steps 1 and 2, except for the use of the water bath. The step response in this case is monitored by pH measurements at room temperature.

8. The sample is changed from deionized water to 200 mg/dL glucose solution at time zero. The solution is gently mixed with a small magnetic bar on a stirrer plate. The pH of the small volume solution is monitored every 5 minutes for 4.5 hours or until pH remains without significant variation for one hour. An IQ Scientific pH meter instrument was used.

**Appendix 6.5.  Insulin Release Experiment Protocol**

*Loading of hydrogels with insulin*

1. PBS buffer solutions are prepared for pH 5 and 7 with a molar strength of 0.1 M, according to the following recipes:


1. Disc samples cut from a recently washed film under refrigeration are set in 5 pH buffer solution at room temperature.

2. Glassware to be used is cleaned and treated with Sigmacote® to prevent protein adhesion to the glass.

3. A solution of 0.5 g/L of insulin is prepared in the following way:  5 pH buffer is mixed with 0.1N HCl to lower the pH, insulin is added and dissolved, and finally 0.1N NaOH is added to recover the original pH. The total volume of the solvent of the loading solution is formed by 80% buffer, 10% 0.1 N HCl and 10% 0.1 N NaOH.

4. A small volume (2 mL) of the loading solution is reserved to prepare standards. Standards of 0.25, 0.125, 0.0625 and 0.03125 g/L are obtained by consecutive dilutions with pH 5 buffer (these solutions serve as a reference to calculate the final insulin concentration in the loading solution after a period of absorption by the hydrogel). Standards are also prepared using 7 pH buffers for the analysis of the delivery medium.

5. Each hydrogel membrane is placed in 20 mL of loading solution for 4 hours, with continuous mixing, at room temperature.

6. A sample of 0.2 mL of the loading solution is taken after 4 hours of insulin absorption by the disc, in order to quantify the loaded insulin.

*Insulin release*

7. Buffer solution of pH 7 is used as a delivery medium in a dissolution apparatus with constant stirring and controlled temperature of 37°C.  The time of the experiment is started at the moment that an insulin loaded hydrogel disc is placed in the 7 pH buffer.

8. Samples of 0.2 mL of the delivery medium are taken at times 5, 10, 15 20, 25, 30, 60, 120, 180, 240 min.  The 0.2 mL volume of the sample is replaced immediately with 7 pH buffer.  The sample is filtered and injected into HPLC vials for the posterior analysis.

9. The samples and the standards are analyzed in a Waters HPLC.

## 7. Mechanical Modulus and Mechanochemical Compliance

A three-dimensional mechanochemical compliance relates the spatial deformation of the hydrogel sample to pH changes in the medium, through the volume-swelling ratio, and can be determined from dynamic swelling experiments as discussed in Chapter 6. Alternatively, the viscoelastic response can be analyzed in terms of a characteristic length or a single dimension to determine a mechanochemical compliance analogous to the mechanical compliance determined from mechanical tests, where a force with a specific direction is applied or exerted.

In this chapter, the mechanical modulus of P(MAA-g-EG) hydrogel samples is characterized by subjecting samples hydrated or swollen at different pH to tensile experiments. The one-dimensional mechanochemical compliance is determined from the same sequence of pH step experiments used for the characterization of three-dimensional mechanochemical compliance in Section 6.1. The time-temperature superposition technique is adapted to generate a time function for the mechanical modulus and the mechanochemical compliance at a neutral pH.

### 7.1. Fundamentals

### 7.1.1. Mechanical Variables and Parameters

As viscoelastic materials, hydrogels are capable of deformation under the action of an external tensile or shear force. The deformation and the force are quantified and their relation is described by characteristic parameters that may depend on the range of deformation or vary with time. Shear and tensile parameters can be associated by Poisson's ratio [1].

Tensile experiments were used in this work to characterize hydrogel materials. The stress $\sigma$ is the magnitude of the tensile force F per unit of transverse area A, which is considered constant. The strain $\varepsilon$ is the fractional extension of the gel along the direction of F. A tensile experiment is based on an elongation ramp function. The gel sample is clamped on the extremes (equipment presented in Section 7.2). One of the clamps is displaced at a constant speed, which represents the extension ratio applied to the material. The load F and the displacement of the clamp or elongation of the material x were measured, and the stress and strain were calculated as a function of time:

$$\sigma(t) = \frac{F(t)}{wb}, \tag{1}$$

$$\varepsilon(t) = \frac{x(t)}{l_0}, \tag{2}$$

where w, b and $l_0$ are width, thickness and initial length of the sample [1, 2].

The mechanical modulus, E, and mechanical compliance, D, are approximated to the slope of the strain-stress curve in a tensile experiment as [2]:

$$E(\varepsilon) = \frac{d\sigma(\varepsilon)}{d\varepsilon} = \frac{1}{D(\varepsilon)}. \tag{3}$$

Since the elongation rate r is controlled during the experiment, each strain value is related to a specific time t by:

$$t = \frac{l_0 \varepsilon}{r}, \tag{4}$$

and the mechanical modulus and compliance can be expressed as time functions:

$$E(t) = \frac{1}{D(t)} = E\Big|_{\varepsilon = \frac{rt}{l_0}}. \tag{5}$$

Other experiments consist in the application of a constant load or a constant deformation. In a creep experiment, $\sigma(t) = \sigma_0$ and D(t) can be determined directly [2]:

$$D(t) = \frac{\varepsilon(t)}{\sigma_0}. \tag{6}$$

In a stress relaxation experiment, $\varepsilon(t) = \varepsilon_0$ and the calculation of E(t) is straightforward [2]:

$$E(t) = \frac{\sigma(t)}{\varepsilon_0}. \tag{7}$$

The disadvantage of these experiments is that it is not possible to relate the parameters obtained from both, since [2]:

$$E(t)\Big|_{\text{stress relaxation}} \neq \frac{1}{D(t)\Big|_{\text{creep}}}. \tag{8}$$

The values of the mechanical modulus and compliance parameters depend on the experiment carried out for their calculation. All experiments are rough simplifications of the actual conditions of the use of the materials, but are precise references for their differentiation.

### 7.1.2. Boltzmann Supe rposition Principle

The Boltzmann superposition principle states that the strain observed in a material is the result of the addition of the individual effect of each stress change or input. Alternatively, the stress response to a specific strain superposes or adds to the response to previous strains to give the total stress developed on the material [2].

The expression for the Boltzmann superposition principle can be explained by considering creep experiments monitored at discrete times $t_k$. Creep compliance allows to calculate the strain $\varepsilon_0(t_k)$ due to the constant stress $\Delta\sigma_0$ (or $\sigma_0$ since the material is supposed to be initially relaxed) applied at time $t_0$:

$$\varepsilon_0(t_0) = \sigma_0 D(t_0); \ \varepsilon_0(t_1) = \sigma_0 D(t_1); \varepsilon_0(t_2) = \sigma_0 D(t_2); \dots \tag{9}$$

The strain $\varepsilon_1(t_k)$ caused by an additional stress $\Delta\sigma_1$ applied at time $t_1$, would be:

$$\varepsilon_1(t_0) = 0; \ \varepsilon_1(t_1) = \Delta\sigma_1 D(t_0); \varepsilon_1(t_2) = \Delta\sigma_1 D(t_1); \dots \tag{10}$$

After applying n stress changes, the total strain $\varepsilon(t_n)$ would be given by:

$$\varepsilon(t_n) = \varepsilon_0(t_n) + \varepsilon_1(t_n) + \dots + \varepsilon_n(t_n) = \sum_{j=0}^{n} \Delta\sigma_j D(t_{n-j}). \tag{11}$$

Equation (11) gives a numerical algorithm for the evaluation of Boltzmann principle that is detailed in Appendix 7.1.

The effect of the n stress steps at any time t in a continuous domain is given by:

$$\varepsilon(t) = \sum_{j=0}^{n} \Delta\sigma_j D(t - u_j), \tag{12}$$

where $u_j = t_j$.

Considering a continuous stress application, the changes $\Delta\sigma_j$ can be substituted by de derivative of $\sigma(t)$, and the sum by an integral operator over the complete history of the material [2]:

$$\varepsilon(t) = \int_{-\infty}^{t} \frac{\partial\sigma(u)}{\partial u} D(t - u) du, \tag{13}$$

where t is the time of the observation, u is the integration variable and D is the mechanical compliance determined by a creep experiment.

Similarly, the superposition principle when the stress is observed before a continuous strain input gives [2]:

$$\sigma(t) = \int_{-\infty}^{t} \frac{\partial\varepsilon(u)}{\partial u} E(t - u) du, \tag{14}$$

where E is the mechanical modulus from a stress relaxation experiment.

The Boltzmann superposition principle applied in the Peppas model for the volume swelling ratio [3, 4] evaluates the strain given a history of exposure to pH changes:

$$\varepsilon(t) = \int_0^t \frac{\partial [H^+](u)}{\partial u} L(t-u) du \ , \tag{15}$$

where L is the mechanochemical compliance determined from the immersion of the material in a buffer solution that resembles the experiment of the application of a constant load or creep experiment.

### 7.1.3. Time-Temperature Superposition

The modulus of a material is a function of time as well as environmental conditions. The temperature affects the behavior of viscoelastic materials. Additionally, the viscoelastic properties of hydrogels have an important pH dependence. The time-temperature superposition technique for amorphous polymers allows the construction of a time function for the modulus at a specific temperature based on a set of short experiments at different temperatures. This technique can be adapted to describe the modulus at a particular pH in time.

The time-temperature superposition technique suggests the substitution of a prohibitively large experiment at a certain temperature by a series of independent experiments at different temperature T (Figure 7.1). The modulus data generated by the different experiments are shifted in order to graphically build a continuous function for the temperature of reference $T_{ref}$ in a large time range [2]:

$$E(T_{ref}, t) = a_V E(T, t/a_T), \tag{16}$$

where $a_V$ and $a_T$ are the vertical and time shifting factors respectively.

Adjusting the magnitude of the modulus, the individual experimental curves are shifted vertically in order to let the final and initial segments or trends to superimpose. Considering that the modulus is proportional to the absolute temperature and is affected by the density of the material [2], the vertical shift is done by:

$$E(T_{ref}, t) = \frac{\rho(T_{ref}) T_{ref}}{\rho(T) T} E(T, t/a_T), \tag{17}$$

where the ratio of the density-temperature products constitutes the vertical shifting factor $a_V$.

The horizontal displacement of the curves is produced by the use of the time shifting factor is given by [2]:

$$a_T = \frac{\eta(T)}{\eta(T_{ref})}, \tag{18}$$

where $\eta$ is the viscosity of the system, which can be calculated with the Doolittle equation [2]:

$$\ln \eta = \ln A + B\left(\frac{V - V_f}{V_f}\right). \tag{19}$$

In this equation, B has been determined to be approximately equal to 1 [2], lnA is cancelled when calculating $\ln(a_T)$ from Equation (18), V is the total volume of the system and $V_f$ is the free volume of the system or volume occupied by the solvent in the case of a hydrogel material in a solution.

Considering:

$$\frac{V_f}{V} = 1 - \frac{1}{Q} \tag{20a}$$

and

$$\frac{V}{V_f} - 1 = \frac{1}{Q - 1}, \tag{20b}$$

Equation (18) can be written as:

$$ln\,a_T = \frac{1}{Q-1} - \frac{1}{Q_{ref}-1}, \tag{21}$$

where Q and $Q_{ref}$ are the equilibrium volume swelling ratios at T and $T_{ref}$, respectively.

The horizontal shifting factor can also be expressed in terms of time constants, $\tau$. The viscosity is the ratio of the shear stress to the velocity of the fluid, and the latter is inversely proportional to the time constant. Therefore, the time scaling factor can be also at different temperatures in the following way:

$$a_T = \frac{\tau(T)}{\tau(T_{ref})}. \tag{22}$$

Clearly, Equations (21) and (22) can be applied to calculate the horizontal shifting factor for the construction of a master curve under any environmental condition. For example, a time factor $a_{pH}$ for a time-pH superposition would be calculated with Q or $\tau$ and $Q_{ref}$ or $\tau_{ref}$ under the same temperature and at a certain pH and the reference pH, respectively.

## 7.2. Experimental Work

The P(MAA-g-EG) hydrogel samples synthesized without enzymes, with TEGDMA and with excess of solvent are tested using the equipment Instron 4300. A scheme of the Instron equipment is shown in Figure 7.2.

Rectangular films (without enzymes) were immersed in different pH solutions until equilibrium. Bell shape samples (Figure 7.3) were cut from the films in preparation for a tensile experiment to determine the mechanical modulus. This parameter depends on the pH of the sample due to the associated density changes of the hydrogel. Tensile experiments, although performed in air at room temperature, are considered to correspond to the pH at which the sample reached equilibrium. Appendix 7.2 presents the parameters and protocol followed for the tensile mechanical tests.

Data from the experiment for the determination of relaxation times (Section 6.1) was used to obtain the mechanochemical compliance function of the hydrogel. In this experiment, a hydrogel sample was changed from buffer solutions maintained at 37°C in a water bath with a period of 24 hours, and the volume was monitored constantly during the first 8 hours. The second half of the sequence of the steps (from 7.2 to 6.2, from 6.2 to 5.8, from 5.8 to 5.4 and from 5.4 to 4.8), was chosen because the hydrogel action would occur from a pH close to 7. A last step from 4.8 to 3.2 was simulated to complete the information of the whole range of swelling of the hydrogel although the expected variation of the mechanochemical compliance is very small.

## 7.3. Results and Discussion

The different tensile tests at a particular pH show repeatability and fit a polynomial equation for the strain-stress relation, shown in the respective Figures 7.4 to 7.7. The first derivative of this equation leads to an expression for the mechanical modulus at each pH in terms of strain. Specific mechanical moduli are reported for strain values of 0, 1 and 2 in Table 7.1.

Time functions for the mechanical compliance can be obtained from the inverse of the mechanical modulus and the strain ratio applied in the tensile experiment as follows:

$$D(t) = \frac{1}{E(t)} = \frac{1}{E(x)\big|_{x=rt/l_o}}, \qquad (23)$$

where x is strain, r is the crosshead speed (mm/s), t is time (s) and $l_o$ is the initial length (mm). Table 7.2 and Figure 7.8 show the family of time curves generated for the mechanical compliance and modulus at different pH values.

A drastic change is observed between the behavior below and above the critical pH. For pH values of 3.2, 4.4 and 5.4, the curves are very similar and approach the function:

$$E(t) = -4E\text{-}10t^6 - 9E\text{-}06t^5 + 0.0054t^4 - 1.2546t^3 + 135.88t^2 - 6823.9t + 142612.$$

(24)

Above the critical pH, at pH 6.6, the behavior before the break point is fitted by:

$$E(t) = 32585e^{-0.0218t}.$$

(25)

Since a breaking point was detected at pH 6.6, there is no reason for a projection of the modulus beyond the time at which it occurs. However, in order to describe the general behavior of hydrogels, the analogous time-pH correspondence technique can be applied to define a tendency of the modulus in the long term.

The pH of 6.6, closest to the physiological condition, is chosen as reference. The shift factors are reported in Table 7.3. The curves shifted vertically and horizontally suggest the use of a single curve shown in Figure 7.9 and given by:

$$E(t) = \begin{cases} -0.0691t^3 + 20.533t^2 - 1688.1t + 54375, & t \leq 30\,\text{s} \\ 20346, & t > 30\,\text{s} \end{cases}.$$

(26)

The master curve (26) is subject to some limitations. The adjusted function assumes that the modulus remains constant at large times. The time range for the shifted curves does not increase with respect to the range of experimental time data.

The mechanical modulus and compliance calculations show values and time dependence characteristic for all hydrogels. Cationic and anionic gel films are expected to experience larger stress forces at higher strain and their mechanical modulus is supposed to decrease with time.

The volume-swelling ratio of the sample can be modified to refer to the volume of the sample with respect to the volume at an initial hydrated equilibrium state. The volume ratio can be expressed in terms of a characteristic length, as indicated in the following equation:

$$\frac{Q}{Qeq} = \frac{V}{Veq} \approx \frac{l^3}{l_{eq}^3} = \left(\frac{l_{eq} + \Delta l}{l_{eq}}\right)^3 = (1+\varepsilon)^3.$$

(27)

The model for the volume swelling ratio of P(MAA-g-EG) gel according to the definition of mechanical compliance, the Boltzmann superposition principle and the volume approximation from a single characteristic length is given by:

132

$$\frac{Q}{Qeq} \approx \left(1 + \int_0^t D(t-u)\frac{\partial\sigma(u)}{\partial u}du\right)^3 . \tag{28}$$

Although the stress can be considered as the input or forcing function of a hydrogel system, the concentration input is of interest for the final use of the material. Numerical evaluation of Equation (28) allows the simulation of the hydrogel behavior before a stress input. In order to simulate the response before a concentration change, a relaxation experiment (with no strain change) in water with a specific feed rate of an acid or basic solution would be necessary for the calculation of a "chemical modulus" (for the chemical input) analogous to the mechanical modulus, as proposed in Figure 7.10. The slope of the stress-hydrogen ion concentration curve from this relaxational experiment would give the chemical modulus $F([H^+])$. The chemical modulus could be expressed in terms of time using the concentration rate. With $F(t)$, the superposition principle could be applied to obtain:

$$\sigma(t) = \int_0^t F(t-u)\frac{\partial[H^+]}{\partial u}du . \tag{29}$$

Substituting Equation (29) in Equation (28), the swelling behavior could be described in terms of hydrogen ion concentration as:

$$\frac{Q}{Qeq} \approx \left(1 + \int_0^t D(t-u)F(t-u)\frac{\partial[H^+]}{\partial u}du\right)^3 . \tag{30}$$

The mechanochemical compliance, as defined by Peppas, correlates the volume changes and the hydrogen ion concentration directly:

$$\frac{Q}{Qeq} = \frac{V}{Veq} \approx (1+\varepsilon)^3 = \left(1 + \int_0^t L(t-u)\frac{\partial[H^+]}{\partial u}du\right)^3 . \tag{31}$$

The relation between the complex mechanochemical compliance in Equation (31) and the elemental parameters (mechanical compliance and chemical modulus) in Equation (30) would be:

L(t-u) = D(t-u) F(t-u). \hfill (32)

The input for the model given by (31) is the change in hydrogen ion concentration and the output is the volume ratio. The experiments for the determination of relaxation times (Section 6.1), where the volume of the material is monitored continuously before pH step changes, allow for the characterization of the time function of the mechanochemical compliance. Each immersion of the hydrogel sample in a buffer solution at a certain pH resembles a creep experiment where the deformation is measured under a specific load.

Instantaneous values of the mechanochemical compliance are calculated assuming a constant value:

$$L = \frac{\left(\dfrac{Q(t)}{Qeq}\right)^{\frac{1}{3}} - 1}{[H^+](t) - [H^+]_{eq}},$$  (33)

where $Q_{eq}$ and $[H^+]_{eq}$ are the initial equilibrium swelling ratio and hydrogen ion concentration for each dynamic experiment, and $[H^+](t)$ is the concentration of hydrogen ions in the microenvironment of the gel. The local concentration $[H^+](t)$ can be calculated from the hyperbolic tangent functions obtained from equilibrium experiments. At equilibrium in a batch experiment, diffusion of hydrogen ions is assumed to stop because the concentration in the vicinity of the hydrogel is equal to the concentration in the bulk solution. The pH of the microenvironment of the hydrogel is known at equilibrium because it is considered to be equal to the pH of the buffer solution. The pH-volume swelling ratio curve obtained in section 5.1 is useful not only to predict equilibrium conditions but to know the local pH from the observed volume swelling ratio through the inverse function:

$$pH = \frac{1}{c}\left[ tanh^{-1}\left(\frac{Q-a}{b}\right) - d\right]$$  (34)

The sign of the L quantities calculated with (33) is determined by the type of hydrogel materials. For an anionic hydrogel, the mechanochemical compliance is negative because the material collapses $(Q(t)/Q_{eq}<1)$ when pH decreases $([H^+](t) > [H^+]_{eq})$ and viceversa. In the case of a cationic hydrogel, the mechanochemical values from (33) are positive.

The sign may be separated from the reported mechanochemical compliance values by writing for an anionic hydrogel:

$$\frac{Q}{Qeq} \approx \left(1 - \int_0^t L(t-u)\frac{\partial[H^+]}{\partial u}du\right)^3.$$  (35)

However, the sign as part of the definition of the mechanochemical compliance is preferred in this discussion.

The time tendency of the magnitude of the mechanochemical compliance can be verified by inspection of Equations (31) and (32). The magnitude of the mechanical compliance of viscoelastic materials, D, is expected to augment because the application of a particular stress causes a bigger deformation as time passes. The absolute value of the chemical modulus, F, is expected to decrease because a certain pH change is expected to produce a smaller stress in the material as it is used. Therefore the product in the right hand of Equation (32) is expected to tend to zero at large times. Accordingly, if a pH change

may be less effective on the volume of the gel in the long term, L in Equation (31) is expected to decrease in time. These considerations agree with the proposal of decaying exponential L functions in previous works ([3]). However, the product of an increasing curve with a decreasing curve gives a function with zero initial and final values and a maximum magnitude. Regarding the initial value of the mechanochemical compliance, a value different from zero is assumed since the material is sensitive to stress and chemical changes particularly from the equilibrium relaxed state. A peak or oscillation of L at other times is possible due to the product of opposite trends for D and F.

A family of experimental mechanochemical compliance curves is managed with a procedure analogous to the time-temperature superposition technique. Figure 7.11 presents the individual mechanochemical compliance curves to align. The horizontal shift is done considering the real time of the measurements in the consecutive step experiments and the respective time constants determined in Section 6.1 to apply Equations (22) and (16). The magnitude is also adjusted to the pH of reference.

The mechanochemical compliance values are recalculated to produce a vertical shift of the curves, in the following way:

$$L(t)\big|_{pH\,ref} = \frac{\left(\dfrac{Q(t)}{Q_{ref}}\right)^{1/3} - 1}{[H^+](t) - [H^+]_{ref}}, \tag{36}$$

where $Q_{ref}$ and $[H^+]_{ref}$ are the equilibrium volume swelling ratio and hydrogen ion concentration at the pH of reference 7.2.

The curves resulting from the time and magnitude shifts constitute the master curve given by (Figure 7.12). The master curve is fitted by sections for the following mathematical representation:

$$L(t) = \begin{cases} -37625, & t \leq 87 \ min \\ -110000 + 75000\,exp\left(-0.00115(t - 86.9565)\right), & 87 \leq t < 8371\,min \\ -84715 + 22626\,tanh\left(0.001888t - 33.0442\right), & t \geq 8371\,min \end{cases} \tag{37}$$

The utility of Equation (37) should be evaluated with the prediction of the swelling ratio. The numerical evaluation of the swelling ratio Equation (31) can be done with the algorithm for the rectangular integration of Appendix 7.1. The data of the steps from 6.2 to 7 and from 7 to 6.2 are used for the simulation and the comparison. If the equilibrium swelling ratio is not changed for the second step experiment and the history of pH changes is conserved, Figure 7.13 shows that the calculated volume swelling ratio during the first step is approximated to the real behavior, but not during the second step. The integration over all the pH experienced by the gel produces a great inertia effect that impedes to modify the direction of volume changes as fast as they occur experimentally. If the

equilibrium swelling ratio is updated and the integration is calculated from the time of the application of the second step (not from time zero), the simulation can approximate the real behavior (Figure 7.14). The disadvantage of the evaluation of (31) is the increasing time and memory involved in the integration during a continuous simulation.

## 7.4. Conclusions

The elastic moduli of hydrogels at different pH show a clear change around the critical pH or transition pH of the material as observed for other intensive properties such as density and mesh size.

Viscoeleastic properties as continuous time functions were obtained to characterize the long term behavior of the material disregarding rupture. While the mechanical modulus is an important parameter for the description of the hydrogel, the mechanochemical compliance is useful for the simulation of its pH responsive behavior.

The volume swelling ratio of the hydrogel was simulated using the Boltzmann superposition theorem. This theorem does not account for a changing dynamic as a result of the aging of the material. This theorem is used considering the same mechanochemical compliance function is valid to describe the additive effect of a concentration change from the moment it occurs. The aging of the hydrogel is related to a degradation process, which is not approached in this work. The late response of the material is related to the asymptotic behavior observed at high (or low) pH values in an experiment, similarly to high elongation or stress developed at the end of a mechanical test.

The use of one-dimensional mechanochemical compliance and the Boltzmann theorem produces a bias error. For this reason, the update of the equilibrium volume swelling ratio and the reset of the integral at a steady state condition improve the estimation of the transitory volume swelling ratio. The same procedure is necessary for the evaluation of the first order models with a tridimensional compliance, however, the calculated output reproduces the experimental volume swelling ratio with a superior precision (Section 6.1). Moreover, the reset of the integral and the update of the initial volume swelling ratio take place only when there is a change in operation zone, according to previously defined pH ranges and the direction of change.

Important differences can be pointed out between the one and the three dimensional mechanochemical compliances, beside the number of coordinates considered to represent the swelling of the hydrogel material. The one-dimensional compliance is expressed as a time function, and determines not only the sensitivity, but also the speed of the hydrogel response to pH changes. The three-dimensional compliance is a constant value dependent on the operation zone and represents only the sensitivity of the hydrogel, although it also affects the velocity of the response. The dynamic behavior is characterized with the combination of the tridimensional compliance and the relaxational time. The non-linearity of the hydrogel swelling process is modeled with the non-linear one-dimensional compliance function, while accounted by a set of a first order models with a tridimensional compliance and a relaxation time.
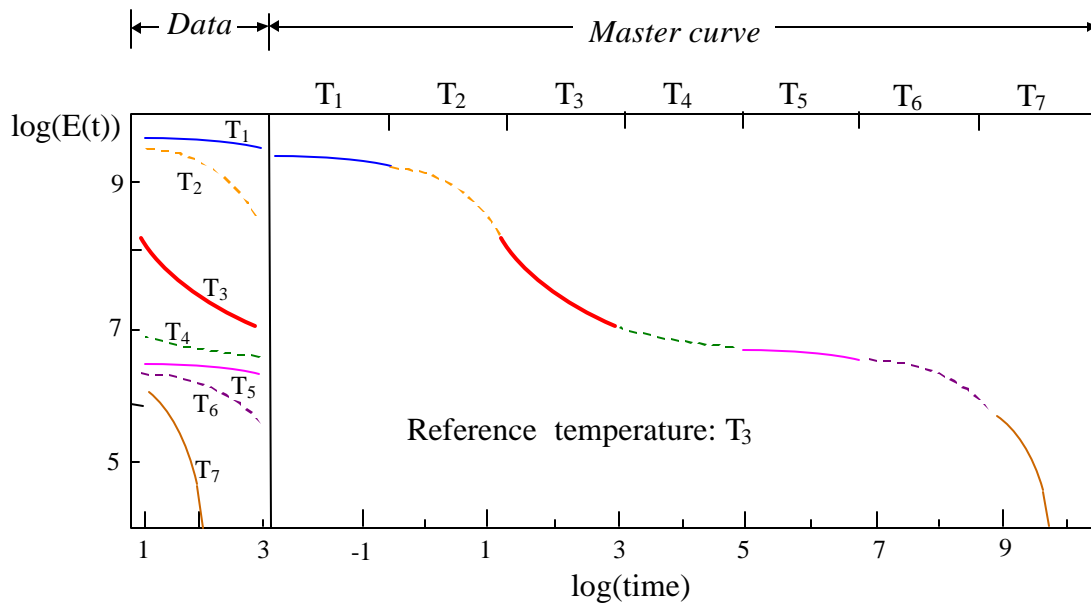
**Figure 7.1. Time-Temperature Superposition Technique.** Independent short experiments at different temperatures are used for the construction of a master curve of the mechanical modulus in a wide range of time at a specific temperature. Figure adapted from [2].
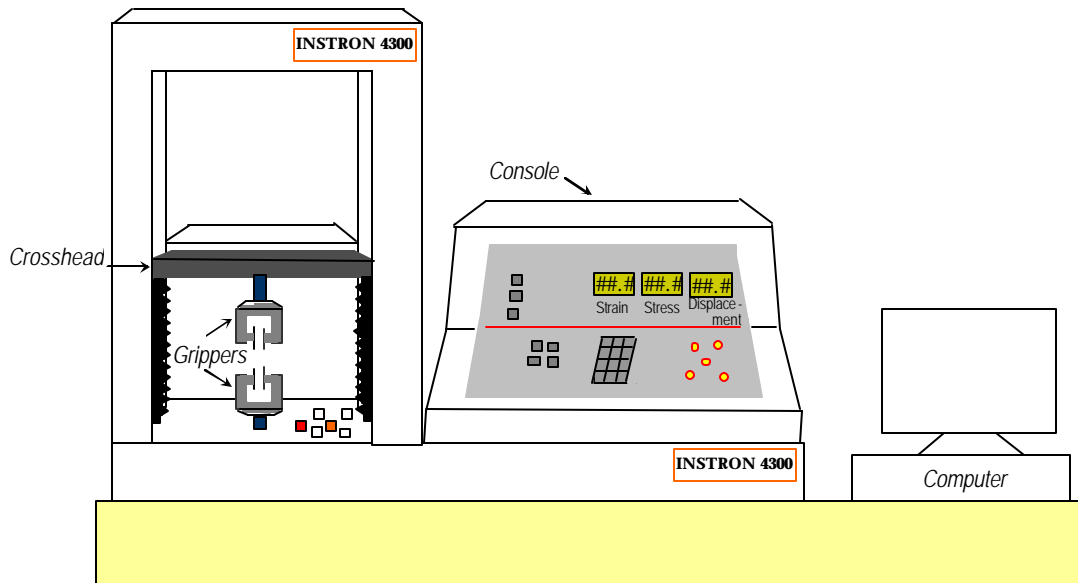


**Figure 7.2. Scheme of Instron Instrument.** Tensile tests were programmed in the computer. The console was used to move the crosshead manually in preparation for the experiment or to stop a test. The clamped sample was stretched by displacing the crosshead.

137
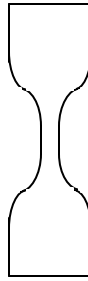
**Figure 7.3**. **Bell shape**. The samples were cut in this form for the mechanical tests.


**Table 7.1.  Mechanical Modulus E at Different pH and Strain Values.** Samples at pH 6.6 broke before a change of length of 200% (* at strain of 2).  The times associated with the strain values of 0, 1 and 2 are 0, 60 and 120 seconds.

| pH | Strain | E (Pa) | E (lb/in$^2$) |
|---|---|---|---|
| 3.2 | 0 | 155789 | 22.6 |
|  | 1 | 12133 | 1.8 |
|  | 2 | 19719 | 2.9 |
| 4.4 | 0 | 125651 | 18.2 |
|  | 1 | 15382 | 2.2 |
|  | 2 | 15676 | 2.3 |
| 5.4 | 0 | 146769 | 21.3 |
|  | 1 | 17168 | 2.5 |
|  | 2 | 17863 | 2.6 |
| 6.6 | 0 | 32383 | 4.7 |
|  | 1 | 11297 | 1.5 |
|  | 2 | ---* | ---* |

$y = -1174.8x^6 + 14565x^5 - 71829x^4 + 177842x^3 - 227821x^2 + 155789x$

$R^2 = 0.9956$
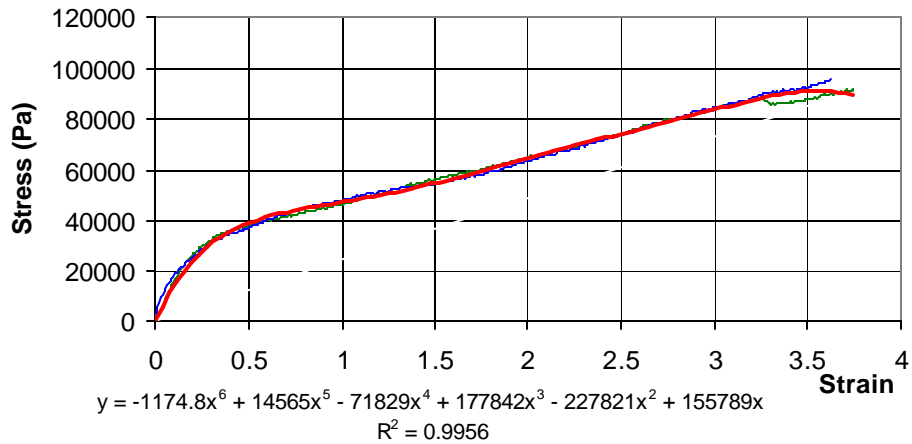
**Figure 7.4. Tensile Experiment at pH 3.2.** Two samples initially at equilibrium in pH 3.2 solutions at 25°C were submitted to a stretching rate of 10 mm/min in air (the individual experiments are shown in green and blue). Initial separation between grips was 10 mm; sample width and thickness were 5.63 mm and 0.7 mm, respectively. A polynomial (red line) is fitted to calculate the mechanical modulus by derivation.



$y = -967.39x^6 + 11737x^5 - 56153x^4 + 135129x^3 - 171962x^2 + 125651x$

$R^2 = 0.9578$
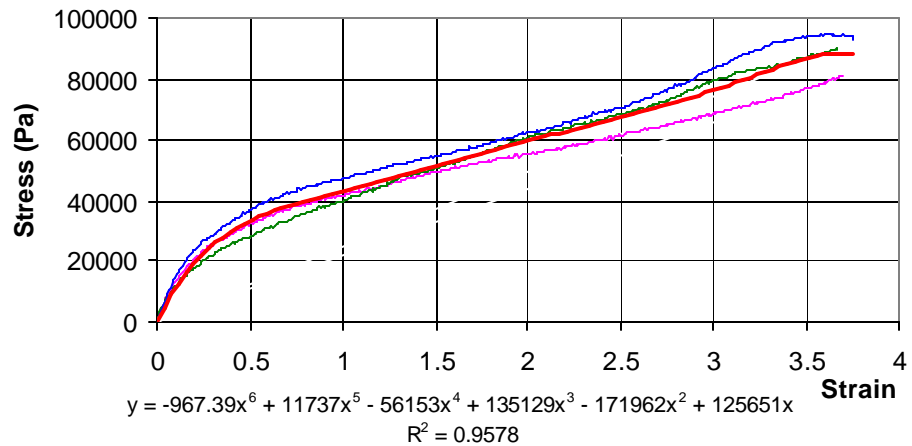
**Figure 7.5. Tensile Experiment at pH 4.4.** Three samples initially at equilibrium in pH 4.4 solutions at 25°C were submitted to a stretching rate of 10 mm/min in air (the individual experiments are shown in green, pink and blue). Initial separation between grips was 10 mm; sample width and thickness were 5.63 mm and 0.7 mm, respectively. A polynomial (red line) is fitted to calculate the mechanical modulus by derivation.

$$y = -1435.3x^6 + 16884x^5 - 78028x^4 + 179907x^3 - 216509x^2 + 146769x$$
$$R^2 = 0.9381$$
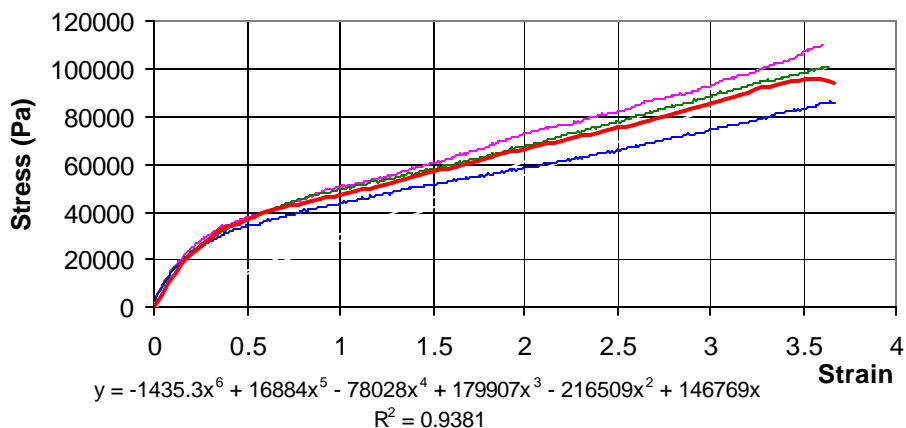
**Figure 7.6. Tensile Experiment at pH 5.4.** Three samples initially at equilibrium in pH 5.4 solutions at 25°C were submitted to a stretching rate of 10 mm/min in air (the individual experiments are shown in green, pink and blue). Initial separation between grips was 10 mm, sample width and thickness were 5.63 mm and 0.7 mm, respectively. A polynomial (red line) is fitted to calculate the mechanical modulus by derivation.



$$y = 5806.8x^3 - 19837x^2 + 32383x$$
$$R^2 = 0.9947$$
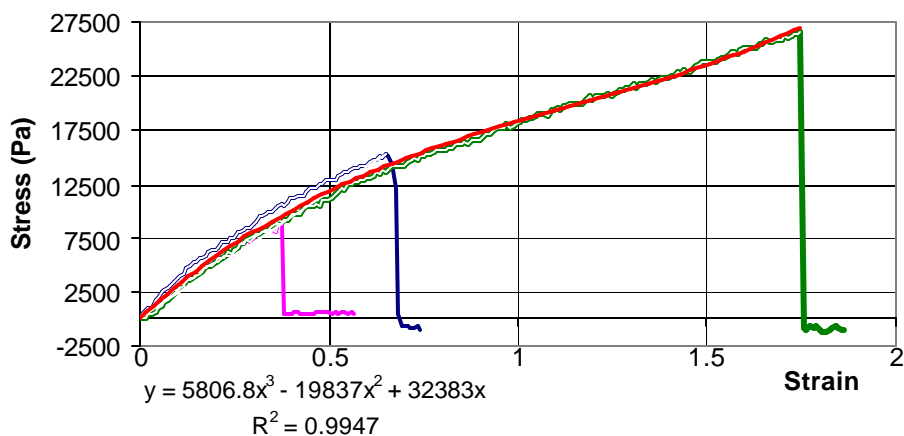
**Figure 7.7. Tensile Experiment at pH 6.6.** Three samples initially at equilibrium in pH 6.6 solutions at room temperature were submitted to a stretching rate of 10 mm/min in air (the individual experiments are shown in green, pink and blue). Initial separation between grips was 10 mm; sample width and thickness were 5.63 mm and 0.7 mm, respectively. A polynomial (red line) is fitted to calculate the mechanical modulus by derivation.

140

**Table 7.2.  Mechanical Compliance Functions D(t).**  P(MAA-g-EG) hydrogel with TEGDMA, excess of solvent and no enzymes was analyzed.  Compliance D in Pa$^{-1}$; modulus E in Pa; time t is in seconds.

| pH | Mechanical compliance D(t)=1/E(t) | t range |
|----|------------------------------------|---------|
| 3.2 | $1/(-9E\text{-}6\ t^5 + 0.0056\ t^4 - 1.33\ t^3 + 148.2\ t^2 - 7594.03\ t + 155789)$ | 0-231 (192) |
| 4.4 | $1/(-7E\text{-}6\ t^5 + 0.0045\ t^4 - 1.04\ t^3 + 112.6\ t^2 - 5732.07\ t + 125651)$ | 0-225 (209) |
| 5.4 | $1/(-1.11E\text{-}5\ t^5 + 0.0065\ t^4 - 1.44\ t^3 + 159\ t^2 - 7216.97\ t + 146769)$ | 0-216 (189) |
| 6.6 | $1/(4.839\ t^2 - 661.233\ t + 32383)$ | 0-34 |
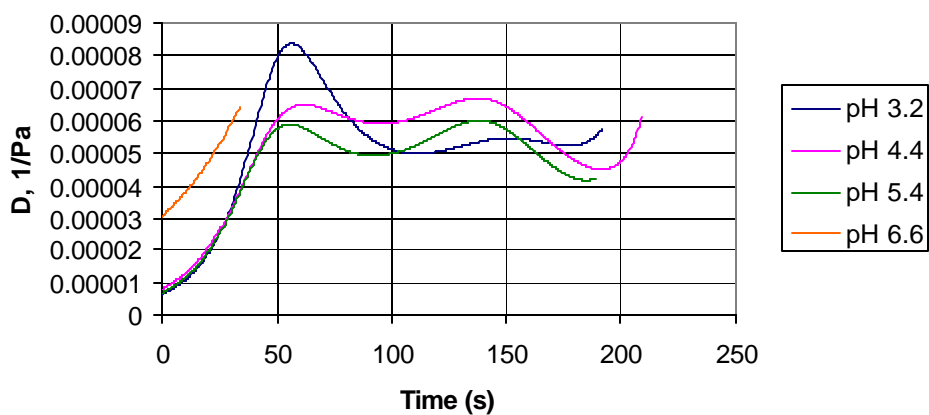


(a)
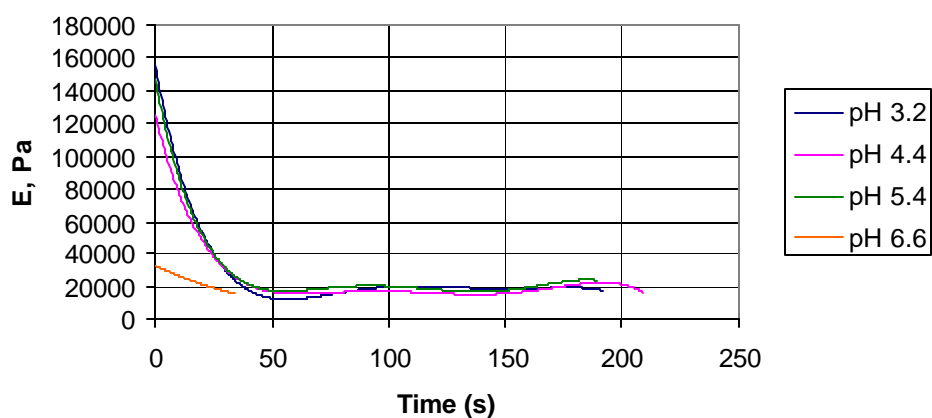


(b)

**Figure 7.8. Sets of Curves for the Mechanical Compliance (a) and Modulus (b).**  The individual functions are presented in Table 7.2.

**Table 7.3. Shifting Factors.** The density ρ, the mechanical modulus magnitude shifting factor, the volume swelling ratio Q and the mechanical modulus time shifting factor $a_{pH}$ are given for each pH value.

| pH | ρ, mg/mL | $\dfrac{\rho\vert_{pH\,ref}\,pH_{ref}}{\rho\vert_{pH}\,pH}$ | Q | $a_{pH}$ |
|---|---|---|---|---|
| 3.2 | 1.238 | 1.708 | 1.24 | 65.30 |
| 4.4 | 1.186 | 1.297 | 1.47 | 7.84 |
| 5.4 | 1.037 | 1.208 | 6.23 | 1.13 |
| 6.6 | 1.025 | 1 | 15.7 | 1 |
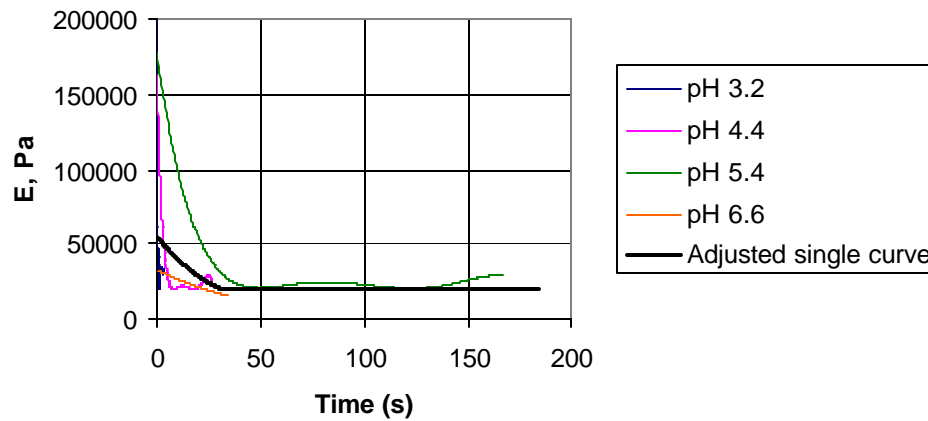


**Figure 7.9. Mechanical Modulus Curve.** A single curve is adjusted from the shifted individual E(t) functions.

142
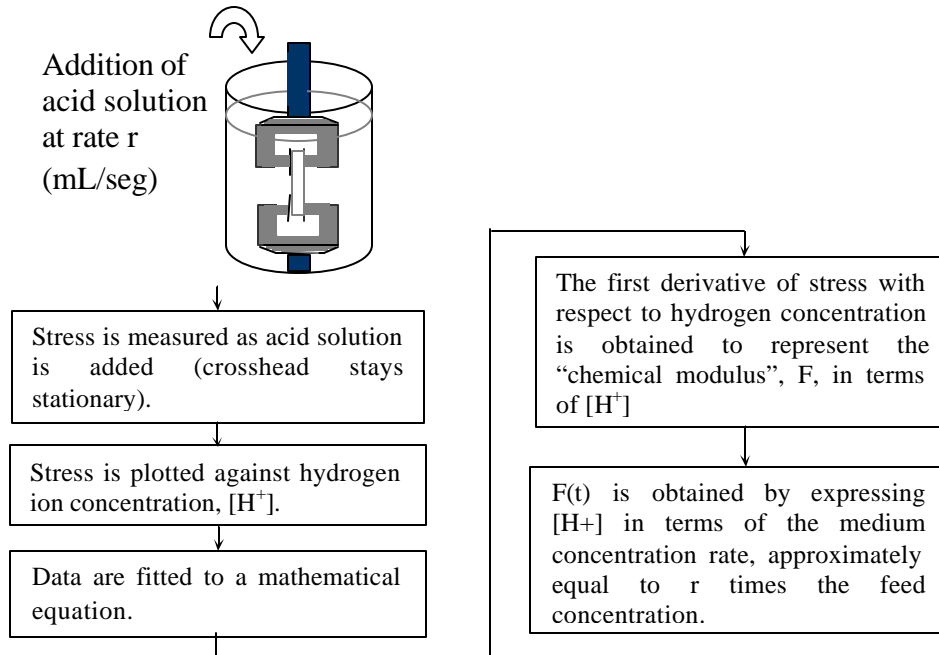
**Figure 7.10. Experiment and Determination of Chemical Modulus.** The laboratory procedure is analogous to a tensile or compression experiment because of the rate of change in the pH of the solution. The procedure is similar to a stress relaxation experiment since the strain is constant. Several difficulties would need to be solved: mixing, temperature control at 37°C and continuous addition of acid solution without disturbing stress measurements.
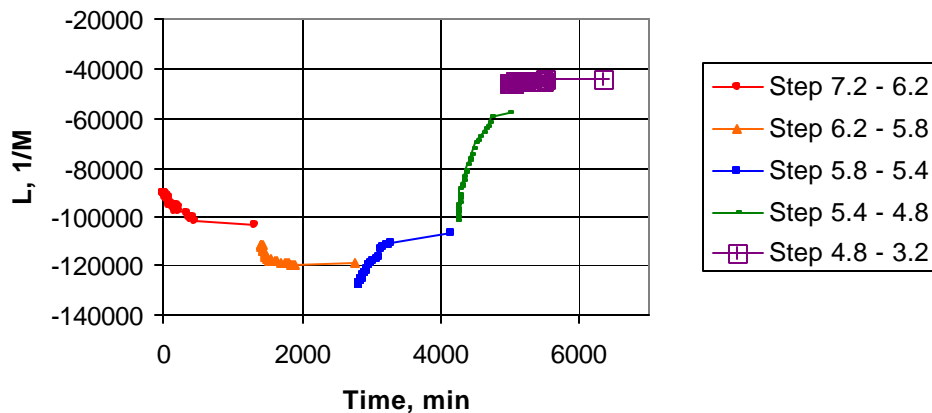


**Figure 7.11. Set of Mechanochemical Compliance Curves.** Horizontal and vertical shifts have not been applied (experiments were carried out consecutively).

143
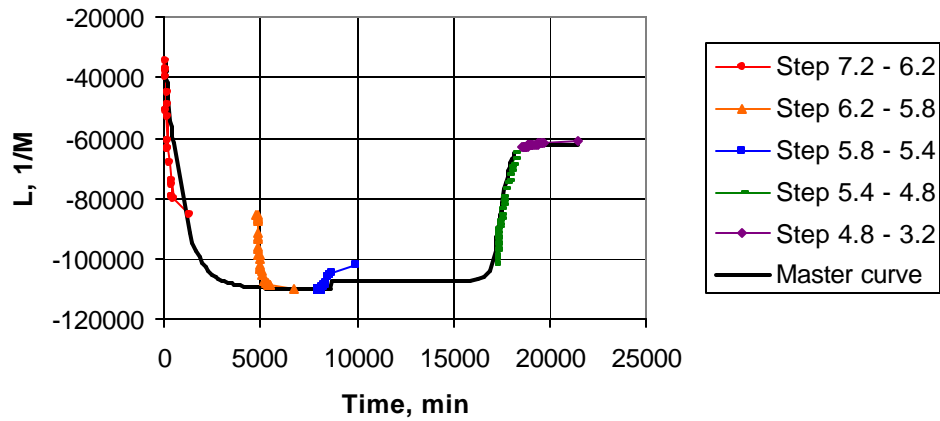
**Figure 7.12.   Master Curve of Mechanochemical Compliance at pH 7.2.**   Set of mechanochemical compliance curves after horizontal and vertical shifts.   The master curve is fitted by sections: an exponential function for the first part and a hyperbolic tangent function for the rest.
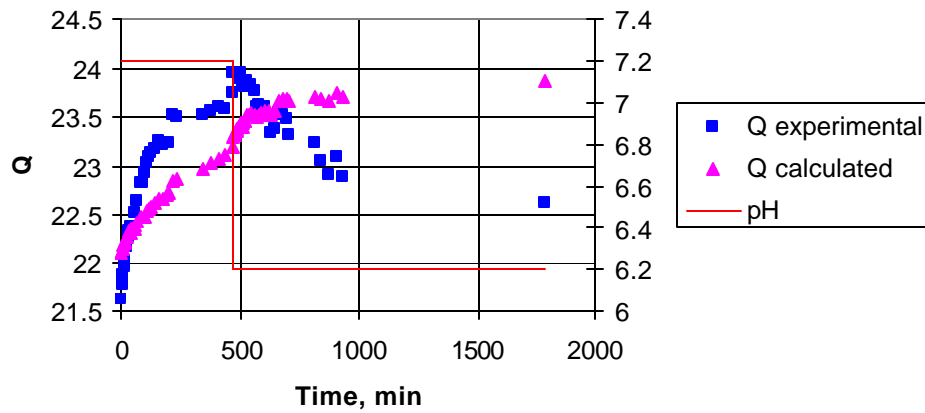


**Figure 7.13. Simulation of the Volume Swelling Ratio with the Master Function of the Mechanochemical Compliance.**  Two pH steps are applied from 6.2 to 7.2 and from 7.2 to 6.2.  The hydrogen ion concentration for Equation (31) is calculated from the experimental Q. The equilibrium volume swelling ratio is the initial condition for the first experiment and the integration in Equation (31) is calculated from time 0 min.
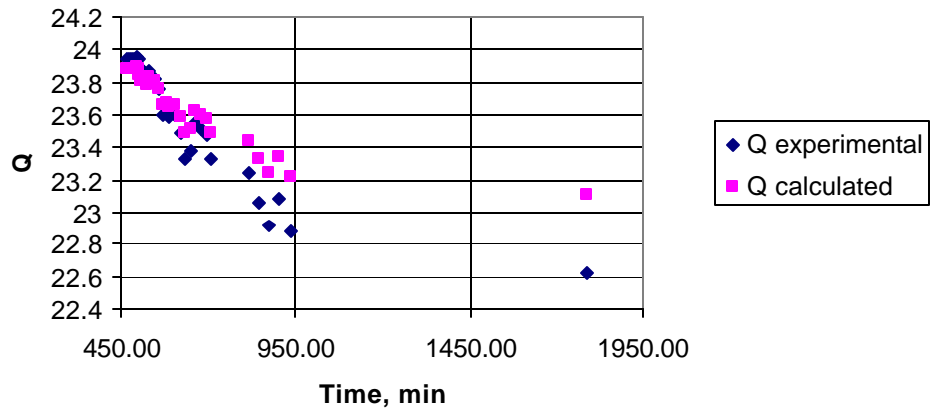
**Figure 7.14. Simulation of the Volume Swelling Ratio with the Master Function of the Mechanochemical Compliance.** A pH step from 7.2 to 6.2 is applied at time 470 min, after a first step from 6.2 to 7.2. The hydrogen ion concentration for Equation (31) is calculated from the experimental Q. The equilibrium volume swelling ratio is updated and the integration in Equation (31) is calculated from time 470 min.

**References**

1. Dowling NE. Mechanical behavior of materials: engineering methods for deformation, fracture and fatigue. Upper Saddle River, NJ: Pearson Prentice Hall, 2007.

2. Aklonis JJ, MacKnight WJ. Introduction to polymer viscoelasticity ($2^{nd}$ edition). New York: John Wiley & Sons, Inc., 1983.

3. Brannon-Peppas L, Peppas N. Time-dependent response of ionic polymer networks to pH and ionic strength changes. Int J Pharm, 1991;70:53-57.

4. Podual K, Peppas N. Relaxational behavior and swelling-pH master curves of poly[(diethylaminoethyl methacrylate)-graft-(ethylene glycol)] hydrogels. Polym Int 2005;54:581-593.

**Appendix 7.1. Numerical Evaluation of the Boltzmann Superposition Principle**

The expression for the Boltzmann superposition principle can be explained by considering creep experiments monitored at discrete times $t_k$ [2]. Creep compliance allows to calculate the strain $\varepsilon_0(t_k)$ due to the constant stress $\Delta\sigma_0$ applied at time $t_0$:

$$\varepsilon_0(t_0) = \Delta\sigma_0 D(t_0);\ \varepsilon_0(t_1) = \Delta\sigma_0 D(t_1);\ \varepsilon_0(t_2) = \Delta\sigma_0 D(t_2);\ ... \tag{a7.1}$$

The strain $\varepsilon_1(t_k)$ caused by a stress change $\Delta\sigma_1$ applied at time $t_1$, would be:

$$\varepsilon_1(t_0) = 0;\ \varepsilon_1(t_1) = \Delta\sigma_1 D(t_0);\ \varepsilon_1(t_2) = \Delta\sigma_1 D(t_1);\ ... \tag{a7.2}$$

After applying $\Delta\sigma_2$ at time $t_2$, the total strain $\varepsilon(t_k)$ would be given by:

$$\varepsilon(t_0) = \Delta\sigma_0 D(t_0),$$

$$\varepsilon(t_1) = \Delta\sigma_0 D(t_1) + \Delta\sigma_1 D(t_0) \tag{a7.3}$$

$$\varepsilon(t_2) = \Delta\sigma_0 D(t_2) + \Delta\sigma_1 D(t_1) + \Delta\sigma_2 D(t_0)$$

For any discrete time $t_k$:

$$\varepsilon(t_k) = \sum_{j=0}^{k} \Delta\sigma_j D(t_{k-j}) \tag{a7.4}$$

where $\Delta\sigma_0 = \sigma_0$, $\Delta\sigma_1 = \sigma_1 - \sigma_0$, $\Delta\sigma_2 = \sigma_2 - \sigma_1$, ..., $\Delta\sigma_k = \sigma_k - \sigma_{k-1}$ and the total stress acting on the material at any time $t_k$ is $\sigma_k = \sigma_0 + \Delta\sigma_1 + \Delta\sigma_2 + ... + \Delta\sigma_{k-1} + \Delta\sigma_k$.

Equation (a7.4) implements a rectangular integration of the continuous Equation (13). The discrete evaluation of the strain requires recording all the history of stress changes and compliance values, since all the terms of the summation have to be recalculated each time

In terms of a pH input and the mechanochemical compliance, the Boltzmann superposition principle can be evaluated numerically as:

$$\varepsilon(t_k) = \sum_{j=0}^{k} \Delta[H^+]_j L(t_{k-j}). \tag{a7.5}$$

The following pseudocode allows the calculation of the strain at each $t_k$.

1. Initialize array A, whose rows will contain the information of each integration step. The fist element of a row is for L and the second for $\Delta[H^+]$: A=[0 0]

2. Save array A in archive.

3. At each integration step, different from the initialization step:

   - Read array A
   - Determine the number of rows n
   - Form vectors L and DH with the first and second column of A
   - Initialize the variable strain in zero
   - Calculate $L(n+1)$ from the simulation time
   - Assign recent $\Delta[H^+]$ to $DH(n+1)$
   - Initialize a counter j with the index of the first element with simulation data in L or DH arrays (j=2, since $L(1)=0$ and $DH(1)=0$)
   - While $j<=n+1$
       - Strain=strain + $H(j)*L(n+1-(j-1))$
       - Increment counter $j=j+1$

4. Assign $L(n+1)$ and $DH(n+1)$ to $A(n+1, 1)$ and $A(n+1, 2)$
5. Save array A in archive and repeat steps 3-5 until the simulation is stopped

**Appendix 7.2. Tensile Experiments Protocol**

1. Hydrogel films are equilibrated in different pH solutions for 24 hours (three films per pH value).

2. A bell shape Teflon template is produced and enveloped with aluminum paper for easy visualization (when placing on the transparent film) and handling (the aluminum paper prevents adhesion of the template onto the film).

3. A test method is defined with the Series IX (version 8.08.00) software with the following parameters:

| | |
|---|---|
| Test type: Tensile | First crosshead speed: 10 mm/min |
| Number of specimens: 3 | Temperature: 25°C |
| Geometry: rectangular | Humidity: 50 % |
| Number of channels: 2 | Auto-start: Disabled |
| Machine type: 4200/4300/4400 | Separate dimension entry: Enabled |
| Machine control: Standard | Width: 5.6300001 mm |
| Data rate; 2 pts/sec | Thickness: 1.0000000 mm |
| Extensometer: Disabled | Specific gauge length:  10.0000000 mm |

4. The crosshead of the Instron is moved manually (using the buttons of the console and the buttons close to the fixed gripper) until the pending gripper is 10 mm apart from the top of the lower fixed gripper.  This distance is called specific gauge length.

5. A film is taken out of the buffer solution, and the bell shape template is used to cut the sample.  This shape allows for tightening the sample from the wider parts with the grippers and exposing a rectangular geometry to stretch.

6.  The sample is placed in the Instron using the grippers.  The sample must be firmly but still gently tightened (to keep the integrity of the sample).

7. The test is started from the computer. When the sample is broken, the crosshead is stopped from the console, which interrupts the test run in the computer.

8. Steps 3 through 7 are repeated to complete the number of specimens indicated in the definition of the test.

9. A new test method may be define with the same parameters, but different names and comments for the results archives corresponding to specimens of sample films equilibrated at a different pH.

## 8. Mathematical Modeling of Physiologic Process and Hydrogel System

The mathematical models for glucose metabolism in a diabetic patient and the hydrogel monolithic system are discussed in this chapter. The models of the glucose-insulin physiologic process according to Ackerman [1] and Sorensen [2] are presented as the basis for the study of closed loop treatment systems. The interaction of a hydrogel-based system with the glucose-insulin metabolism is represented with the Sorensen model for a better description in terms of the specific location of the insulin delivery system.

This chapter is organized in five sections. The first two sections give a general description of the physiological models by Ackerman and Sorensen. In both models, a proper manipulation variable for an explicit controller is identified. In the third section, the Sorensen model is modified with the addition of a compartment for a hydrogel implant in the peritoneum. The hydrogel compartment is developed from the previously presented experimental characterization results (Chapter 6). The fourth section presents and discusses simulation results, and the fifth section concludes the chapter.

## 8.1. Ackerman Physiological Model for Glucose-Insulin Metabolism

Compartmental or mechanistic models are based on variables that correspond directly to physical quantities related to physiological entities. The compartments are defined through mass balances. The Ackerman's model [1] is widely known because of its simplicity, since it considers one compartment (Figure 8.1) that represents the global glucose-insulin dynamics in the human body. This model is proposed from data of glucose tolerance tests where the basal level is disturbed by the intake of glucose.

The assumptions behind the Ackerman model are the following:

- The duration of glucose tolerance tests allows for neglecting the effect of chemicals through slower metabolic processes.
- The hormonal level can be interpreted directly as the blood insulin level since this is the main active hormone during hyperglycemia. Insulin promotes consumption and storage of glucose.
- Glucagon dynamics is disregarded because glucagon has no significant action when blood glucose level is high, as it occurs in a glucose tolerance test or in a diabetic person, although it has an essential role to correct a hypoglycemic condition.

The non-linear interaction between glucose and insulin is described by:

$$G'(t) = f_1(G, H) + p(t) \tag{1a}$$

$$H'(t) = f_2(G, H) + u(t) \tag{1b}$$

with $G(t=0)=G_0$, $H(t=0)=H_0$, $p(t=0)=0$ and $u(t=0)=0$, where $G(t)$ is the glucose level, $H(t)$ is the hormone level, $p(t)$ is the external glucose supply rate and $u(t)$ is the insulin infusion

rate at time t. In this model, p(t) allows to simulate the ingestion of glucose, and the term of u(t) represents the control action in a medical treatment either in open loop or in a controller closed loop.

Considering the deviation variables $g(t) = G(t) - G_0$ and $h(t) = H(t) - H_0$, and applying the linearization procedure with Taylor series, the non-linear functions $f_1$ and $f_2$ can be approximated by:

$$f_1(G,H) = f_1\big|_{G_0,H_0} + \frac{\partial f_1}{\partial g}\bigg|_{G_0,H_0} g + \frac{\partial f_1}{\partial h}\bigg|_{G_0,H_0} h \qquad (2a)$$

$$f_2(G,H) = f_2\big|_{G_0,H_0} + \frac{\partial f_2}{\partial g}\bigg|_{G_0,H_0} g + \frac{\partial f_2}{\partial h}\bigg|_{G_0,H_0} h \qquad (2b)$$

The analysis of each term of equation (2) produces the simplification of the model:

- Evaluation of equation 1 in steady state determines $f_1(G_0, H_0) = f_2(G_0, H_0) = 0$.

- At a high level of glucose (g>0), with no change in hormonal level (h=0) and no glucose ingestion (p=0), part of the glucose is used by tissue cells and the excess is stored in the liver as glycogen. Consequently, the blood glucose concentration decreases (g'(t)=0) and

$$\frac{\partial f_1}{\partial g}\bigg|_{G_0,H_0} = -m_1, \quad m_1 > 0. \qquad (3)$$

- When the insulin level is high (h>0), the glucose concentration diminishes (g'(t)<0) because the glucose uptake by the tissue is eased and glucose conversion to glycogen is augmented. Therefore,

$$\frac{\partial f_1}{\partial h}\bigg|_{G_0,H_0} = -m_2, \quad m_2 > 0. \qquad (4)$$

- The metabolism tends to reduce insulin concentration (h'(t)<0), when its level is high (h>0), which is represented by:

$$\frac{\partial f_2}{\partial h}\bigg|_{G_0,H_0} = -m_3, \quad m_3 > 0. \qquad (5)$$

- Endocrine glands stimulate the production of insulin (h'(t)>0) when the glucose level is high (g>0). This capacity of the organism is indicated by:

$$\left.\frac{\partial f_2}{\partial g}\right|_{G_0,H_0} = m_4, \quad m_4 \geq 0. \tag{6}$$

The above considerations lead to the linear version of the Ackerman model:

$$g'(t) = -m_1 g(t) - m_2 h(t) + p(t), \tag{7a}$$
$$h'(t) = m_4 g(t) - m_3 h(t) + u(t). \tag{7b}$$

Here, the terms containing $m_1$ and $m_3$ account for self-removal of glucose and insulin, and the terms with $m_2$ and $m_4$ describe the therapeutic effect of insulin and the capacity of the body to produce insulin, respectively. The parameters $m_1$, $m_2$, $m_3$ and $m_4$ have been obtained from experimental data [3]. In the case of a type I diabetic patient, $m_4=0$. The reported values in $\min^{-1}$ for the rest of the parameters are $m_1=0.0009$, $m_2=0.0031$ and $m_3=0.0415$.

The Ackerman model offers a comprehensive and general representation of glucose-insulin metabolism. This second order model with dynamic interaction between the glucose and insulin levels may be useful for the discussion of control or treatment issues, which can be solved before using broader models.


## 8.2. Sorensen Physiologic Model for Glucose-Insulin Metabolism

The compartmental technique applied to the main organs of the human body involved in the glucose-insulin dynamics, the consideration of convection and diffusion transport mechanisms and the representation of the underlying kinetics have led to the nonlinear 19th order model contributed by Sorensen [2]. This model has been the base for research on meal and exercise effects on glucose-insulin metabolism and investigation on blood glucose control. The present work takes the Sorensen's model with the inclusion of meal disturbance modeling and the corresponding physiologic parameters available in the literature [4]. Figure 8.2 shows a schematic representation of the Sorensen's model.

The Sorensen model has the following limitations:
- The effects of adrenalin, cortisol and growth hormone are not included.
- The interaction of amino acid and free fatty acid with the hepatic metabolism is not considered.
- The initial conditions for the model reflect normal basal postabsorptive metabolism.
- The parameters of the model correspond to a 70 kg man.

Each compartment in the Sorensen model assumes a capillary blood space fed by the arterial blood flow and drained by the venous blood flow. These flows realize the convective transport of glucose and insulin through the compartment. The brain and the periphery (skeletal muscle and adipose tissue) compartments include an interstitial space that interacts with the capillary blood space by the diffusion of glucose and insulin.

Metabolic sources and sinks for glucose and insulin are represented by production and consumption terms in the mass balances of the proper compartments. Figure 8.3 shows a schematic representation of a compartment. The following balances define a compartment considering perfect mixing or the same concentration for the interior and the output flow of the compartment:

$$V_X \frac{dC_X}{dt} = Q_X(C_{Xi} - C_X) + PA\left(C_X^T - C_X\right) \pm \Gamma, \tag{8}$$

$$V_X^T \frac{dC_X^T}{dt} = -PA\left(C_X^T - C_X\right) \pm \Gamma^T. \tag{9}$$

Here, X is a specific organ in the physiological model; V is the volume of the compartment, C is the concentration of a particular species (glucose, G, insulin, I, or glucagon, N); Q is the volumetric blood flow through the constant volume capillary space; PA is the permeability-area product that determine the diffusion transport between the interstitial or tissue space, T, and the capillary space, and $\Gamma$ is a metabolic source of sink.

The metabolic sources and sinks are calculated from a basal rate, $\Gamma_{basal}$, considering multiplying effects of glucagon ($M^N$), insulin ($M^I$) and glucose ($M^G$) according to the following equation:

$$\Gamma = M^N M^I M^G \Gamma_{basal}, \tag{10}$$

where each factor $M^C$ (C can be N, I and G) is dimensionless and describes a sigmoidal non-linearity fitted by a hyperbolic tangent function with parameters a, b, d and e:

$$M^C = a + b\,tanh[d(C(t) - e)]. \tag{11}$$

The time variation of the multiplying factors is represented by first order dynamics. Appendix 8.1 presents the equations and parameters used for all the compartments of the Sorensen model.

The hyperbolic tangent function used for the metabolic sources and sinks in the Sorensen model also describes the pH dependence of the volume swelling ratio of the hydrogel membranes, which may suggest a convenient characteristic for insulin delivery for being similar to the normal metabolic source.

In the Sorensen model, insulin venous infusion can be proposed as the manipulated variable and the arterial blood glucose concentration as the process variable for a closed loop treatment with an explicit controller. A metabolic source is defined to simulate a meal disturbance (Figure 8.2).

A numeric relation between the models by Sorensen and Ackerman can be established. If the Sorensen model is used for the simulation of the glucose-insulin metabolism in a diabetic patient, the linear Ackerman model can be fitted to the Sorensen

model dynamics by an identification procedure for the controller design, as shown in Chapter 10.

## 8.3. Coupled Dynamics of the Hydrogel and Glucose-Insulin Physiologic Systems

The Sorensen model is modified to include a hydrogel based system as an artificial metabolic source of insulin (Figure 8.4). A hydrogel implant in the peritoneum is proposed. The peritoneum is the serous membrane that lines up the walls of the abdominal cavity and invests its viscera [5]. For this reason, the hydrogel is added as a subcompartment of the stomach and the insulin delivery is supposed to occur through the portal vein, similarly to a healthy pancreas insulin production.

The experimentation with P(MAA-g-EG) hydrogel shows that glucose diffuses from the solution to the membrane causing a contraction; however no macroporous are formed to produce a squeezing delivery of insulin. Therefore, the characteristics of the fabricated P(MAA-g-EG) hydrogel are used to model diffusion mechanisms for glucose sensing and insulin delivery.

### 8.3.1. Stomach-Hydrogel Glucose Compartment

The equations for the stomach compartment are modified with the addition of diffusion terms for the interaction with the hydrogel system. The glucose balance in the stomach is given by:

$$v_S \frac{dG_S(t)}{dt} = q_S(G_H(t) - G_S(t)) + \Gamma_{meal}(t) - \Gamma_{SU} - \frac{D_G(t)A_M(t)}{b}(G_S(t) - G_M(t)),$$

(12)

where $v_S$ is the volume of the stomach capillary compartment and $q_S$ is the blood flow through the stomach for the glucose balance, $G_H$ is the output glucose concentration of the heart compartment, $G_S$ is the output glucose concentration of the stomach compartment, $\Gamma_{meal}$ is the metabolic glucose addition by a meal (disturbance variable for the closed loop system), $\Gamma_{SU}$ is the glucose uptake in the stomach, $D_G$ is the diffusion coefficient of glucose through the membrane, $A_M$ and $b$ are the transverse area and the thickness of the membrane, and $G_M$ is the concentration of glucose in the membrane.

The output diffusion terms in (12) correspond to glucose input terms in the balance at the hydrogel subcompartment. The enzymatic reactions within the hydrogel consume glucose and produce hydrogen ions at the same rate characterized by the overall kinetic constant determined previously. Hydrogen ions diffuse through the membrane depending on a gradient between a variable interior concentration and a fixed exterior concentration determined by the assumed constant pH at the peritoneum (approximately 6.5). The glucose mass and hydrogen ion molar balances are stated by the following equations:

154

$$\frac{d(G_M(t)V_M(t))}{dt} = \frac{D_G(t)A_M(t)}{b}(G_S(t) - G_M(t)) - kG_M(t)V_M(t), \qquad (13)$$

$$\frac{d(H_M^+(t)V_M(t))}{dt} = \frac{D_H(t)A_M(t)}{b}(H_P^+ - H_M^+(t)) + x(t)V_M(t), \qquad (14)$$

where $V_M$ is the variable volume of the membrane, $H_M^+$ is the hydrogen ion concentration in the membrane, $H_P^+$ is the hydrogen concentration in the peritoneum, k is the kinetic constant of the oxidation process of glucose in the membrane and x is the rate of production of moles of hydrogen ions per volume unit.

The production of hydrogen ions depends on the dissociation of the produced gluconic acid, characterized by the dissociation constant $K_a$:

$$K_a = \frac{[H^+][Gluconate^-]}{[Gluconic\ acid]}, \qquad (15)$$

where the rectangular parenthesis indicate molar concentration. Since there is an equimolar relation between the consumed glucose and the produced gluconic acid and between the dissociated gluconic acid and each ionic species, the previous equation can be transformed into a quadratic function of hydrogen ion molar concentration by substituting:

$$[Gluconate^-] = [H^+], \qquad [Gluconic\ acid] = [Glucose]_M - [H^+], \qquad (16)$$

where $[Glucose]_M$ is the molar concentration of glucose in the membrane.

The production rate of hydrogen ions may be determined by the same rate constant for glucose oxidation and is expressed as:

$$x(t) = k[H^+]. \qquad (19)$$

The concentrations in the membrane at any time are calculated from the accumulated mass and the instantaneous volume of the hydrogel system. The glucose concentration is obtained by integrating the accumulation given by (13) and dividing over the volume of the hydrogel membrane:

$$G_M(t) = \frac{\int_0^t (G_M(t)V_M(t))'\ dt}{V_M(t)}, \qquad (20)$$

where $G_M(0) = 0$. Similarly, the local pH of the membrane, $pH_M$, is calculated as:

$$pH_M(t) = -log_{10}\left( \frac{H_P^+V_M(0) + \int\limits_0^t \left(H_M^+V_M\right)'\, dt}{V_M(t)} \right),$$

(21)

where the initial pH of the membrane is equal to the pH of the peritoneum (the membrane is pre-equilibrated at the pH of the peritoneum before implantation).

## 8.3.2. Stomach-Hydrogel Insulin Compartment

The insulin balance in the stomach is affected by the insulin delivery from the hydrogel membrane by a diffusion mechanism, according to the following equation:

$$V_S \frac{dI_S}{dt} = Q_S(I_H - I_S) + \frac{D_I A_M}{b}(I_M - I_S),$$

(22)

where $V_S$ is the volume of the stomach capillary compartment and $Q_s$ is the blood flow through the stomach for the insulin balance, $I_H$ is the output insulin concentration of the heart compartment, $I_S$ is the output insulin concentration of the stomach compartment, $D_I$ is the diffusion coefficient of insulin through the membrane, and $I_M$ is the concentration of insulin in the membrane.

The input diffusion terms in (22) correspond to the insulin delivery rate from the hydrogel subcompartment, $\Gamma_{ID}$, which determines the insulin depletion from the membrane indicated in the next equations:

$$\frac{d(I_M V_M)}{dt} = -\frac{D_I A_M}{b}(I_M - I_S) = -\Gamma_{ID},$$

(23)

$$I_M = \frac{\text{Loaded insulin} - \int\limits_0^t \Gamma_{ID} dt}{V_M}.$$

(24)

## 8.3.3. Hydrogel Subcompartment Volume

The mass balances determine the local pH at the hydrogel membrane that affects its volume. The equilibrium volume ratio of the membrane at the estimated $pH_M$ drives the direction of the volume changes with the dynamics characterized by the mechanochemical compliance and relaxation time (Table 6.1.1).

In order to represent not only the swelling dynamics and sensitivity before pH changes, but also the pH-volume operation points, the swelling process is represented as a closed loop system, as shown in Figure 8.5. The volume swelling ratio set point is established from the equilibrium pH dependence and the local pH. A compensator is used

156

to produce the volume changes with the relaxation time corresponding to the operation zone of the hydrogel. The instantaneous volume swelling ratio output of the closed loop model determines the diffusivities through the gel, which affect the pH of its microenvironment. The diagram of Figure 8.6 models the continuous interaction between the pH of the membrane and its volume.

The equilibrium information is derived from the steady sate pH-volume points from the sequence of steps applied in the characterization of the swelling behavior (Section 6.1). The pH-volume operation points define different equilibrium trajectories for ascending and descending pH values, and fit hyperbolic tangent functions with four constant parameters a, b, c and d:

$$Q = a + b\,tanh\left(c(pH) + d\right)_.$$  (25)

The set point of volume swelling ratio is calculated with the membrane pH value from equation (21) and the proper hyperbolic tangent function (25) according to the membrane pH trend (ascending or descending).

The function of the compensator, Gc(s), is determined to attain the characteristic time constant and reach the equilibrium volume swelling ratio corresponding to the pH calculated in the microenvironment of the membrane:

$$Gc(s) = \frac{1}{K}\left(1 + \frac{1}{\tau s}\right),$$  (26)

where Gc is defined in the domain of the Laplace variable s, K and $\tau$ are the parameters of the first order dynamic model in a specific operation zone, and the integration represented by $s^{-1}$ is reset when the parameters K and $\tau$ change. Appendix 8.2 explains the equivalence of Figure 8.5 to the set of first order models proposed in Chapter 6.

Although an anionic hydrogel material is characterized experimentally in this investigation, the parameters for a cationic hydrogel are proposed based on the order of magnitude of the parameters of the first and the qualitative behavior of the latter. Cationic materials may be represented by considering a negative gain since a decrement in pH would cause the volume of the cationic membrane to augment. A cationic hydrogel is simulated with gains of the same magnitude and opposite sign than those calculated for the anionic gel. The pH-volume operation points for the cationic gel are proposed by switching those observed for the anionic gel to relate high volume swelling ratios to low pH values and vice versa. Figure 8.6 and Table 8.1 show the adjustments for the simulation of the cationic gel.

## 8.4. Simulation Results and Discussion

In order to test the effect of the hydrogel system on the glucose-insulin physiological procress, the recovery of a normal glycemic value from a 300 mg/dL arterial blood glucose concentration is simulated. The initial hyperglycemic condition is achieved

by setting the meal input equal to a consumption rate of 409 mg of carbohydrates per minute until 300 mg/dL of arterial glucose concentration is stabilized for the diabetic patient model.

In order to have a reference for the results with the hydrogel system, the physiological process is first simulated without administration of exogeneous insulin using the models for the healthy and diabetic individuals (Appendix 8.1). Figure 8.7 shows the response of the diabetic and normal metabolisms once the cause of the hyperglycemic level is suspended (meal glucose metabolic source of 409 mg carbohydrates/min). While the initial arterial glucose level of the diabetic patient reaches 300 mg/dL, the same variable for the healthy body model has an initial steady state value of 92 mg/dL. The final glucose concentrations assume the basal values of 120 and 60 mg/dL for the diabetic and normal cases, respectively. A different velocity of response can also be observed. The diabetic physiological process is three times slower than the normal process, according to the stabilization times of 600 and 200 min, respectively.

According to Figure 8.8, the original Sorensen model for the diabetic patient returns to a normal steady state glucose concentration of 120 mg/dL in approximately 600 min. A hydrogel implant is considered loaded with insulin in 5% of its dry weight (0.9 mg approximately). The physiological process with a cationic hydrogel implant takes about 125 min to return glucose concentration into a normal range considered between 80 and 120 mg/dL. As the simulated hydrogel membrane is depleted, the glucose concentration converges to 120 mg/dL as the original model. The higher speed of response and the lower glucose concentration levels are due to the insulin administration from the hydrogel system. The cationic hydrogel is assumed to be initially contracted and preequilibrated at neutral pH. When the exposure to a hyperglycemic condition is considered, the local pH of the membrane is reduced, the polymeric structure opens (Figure 8.10) and insulin is delivered.

Although the anionic polymer structure closes as the pH decreases, it resulted effective to correct the simulated hyperglycemic condition. The anionic hydrogel produces slightly lower concentrations in the transitory response (Figure 8.9a). The higher initial release is due to the higher volume of the membrane at neutral pH (Figure 8.9b). As the glucose reaction proceeds, the anionic hydrogel contracts (Figure 8.10), but not sufficiently to stop insulin release.

The transient blood glucose response with the hydrogel delivery systems has a very long duration in comparison with the transitory response of the diabetic physiological process without treatment, because of the large relaxation times of the hydrogel material. However, this response may be beneficial considering the effect of daily meals. Hypoglycemia is prevented by limiting the amount of insulin loaded in the system. Simulation of a regular diet is presented in a posterior chapter for the evaluation and comparison of the performance of hydrogel monolithic systems for insulin delivery.

## 8.5. Conclusions

The compartmental Sorensen model offers the possibility to analyze a specific implantation site for a hydrogel-based system. The proposed modifications for the integration of hydrogel-therapeutic membrane could be applied in the periphery compartment, for example. However, the stomach compartment is chosen assuming a more effective intervention of the hydrogel system before meal disturbances because insulin would be delivered closer to the place where glucose concentration starts augmenting.

A strong dynamic interaction between the pH and glucose effects on the hydrogel system exists since there is a bidirectional dependence between them. The glucose concentration in the medium causes a change in pH, which in turn produces a volume change of the hydrogel. Simultaneously, the glucose concentration in the gel is affected by its degree of swelling, which affects the hydrogen concentration inside and in the close vicinity of the gel. Obviously, interactions among the different compartments of the Sorensen model also affect the behavior of concentrations and volume of the hydrogel system.

Parameters for the modelling of a hydrogel-closed loop treatment are obtained from experimental characterization with P(MAA-g-EG) hydrogel for an anionic hydrogel implant. The operation points and the parameters are adjusted to model a cationic material for the application in blood glucose regulation in diabetic patients.

Simulation of the recovery of a normal glucose concentration from an initial state of 300 mg/dL shows a logical interaction between the hydrogel-based delivery system and the physiological process. Further analysis is necessary to evaluate the effect of maintaining the glucose level in a normal range with slow variations below the steady state value of 120 mg/dL, and the overall performance of a hydrogel implant. This analysis is developed in Chapter 10.
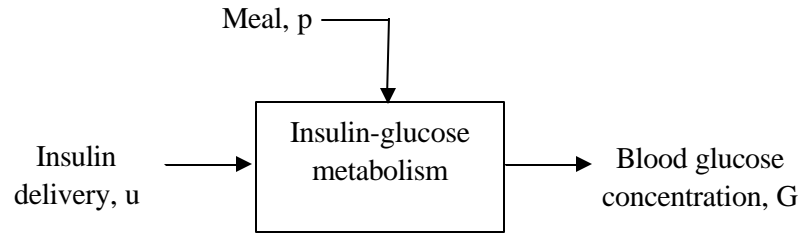
**Figure 8.1. Ackerman Model for Glucose-Insulin Metabolism.** Insulin delivery and glucose from a meal are the inputs and the arterial glucose level is the output of the single body compartment.
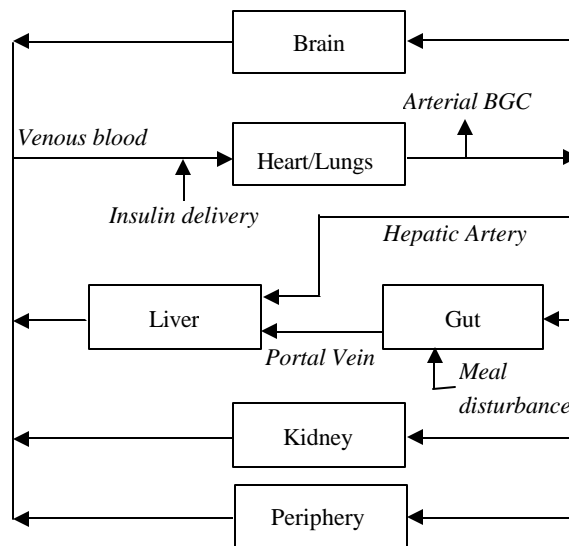


**Figure 8.2. The Sorensen Compartmental Model for the Glucose-Insulin Metabolism** (BGC: blood glucose concentration).
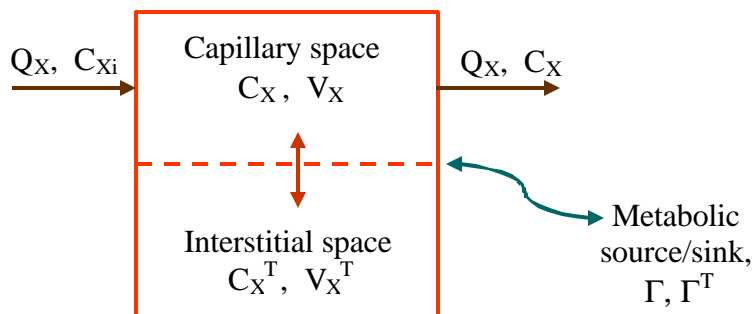


**Figure 8.3. Compartme nt of the Sorensen Model.** C represents the concentration of either glucose (G), insulin (I) or glucagons (N). Q is the volumetric flow at the input and the output of the compartment. V is the volume of a particular space. Subscript X refers to an organ in glucose-insulin metabolism. Subscript I indicates an input condition. Superscript T designates the tissue or interstitial space of the compartment. Metabolic sources and sinks, $\Gamma$, may be defined in both capillary blood and interstitial spaces.

160
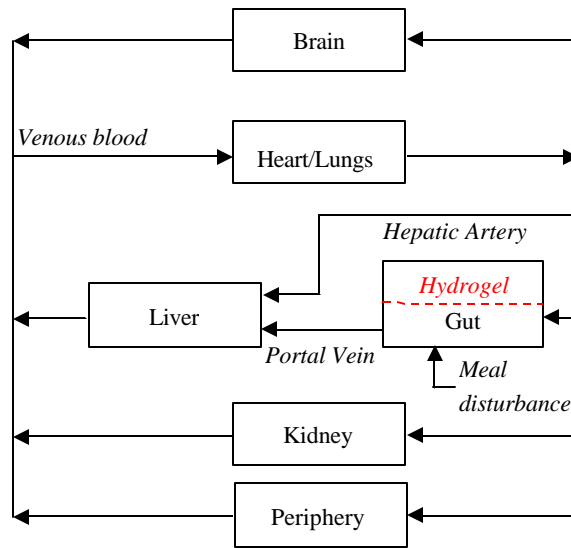
**Figure 8.4. Modification of the Sorensen Model with a Hydrogel Compartment.** A hydrogel implant in the peritoneum is proposed by a subcompartment in the stomach compartment.
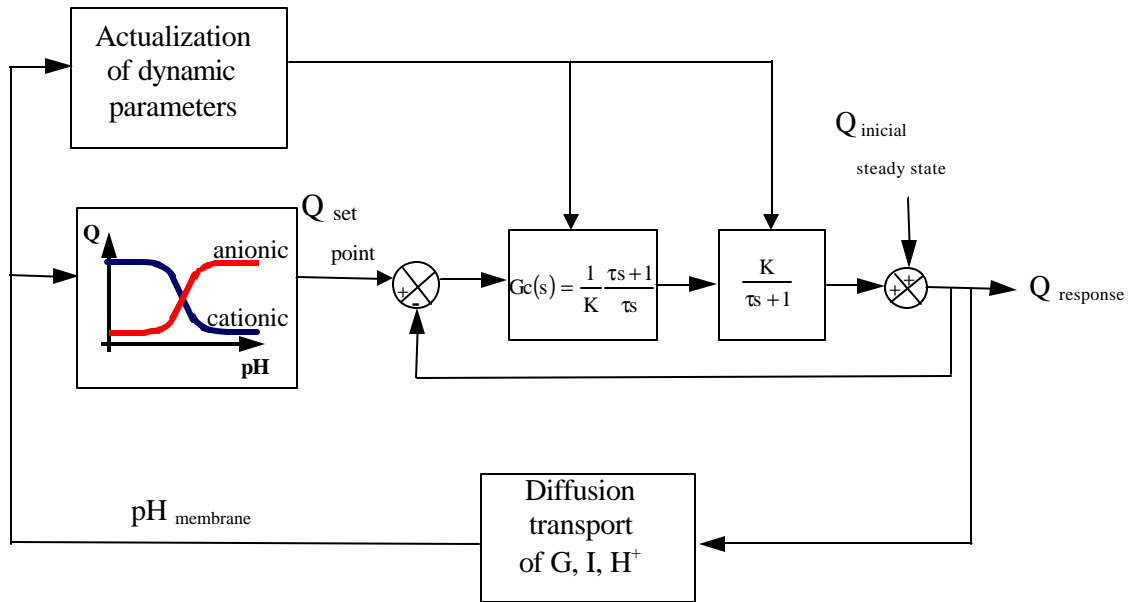


**Figure 8.5. Volume Swelling Ratio Closed Loop Model.** The system shown reproduces the swelling dynamics as well as the volume operation points of a hydrogel system.
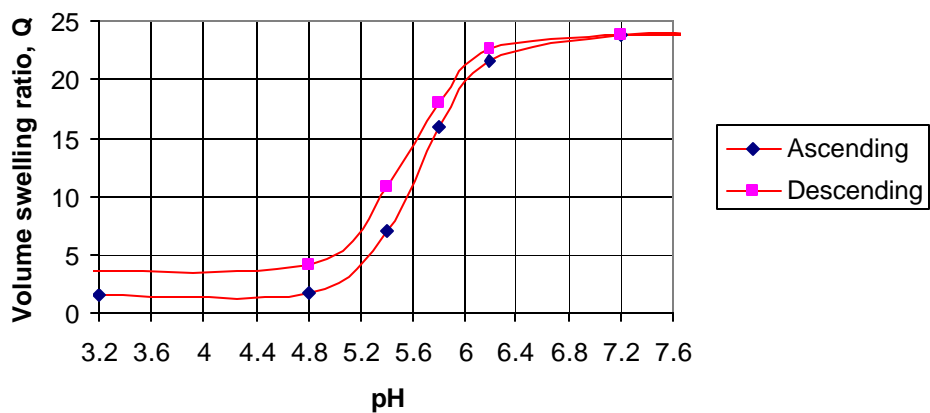
(a) Anionic hydrogel
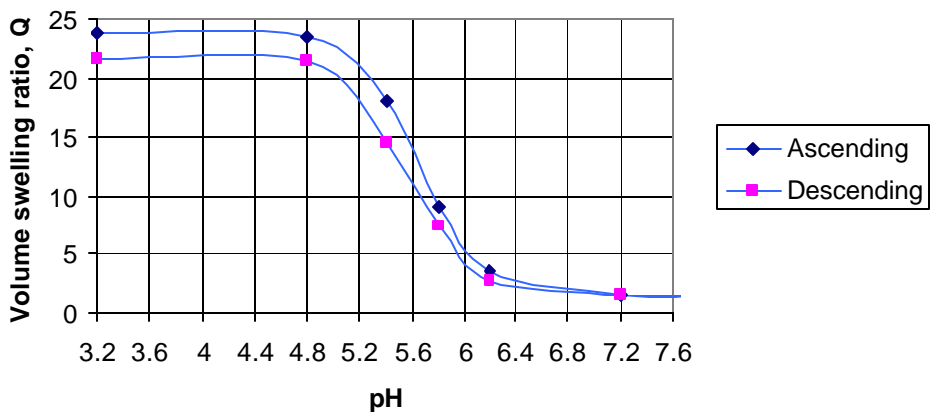


(b) Cationic hydrogel

**Figure 8.6. Equilibrium Operation Points for Anionic and Cationic Hydrogels.** The behavior of the anionic material was obtained experimentally with P(MAA-g-EG) hydrogel (a), and used as a basis to propose the behavior of a cationic hydrogel material (b).

**Table 8.1. Model Parameters for Anionic and Cationic Hydrogels.** The parameters for the anionic P(MAA‑g‑EG) hydrogel are adapted to fit the qualitative behavior of cationic hydrogels.

| pH range and change direction | 3D Mechanochemical Compliance | | Relaxation Time (min) |
|---|---|---|---|
| | *Anionic* | *Cationic* | |
| 3.2 to 4.8 | 0.15 | -0.15 | 625 |
| 4.8 to 5.4 | 8.96 | -8.96 | 588 |
| 5.4 to 4.8 | 11.46 | -11.46 | 170 |
| 5.4 to 5.8 | 22.46 | -22.46 | 333 |
| 5.8 to 5.4 | 17.75 | -17.75 | 238 |
| 5.8 to 6.2 | 13.92 | -13.92 | 222 |
| 6.2 to 5.8 | 11.63 | -11.63 | 256 |
| 6.2 to 7.2 | 2.12 | -2.12 | 167 |
| 7.2 to 6.2 | 1.32 | -1.32 | 357 |
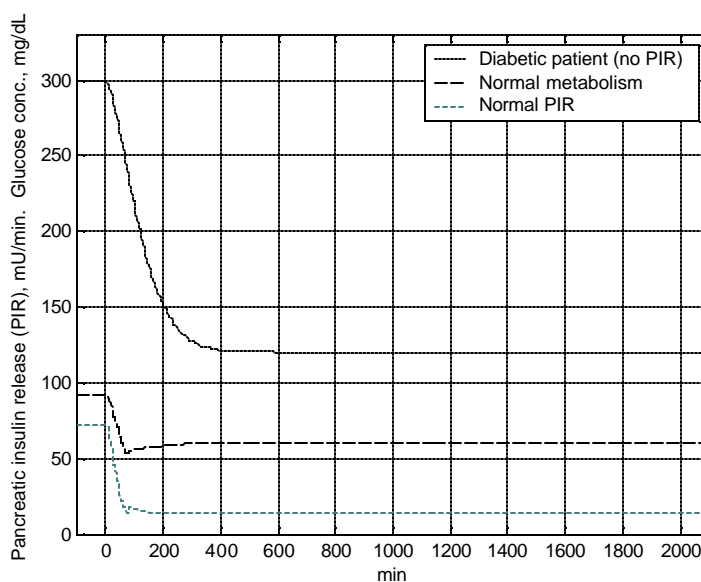


**Figure 8.7. Simulation of Sorensen Model for the Diabetic and Normal Cases.** A meal glucose metabolic source of 409 mg carbohydrates/min is maintained until a steady initial arterial glucose concentration is reached (300 mg/dL for the diabetic case and 92 for the normal or healthy case). At time 0, the meal metabolic source is suspended. The glucose level of the diabetic patient model recovers the final value of 120 mg/dL slower than the glucose level response of the normal model to reach the concentration of 60 mg/dL. Final values are practically equal to basal values, since no other meal is simulated.
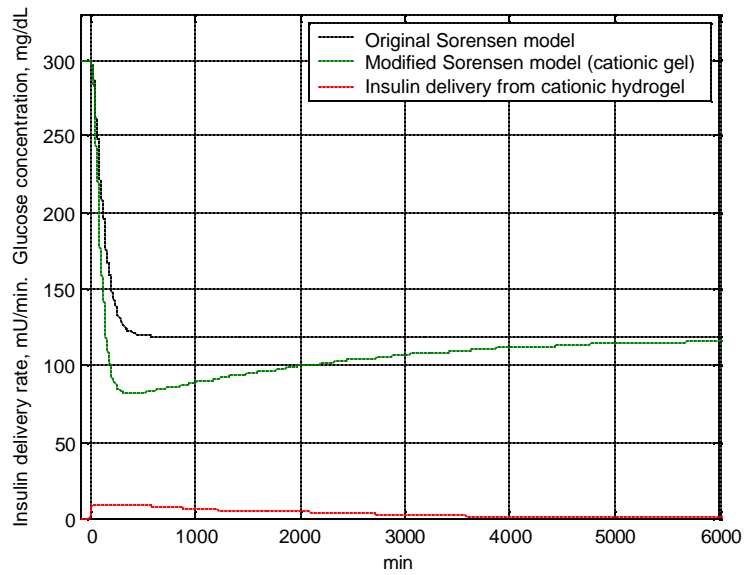
**Figure 8.8. Simulation of Glucose Response with a Cationic Hydrogel.** Correction of a hyperglycemic initial condition of 300 mg/dL in arterial blood concentratioin. The original Sorensen model evaluation corresponds to the diabetic case.
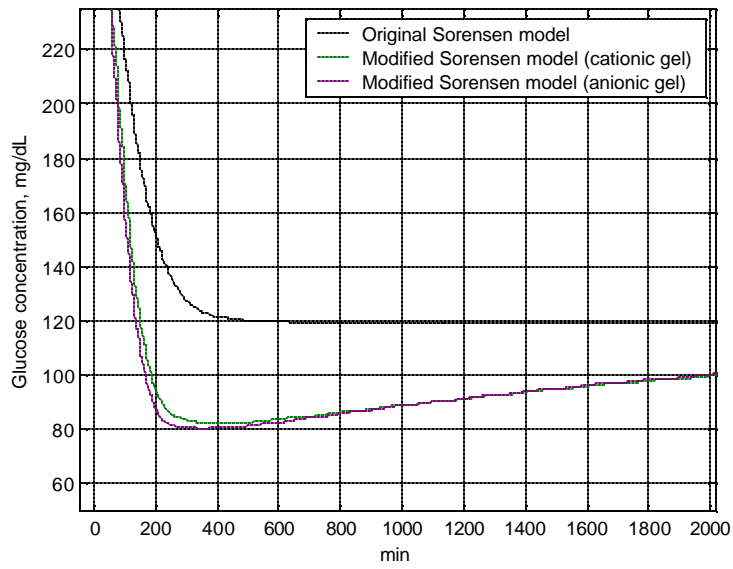
(a)
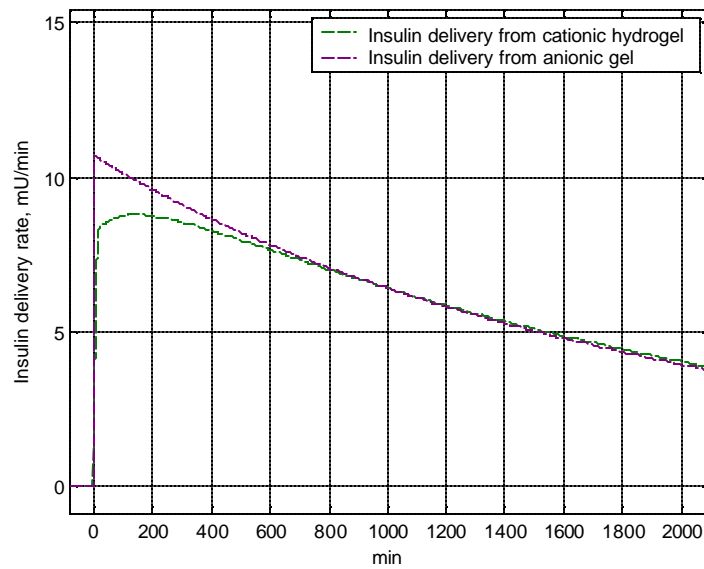


(b)

**Figure 8.9. Simulation of Glucose Response with Cationic and Anionic Hydrogels.** Correction of a hyperglycemic initial condition of 300 mg/dL in arterial blood concentration. Glucose concentration (a) and insulin release (b) curves are shown.
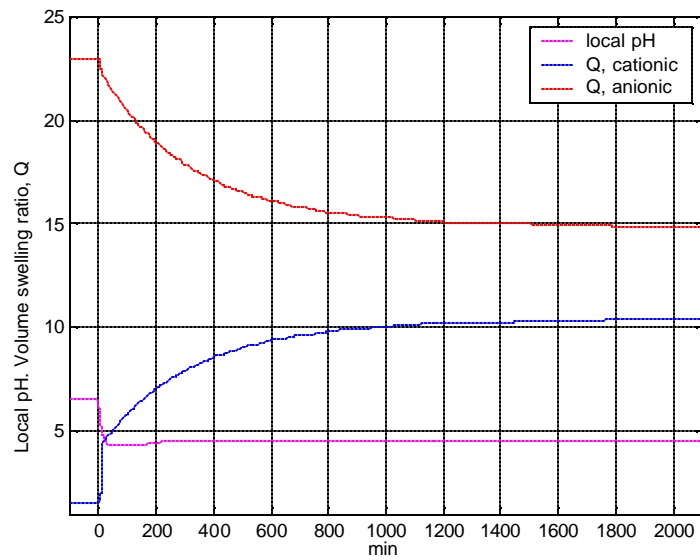
**Figure 8.10. Simulation of Swelling Behavior of Cationic and Anionic Hydrogels.** Correction of a hyperglycemic initial condition of 300 mg/dL in arterial blood concentration. The curve of local pH is the same for both simulation cases, with the cationic and the anionic hydrogels.

## References

1.  Ackerman E, Gatewood L, Rosevear J, Molnar G. Model studies of blood-glucose regulation. Bull Mathem Biophys. 1965;27:21-38.

2.  Sorensen J. A physiologic model of glucose metabolism in man and its use to design and assess improved insulin therapies for diabetes. PhD thesis. Dept. of Chemical Engineering, MIT, 1985.

3.  Yipintsol T, Gatewood L, Ackerman E, Spivak P, Molnar G, Rosevear J, Service F. Mathematical analysis of blood glucose and plasma insulin responses to insulin infusion in healthy and diabetic subjects. Comput Biol Med. 1973;3:71-78.

4.  Parker R, Doyle III F, Ward J, Peppas N. Robust $H_8$ glucose control in diabetes using a physiological model. AIChE J. 2000;46(12):2537-2549.

5.  Van De Graaff KM, Fox SI, LaFleur KM. Synopsis of human anatomy & physiology. Dubuque, IA: Wm. C. Brown Publishers, 1997.

## Appendix 8.1.  Sorensen Model for Glucose-Insulin Metabolism
The following nomenclature and equations describe the compartmental model by Sorensen for the glucose-insulin metabolism for either a healthy person or a diabetic patient [2].

Model variables

A: auxiliary equation state (dimensionless)
B: fractional clearance (I, dimensionless; N, L/min)
G: glucose concentration (mg/dL)
I: insulin concentration (mU/L)
N: glucagons concentration (normalized, dimensionless)
Q: vascular plasma flow rate (L/min)
q: vascular blood flow rate (dL/min)
T: transcapillary diffusion time constant (min)
V: volume (L)
v : volume (dL)
$\Gamma$ : metabolic source or sink rate (mg/min or mU/min)
Variables in pancreatic insulin release model in healthy body:
W: potentiator (dimensionless)
Y: inhibitor (dimensionless)
R: labile insulin (U)
Z: secretion rate (U/min)
$X, W_8$ : intermediate variables (dimensionless)

Model sub and superscripts

A: hepatic artery
B: brain  /  basal value in insulin pancreatic release model
BU: brain uptake
G: glucose
H: heart and lungs
HGP: hepatic glucose production
HGU: hepatic glucose uptake
I: insulin
IHGP: insulin effect on HGP
IHGU: insulin effect on HGU
IVI: intravenous insulin infusion
K: kidney
KC: kidney clearance
KE: kidney excretion
L: liver
LC: liver clearance
N: glucagon
NHGP: glucagons effect on HGP
P: periphery (muscle/adipose tissue)
PC: peripheral clearance
PGU: peripheral glucose uptake
PIR: pancreatic insulin release
PNC: pancreatic glucagon clearance

PNR: pancreatic glucagon release (normalized)
RBCU: red blood cell uptake
S: gut (stomach/intestine)
SIA: insulin absorption into blood stream from subcutaneous depot
SU: gut uptake
T: tissue or interstitial space


Glucose mass balance equations

$$v_B \frac{dG_B(t)}{dt} = (G_H(t) - G_B(t))q_B - (G_B(t) - G_B^T(t))\frac{v_B^T}{T_B}$$ (a8.1.1)

$$v_B^T \frac{dG_B^T(t)}{dt} = (G_B(t) - G_B^T(t))\frac{v_B^T}{T_B} - \Gamma_{BU}$$ (a8.1.2)

$$v_H \frac{dG_H(t)}{dt} = G_B(t)q_B + G_L(t)q_L + G_K(t)q_K + G_P(t)q_P - G_H(t)q_H - \Gamma_{RBCU}$$ (a8.1.3)

$$v_S \frac{dG_S(t)}{dt} = (G_H(t) - G_S(t))q_S + \Gamma_{meal} - \Gamma_{SU}$$ (a8.1.4)

$$v_L \frac{dG_L(t)}{dt} = G_H(t)q_A + G_S(t)q_S - G_L(t)q_L + \Gamma_{HGP} - \Gamma_{HGU}$$ (a8.1.5)

$$v_K \frac{dG_K(t)}{dt} = (G_H(t) - G_K(t))q_K - \Gamma_{KE}$$ (a8.1.6)

$$v_P \frac{dG_P(t)}{dt} = (G_H(t) - G_P(t))q_P + (G_P^T(t) - G_P(t))\frac{v_P^T}{T_P^G}$$ (a8.1.7)

$$v_P^T \frac{dG_P^T(t)}{dt} = (G_P(t) - G_P^T(t))\frac{v_P^T}{T_P^G} - \Gamma_{PGU}$$ (a8.1.8)


Glucose metabolic sinks and sources (mg/min):

$$\Gamma_{BC} = 70$$ (a8.1.9)
$$\Gamma_{RBCU} = 10$$ (a8.1.10)

$$\Gamma_{SU} = 20 \tag{a8.1.11}$$

$$\Gamma_{HGP} = 155A_{IHGP}(t)[2.7\,tanh(0.388N(t)) - A_{NHGP}(t)]$$
$$\times\left[1.425 - 1.406\,tanh\left\{0.6199\left(\frac{G_L(t)}{101} - 0.4969\right)\right\}\right] \tag{a8.1.12}$$

$$\frac{dA_{IHGP}(t)}{dt} = \frac{1}{25}\left[1.2088 - 1.138\,tanh\left(1.669\frac{I_L(t)}{21.43} - 0.8885\right) - A_{IHGP}(t)\right] \tag{a8.1.13}$$

$$\frac{dA_{NHGP}(t)}{dt} = \frac{1}{65}\left[\frac{2.7\,tanh(0.388N(t)) - 1}{2} - A_{NHGP}(t)\right] \tag{a8.1.14}$$

$$\Gamma_{HGU}(t) = 20A_{IHGU}(t)\left[5.6648 + 5.6589\,tanh\left\{2.4375\left(\frac{G_L(t)}{101} - 1.48\right)\right\}\right] \tag{a8.1.15}$$

$$\frac{dA_{IHGU}(t)}{dt} = \frac{1}{25}\left[2\,tanh\left(0.549\frac{I_L(t)}{21.43}\right) - A_{IHGU}(t)\right] \tag{a8.1.16}$$

$$\Gamma_{KE}(t) = \begin{cases} 71 + 71\,tanh[0.011(G_K(t) - 460)], & \text{for } G_K < 460\text{ mg/dL} \\ 0.872G_K(t) - 300, & \text{for } G_K > 460\text{ mg/dL} \end{cases} \tag{a8.1.17}$$

$$\Gamma_{PGU}(t) = \frac{35G_P^T(t)}{86.81}\left[7.035 + 6.51623\,tanh\left\{0.33827\left(\frac{I_P^T(t)}{5.304} - 5.82113\right)\right\}\right] \tag{a8.1.18}$$

Insulin mass balance equations

$$V_B\frac{dI_B(t)}{dt} = (I_H(t) - I_B(t))Q_B \tag{a8.1.19}$$

$$v_H\frac{dI_H(t)}{dt} = I_B(t)Q_B + I_L(t)Q_L + I_K(t)Q_K + I_P(t)Q_P - I_H(t)Q_H + \Gamma_{IVI} \tag{a8.1.20}$$

$$V_S\frac{dI_S(t)}{dt} = (I_H(t) - I_S(t))Q_S \tag{a8.1.21}$$

$$V_L\frac{dI_L(t)}{dt} = I_H(t)Q_A + I_S(t)Q_S - I_L(t)Q_L + \Gamma_{PIR} - \Gamma_{LC} \tag{a8.1.22}$$

$$V_K \frac{dI_K(t)}{dt} = \left(I_H(t) - I_K(t)\right)Q_K - \Gamma_{KC} \tag{a8.1.23}$$

$$V_P \frac{dI_P(t)}{dt} = \left(I_H(t) - I_P(t)\right)Q_P - \left(I_P(t) - I_P^T(t)\right)\frac{V_P^T}{T_P^I} \tag{a8.1.24}$$

$$V_P^T \frac{dI_P^T(t)}{dt} = \left(I_P(t) - I_P^T(t)\right)\frac{V_P^T}{T_P^I} + \Gamma_{SIA} - \Gamma_{PC} \tag{a8.1.25}$$

Insulin metabolic sources and sinks (mU/min)

$\Gamma_{IVI}$ and $\Gamma_{SIA}$ are the terms for insulin administration in medical treatments using the intravenous and the subcutaneous routes, respectively.

$$\Gamma_{LC}(t) = F_{LC}\left(I_H(t)Q_A + I_S(t)Q_S + \Gamma_{PIR}\right) \tag{a8.1.26}$$

$$\Gamma_{KC}(t) = F_{KC}I_K(t)Q_K \tag{a8.1.27}$$

$$\Gamma_{PC}(t) = \frac{I_P^T(t)}{\dfrac{1 - F_{PC}}{F_{PC}}\dfrac{1}{Q_P} - \dfrac{T_P^I}{V_P^T}} \tag{a8.1.28}$$

$$\Gamma_{PIR} = 0 \qquad \text{no pancreatic insulin release in diabetic patient} \tag{a8.1.29}$$

$$\Gamma_{PIR}(t) = \frac{Z(G_H)}{Z(G_H^B)}\Gamma_{PIR}^B \qquad \text{pancreatic insulin release for a healthy person} \tag{a8.1.30a}$$

$$\frac{dW(t)}{dt} = \alpha\left[W_\infty(t) - W(t)\right] \tag{a8.1.30b}$$

$$\frac{dY(t)}{dt} = \beta\left[X(t) - Y(t)\right] \tag{a8.1.30c}$$

$$\frac{dR(t)}{dt} = k\left[R_0 - R(t)\right] + \gamma W(t) - Z(t) \tag{a8.1.30d}$$

$$Z(t) = \left\{M_1 W_\infty(t) + M_2\left[X(t) - Y(t)\right]\right\}R(t) \tag{a8.1.30e}$$

171

$$X(t) = \frac{[G_H(t)]^{3.27}}{132^{3.27} + 5.93[G_H(t)]^{3.02}} \qquad \text{(a8.1.30f)}$$

$$W_\infty(t) = [X(t)]^{1.11} \qquad \text{(a8.1.30g)}$$

Glucagon mass balance

$$V_N \frac{dN(t)}{dt} = (\Gamma_{PNR}(t) - N(t)) F_{PNC} \qquad \text{(a8.1.31)}$$

Glucagon metabolic source (dimensionless)

$$\Gamma_{PNR}(t) = \left[ 1.3102 - 0.61016 \, tanh \left\{ 1.0571 \left( \frac{I_H(t)}{15.15} - 0.46981 \right) \right\} \right]$$
$$\times \left[ 2.9285 - 2.095 \, tanh \left\{ 4.18 \left( \frac{G_H(t)}{91.89} - 0.6191 \right) \right\} \right] \qquad \text{(a8.1.32)}$$

Parameter values

| Volumes | Flows | Diffusion time constants | Dimensionless factors |
|---|---|---|---|
| $v_B$=3.5 dL | $q_B$=5.9 dL/min | $T_B$=2.1 min | |
| $v_B^T = 4.5\,dL$ | | | |
| $v_H$=13.8 dL | $q_H$=43.7 dL/min | | |
| $v_S$=11.2 dL | $q_S$=10.1 dL/min | | |
| $v_L$=25.1 dL | $q_L$=12.6 dL/min | | |
| | $q_A$=2.5 dL/min | | |
| $v_K$=6.6 dL | $q_K$=10.1 dL/min | | |
| | | | |
| $v_P$=10.4 dL | $q_P$=15.1 dL/min | $T_P^G = 5.0\,min$ | |
| $v_P^T = 67.4\,dL$ | | | |
| $V_B$=0.265 L | $Q_B$=0.45 L/min | | |
| $V_H$=0.985 L | $Q_H$=3.12 L/min | | |
| $V_S$=0.945 L | $Q_S$=0.72 L/min | | |
| $V_L$=1.14 L | $Q_L$=0.9 L/min | | $F_{LC}$=0.4 |
| | $Q_A$=0.18 L/min | | |
| $V_K$=0.505 L | $Q_K$=0.72 L/min | | $F_{KC}$=0.3 |
| $V_P$=0.735 L | $Q_P$=1.05 L/min | $T_P^I = 20\,min$ | $F_{PC}$=0.15 |
| $V_P^T = 6.3\,dL$ | | | |
| $V_N$=11.31 L | $F_{PNC}$=0.0091 L/min | | |

Constants for insulin release model in healthy body:

$\alpha$=0.0482 min$^{-1}$
$\beta$=0.931 min$^{-1}$
k=0.00794 min$^{-1}$
$M_1$=0.00747 min$^{-1}$
$M_2$=0.0958 min$^{-1}$
$\gamma$=0.575 U/min
$R_0$=6.33 U

General initialization procedure

The following procedure produces the initial or basal values for the model. Specific differences for the diabetic patient and the normal subject representations are emphasized.

1. $I_H = 0$ for the diabetic patient modelling case

2. $I_H = 15.2$ (a value between 10 and 20 mU/L for the normal case [2])

3. $I_P = I_H(1 - F_{PC})$

4. $I_K = I_H(1 - F_{KC})$

5. $I_B = I_H$

6. $I_S = I_H$

7. $I_P^T = I_P - \left[ \dfrac{Q_P T_P^I}{V_P^T}(I_H - I_P) \right]$

8. $I_L = I_H(1 - F_{LC})$ (for the model of the diabetic patient)

9. $I_L = \dfrac{1}{Q_L}(I_H Q_H - I_B Q_B - I_K Q_K - I_P Q_P)$ (for the model of the normal subject)

10. $\Gamma_{PIR}^B = \dfrac{Q_L}{1 - F_{LC}} I_L - I_S Q_S - I_H Q_A$ (for the model of the normal subject)

11. Assume $G_H$

12. Evaluate $\Gamma_{PNR}$ (a8.1.32)

13. $G_B = G_H - \dfrac{\Gamma_{BU}}{q_B}$

14. $G_S = G_H - \dfrac{\Gamma_{SU}}{q_S}$

15. $M_{PGU}^I = 7.035 + 6.51623\, tanh\left\{ 0.33827\left( \dfrac{I_P^T}{5.304} - 5.82113 \right) \right\}$

16. $G_P = \dfrac{G_H}{1 + \dfrac{v_P^T M_{PGU}^I (35)}{q_P v_P^T (86.81) + T_P^G q_P M_{PGU}^I (35)}}$

17. Assume $G_K$

18. Evaluate $\Gamma_{KE}$ (a8.1.17)

19. $G_K = G_H - \dfrac{\Gamma_{KE}}{q_K}$, check assumption in step 17, repeat 18 and 19 until convergence

20. Assume $G_L$

21. Evaluate $\Gamma_{HGP}$ (a8.1.12) and $\Gamma_{HGU}$ (a8.1.15)

22. $G_L = \dfrac{1}{q_L} \left( G_H q_A + G_S q_S + \Gamma_{HGP} - \Gamma_{HGU} \right)$, check assumption in step 20, repeat 21 and 22 until convergence

23. $G_H = \dfrac{1}{q_H} \left( G_B q_B + G_L q_L + G_K q_K + G_P q_P - \Gamma_{RBCU} \right)$, check assumption in step 11, repeat steps 12 to 23 until convergence

24. $G_P^T = \dfrac{G_P}{1 + \dfrac{T_P^G M_{PGU}^I (35)}{v_P^T (86.81)}}$

25. $G_B^T = G_B - \dfrac{T_B \Gamma_{BU}}{v_B^T}$

26. Evaluate X (a8.1.30f) and $W_8$ (a8.1.30g) (for the model of the normal subject)

27. $W = W_8$ (for insulin model in normal subject)

28. $Y = X$ (for insulin model in normal subject)

29. $R = \dfrac{kR_0 + \gamma W_\infty}{k + M_1 W_\infty}$ (for insulin model in normal subject)

30. $Z = M_1 W_\infty R$ (for insulin model in normal subject)

## Appendix 8.2. Compensator Function in the Hydrogel Volume Closed Loop Model

The evaluation of the modified Sorensen model with the balances at the hydrogel gives the pH of the membrane. Since operation points are specified from the calculated pH of the membrane and the equilibrium volume swelling ratio-pH function, the gain or static effect of the mechanochemical compliance of the hydrogel volume process is already represented. The dynamic behavior is modeled by a closed loop system that reaches the specified volume-swelling ratio determined at the operative pH of the membrane with a velocity of response characterized by a relaxation time. The compensator is designed for this function in the domain of the variable of Laplace.

The design of the compensator element in the model of the volume of the hydrogel requires the use of deviation variables. The closed loop elements are represented by transfer functions whose inputs and outputs signals or variables describe deviation values. The next diagram allows the analysis of the overall dynamics of the internal loop in terms of changes in the desired (R) and present (Y) volume swelling ratios.
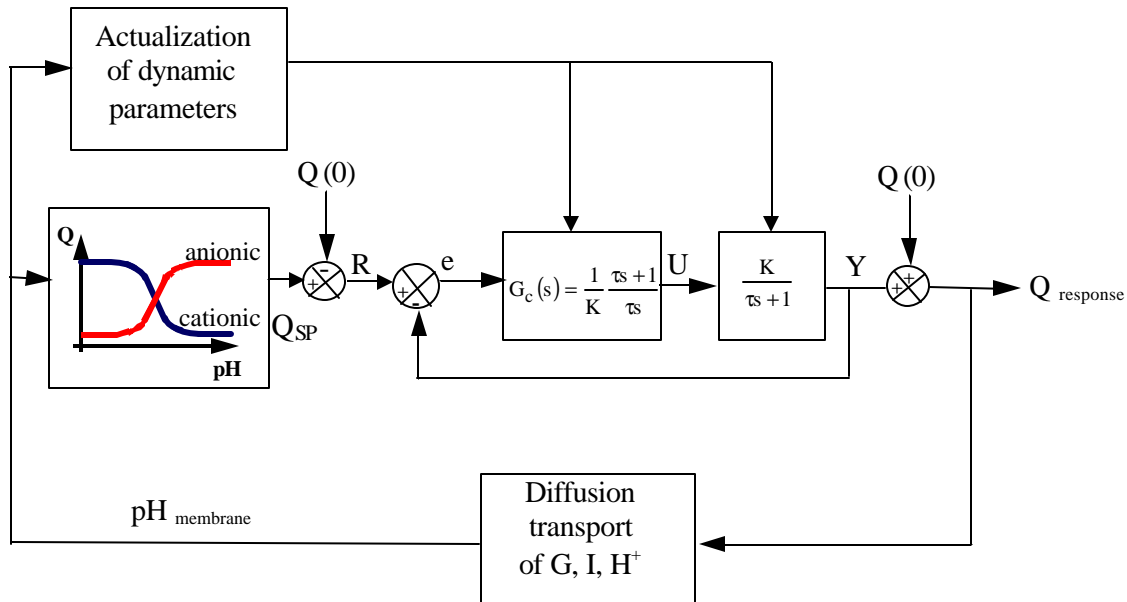


**Figure a8.2.1. Volume Swelling Ratio Closed Loop Model.** This diagram is equivalent to the one in Figure 8.5. Deviation variables R (set point), e (error), U (manipulation) and Y (change in volume swelling ratio) are shown.

The response of the change in volume swelling ratio, Y, before changes driven by the tendency to equilibrium, R, is given by:

$$\frac{Y(s)}{R(s)} = \frac{Gc(s)\dfrac{K}{\tau s + 1}}{1 + Gc(s)\dfrac{K}{\tau s + 1}},$$
(a8.2.1)

where $\tau$ is the relaxation time of the hydrogel. This closed loop function is specified in such a way that the resultant constant time is equal to the relaxation time of the hydrogel, and the changes in R are reached at the end in Y, or a unit gain is attained, additionally, the experimental first order dynamics should be reproduced:

$$\frac{Y(s)}{R(s)} = \frac{1}{\tau s + 1} \qquad (a8.2.2)$$

By equating (a8.2.1) and (a8.2.2), the compensator Gc(s) can be calculated. The solution for Gc(s) fits the structure of a proportional integral or PI controller:

$$Gc(s) = \frac{1}{K}\frac{\tau s + 1}{\tau s} \qquad (a8.2.3)$$

The parameters of this compensator are updated according to the operation zone of the hydrogel material to represent its non-linear behavior.

## 9. Optimal Controller Design

The conventional feedback system uses a mathematical controller algorithm to adjust insulin administration according to the blood glucose concentration. In this chapter, a controller is designed from the dynamic characteristics of the glucose-insulin physiological process. The linear quadratic regulatory problem (LQRP) formulation is applied to obtain the structure and the parameters of the controller. The linear Ackerman model [1] is used preliminarily to compare the regulatory and servocontrol design approaches. After the controller design approach is selected, the calculations are based on the dynamics of the Sorensen model [2] for the diabetic patient and the Ackerman structure. Specific issues such as limited measured variables, changing process dynamics, noisy measurements and tuning requirements are addressed to discuss the robustness and the flexibility of the controller.

## 9.1. State Space Representation of the Physiological Model

The state space representation of the process is necessary for the calculation of an optimal controller. A state space model is given by:

$$x'(t) = Ax(t) + Bn(t) \ , \qquad\qquad (1a)$$
$$y'(t) = Cx(t) + Dn(t) \ , \qquad\qquad (1b)$$

where x is the vector of state variables, y is the vector of output variables, n is the vector of input variables, and the transition matrix A and the vectors B, C and D contain the parameters of the model.

The linearized Ackerman model with deviation variables and constant parameters $m_1$, $m_2$, $m_3$ and $m_4$ (Section 8.1) is given by:

$$g'(t) = -m_1 g(t) - m_2 h(t) + p(t), \qquad\qquad (2a)$$
$$h'(t) = m_4 g(t) - m_3 h(t) + u(t), \qquad\qquad (2b)$$

where g(t) is the blood glucose level deviation, h(t) is the insulin concentration deviation, u(t) is the insulin infusion rate for diabetes treatment, p(t) is the external glucose supply rate from meals, and all initial values are zero. The output of the model or response variable of the process is the blood glucose deviation, this implies that only this variable is measured. The term p(t) is eliminated for the calculations of the controller since only the dynamics before the manipulated input variable is required.

The single input – single output glucose-insulin state space model is:

$$x'(t) = Ax(t) + Bu(t) \ , \qquad\qquad (3a)$$
$$y'(t) = Cx(t) \ , \qquad\qquad (3b)$$

This representation is obtained from Equation (1) by defining the following matrices:

$$x(t) = \begin{bmatrix} x_1(t) \\ x_2(t) \end{bmatrix} = \begin{bmatrix} g(t) \\ h(t) \end{bmatrix},$$ (4)

$$y(t) = x_1(t) = g(t),$$ (5)

$$A = \begin{bmatrix} -m_1 & -m_2 \\ 0 & -m_3 \end{bmatrix},$$ (6)

$$B = \begin{bmatrix} 0 \\ 1 \end{bmatrix},$$ (7)

$$C = \begin{bmatrix} 1 & 0 \end{bmatrix},$$ (8)

$$D = \begin{bmatrix} 0 \end{bmatrix}.$$ (9)

The parameters for the state space model (3) are directly proposed in the work by Yipintsol et al ($m_1$=0.0009, $m_2$=0.0031, $m_3$=0.0415, $m_4$=0) [3], but can also be obtained from the Sorensen model through its order reduction and linearization performed by the calculation of the transition matrix A as the following Jacobian matrix [4]:

$$A = \begin{bmatrix} -m_1 & -m_2 \\ m_4 & -m_3 \end{bmatrix} = \begin{bmatrix} \partial f_1 / \partial x_1 & \partial f_1 / \partial x_2 \\ \partial f_2 / \partial x_1 & \partial f_2 / \partial x_2 \end{bmatrix},$$ (10)

with $m_4 = \delta f_2 / \delta x_1 = 0$, where $f_1$ and $f_2$ are the first time derivatives of glucose ($x_1$) and insulin ($x_2$) concentrations, respectively, in the heart and lungs compartment. This linearization procedure preserves meaningful parameters and states, as well as mathematical precision, since the simplified model considers explicitly the main physiologic variables in diabetes.

## 9.2. Design of Optimal Controller

### 9.2.1. Linear Quadratic Control Problem

The optimal controller design according to the linear quadratic technique is explained based on references [5] and [6]. The linear quadratic control (LQC) problem consists of determining a control equation or control law, u(t), to minimize the cost function given by the next equation:

$$J(\,u\,) = \frac{1}{2}e^T(t_f)Se(t_f) + \frac{1}{2}\int_{t0}^{t_f}\left[e^T(t)Q(t)e(t) + u^T(t)R(t)u(t)\right]dt\,, \qquad (11)$$

where u(t) appears *quadratically*; e(t) is the error vector, S is a constant matrix; Q and R may vary with time; Q, R and S are symmetric matrices; S and Q are positive semidefinite, and R is positive definite.

The control law u(t) is the input of the state-space model with the general form:

$$x'(t) = A(t)x(t) + B(t)u(t),\ x(t_0) = x_0,\ t \in [t_0,\ t_f],\qquad (12)$$

where u(t) is included *linearly*, and the state transition matrix A(t) and the input matrix B(t) may be time variant in general. An optimal control law u*(t) is assumed to exist for this problem in [$t_0$, $t_f$]. An optimal trajectory x*(t) is associated with u*(t). The control signal and the state vector can be expressed as:

$$u(t) = u^*(t) + \varepsilon\upsilon(t), \qquad\qquad\qquad (13a)$$
$$x(t) = x^*(t) + \varepsilon\ y(t)\,, \qquad\qquad\qquad (13b)$$

where $\varepsilon$ is a small positive number and $\upsilon(t)$ is arbitrary.

The optimal control law is obtained when $\varepsilon = 0$, which makes $dJ(\varepsilon)/d\varepsilon = 0$ [5, 6]. The solution is detailed in Appendix 9.1 and leads to the control law:

$$u(t) = -R(t)^{-1}B(t)^T\lambda(t), \qquad\qquad (14)$$

here $\lambda(t)$ is the coestate vector defined as:

$$\lambda(t) = P(t)x(t) + \mu(t), \qquad\qquad (15)$$

where P is a symmetric positive semidefinite matrix and $\mu$ is a column vector and the dynamic behavior of the coestate vector is given by:

$$\lambda'(t) = -Q(t)e(t) - A^T(t)\lambda(t)\,. \qquad\qquad (16)$$

The particular structure of the control law depends on the design approach used in the formulation of the linear quadratic problem as explained in the following section.

### 9.2.2. Servocontrol and Regulatory Design Schemes

Two controller design schemes can be considered according to the control objective: servocontrol and regulation. The servocontrol scheme focuses on the control of blood

glucose concentration, G, when the desired glucose level, $G_d$, is changed. The regulatory scheme emphasizes the correction of the deviations from a constant $G_d$, caused by disturbances.

### 9.2.2.1. Servocontrol Design

Under the servocontrol approach, $x_d$ is the desired glucose change in a diabetic person from the initial steady state level ($G_0$):

$$x_d = G_d - G_0. \tag{17}$$

The deviation of the blood glucose level from its desired value ($x_l - x_d = G - G_d$) and the insulin infusion must be minimized. The objective function is:

$$J(u) = \int_0^\infty \left[ \eta (x_1(t) - x_d)^2 + \rho u^2(t) \right] dt \tag{18}$$

where $\eta$ and $\rho$ are positive weighting factors. By comparing Equations (18) and (11), it can be identified that $S = \begin{bmatrix} 0 & 0; & 0 & 0 \end{bmatrix}$, $Q = \begin{bmatrix} 2\eta & 0; & 0 & 0 \end{bmatrix}$, $R = 2\rho$, $t_0 = 0$ and $t_f = \infty$.

The open loop system is represented by a state space model with constant parameters. The closed loop dynamics achieved with the optimal control law is obtained by combining Equations (12) and (14):

$$x'(t) = Ax(t) - BR^{-1}B^T\lambda(t) \tag{19}$$

From Equations (15) and (16), the first derivative of the coestate vector is:

$$Px' = -Q(t)[x(t) - x_D] - A^T Px(t) - A^T \mu \tag{20}$$

where $x_D$ is the vector of desired deviation values for the state variables and $x_D(1) = x_d$.

Replacing $x'(t)$ with Equation (19) in (20) gives:

$$\left( PA + A^T P - PBR^{-1}B^T P + Q \right) x(t) = \left( PBR^{-1}B^T - A^T \right)\mu + Qx_D \tag{21}$$

The matrix P is chosen to satisfy the Riccati equation:

$$PA + A^T P - PBR^{-1}B^T P + Q = 0 \tag{22}$$

Then, from equation (21), $\mu$ can be calculated ($\mu \neq 0$). The optimal control law is:

$$u(t) = -K_c x + K \tag{23}$$

where $K_c = \begin{bmatrix} K_{c1} & K_{c2} \end{bmatrix}$ and the parameters are calculated as:

$$K_{c2} = \sqrt{m_1^2 + m_3^2 + 2\sqrt{m_1^2 m_3^2 + m_2^2 \rho^{-1} \eta}} - (m_1 + m_3) \tag{24}$$

$$K_{c1} = -\left(K_{c2}^2 + 2m_3 K_{c2}\right)\big/ 2m_2 \tag{25}$$

$$K = -m_2 x_d \rho^{-1} \left(m_1^2 m_3^2 + m_2^2 \rho^{-1} \eta\right)^{-0.5} \tag{26}$$

With $\eta = 1$, $\rho = 10$ min$^2$ and $x_d = -200$ mg/dL (for the simulation case of the correction of a hyperglycemic condition of 300 mg/dL studied in Section 8.4) and the Ackerman model parameters (Section 9.1), the resulting parameters of the control law are:

$$K_{c1} = -0.2991 \text{ min}^{-1}, \; K_{c2} = 0.0183 \text{ min}^{-1}, \; K = 63.1997 \text{ (mg/dL)/min.} \tag{27}$$

### 9.2.2.2. Regulatory Design

For the regulatory approach, a normal glucose level is referred as the initial steady state ($G_d = G_0$). Any deviation from this value is a disturbance, since

$$x_d = G_d - G_0 = 0. \tag{28}$$

Therefore, $x_l$ is the deviation of glucose level from the desired value ($x_l = G - G_d$) and the performance criterion is expressed as:

$$J(u) = \int_0^\infty \left[ \eta\, x_1^2(t) + \rho\, u^2(t) \right] dt \tag{29}$$

Considering the linear state space process model, the performance criterion represented by equation (29) and the application of equations (19) through (22), $\mu = 0$ and the control law is:

$$u(t) = -K_c x(t). \tag{30}$$

With $\boldsymbol{h} = 1$, $\boldsymbol{r} = 10$ min$^2$ and the Ackerman model parameters of Section 9.1:

$$K_c = [-0.2991 \; 0.0183]. \tag{31}$$

Equations (24), (25) and (26) for the servocontrol and regulatory controller parameters can be evaluated with the elements of the Jacobian matrix indicated in Equation (10), when the dynamics of the Sorensen model for the diabetic patient is used.

### 9.2.3. State Estimation

The control law in both approaches is a function of the two states of the system, glucose ($x_1$) and insulin ($x_2$) concentrations. The glucose concentration measurement is supposed to be available while the insulin concentration needs to be estimated.

The design of the control law and the design of the state observer are independent. The observer model is given by:

$$\tilde{x}'(t) = A\tilde{x}(t) + Bu(t) + K_e[y(t) - C\tilde{x}(t)] \qquad (32)$$

where $y(t) - C\tilde{x}(t)$ is the observation error.

The Ackerman's model is an observable system. The state observer is designed according to the classical control theory using the parameters given in Section 9.1. The gain vector $K_e = [0.2021 \ -2.1023]^T$ produces a faster observer response (natural frequency $\omega_n = 0.122$ rad/min and damping ratio $\zeta = 1$), with respect to the closed loop behavior ($\omega_n = 0.031$ rad/min and damping ratio $\zeta = 0.97$). The state observer design and the dynamic analysis are documented in Appendix 9.2.

If the physiologic process is represented by the Sorensen nonlinear model, the best linear approximation may vary with time, which causes "process noise" [4]. Additionally, noisy sensor measurements can be considered to justify the use of a Kalman filter for the sate estimation.

### 9.3. Simulation of the Controller Closed Loop System

The simulation problem consists of a situation of hyperglycemia in a type I diabetic patient with an initial glucose level of 300 mg/dL. The closed loop system should reach a normal steady state level (100 mg/dL for the Ackerman model or 120 mg/dL with the Sorensen model) with a relatively fast response and without inducing hypoglycemia. The sensor and actuator are assumed to be ideal systems and the open loop dynamics is supposed to be dominated by the model of the patient or physiologic process to be controlled.

### 9.3.1. Closed loop with a Linear Process Model

The servocontrol and the regulatory control design schemes are explored using the second order linear glucose-insulin model by Ackerman. The simplicity of the Ackerman model allows for the discussion of control design approaches, before using the broader Sorensen model. The designs are evaluated in the context of the correction of hyperglycemia.

The open loop response of the Ackerman physiological model provides a basic reference to appreciate the effect of the controller. The extremely slow recovery of a normal glucose level of 100 mg/dl, with the elimination of the cause of the hyperglycemic condition and without supply of exogenous insulin, is shown in Figure 9.1. The control loop is closed with the classical state observer and the optimal controller as illustrated in Figure 9.2. This configuration allows the comparison with reported results for the stated simulation problem [7].

Under a servocontrol approach, the initial deviation value is zero assuming an initial stable state in the hyperglycaemic condition (300 mg/dL). The glucose change to be achieved is -200 mg/dL. Simulation results are shown in Figure 9.3. The transient period elapses 4 hours, a steady state error of 0.3 mg/dL is detected and the cost function grows indefinitely.

For the regulatory approach, the reference steady state is the normal condition of glucose level at 100 mg/dL, so the initial deviation of 200 mg/dL is considered a disturbance to the closed loop system. No offset error is obtained and the cost function converges, as Figure 9.4 shows.

A linearized and low order glucose-insulin model may cause uncertainty as non-linear high order models do. Although a more complete model may be suitable to manage characterized uncertainty [8], all effects may not be represented, which justifies a random variation of model parameters to analyze controller robustness.

A Monte Carlo simulation tests the robustness of the control system. The parameters of the Ackerman model are changed following a stochastic process, while the controller parameters are not altered. To illustrate the variability in the performance of the closed loop system before changes in process dynamics, Figure 9.5 presents box and whisker plots for the cost function and the offset of the closed loop response under different percentages of variation. These graphs were computed by 30 independent runs of the simulation test. Beyond 60% parameter variation, the servocontrol system shows unacceptable performance. The regulatory design performs with no significant difference with more than 50% variation.

### 9.3.2. Closed Loop with a Non-linear Process Model

A second closed loop system is proposed using the Sorensen model to simulate the glucose-insulin metabolism in a diabetic patient. This model considers the nonlinear nature of the real process. The model response converges to a normal steady state glucose

concentration of 120 mg/dL with no infusion of insulin. Therefore, the simulation problem is slightly modified by the consideration of the final normal glucose concentration of 120 mg/dL. The hyperglycemic condition is produced by the simulation of a glucose meal input to the gut compartment of the Sorensen model. The glucose meal input is increased exponentially from zero and kept at 408.7 mg/min to stabilize the arterial glucose concentration in 300 mg/dL. Then, the glucose meal input is suspended and the metabolism of the diabetic patient takes about 8 hours to reach a steady glucose concentration of 120 mg/dL without insulin delivery, as shown in Figure 9.6.

The control system includes a linearization module, a Kalman filter and the optimal controller, as indicated in Figure 9.7. The linearization module is used for the calculation of the parameters of the control law and the Kalman estimator gain vector. The Kalman filter is needed to estimate the blood insulin concentration. The control approach to apply is the regulatory one, since it produces higher performance with a simpler configuration (Section 9.3.1). The simulation diagram of Figure 9.7 helps to evaluate the adequacy of the control law structure and regulatory approach for a nonlinear process in the presence of noise.

The weighting factors $\eta$ and $\rho$ of the cost function are adjusted to avoid oscillation. The normal glucose level can be restored after 250 min, according to the simulation results shown in Figure 9.8. The closed loop system reduces the open loop settling time (Figure 9.6), but the difference is less drastic than in the case of the system of Figure 9.2, as transient responses in Figures 9.1 and 9.4 show, since the controller is not based on the same model used for the glucose-insulin process simulation.

The parameters $\eta$ and $\rho$ of the cost function (29) are varied to show how they affect the system dynamics in Figure 9.9. The magnitude of the initial slope and the undershoot of the closed loop response increase with higher $\eta$ and lower $\rho$. Figure 9.9 also shows the corresponding effect of the weighting factors on insulin delivery (bottom plots). The order of magnitude of $\rho$ needs to be very high in order to prevent saturation and an ON-OFF controller behavior. The values for the weighting factor $\rho$ are very different from the value used with the linear process model of the glucose-insulin metabolism due to the distinct dynamics and different units required for the metabolic source of insulin in the Sorensen model.

### 9.3.3. Discussion of Results

The simulation results are summarized in Table 9.1. The evaluation of the linear control system using the Ackerman representation of the physiological model suggests using the regulatory approach for its higher robustness. In spite of the variable offset obtained with the servocontrol scheme, the correction of the simulated hyperglycemic condition control is effective under the consideration of a desired range of glucose levels instead of a specific target glucose concentration value.

The structure of the control law obtained with the LQC technique corresponds to a proportional controller, which causes an offset except in the steady state condition of the

patient used as reference to define deviation values. If the reference steady state of the patient is the state of normal blood glucose level, the control action proportional to the states can reach the desired glucose level from any abnormal condition. Monte Carlo simulations prove the higher robustness for the regulatory control scheme.

The stated simulation test with the linear system configuration of Figure 9.2 has been presented in the literature [7]. Glucose levels at 1 and 2 hours with the servocontrol approach are very similar to reported values. Glucose levels of 185.98 and 119.86 mg/dl are obtained while previous works report $\approx 183$ and $\approx 119$ mg/dl at these times respectively. For the regulatory approach, glucose concentrations of 166.8 and 112.57 mg/dl are reached at 60 and 120 min. These results differ more from the reported results, however the performance is more satisfactory.

The closed loop implemented with the process dynamics given by the Sorensen's model under a regulatory approach (with $\eta = 1$ and $\rho = 3.3 \times 10^{11}$ min$^2$) achieves 60.87% and 93.06% of the total desired change at 60 and 120 minutes, with no steady state deviation. Reported results show a change in blood glucose concentration of 58.5% and 90.5% at the same times. Thus, the comparison shows agreement with prior researches and validates the present approach for optimal glucose control.

The possibility for external adjustment by the patient or a physician, as a safety feature or extraordinary measure, is also considered by means of the weighting factors of the performance function. A low weighting factor for the glucose level deviation and a high weighting factor for the exogeneous insulin lead to a slower correction of the blood glucose concentration with more restricted supply of insulin (Figure 9.9). Appropriate weighting factors would give the fastest response without oscillations that could imply a hypoglycemia risk, which is also prevented by the observed monotonous decaying controller output or insulin administration.

The stability is a basic requirement of any closed loop system. The preservation of a stable performance or robustness in spite of the variations of the process dynamics was only explored with the linear system. The wide range of model parameter variations in the Monte Carlo simulations (from 0 to more than 50% in magnitude) for the linear system suggested a high degree of robustness, particularly with the regulatory control approach. This appreciation of high robustness is extended to the non-linear system, considering that the variations of the Ackerman model can represent the non-linear dynamics of the Sorensen model of the glucose-insulin metabolic process. Although, the stability analysis of the high order non-linear closed loop system is not proved in this work, no evidence of instability was obtained.

## 9.4. Conclusions

The presented simulation of a closed loop system for diabetes treatment considers a glucose-insulin process model and a mathematical controller. The low order and linearized Ackerman model provides a practical basis for the evaluation of the servocontrol and regulatory controller design approaches. Simulation results with the Ackerman model and

different design approaches show the superiority of the regulatory controller, since it avoids a steady state error in the glucose level and realizes corrections and maintains stability in spite of dynamic variations of the physiological process, which are examined by means of a Monte Carlo simulation.

The advantageous regulatory design is applied to control the glucose-insulin metabolism represented by the Sorensen high order, non-linear model. The closed loop system is refined by considering a more detailed description of the process, a Kalman filter to account for the noise effect in the estimation of the blood insulin concentration, and an adaptive mechanism to update the controller parameters. The added complexity responds to basic requirements for a real application of the proposed system.

Although a closed loop treatment system is designed to perform without human intervention, the user (patient or physician) could make adjustments by modifying the weighting factors $\eta$ for the glucose concentration deviation and $\rho$ for the insulin delivery or controller action. Since the inverse of the weighting factor for the insulin delivery and the weighting factor for the glucose level deviation have similar effects, and the product of both appears in the calculations of the controller gain vector Kc, a single means can be proposed for tuning the system, either $\rho$ or $\eta$ or the product $\rho^{-1}\eta$ itself. A unique parameter for adjustment would ease the interaction of the user with the system.

The results based on the interaction of the optimal controller with a highly nonlinear plant show the robustness of the controller and the adequacy of the design approach for a particular biomedical problem. However, the proposed system lacks of a feedforward or anticipation mechanism that is present even in the traditional open loop treatment based on insulin injections previous to the ingestion of food, for example. The presented closed loop system intends to emulate the response of a healthy body to the blood glucose level resultant from the activity of the patient, trying not to alter his daily routine.
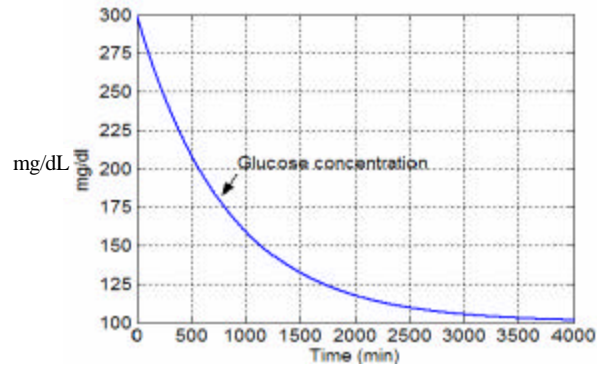
**Figure 9.1. Open Loop Response Using the Ackerman Linearized Model.** The physiological process starts from an initial blood glucose level of 300 mg/dL and recovers a normal value of 100 mg/dL without insulin administration.



**Figure 9.2. Configuration of the Linear Closed Loop System.** The glucose-insulin metabolism is represented by the Ackerman linearized model (BGC: blood glucose concentration, BIC: blood insulin concentration).

(a)

(b)

(c)
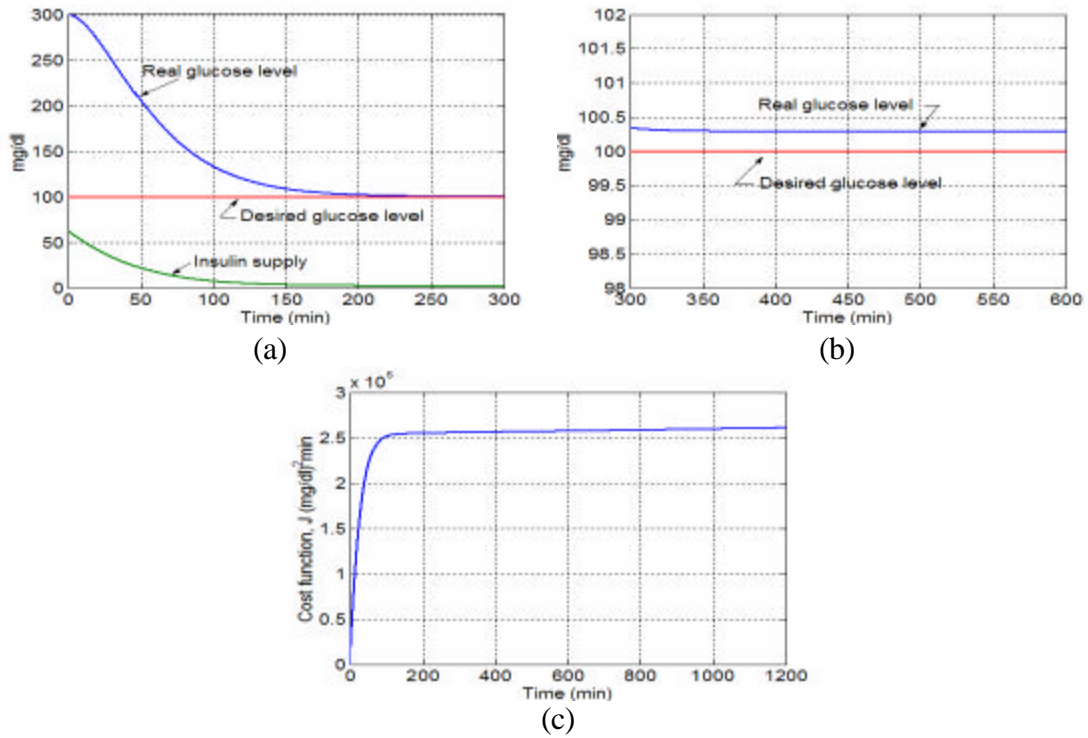
**Figure 9.3. Servocontrol Results with a Linearized Model for Glucose-Insulin Metabolism.** The obtained transient response (a), final steady state (b) and cost function (c) are shown.
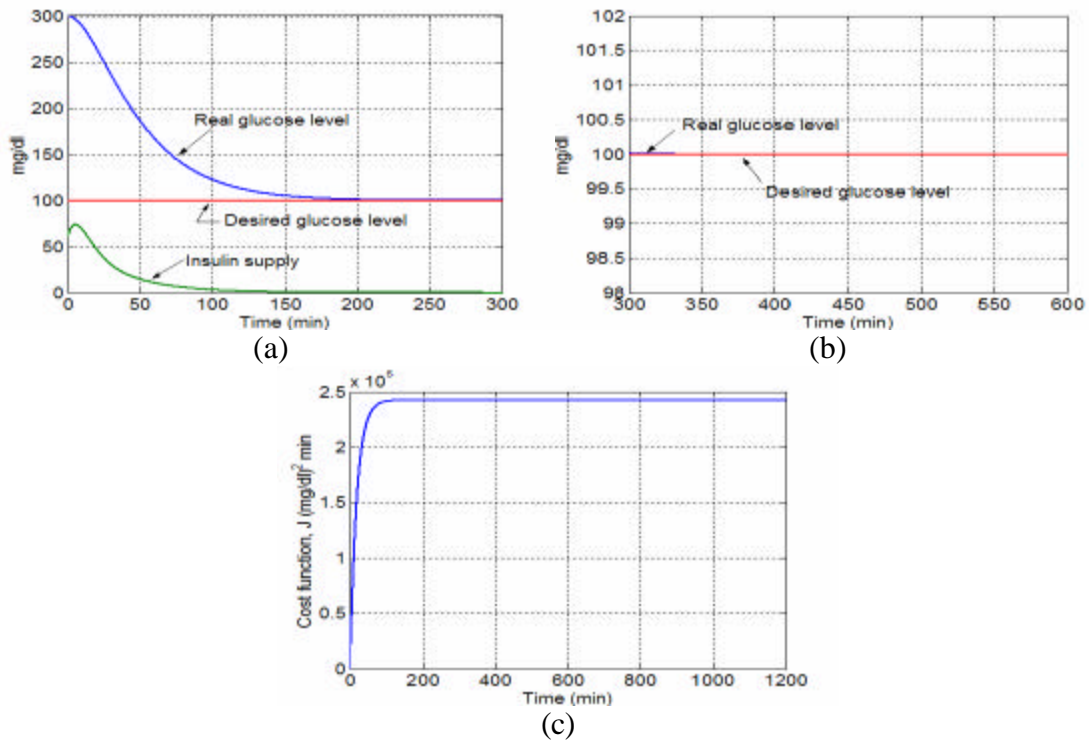
**Figure 9.4. Regulatory Results with a Linearized Model for Glucose-Insulin Metabolism.** The obtained transient response (a), final steady state (b) and cost function (c) are shown.

190
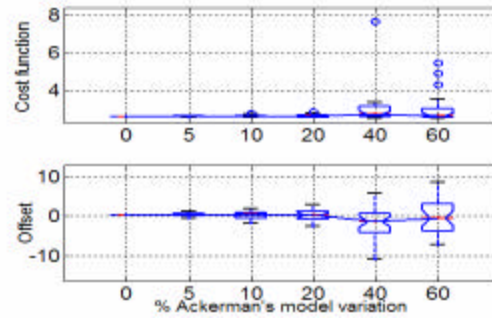
(a)
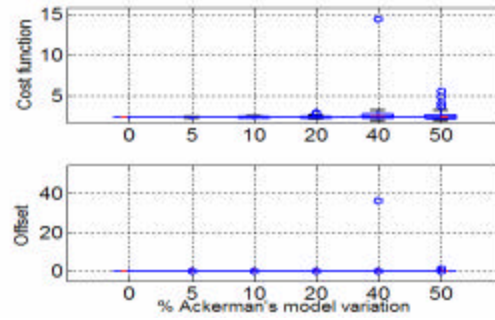


(b)

**Figure 9.5. Robustness Tests for the Linear System.** The servocontrol approach (a) and the regulatory approach (b) are compared before random variations of the dynamic of the process. The cost function, J, given by Equation (18) or Equation (29), is reported in $(mg/dL)^2$ min $\times 10^{-6}$ ; the offset is reported in mg/dL. The boxes have lines at the lower quartile, median, and upper quartile values. The whiskers are lines extending from each end of a box to show the extent of the rest of the data. The boxes are notched. Notches represent a robust estimate of the uncertainty about the medians for box-to-box comparison. Outliers are data values beyond the ends of the whiskers; outliers are shown as circles.
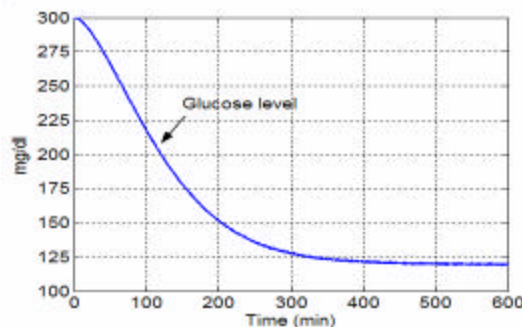


**Figure 9.6. Open Loop Response Using the Sorensen Non-linear Model.** The physiological process starts from an initial blood glucose level of 300 mg/dL and recovers a normal value of 120 mg/dL without insulin administration.
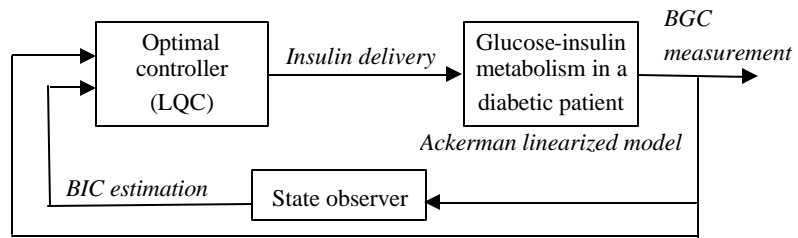
191
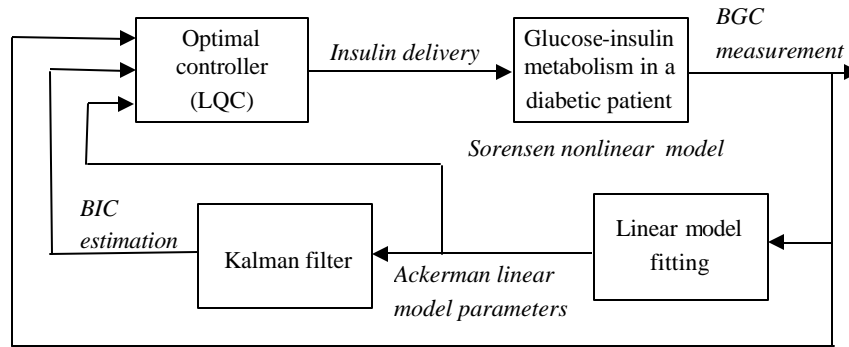
**Figure 9.7. Configuration of the Non-linear Closed Loop System.** The glucose-insulin metabolism is represented with the Sorensen non-linear model. (BGC: blood glucose concentration, BIC: blood insulin concentration).
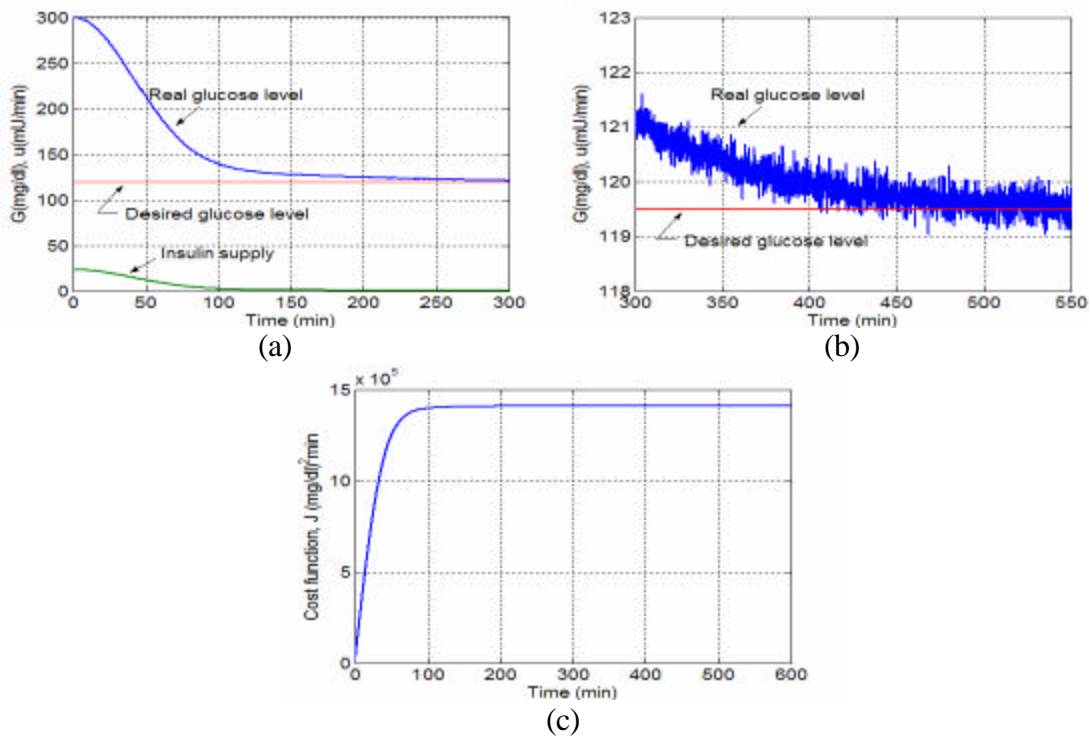


**Figure 9.8. Regulatory Results with the Sorensen Non-linear Model.** The obtained transient response (a), final steady state (b) and cost function (c) are shown.
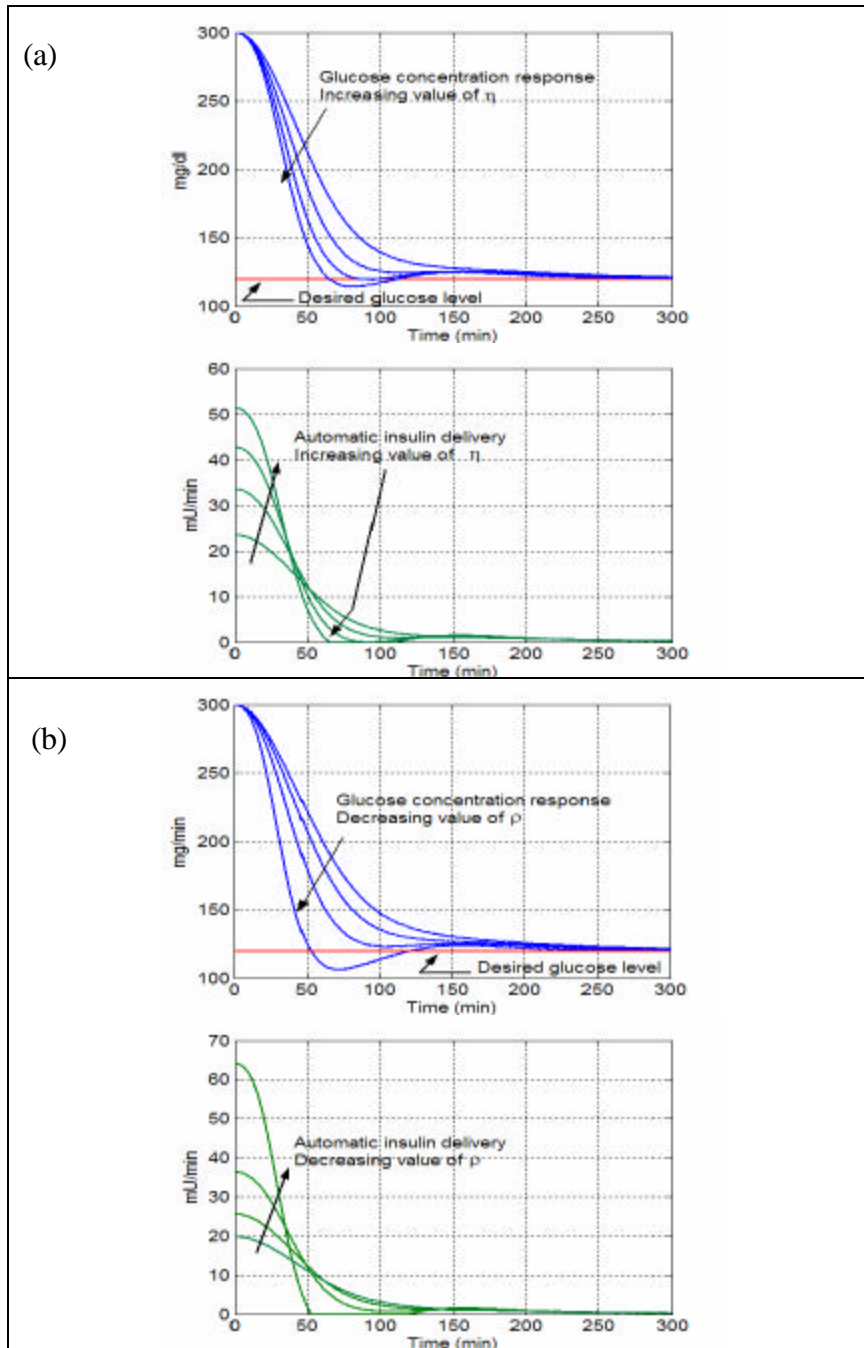
**Figure 9.9. Effect of Weighting Factors on Closed Loop Response**. (a) The values for $\eta$ are 1, 1.5, 2 and 2.5, with $\rho = 3.3 \times 10^{11}$ min$^2$. (b) The factor $\rho$ is varied as 1, 2, 3 and 4 times $10^{11}$ min$^2$ with $\eta = 1$.

**Table 9.1. Simulation Results for the Correction of a Hyperglycemic Condition of 300 mg/dL.** An optimal LQ controller is used en each case.

| Physiological model | Ackerman | | Sorensen |
|---|---|---|---|
| Open loop settling time | 3500 min | | 450 min |
| Control approach | Servocontrol | Regulatory | Regulatory |
| Closed loop settling time | 230 min | 200 min | 250 min |
| Closed loop offset | Variable | Null | Null |

**References**

1. Ackerman E, Gatewood L, Rosevear J, Molnar G. Model studies of blood-glucose regulation. Bull Mathem Biophys. 1965;27:21-38.

2. Sorensen J. A physiologic model of glucose metabolism in man and its use to design and assess improved insulin therapies for diabetes. PhD thesis. Dept. of Chemical Engineering, MIT, 1985.

3. Yipintsol T, Gatewood L, Ackerman E, Spivak P, Molnar G, Rosevear J, Service F. Mathematical analysis of blood glucose and plasma insulin responses to insulin infusion in healthy and diabetic subjects. Comput Biol Med. 1973;3:71-78.

4. Haykin S. Adaptive filter theory (4$^{th}$ edition). New Jersey: Prentice Hall, 2001.

5. Naidu D. Optimal Control Systems. Boca Raton: CRC Press, 2003.

6. Vinter R. Optimal control. Boston: Birkhöuser, 2000.

7. Kikuchi M, Machiyama N, Kabei N, Yamada A, Sakurai Y. Homeostat to control blood glucose level. Int Symp Med Inf Syst. 1978:541-545.

8. Parker RS, Doyle FJ III, Ward JH, Peppas NA. Robust $H_\infty$ glucose control in diabetes using a physiological model. AIChE J. 2000;46:2537-2549.

## Appendix 9.1.  Optimal Control:  Linear Quadratic Problem

In optimal control, the manipulation variable, u, is defined in order to minimize a cost function, that is, to optimize a performance criterion. The performance criterion is proposed in terms of a terminal condition and a cumulative quantity:

$$J(u) = \theta[x(t_f)] + \int_{t_0}^{t_f} g(x,u)dt,$$  (a9.1.1)

where J, $\theta$ and g are scalar functions, x is the state vector and u is the input vector or control action vector.

The process dynamics is represented by:

$$x'(t) = f(x,u), \quad x(t_0) = x_0.$$  (a9.1.2)

In the linear quadratic problem, the input vector appears linearly in the process model, f(x,u), and quadratically in the performance criterion, J(u):

$$J(u) = \frac{1}{2}x^T(t_f)Sx(t_f) + \frac{1}{2}\int_{t_0}^{t_f}\left[x^T(t)Q(t)x(t) + u^T(t)R(t)u(t)\right]dt,$$  (a9.1.3)

$$x'(t) = A(t)x + B(t)u, \quad x(t_0) = x_0,$$  (a9.1.4)

where S is constant; Q, R, A and B can vary with time; Q, R and S are symmetric matrices; S and Q are positive semidefinite, and R is positive definite.

An optimal control law u*(t) is assumed to exist for this problem in [$t_0$, $t_f$].  An optimal trajectory x*(t) is associated with u*(t).  The control signal and the state vector can be expressed as:

$$u(t) = u^*(t) + \varepsilon\upsilon(t),$$  (a9.1.5)

$$x(t) = x^*(t) + \varepsilon\, y(t),$$  (a9.1.6)

where $\varepsilon$ is a small positive number and $\upsilon(t)$ is arbitrary.

Substituting u and x with Equations (a9.1.5) and (a9.1.6) in Equation (a9.1.3), $J(u^* + \varepsilon\,\upsilon) = J(\varepsilon)$ is obtained:

$$J(u) = \frac{1}{2} x *^T (t_f) S x * (t_f) + \frac{1}{2} \int_{t_0}^{t_f} \left[ x *^T (t) Q(t) x * (t) + u *^T (t) R(t) u * (t) \right] dt$$

$$+ \varepsilon \left\{ y^T (t_f) S x * (t_f) + \int_{t_0}^{t_f} \left[ y^T (t) Q(t) x * (t) + \upsilon^T (t) R(t) u * (t) \right] dt \right\}$$

$$+ O(\varepsilon^2)$$

(a9.1.7)

where

$$O(\varepsilon^2) = \frac{\varepsilon^2}{2} \left\{ y^T (t_f) S y(t_f) + \int_{t_0}^{t_f} \left[ y^T (t) Q(t) y(t) + \upsilon^T (t) R(t) \upsilon(t) \right] dt \right\} \quad (a9.1.8)$$

Equation (a9.1.5) indicates that the optimal control is obtained when $\varepsilon = 0$. Therefore, $\varepsilon = 0$ optimizes the performance criterion, regardless of the vectors $\upsilon(t)$ y $y(t)$, as expressed by the following equation:

$$\left. \frac{dJ(\varepsilon)}{d\varepsilon} \right|_{\varepsilon=0} = 0.$$

(a9.1.9)

From the development of Equation (a9.1.9), the following condition is obtained:

$$y^T (t_f) S x * (t_f) + \int_{t_0}^{t_f} \left[ y^T (t) Q(t) x * (t) + \upsilon^T (t) R(t) u * (t) \right] dt = 0. \quad (a9.1.10)$$

The following equation is produced from the combination of Equations (a9.1.4) and (a9.1.6):

$$y'(t) = A(t)y + B(t)\upsilon, \quad y(t_0) = 0.$$

(a9.1.11)

The solution of equation (a9.1.11) is given by:

$$y(t) = \int_{t_0}^{t_f} \phi(t,\xi) B(\xi)\upsilon(\xi) d\xi ,$$

(a9.1.12)

where $\phi$ is the fundamental solution of the differential equation:

$$\phi'(t,t_0) = A(t)\phi(t,t_0), \quad \phi(t_0,t_0) = I.$$

(a9.1.13)

By substituting Equation (a9.12) in Equation (a9.10) and changing the integration order, the following expression can be obtained:

$$\int_{t_0}^{t_f} \upsilon^T(t)\left[B^T(\xi)\phi^T(t_f,\xi)Sx*(t_f) + B^T(\xi)\int_{\xi}^{t_f}\left[\phi^T(t,\xi)Q(t)x*(t)dt + R(\xi)u*(\xi)\right]\right]d\xi = 0$$

(a9.1.13)

The costate column vector $\lambda(t)$ is defined as:

$$\lambda(t) = \phi^T(t_f,t)Sx*(t_f) + \int_{t}^{t_f}\phi^T(\xi,t)Q(\xi)x*(\xi)d\xi.$$

(a9.1.14)

Equation (a9.1.13) can be rewritten in the following way:

$$\int_{t_0}^{t_f}\upsilon^T(t)\left[B^T(t)\lambda(t) + R(t)u*(t)\right]dt = 0.$$

(a9.1.15)

Since $\upsilon(t)$ is arbitrary, Equation (a9.1.15) is satisfied when:

$$B^T(t)\lambda(t) + R(t)u*(t) = 0.$$

(a9.1.16)

Matrix R(t) must have an inverse to express the optimal control vector as:

$$u*(t) = -R^{-1}(t)B^T(t)\lambda(t).$$

(a9.1.17)

Differentiating both sides of Equation (a9.1.14) and using:

$$\phi'^T(t_f,t) = -A^T(t)\phi^T(t_f,t), \quad \phi(t,t) = I,$$

(a9.1.18)

the following equation is obtained:

$$\lambda'(t) = \phi'^T(t_f,t)Sx*(t_f) - \phi(t,t)Q(t)x*(t) + \int_{t}^{t_f}\phi'^T(\xi,t)Q(\xi)x*(\xi)d\xi$$

$$= -Q(t)x*(t) - A^T(t)\lambda$$

(a9.1.19)

198

The following equation is defined from Equation (a9.1.14):

$$\lambda(t_f) = Sx*(t_f) \tag{a9.1.20}$$

The following equation results from substituting Equation (a9.1.17) in Equation (a9.1.4):

$$x'(t) = A(t)x - B(t)R^{-1}(t)B^T(t)\lambda(t). \tag{a9.1.21}$$

The costate vector is proposed to have tha following form:

$$\lambda = Px + \mu, \tag{a9.1.22}$$

where P is a symmetric matrix.

The combination of equations (a.19), (a.22) and (a.4) produces:

$$\lambda' = P'x + Px' + \mu' = -Qx - A^T Px - A^T \mu. \tag{a9.1.23}$$

Eliminating $x'$ by using (a.21):

$$P'x + PAx - A^T Px - PBR^{-1}B^T Px + Qx = +PBR^{-1}B^T P\mu - A^T\mu - \mu' \tag{a9.1.24}$$

The Riccati equation is given by:

$$P' + PA - A^T P - PBR^{-1}B^T P + Q = 0. \tag{a9.1.25}$$

Matrix P is proposed to satisfy the Riccati equation, and proceed with the solution of Equation (a9.1.24) for $\mu$ (with the left side equal to 0). The procedure is simplified when P and $\mu$ are constant arrays, as considered in this work by the use of

$$\lambda'(t) = -Q(x - x_d) - A^T\lambda.$$

Finally, the control law is completely specified as:

$$u = -R^{-1}B^T Px - R^{-1}B^T\mu$$

or

$$u = -K_c x + K. \tag{a9.1.26}$$

## Appendix 9.2. State Observer Design

The control law is a function of two state variables of the process: glucose concentration and insulin concentration. Only the measurement of glucose concentration is considered to be available. Therefore, a state observer is necessary for the estimation of the second state. The state observer is designed according to the modern control theory of state space.

The model of the biological process in stae space is given by:

$$\begin{bmatrix} x'_1 \\ x'_2 \end{bmatrix} = \begin{bmatrix} -0.0009 & -0.0031 \\ 0 & -0.0415 \end{bmatrix} \begin{bmatrix} x_1 \\ x_2 \end{bmatrix} \begin{bmatrix} 0 \\ 1 \end{bmatrix} u$$

$$y = \begin{bmatrix} 1 & 0 \end{bmatrix} \begin{bmatrix} x_1 \\ x_2 \end{bmatrix}$$

(a9.2.1)

The observability matrix is determined in the following way:

$$N = \begin{bmatrix} C^T & | & A^T C^T \end{bmatrix} = \begin{bmatrix} 1 & -0.0009 \\ 0 & -0.0031 \end{bmatrix}$$

(a9.2.2)

The rank of matrix N is equal to the number of status or the rank of matriz A, which determines that the system is observable.

The mathematical model of the observer is expressed as:

$$\tilde{x}' = A\tilde{x} + Bu + K_e(y - C\tilde{x}) = (A - K_e C)\tilde{x} + Bu + K_e Cx$$

(a9.2.3)

Substracting the observer model from the process model, the estimation error dynamics is obtained:

$$x' = Ax + Bu$$
$$\tilde{x}' = A\tilde{x} + Bu + K_e(y - C\tilde{x}) = (A - K_e C)\tilde{x} + Bu + K_e Cx$$
$$x' - \tilde{x}' = (A - K_e C)(x - \tilde{x})$$
$$error' = (A - K_e C)error$$

(a9.2.4)

The design of the observer consists in determining the vector $K_e$, so that the matrix $A - K_e C$ is stable (eigenvalues or poles with negative real part). In this way, the error vector will converge to zero regardless of its initial value.

The poles of the observer or eigenvalues of $A - K_e C$ should be chosen to produce a faster dynamics than the one of the controlled process. For this reason, it is necessary to calculate first the poles of the process and the poles of the closed loop system.

The characteristic polynomial of the process is the determinant of A-sI:

$$s^2 + 0.0424s + 0.00003735 = s^2 + a_1 s + a_2 \qquad\qquad (a9.2.5)$$

From the solution of the above equation, the poles of the process can be obtained:

$s_1 = -0.0415$   y   $s_2 = -0.0009$   ($s_2$ is the dominant pole)

These poles produce an open loop response with a damping factor of 3.47 and a natural frequency of 0.0061 rad/min.

The closed loop model is obtained by substituting the control law in the model of the process:

$$x' = Ax + B(-K_c x + K) = (A - BK_c)x + BK \qquad\qquad (a9.2.6)$$

The closed loop poles are calculated from A-BK$_c$ – sI=0:

Los *polos de lazo cerrado* se obtienen al resolver A-BK$_c$ –sI=0
$s_1 = -0.0303525 + 0.0077294i$
$s_2 = -0.0303525 - 0.0077294i$

These poles determine a closed loop behavior with a damping factor of 0.97, which impedes a noticeable oscillation or the occurrence of hypoglycemia when the controller tries to correct hyperglycemia.   The natural frequenc y is 0.031 rad/min, much more bigger than the open loop frequency, which produces a faster response in combination with a low closed loop damping factor.

The poles of the observer are proposed considering a unit damping factor and a natural frequency of 20 times the open loop natural frecuency, which is approximately equal to 4 times the closed loop natural frequency:

$s_1 = s_2 = -0.12223$

The characteristic polynomial of the observer is given by:

$$(s + 0.12223)^2 = s^2 + 0.2445s + 0.0149 = s^2 + \alpha_1 s + \alpha_2 \qquad\qquad (a9.2.7)$$

The following matrix W is formed with the coefficients of the characteristic polynomial of the process:

$$W = \begin{bmatrix} a_1 & 1 \\ 1 & 0 \end{bmatrix} = \begin{bmatrix} 0.0424 & 1 \\ 1 & 0 \end{bmatrix} \qquad\qquad (a9.2.8)$$

The matrix Q$_{obs}$ is calculated as:

$$Q_{obs} = \left(WN^T\right)^{-1} = \begin{bmatrix} 0 & 1 \\ -322.5806 & 13.3871 \end{bmatrix}$$
(a9.2.9)

The gain vector of the observer $K_e$ is calculated in the following way:

$$K_e = Q*\begin{bmatrix} \alpha_2 - a_2 & \alpha_1 - a_1 \end{bmatrix} = \begin{bmatrix} 0.2021 \\ -2.1023 \end{bmatrix}$$
(a9.2.10)

With the obtained vector $K_e$, the model of the state observer is completely determined.

## 10. Comparison of Hydrogel and Controller Based Feedback Systems

Two types of diabetes closed loop treatments, characterized by the continuous feedback of blood glucose level and proper insulin delivery, have been proposed based on the intrinsic multifunctionality of hydrogels as well as on an explicit controller to be supported by separated sensor and actuator units. The objective of this chapter is to evaluate the potential of hydrogel systems for the regulation of blood glucose levels. The performance of the system closed by a hydrogel-based device is explored and compared to the dynamic behavior of a conventional scheme with an explicit controller element. Anionic and cationic hydrogels are discussed for insulin delivery application. Operation limitations of hydrogels are shown and explained in this chapter.

## 10.1. Configuration of Feedback Systems

The hydrogel and controller based diabetes treatment systems are shown in Figure 10.1. The Sorensen compartmental model is used for the representation of the physiological process to be regulated [1]. This model is extended to represent the hydrogel based treatment system of a diabetic patient, that is, a hydrogel compartment is defined similarly to the rest of the organ compartments and coupled through untransmitted variables. The hydrogel compartment represents a membrane implant in the peritoneum that reacts to the glucose concentration in the surroundings by releasing insulin through a diffusion mechanism determined by the volume changes of the hydrogel material. The glucose sensitivity is attained by the enzymatic transformation of glucose into gluconic acid, which affects the pH and the volume of the insulin loaded hydrogel system.

The simulation of the anionic hydrogel membrane is based on the experimental characterization of the P(MAA-g-EG) material. The parameters for the cationic material are proposed based on its qualitative pH swelling response and the quantitative characteristics of the response of the anionic membranes, such as the order of magnitude of the mechanochemical compliance and the values of the reaction and swelling kinetic constants.

The Sorensen model interacts with the mathematical controller through supposed transmission signals from an ideal sensor and to an ideal actuator. The actual implementation of this closed loop system would require a sensing element and a transducer to send a signal proportional to the glucose concentration of physiological fluids to the controller. The controller uses the measurement to estimate other unmeasured physiological variables, such as the blood insulin concentration, and to evaluate a mathematical algorithm to specify the proper insulin infusion rate to maintain a normal glucose level. A transducer converts the specified insulin infusion rate into a signal that operates an actuator for the administration of insulin.

## 10.2. Simulation Test

The performance of a hydrogel-based system for the regulation of blood glucose is evaluated by the simulation of three daily meals until significant insulin diffusion from the hydrogel stops. The meals are represented by pulse functions for the carbohydrates consumption rate, as illustrated in Figure 10.2. The pulse duration is fixed in 30 minutes, and the pulse area represents the ingestion of 66 g of carbohydrates. The carbohydrates total in three meals accounts for 53% of the energy from a 1500 kcal diet, close to the minimum daily recommended energy percentage from carbohydrates [2]. In the case of a higher caloric content diet, low carbohydrate meals are considered for the simulation. This type of diet was selected because the response obtained without insulin administration produced peak glucose concentrations close to the hyperglycemic condition of 300 mg/dL managed in previous simulations (Chapters 8 and 9).

Several assumptions complete the simulation conditions for hydrogel structures for insulin delivery in a diabetic patient. The meal absorption process in the stomach compartment is simulated by a filter with a constant time of 60 minutes, as proposed in the literature [3]. The hydrogel membrane is allowed to reach equilibrium at the physiological pH previous to its implantation. The hydrogel is loaded with insulin in 5% of the dry gel weight to prevent an abrupt descend of glucose level upon implantation. Moreover, the patient is assumed to have a meal after 100 min from implantation to avoid low glucose levels. The meals are programmed at 7:00, 12:00 and 17:00 hours, considering implantation at 5:20. Finally, the insulin therapeutic effect is supposed not to decrease with time and implantation conditions, and the activity of the enzymes and the hydrogel itself are preserved beyond insulin depletion.

## 10.3. Comparison References

The effect of insulin delivery from a hydrogel-based device is contrasted against the open loop response of the physiological model of the diabetic patient and the potential performance of a conventional closed loop system with an explicit controller.

The open loop response before the previously defined test offers a reference to determine when the hydrogel-based system stops being useful for blood glucose control. The glucose metabolism dynamics with the Sorensen model shows the highest glucose deviations and a slow recovery of a normal level when meal disturbances are considered. The differentiation from the open loop response indicates an advantage for the treatment system.

An explicit controller is defined to close a feedback glucose loop, since the action of the hydrogel-based system is reactive to the blood glucose concentration, i.e., no anticipation or adaptive features are considered in the conventional loop for better analogous conditions with respect to the hydrogel closed loop. The controller algorithm is proposed according to the linear quadratic regulatory problem formulation (Chapter 9), to minimize the following cost function, J:

$$J(x_1, u) = \int_0^\infty \left[ \eta x_1^2(t) + \rho u^2(t) \right] dt , \qquad\qquad (1)$$

where $x_1$ is the deviation of glucose level from the desired value, u is the insulin delivery rate, and $\eta$ and $\rho$ are positive weighting factors. The tuning parameters of the controller or weight factors in the cost function are fixed during the simulation of the closed system. The separate sensor and actuator units are considered ideal systems with negligible effect on the overall process dynamics. The controller is simulated assuming that insulin availability is not interrupted.

## 10.4. Simulation Results

A cationic gel is functionally more adequate for insulin delivery, since a decrement in pH caused by the enzymatic glucose oxidation opens the mesh and eases the liberation of the preloaded insulin. Figures 10.3 and 10.4 show the performance of a cationic hydrogel-based system. The diffusion delivery mechanism produces a decreasing release rate with time. Most of the loaded insulin is released upon exposure to glucose in physiological fluids or implantation as shown by the release profile and the first valley of glucose concentration. The insulin hydrogel-based delivery system reduces the glucose concentration relative maximums in the first days. The comparison with the open loop response (Figure 10.3) suggests that the hydrogel membrane would be effective for a three day treatment considering only the amount of insulin loaded. The preloaded drug may be limited to reduce a hypoglycemic reaction upon implantation. In a three day time frame (Figure 10.4), the hydrogel action achieves the same speed of response in the first day or series of three meals, with a significant and higher reduction of glucose levels with respect to the use of the controller. In the second day, the glucose concentration range is similar for both closed loop systems, but the slope of recovery of normoglycemia is smaller in magnitude for the hydrogel system. In the third day, the response of the hydrogel closed loop is as slow as the open loop response and the peak glucose levels are raised above the uniform peaks of the controller closed loop glucose response.

The behavior of the cationic hydrogel can be observed in Figure 10.5. The meal disturbances are reflected in the pH of the microenvironment of the hydrogel, but the produced variations are small and unable to cause an appreciable change in the volume swelling ratio. The initial interaction with the glucose containing physiological fluids dominates the volume response of the membrane over the pH changes caused by the meals. The continuous presence of glucose impedes the full range hydrogel action explored in the laboratory (Section 6.1). These observations explain the monotonous release rate profile obtained for the implanted hydrogel membrane system.

An anionic gel may be used to store insulin and allow its diffusion out to the surroundings. However, the pH dependence of the volume is expected to hinder diffusion when insulin is most needed (or glucose level is high). This disadvantage can be overcome if the contraction of the hydrogel can squeeze out enough insulin to compensate the posterior hindered diffusion at the low pH caused by glucose oxidation. The squeezing

effect is stronger with macroporous materials [4]. Macropores can be formed if the hydrogel is synthesized with excess of solvent by adjusting the pH of the reactive mixture as in the above poly(MAA-g-EG) preparation procedure. The simulation of a poly(MAA-g-EG) membrane, shown in Figure 10.6 and Figure 10.7, gives similar results for the case of a cationic gel membrane. The difference is only noticed in the early interaction causing lower glucose concentration with respect to the initial glucose response with a cationic gel (Figure 10.8). The high initial insulin release is due to both the possible squeezing delivery by the contraction of the gel [5], although discarded for the fabricated P(MAA-g-EG) (Section 6.2), and the diffusion through wide molecular openings in spite of the volume reduction (Figure 10.9). The quantitative simulation results restrict the qualitative appreciation of a hindered diffusion from the anionic membrane in the presence of gluconic acid to relative terms with respect to the diffusion from the same anionic membrane at high pH. This means that the different ranges for the volume swelling ratio of cationic and anionic membranes do not allow establishing an advantage for insulin delivery for a particular type of hydrogel under the conditions of evaluation in this study.

The observed limitation of volume changes of the hydrogel (Figures 10.5 and 10.9) corresponds to the small variations of pH due to a combination of the buffer effect of the blood and its glucose composition. The recovery of a high pH in the hydrogel after a meal implies the diffusion of hydrogen ions out of the membrane that would promote a change of pH in the peritoneum. However, such change may be damped or practically avoided by the buffer characteristic of the blood. Therefore, the hydrogen ion gradient would be fixed on the side of the physiological pH and limit the output of hydrogen ions from the hydrogel (Equation 14 in Chapter 8). The high concentration of hydrogen ions or low pH on the side of the hydrogel results from the generation of hydrogen ions by chemical dissociation of the produced gluconic acid. Even at the fasting glucose level, glucose would tend to diffuse into the gel causing a sustained production of gluconic acid that would oppose the recovery of the higher physiological pH.

The short variability of the pH input and volume swelling ratio output of a hydrogel system can be explained in terms of Donnan equilibrium. The crosslinked backbone of the polymer supports uniformly charged chemical groups that affect the local concentration of ionic species creating an electric bilayer [6]. Ionic species with the same charge of the pending groups of the polymer or co-ions are kept from entering the hydrogel because of electrostatic resistance. The exclusion of co-ions, increases the concentration of counter-ions in the hydrogel. In consequence, species with equal electrochemical potential can be present at different concentrations inside and outside of the hydrogel membrane, which explains the conservation of a local pH different from the pH of the physiological environment.

The controller output in the conventional closed loop scheme is potentially more versatile and adequate to regulate blood glucose concentration before meal disturbances, while the insulin delivery through a hydrogel system provides the benefits of a low continuous decreasing dose. The behavior of the insulin delivery determined by the mathematical controller would only be possible for the hydrogel release profile if volume changes were faster and bigger. The insulin delivery by the hydrogel membrane may be

206

considered more similar to a basal insulin supply, although there is a limited responsiveness to the particular physiological environment.

## 10.5. Conclusions

The simulation results demonstrate limitations in the range of swelling and contraction of hydrogels in a physiological environment. However, peak glucose levels are reduced and a basal insulin delivery from a hydrogel membrane system is produced in the simulation of periodic meal disturbances.

The obtained simulations results are backed with experimental evidence obtained from insulin release studies, in spite of the different scenarios. In the treatment of diabetes mellitus, the insulin release rate from the hydrogel is more effective to correct glucose levels during the first meals after implantation. The high initial release in neutral pH buffer solutions at 37°C in a dissolution apparatus is also observed and differentiated for each glucose concentration (Figure 6.5.7 in Section 6.5). The later coincidence of the experimental profiles of insulin released fractions in the different glucose concentration solutions, indicate that glucose in the delivery medium is in enough excess to maintain the same constant local pH allowing for no difference in diffusivities. This observation in the laboratory supports the pH and volume behavior with little variations in spite of the meal disturbances in the simulation.

The arguments given about the effects of the buffer physiological medium, the continuous presence of glucose and the Donnan equilibrium suggest that the discussed limitations may be present regardless of the size of the hydrogel system. Hydrogel microparticles show very low time constants [7], but the local pH variations may be restricted in magnitude as in the membrane systems. Limitations of hydrogel monolithic systems or membranes for continuous blood glucose regulation may be overcome by hydrogel based devices. Hydrogels may be used in composite systems for a more effective insulin delivery [8, 9].

The comparison of closed loop systems based on a single smart material device and on a traditional scheme of a device per function serves the purpose of setting a reference for the discussion of hydrogel-based systems and alternatives of diabetes treatment. The short range of actuation of the hydrogel due to the small changes in the local pH limits the dynamic performance of a hydrogel membrane in comparison with a controller closed loop system. Nevertheless, both closed loop systems share issues regarding insulin availability and effectiveness. The higher level of integration offered by a hydrogel based system is potentially more advantageous for implantation and, ultimately, for the comfort of the patient.
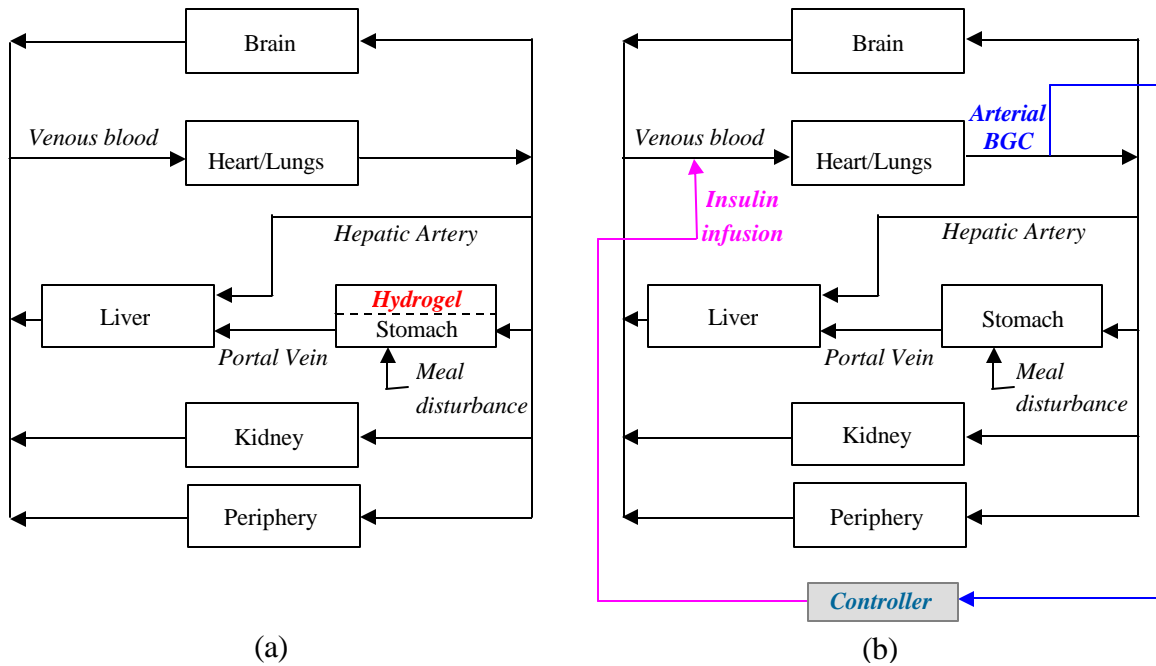
**Figure 10.1. Feedback Control Systems.** Two systems are proposed for the closed loop treatment of diabetes: using a hydrogel system (a) and an optimal controller (b). The Sorensen model is used for the representation of the glucose-insulin metabolism of the diabetic patient.
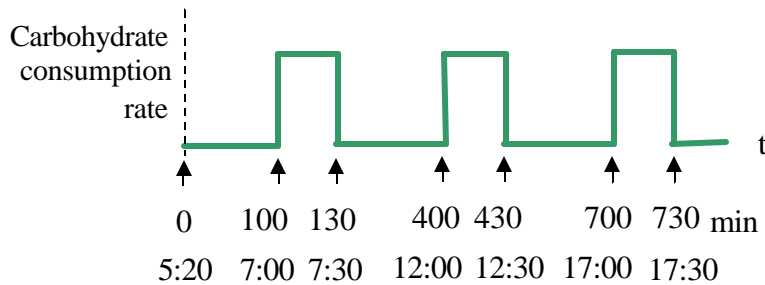


**Figure 10.2. Simulation test.** The hydrogel is implanted at time zero. A meal is represented by a pulse with duration of 30 min and area proportional to the consumption of 66 g of carbohydrates. Three daily meals are simulated.

**Figure 10.3. Cationic Hydrogel and Open Loop Performances.** The open loop response (dotted line) is obtained without insulin administration. The insulin delivery (monotonous decreasing curve) from the cationic hydrogel produces a better glucose response (oscillatory continuous line) in the first three days.



**Figure 10.4.  Cationic Hydrogel, Controller and Open Loop Performances.** The glucose level response for the hydrogel based system (continuous line), the controller based system (dashed line) and the open loop system (dotted line) are shown in the range from 80 to 300 mg/dL.  The insulin delivery profiles from the hydrogel (continuous line) and the controller (dashed line) are shown in the range from 0 to 25 mU/min.

**Figure 10.5. Volume Swelling Ratio and pH of Implanted Cationic Hydrogel Membrane System.** The volume swelling ratio, Q, increases form the pre-equilibrium value of 1.5. The initial descend in pH occurs upon implantation of the hydrogel and the oscillations correspond to the effect of the meals.
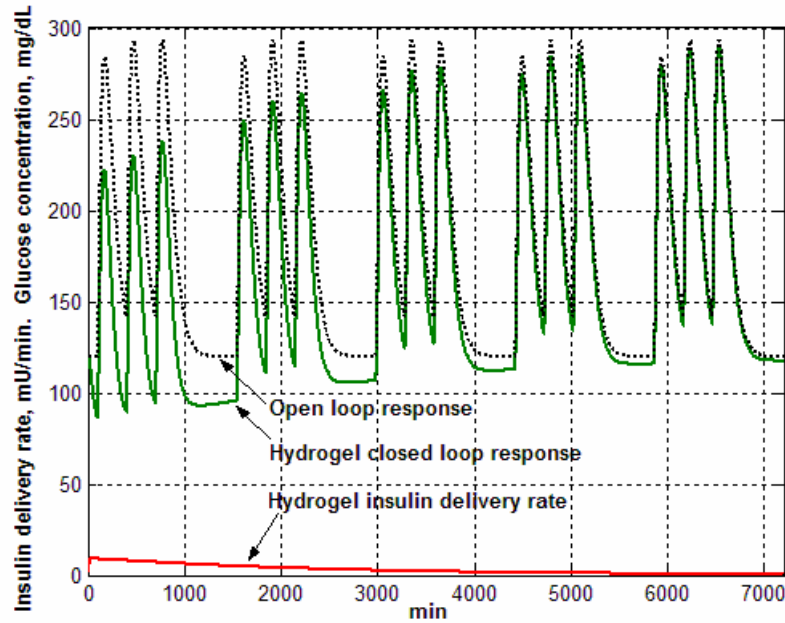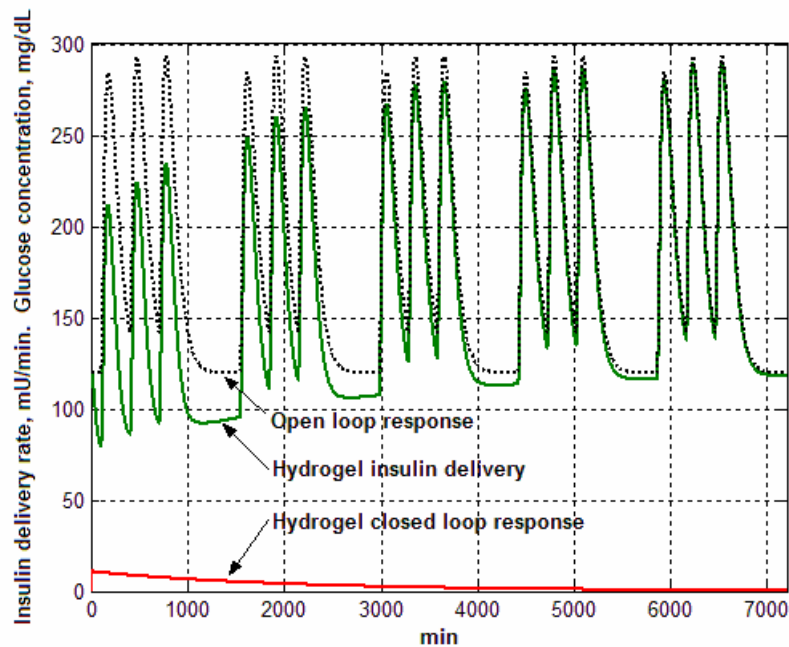


**Figure 10.6. Anionic Hydrogel and Open Loop Performances.** The open loop response (dotted line) is obtained without insulin administration. The insulin delivery (monotonous decreasing curve) from the anionic hydrogel produces a better glucose response (oscillatory continuous line) in the first three days.
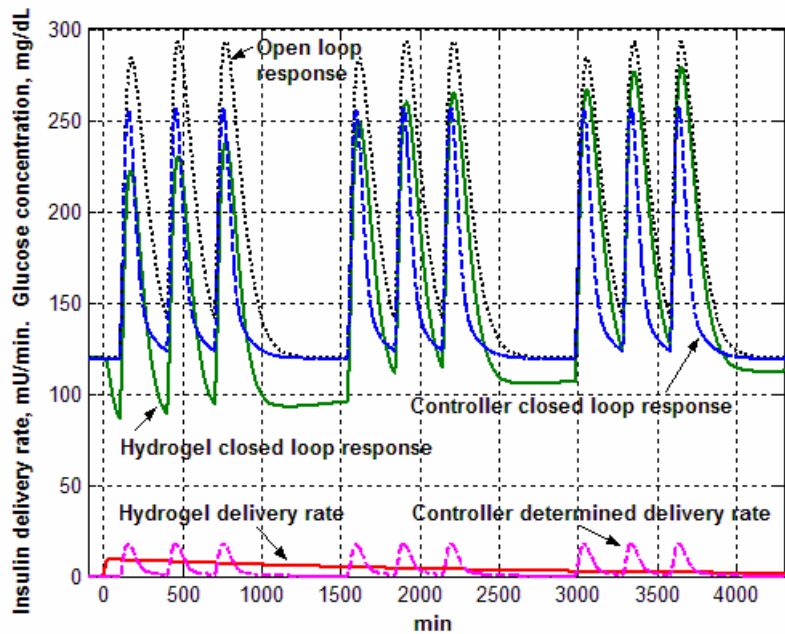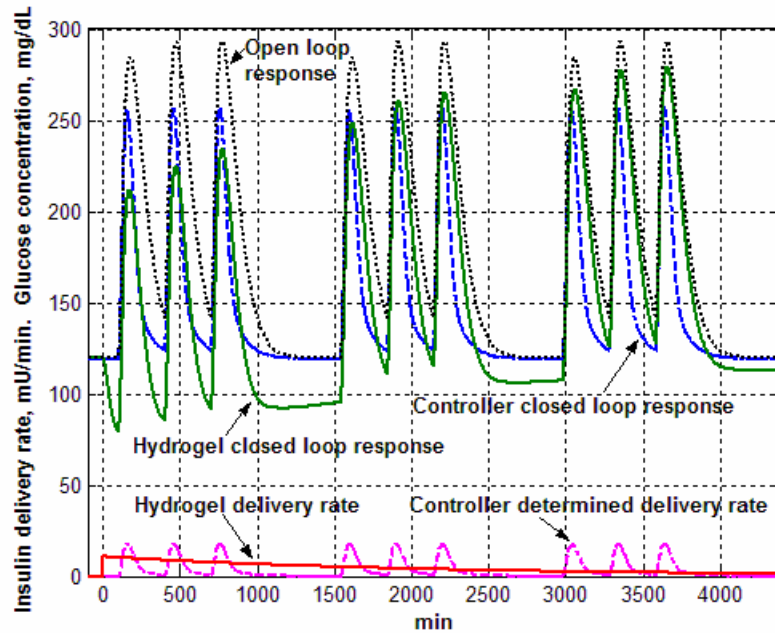
**Figure 10.7. Anionic Hydrogel, Controller and Open Loop Performances.** The glucose level response for the hydrogel based system (continuous line), the controller based system (dashed line) and the open loop system (dotted line) are shown in the range from 80 to 300 mg/dL. The insulin delivery profiles from the hydrogel (continuous line) and the controller (dashed line) are shown in the range from 0 to 25 mU/min.
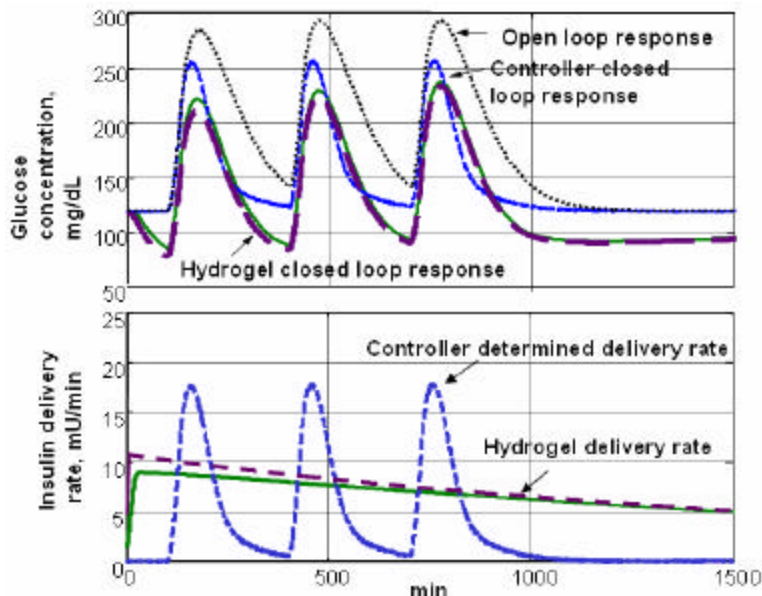


**Figure 10.8. Comparison of Cationic and Anionic Hydrogel Based Systems.** The glucose concentration curves with both types of hydrogels overlap, except for the duration of the first meal, when the glucose level reaches the lowest value (dashed line) since more insulin is delivered from the anionic gel (monotonous dashed curve).
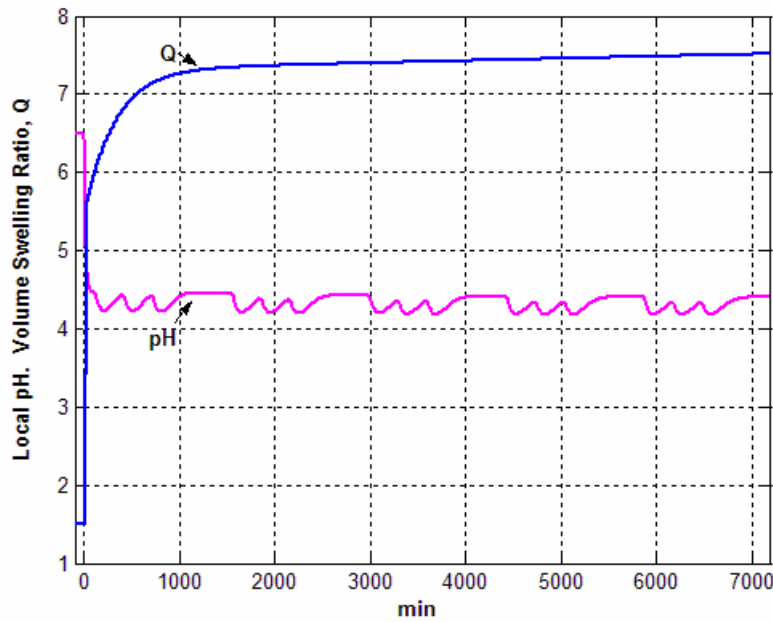
211
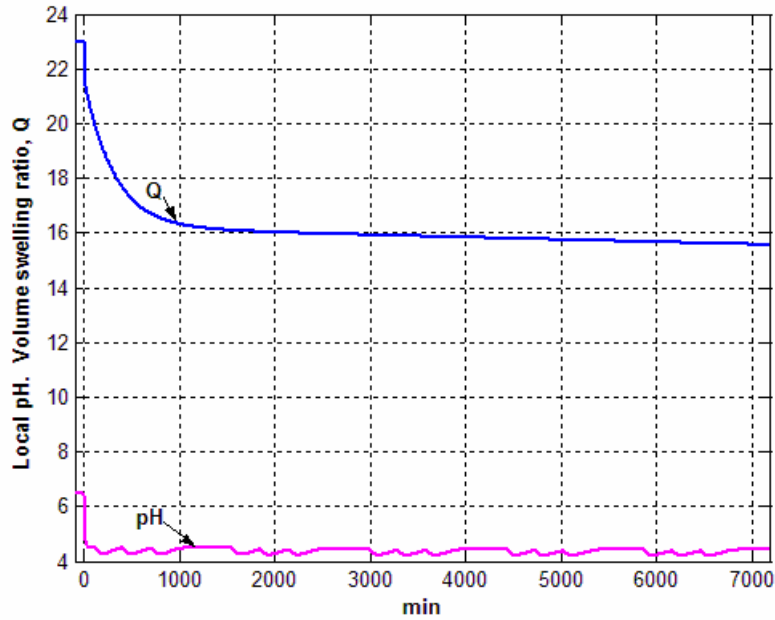
**Figure 10.9. Volume Swelling Ratio and pH of Implanted Anionic Hydrogel Membrane System.** The volume swelling ratio, Q, decreases form the pre-equilibrium value of 23. The initial descend in pH occurs upon implantation of the hydrogel and the oscillations correspond to the effect of the meals.

## References

1. Sorensen J. A physiologic model of glucose metabolism in man and its use to design and assess improved insulin therapies for diabetes. PhD thesis. Dept. of Chemical Engineering, MIT, 1985.

2. Whitney E, Rolfes SR. Understanding nutrition ($10^{th}$ edition), Belmont, CA: West Group, 2005.

3. Parker R, Doyle III F, Peppas NA. Model-based algorithm for blood glucose control in type I diabetic patients. IEEE T Bio-Med Eng. 1999;46(2):148-157.

4. Pradny M, Lesny P, Fiala J, Vacik J, Slouf M, Michalek J, Sykova E. Macroporous hydrogels based on 2-hydroxyethyl methacrylate with methacrylic acid. Collect Czech Chem C. 2003;68:812-822.

5. Huang X, Brazel CS. On the importance and mechanisms of burst release in matrix-controlled drug delivery systems. J Control Release. 2001;73:121-136.

6. Webster J. Medical instrumentation: application and design ($3^{rd}$ edition), New York: John Wiley & Sons, Inc., 1998.

7. Podual K, Doyle III FJ, Peppas NA. Dynamic behavior of glucose oxidase-containing microparticles of poly(ethylene glycol)-grafted cationic hydrogels in an environment of changing pH. Biomaterials. 2000;21:1439-1450.

8. Gutowska A, Bark J S, Kwon IC, Bae YH, Cha Y. Squeezing hydrogels for controlled oral drug delivery. J Control Release. 1997;48:141-148.

9. Shin Y, Chang JH, Liu J, Williford R, Shin YK, Exarhos GJ. Hybrid nanogels for sustainable positive thermosensitive drug release. J Control Release. 2001;73:1-6.

## 11. Conclusions

In this work, the evaluation of the potential of hydrogel implantable closed loop insulin delivery systems highlights some limitations linked to the particular characteristics of the synthesis of the hydrogel material, as well as to general conditions of the application context. This chapter concludes about the proposed objectives, the contributions of the thesis and future work on feedback systems for medical treatments.

## 11.1. Fulfillment of objectives

Regarding the hydrogel synthesis, characterization and simulation objectives (Chapter 3), the following conclusions were obtained.

The excess of solvent, produced by pH adjustments of the reactive mixture for the synthesis of hydrogels, has a clearer effect on the mesh size of the resultant material than the variation of the length of the crosslinking agent with the same molar concentration or the discrete presence of enzymes (Chapter 4). This result was obtained mathematically and corroborated by the porosimetry study of dry samples (Chapter 5). The mesh size at a neutral pH was in average 12 times the hydrodynamic diameter of insulin (Chapter 4) which explains the similarity among the release profiles obtained.

The equilibrium volume response to the environmental pH shows a transition or critical point at a low pH of 5.6, which determines smaller volume variations at the physiological pH (Chapter 5). The displacement of the critical pH to a higher value could help to obtain effective volume variations before the damped pH changes caused by meal disturbances in physiological fluids.

The syneresis of the fabricated hydrogels did not cause the formation of macropores that could produce a squeezing delivery effect. Therefore, the release mechanism was mainly diffusion. This conclusion led to an apparent inconsistency between the operation of anionic hydrogels and their application as insulin delivery systems for diabetes treatment (Chapter 6).

Other transport and reaction parameters were obtained. Mechanisms of enzymatic reactions justified their incorporation as sensing mechanism in the hydrogel membranes. The overall reaction system was represented with a first order kinetics. Diffusion coefficients were obtained by the Stokes equation, which is particularly convenient for the small glucose molecules and hydrogen ions (Chapter 6).

The time-pH superposition technique and the required experimentation were proposed for the calculation of the fundamental mechanochemical compliance defined in the direction of tensile elongation and produced stress forces. The simulation of the volume behavior of a hydrogel system using operation zone dependent relaxation times and three-dimensional mechanochemical compliances reproduced better the real behavior than the use of a one-dimensional mechanochemical compliance function with the Boltzmann superposition principle (Chapter 7).

A multiple-compartment model is used as the representation of diabetic metabolism. However, the controller calculations require a linear and low order representation in order to obtain a numerical solution for the optimization control problem (Chapter 9). On the other hand, the hydrogel at a particular implantation site can be incorporated in the detailed multiple-compartment model. The hydrogel compartment is defined by mass balances for glucose, insulin and hydrogen ions and a closed loop model for the non-linear swelling behavior (Chapter 8).

Servocontrol and regulatory control laws or algorithms were first evaluated with the one-compartment model in order to make a selection of the design approach to apply with the high order non-linear physiological model. The regulatory approach showed higher robustness and lower risk of hypoglycemia. Flexibility is introduced to the control law by proposing the weighting factors in the cost function as tuning parameters that can be adjusted to balance the velocity of the controller and the risk of hypoglycemia.(Chapter 9).

Both controller and hydrogel closed loop treatment systems are simulated before a hyperglycemic condition (Chapters 8 and 9) and before periodic meal disturbances (Chapter 10). The anionic hydrogel gave a similar effect than the cationic in spite of the apparent disadvantage with respect to cationic hydrogels. The hydrogel produced a monotonous release profile that would reduce the induction of hypoglycemic events and could perform as a source of basal insulin. The controller showed a release profile with opportune and rapid variations to correct the effect of meal disturbances; however, after an initial fast elevation followed a relatively slow monotonous decrease. The limited performance of the hydrogel-based system with respect to the use of the controller is explained by the glucose composition of the blood and saturation of the enzymatic system, the buffer effect of physiological fluids and the Donnan equilibrium unequal distribution of hydrogen ions that impede the recovery of a neutral pH after the exposure to high glucose concentrations (Chapter 10).

The proposed simulations responded to the stated hypothesis (Chapter 3) by identifying advantages and limitations of hydrogel-based systems with respect to the use of controller algorithms as treatment options. The shown advantage of the integration of sensor, controller and actuator functions is added to the biocompatibility and enhanced protein activity attributed to pegylated hydrogels. The limitations refer to the shown restricted volume changes of hydrogel structures in the physiological medium.

The mesh size of the hydrogel material needs to show variations around the size of insulin at a physiological pH in order to produce a flexible delivery profile similar to the one obtained with the optimal controller. More synthesis specifications can affect the mesh size, such as the type of functional groups as well as the molar concentration of the monomer in order to obtain a more effective molecular valve. Improvements regarding the simulation work may include the analysis of exercise disturbances and more flexible dietary regimens.

## 11.2. Contributions

The main contribution of this thesis work is the study of the performance of hydrogel-based systems for the closed loop control of glucose levels to restitute this lost or diminished natural regulation function. The simulation of hydrogel-closed loop diabetes treatment considered a theoretical model with parameters obtained from experimentation. The evaluation and explanation of the results point out limitations of hydrogels and their causes.

In the development of this thesis, several products were obtained. These products are the following: contributions to the synthesis of hydrogels, through the study of the effects of fabrication conditions such as the pH of the reactive mixture and length of crosslinking agent; the extension of the time-temperature superposition technique for the obtention of a time function for the one-dimensional mechanochemical compliance; the characterization of a three-dimensional mechanochemical compliance, that allows for the simulation of the time response of the hydrogel material; an integral model for hydrogels, that incorporates the different functionalities of this type of smart materials in a physiological context, and that is supported by the analysis of experimental *in vitro* data; the evaluation of servocontrol and regulatory schemes in the design of the optimal controller (LQRP); the Donnan equilibrium effect as a resistance for reversible volume changes of hydrogels; a critical evaluation of the potential of hydrogels in a continuous closed-loop application as an implantable insulin delivery system.

The obtained results from experimentation and simulation allowed the evaluation of the performance of hydrogel-based systems in the context of the diabetes disease. The fabricated hydrogels and the experimental and simulation methods of this thesis allowed the demonstration of the potential of a basal insulin delivery and its duration for the closed loop treatment of diabetes. The assumptions behind the presented results make them a reference for the maximum therapeutic effectiveness that can be expected from these materials, although they could be redesigned for an active regulation. The observed limitations of the swelling and contracting behavior are valid regardless of the regimen of the process: continuous in the simulation work by considering the circulation of the blood, and batch in the *in vitro* laboratory experiments where closed dissolution systems (with no input nor output flows) with a specific glucose concentration constituted the release medium.

## 11.3. Future Work and Final Comments

The continuation of this work may focus on different aspects. The following are related to the experimental basis of the research. Further studies can be done regarding the impact of the variation of synthesis parameters on the equilibrium and dynamic properties of the reference material of this investigation. Hydrogel materials with temperature and glucose sensitivity can be suggested from the possibility to couple the energy produced by the enzymatic reaction of glucose to the modulation of molecular openings and drug delivery. Their potential for diabetes closed loop treatment could be studied with the guidelines proposed by the development of this work.

Other suggestions can be made for the continuation of the simulation work. The Sorensen physiological model can be used to investigate the effect of the implantation site on the closed loop performance of hydrogel-based systems; for instance, a subcutaneous hydrogel membrane implant could be compared against the implant at the peritoneum considered in the simulation work of this dissertation. The simulation of the mathematical controller-closed loop system used as a comparison reference can be enriched by the incorporation of the models of the sensor and the actuator, even when their dynamic response must not dominate over the one of the physiological process in order to be a useful reference for the evaluation of alternative hydrogel-closed loop systems for diabetes treatment. The application of stability analysis techniques in the proposed closed loop systems for medical treatment can generate valuable information about critical physiological conditions through the prediction of unacceptable variations in particular parameters.

Practical limitations arise regarding the implementation of the closed loop system. The system relies on a continuous meter of glucose levels and an analogous insulin pump. Although both types of devices have been studied and developed, their continuous operation still has to be improved for a smooth functioning, according to the general perception shared at recent scientific conventions (Diabetes Technology Meeting 2006) [1]. The models of a glucose sensor and an actuator to deliver insulin should be considered specifically for an evaluation of the closed loop treatment from the perspective of the comfort of the patient, as well as from the dynamics point of view in future work.

In addition to the instrumentation challenges, unavailable measurements and the complexity of physiological processes demand reliable state estimation which needs noise management and on line identification. Further investigation could be oriented to the use of unscented particle filters for nonlinear processes to improve blood insulin state estimation [2]. The tests for the closed control system should include the regulation during prolonged disturbances, such as exercising, which may require the extension of the physiologic model for simulation analysis.

Continuous feedback control systems for disease treatment are potentially bloodless, painless and more precise therapies. The successful application of explicit controller algorithms in biomedicine requires the development of microsystems with reliable sensors and actuators and embedded control algorithms. Modeling and computer simulation assist the integration of sensing, actuating and controlling components and the evaluation of their interaction with the process or medical situation. This supports the need of interdisciplinary collaboration for research and development of biomedical systems.

Even when hydrogels potentially allow high levels of integration, hydrogels are a suitable option for the development of individual sensor and actuator devices. Hydrogels may be synergically used in integral or multifunctional systems where other types of materials and other physical principles are combined to fit a particular application.

The evaluation of hydrogel macrosystems prompts the consideration of the detected pros and contras in hydrogel microsystems potentially injectable [3] for closed loop treatment. The benefits of biocompatibility and the therapeutic effect of continuous and

potentially reduced drug delivery [4] must be balanced against problems such as drug replenishment, implant replacement (in case of drug depletion as well as degradation or elimination of the system by the body), preservation of therapeutic activity, and functional limitations due to the continuous exposure to physiological medium with a buffer effect and a non-zero glucose concentration, and the tendency to equilibrium with unequal concentrations of ionic permeable species inside and outside the hydrogel.

In spite of the emphasis on science application for the treatment of diabetes in the present work, prevention systems are most convenient to face the diabetes epidemic. From this perspective, engineering beside educational sciences are also required.

**References**

1.  Diabetes Technology Meeting (2006). Sixth Annual Meeting. Chair D. Klonoff. Atlanta, GA.

2.  Morales-Menéndez R, Mutch J, de Freitas N,  Poole D, Guedea-Elizalde F. Dynamic modelling and control of industrial processes with particle filtering algorithms. ESCAPE-14. Barbosa-Póvoa, Matos H, editors. Lisbon Portugal. 2004: 721-726.

3.  Farmer T, Peppas NA, Edgar T.  Design of a polymeric insulin infusion system for blood glucose control. Proceed Amer Control Conf. 2007;(1):607-612.

4.  DeWitt DE, Hirsch IB. Outpatient Insulin Therapy in Type 1 and Type 2 Diabetes Mellitus. JAMA. 2003;289(17):2254-2264.

**Bibliography**

Accu Chek. http://www.accu-chek.es/es_ES/image/insulin_pump_sensor_system.gif as seen on 12/13/07.

Ackerman E, Gatewood L, Rosevear JW, Molnar GD. Model studies of blood-glucose regulation. Bull Mathem Biophys. 1965;27:21-38.

Ahmed A, Bonner C, Desai TA. Bioadhesive microdevices for drug delivery: a feasibility study. Microdev. 2001;3:89-95.

Aklonis JJ, MacKnight WJ. Introduction to polymer viscoelasticity ($2^{nd}$ edition). New York: John Wiley & Sons, Inc., 1983.

Albin GW, Horbett TA, Miller SR, Ricker NL. Theoretical and experimental studies of glucose sensitive membranes. J. Controlled Release. 1987;6:267-291.

Albisser AM, Leibel BS, Ewart TG, Davidovac Z, Botz CK, Zingg W. An Artificial endocrine pancreas. Diabetes. 1974;23:389-396.

American Diabetes Association. http://www.diabetes.org/diabetes-statistics.jsp (as seen on June 18, 2007).

AutoPore III 9420 Analyzer Operator's Manual v1.01. Micromeritics, Inc. 1996.

Baker R W, Lonsdale H K. Controlled release: mechanisms and rates. In Controlled Release of Biologically Active Agents, Tanquary A C, Lacey R E (eds.). Plenum Press, New York,1974, pp. 15-71.

Barbieri R, Quaglia M, Delfini M, Brosio, E. Investigation of water dynamic behaviour in poly(HEMA) and poly(HEMA-co-DHPMA) hydrogels by proton $T_2$ relaxation time and self-diffusion coefficient n.m.r, measurements. Polymer. 1998;39(5):1059-1066.

Barceló A, Aedo C, Rajpathak S, Robles S. The cost of diabetes in Latin America and the Caribbean. Bulletin of the World Health Organization 2003;81(1):19-27.

Barceló A, Vovides Y. The Pan American Health Organization and World Diabetes Day. Pan Am J Public Health. 2001;10(5):297-298.

Barton AFM. CRC handbook of polymer-solvent interaction parameters ($1^{st}$ edition). Ann Arbor, MI: CRC Press, 1990.

Bell CL, Peppas NA. Water, Solute and Protein Diffusion in Physiologically-Responsive Hydrogels of Poly(methacrylic acid-g-ethylene glycol). Biomaterials. 1996;17:1203-1218.

Bellazi R, Nucci G, Cobelli C.  The subcutaneous route to insulin-dependent diabetes therapy.  IEEE Eng Med Biol. 2001;20(1):54-64.

Benard WL, Kahn H, Heuer AH, Huff MA. A titanium-nickel shape-memory alloy actuated micropump. Internacional Conference on  Transducers, Solid-State Sensors, Actuators and Microsystems. 1997;1:361-364.

Bequette BW. A critical assessment of algorithms and challenges in the development of a closed-loop artificial pancreas. Diabetes Technology and Therapeutics. 2005;**7:**28-47.

Bergman RN, Phillips LS, Cobelli C. Physiologic evaluation of factors controlling glucose tolerance in man. J Clin Invest. 1981;68:1456-1467.

Bhandare P, Stohr E, Mendelson Y, Perua  RA. IR spectrophotometric measurement of glucose in phosphate buffered saline solutions: effects of temperature and pH. Proceedings of the 1992 Eighteenth IEEE Annual Northeast Bioengineering Conference. 1992:103-104.

Bode BW, Sabbah HT, Gross TM, Fredrickson LP, Davidson PC. Diabetes management in the new millennium using insulin pump therapy. Diabetes Metab Res Rev. 2002;18(1):14-20.

Boon EM, Downs A, Marcey D.   Catalase Structural Tutorial Text. http://www.callutheran.edu/Academic_Programs/Departments/BioDev/omm/catalase/cat1.htm  (as seen on November 14, 2007).

Brandrup J, Immergut EH. Polymer handbook (3rd edition).  New York: John Wiley & Sons, Inc., 1989.

Brannon-Peppas L. Biomaterials-Polymers in Controlled Drug Delivery. Polymers in Controlled Drug Delivery (MPB archive, Nov 97). http://www.devicelink.com/mpb/archive/97/11/003.html.

Brannon-Peppas L, Peppas N. Time-dependent response of ionic polymer networks to pH and ionic strength changes. Int J Pharm, 1991;70:53-57.

Bryant SJ, Nuttelman CR, Anseth KS. Cytocompatibility of UV and visible light photoinitiating systems on cultured NIH/3T3 fibroblasts. J Biomat Sci.-Polym E. 2000;11:439-457.

Cardosi, M.   http://www-biol.paisley.ac.uk/ (Chemscape Chime plug in by MDL Information Systems, Inc.) (as seen on November 16, 2007)

Chakrabarti S,  Sahu J, Biswas A, Acharya HN. Relationship between weight loss and shrinkage during gel drying. J Mater Sci Letters. 1992;11:763-766.

Chee F, Fernando T, van Heeden P. Expert PID control system for blood glucose control in critically ill patients. IEEE T Info Technol B. 2003;7(4):419-425.

Clemens AH. Feedback control dynamics for glucose controlled insulin infusion systems. Med. Prog. Technol. 1979;6:91-98.

Connolly P, Cotton C, Morin F. Opportunities at the skin interface for continuous patient monitoring: a development model based on lactate and glucose. Proceedings of the IEEE-EMBS Special Topic Conference on Molecular, Cellular and Tissue Engineering. 2002:50 – 51.

Coughanowr DR. Process systems analysis and control (2nd edition). Boston: McGraw-Hill, 1991.

Damiano E. Closed-loop blood-glucose control using dual subcutaneous infusion of insulin and glucagons in vivo. Diabetes Technology Meeting 2006, Atlanta, Georgia: S12.

Davidson III R. Peppas N. Solute and penetrant diffusion in swellable polymers. J Controlled Release. 1986;3:243-258.

DeWitt DE, Hirsch IB. Outpatient Insulin Therapy in Type 1 and Type 2 Diabetes Mellitus. JAMA. 2003;289(17):2254-2264.

Diabetes Atlas, third edition ©International Diabetes Federation 2006.

Diabetes Technology Meeting (2006). Sixth Annual Meeting. Chair D. Klonoff. Atlanta, GA.

Donsmark M. Physiological Aspects and Pharmacology of Commercial Glucagon preparations. Diabetes Technology Meeting 2006, Atlanta, Georgia: S14.

Dowling NE. Mechanical behavior of materials: engineering methods for deformation, fracture and fatigue. Upper Saddle River, NJ: Pearson Prentice Hall, 2007.

Dudde R, Vering T. Advanced insulin infusion using a control loop (ADICOL) concept and realization of a control-loop application for the automated delivery of insulin. 4th International IEEE EMBS Special Topic Conf. on Info. Tech. App. in Biomed. 2003:280-282.

Farmer T, Peppas NA, Edgar T. Design of a polymeric insulin infusion system for blood glucose control. Proceed Amer Control Conf. 2007;(1):607-612.

Fisher ME. A semiclosed-loop algorithm for the control of blood glucose levels in diabetics. IEEE Trans. Biomed. Eng. 1991;38:57-61.

Franciosi M, Pellegrini F, De Berardis G. The impact of blood glucose self-monitoring on metabolic control and quality of life in type 2 diabetic patients. Diabetes Care. 2001;24:1870-1877.

Furler SM, Kraegen EW, Smallwood RH, Chisolm DJ. Blood glucose control by intermittent loop closure in the basal mode: computer simulation studies with a diabetic model. Diabetes Care. 1985;8:553-561.

Grayson ACR, Shawgo RS, Johnson AM, Flynn NT, Yawen LI, Cima MJ, Langer R. A BioMEMS review: MEMS technology for physiologically integrated devices. Proceedings of the IEEE. 2004;92(1):6-21.

Gregory CM. Fabrication methods for integrated biosensors. IEE Colloquium on Advances in Sensors. 1995:10/1-10/5.

Gutowska A, Bark J S, Kwon IC, Bae YH, Cha Y. Squeezing hydrogels for controlled oral drug delivery. J Controlled Release. 1997;48:141-148.

Harsanyi T, Santha H. Polytronics for biotronics: unique possibilities of polymers in biosensors and bioMEMS? Polymers and Adhesives in Microelectronics and Photonics. 2nd International IEEE Conference. 2002:211-215.

Hasselblatt A, Bruchhausen F, eds. Handbook of experimental pharmacology. Heffler-Heubner New Series XXXII/2 (Altzuler). Springer Verlag New York 1975

Haykin S. Adaptive filter theory (4th edition). New Jersey: Prentice Hall, 2001.

Heller A. Integrated medical feedback systems for drug delivery. AIChE J. 2005;51(4):1054-1066.

Heller J, Hoffman A. Drug delivery Sistems in Chapter 7 Application of Materials in Medicine, Biology and Artificail Organs. Biomaterials Science, 2nd edition, Ratner B D, Hoffman A S, Schoen F J, Lemons J E, eds. Elsevier Academic Press, San Diego, 2004, 628-648.

Henry S, McAllister DV, Allen MG, Prausnitz MR. Microfabricated microneedles: a novel approach to transdermal drug delivery. J. Pharm. Sci. 1998;87:922–925.

Hilt JZ, Gupta AK, Bashir R, Peppas NA. Ultrasensitive BioMEMS sensors based on microcantilevers patterned with environmentally responsive hydrogels. Biomed Microdev. 2003;5(3):177-184.

Hilt JZ, Gupta AK, Bashir R, Peppas NA. A bioMEMS sensor platform based on a cantilever with a precisely patterned environmentally sensitive hydrogel. EMBS/BMES Conference Proceedings. 2002;2:1650–1651.

Hoffman AS. Applications of smart polymers as biomaterials. In: Ratner BD, Hoffman AS, Schoen FJ, Lemons JE. Biomaterials Science (2$^{nd}$ edition). California: Elsevier Academic Press, 2004:107-115.

Huang X, Brazel CS. On the importance and mechanisms of burst release in matrix-controlled drug delivery systems. J Controlled Release. 2001;73:121-136.

Hyams D. CurveExpert Version 1.37 Copyright C 1995-2001.

Jones P, Suggett A. The cata-ase-hydrogen peroxide system. A theoretical appraisal of the mechanism of catalase action. Biochem J. 1968:110(4):621-629.

Kaiser N. Laser absorption spectroscopy with an ATRprism-noninvasive in vivo determination of glucose. In: Hepp KD. Feedback-controlled and preprogrammed insulin infusion in diabetes mellitus. New York: Thieme Verlag, 1979:30-33.

Khoo M, Liu C. A novel micromachined magnetic membrane microfluid pump. Proceedings of the 22nd Annual Internacional Conference on the IEEE Engineering in Medicine and Biology Society. 2000;3:2394-2397.

Kikuchi M, Machiyama N, Kabei N, Yamada A, Sakurai Y. Homeostat to control blood glucose level. Int Symp Med Inf Syst. 1978:541-545.

Kima B, Peppas NA. Analysis of molecular interactions in poly(methacrylic acid-g-ethylene glycol) hydrogels. Polymer. 2003;44: 3701–3707.

Lane AM. Interpretation of Mercury Porosimetry Data (catalysis, morphology, pores). University of Massachusetts Amherst, 1984.

Langer R S, Peppas N A. (1983). Chemical and physical structure of polymers as carriers for controlled release of bioactive agents: a review. Rev. Macromol. Chem Phys. C23:61-126.

Lehninger, A. 1975. Biochemistry: the molecular basis of cell structure and function. Worth Publishers, Inc. New York.

Lentner C (editor). Geigy scientific tables (8th, rev. and enl. ed.). Basle, Switzerland: Ciba-Geigy. 1981;278-283.

Lewandowsky JJ. Amperometric glucose sensor: short-term, in-vivo test, Diabetes Care. 1982;5(3):238-244.

Lin Y, Lu F, Tu Y, Ren Z. Glucose biosensors based on carbon nanotube nanoelectrode ensembles. Nano Letters. 2004;4(2):191-195.

Lowman AM, Dziubla TD, Bures P, Peppas NA. Structural and dynamic response of neutral and intelligent networks in biomedical environments. In: Peppas NA, Sefton

223

MV. Molecular and Cellular Foundations of Biomaterials. New York: Elsevier Academic Press, 2004;29:75-130.

Lowman AM, Morishita M, Kajita M, Nagai T, Peppas NA. Oral delivery of insulin using pH-responsive complexation gels. J Pharm Sci. 1999;88:933-937.

Lowman AM, Peppas NA. Analysis of the complexation/decomplexation phenomena in graft copolymer networks. Macromolecules. 1997;30:4959-4965.

Lowman AM, Peppas NA. Analysis of the complexation/decomplexation phenomena in graft copolymer networks. Macromolecules. 1997;30:4959-4965.

Lowman AM, Peppas NA. Solute transport analysis in pH-responsive, complexing hydrogels of poly(methacrylic acid-g-ethylene glycol). J Biomater Sci Polymer Edn. 1999;10(9):999-1009.

Lowman AM and Peppas NA, Solute transport analysis in pH-responsive, complexing hydrogels of poly(methacrylic acid-g-ethylene glycol). J Biomater Sci, Polym Ed. 1999;10:999-1009.

Lynch SM, Bequette BW. Estimation-based model predictive control of blood glucose in type I diabetics: a simulation study. Proceedings of the IEEE 27th Annual Northeastern Bioengineering Conference, Storrs, CT. 2001:79-80.

Madou M, Morrison SR. Chemical Sensing with Solid State Devices. Academic Press, Inc. 1988.

Maillefer D, Van Lintel H, Rey-Mermet G, Hirschi R. A high-performance silicon micropump for an implantable drug delivery system. IEEE International Conference on Micro Electro Mechanical Systems. 1999: 541-546.

Morales-Menéndez R, Mutch J, de Freitas N, Poole D, Guedea-Elizalde F. Dynamic modelling and control of industrial processes with particle filtering algorithms. ESCAPE-14. Barbosa-Póvoa, Matos H, editors. Lisbon Portugal. 2004: 721-726.

Moussy, F. Implantable glucose sensor: progress and problems. Proceedings of IEEE Sensors. 2002;1:12-14.

Naidu D. Optimal Control Systems. Boca Raton: CRC Press, 2003.

Odian G. Principles of polymerization (3rd edition). New York: John Wiley and Sons, Inc., 2004.

Ollerton RL. Application of optimal control theory to diabetes mellitus. Int J Control. 1989;50:2503-2522.

O'Malley J, Weaver J. Subunit structure of glucose oxidase from Aspergillus niger. Biochem. 1972;11:3527

Parker R, Doyle III FJ, Peppas NA. The intravenous route to blood glucose control. IEEE Eng Med Biol. 2001;20(1):65-73.

Parker R, Doyle III FJ, Peppas NA. Model-based algorithm for blood glucose control in type I diabetic patients. IEEE T Bio-Med Eng. 1999;46(2):148-157.

Parker RS, Doyle III FJ, Ward JH, Peppas NA. Robust $H_8$ glucose control in diabetes using a physiological model. AIChE J. 2000;46:2537-2549.

Peppas NA, Barr-Howell BD. Characterization of crosslinked structure of hydrogels. In: Peppas NA. Hydrogels in medicine and pharmacy. Boca Raton: CRC Press, 1986;1:28-55.

Peppas NA, Bures P, Leobandung W, Ichikawa H. Hydrogels in pharmaceutical formulations. Eur J Pharm Biopharm. 2000;50:27-46.

Peppas NA, Hydrogels. In Biomaterials Science. Ratner, BD, Hoffman AS, Schoen FJ, Lemons JE, Eds. Academic Press, NY. 2004:100-107.

Peppas NA, Kavimandan NJ. Nanoscale analysis of protein and peptide absorption: Insulin absorption using complexation and pH-sensitive hydrogels as delivery vehicles. Eur J Pharm Sci. 2006;29:183–197.

Peppas NA, Keys KB, Torres-Lugo M, Lowman A. Poly(ethylene glycol)-containing hydrogels in drug delivery. J Controlled Release. 1999;62:81–87.

Peppas NA, Klier J. Controlled release by using poly(methacrylic acid-g-ethylene glycol) hydrogels. J Controlled Release. 1991;(16):203-214.

Peppas NA, Wood KM, Blanchette J. Hydrogels for oral delivery of therapeutic proteins. Expert Opin Biol Ther. 2004;4(6):881-887.

Peppas NA. Is there a future in glucose-sensitive, responsive insulin delivery systems? J Drug Del Sci Tech. 2004;14(4):247-256.

Pereira C, Oliveira J, Silva R, Silva F. Amperometric glucose biosensor based on assited ion transfer through gel-supported microinterfaces. Anal. Chem. 2004;76:5547-5551.

Perry RH, Green DW, Maloney JO. Perry's Chemical Engineers' Handbook (6th edition). New York: McGraw Hill, 1984.

Peterson JI. A miniature pH sensor potentially suitable for glucose measurements. Diabetes Care. 1982;5(3):272-274.

Peura RA. Blood glucose biosensors - A review. IEEE Cast Studies in Medical Instrument Design. 1991:51 – 64.

Pillarella MR, Zydney AL. Theoretical analysis of the effect of convective flow on solute transport and insulin release in a hollow fiber bioartificial pancreas. J Biomech Eng-T ASME. 1990;112:220-228.

Podual K, Dolye FJ III, Peppas NA. Insulin release from pH sensitve cationic hydrogels. Proceed Intern Symp Control Rel Biact Mater. 1998;25:56-57.

Podual K, Doyle FJ III, Peppas NA. Preparation and dynamic response of cationic copolymer hydrogels containing glucose oxidase. Polymer. 2000;41:3975-3983.

Podual K, Doyle III FJ, Peppas NA. Dynamic behavior of glucose oxidase-containing microparticles of poly(ethylene glycol)-grafted cationic hydrogels in an environment of changing pH. Biomaterials. 2000;21:1439-1450.

Podual K, Doyle III FJ, Peppas NA. Glucose-sensitivity of glucose oxidase-containing cationic copolymer hydrogels having poly(ethylene glycol) grafts. J Controlled Release. 2000; 67:9-17.

Podual K, Peppas N. Relaxational behavior and swelling-pH master curves of poly[(diethylaminoethyl methacrylate)-graft-(ethylene glycol)] hydrogels. Polym Int 2005;54:581-593.

Polla DL. BioMEMS applications in medicine. Proceedings of International Symposium on Micromechatronics and Human Science. 2001:13-15.

Pradny M, Lesny P, Fiala J, Vacik J, Slouf M, Michalek J, Sykova E. Macroporous hydrogels based on 2-hydroxyethyl methacrylate with methacrylic acid. Collect Czech Chem C. 2003;68:812-822.

RCSB Protein Data Bank http://www.rcsb.org/pdb/home/home.do. (as seen on November 20, 2007) Jmol Viewer.

Reynaerts D, Peirs J, Van Brussel H. Design of a SMA-actuated implantable drug delivery system. Proceedings of the Sixth International Symposium on Micro Machine and Human Science. 1995:111.

Salud: México 2001-2005. http://evaluacion.salud.gob.mx/saludmex2005/sm2005.htm (as seen on June 18, 2007).

Santini JT, Cima MJ, Langer R. A controlled-release microchip. Nature 1999;397:335-338.

Seely RR, Stephens TD, Tate P. Anatomy & physiology. St Louis: 1995. Seeley, R.R, Stephens, T.D., and Tate, P. (1995) Anatomy & physiology (3rd edition). St Louis: Mosby-Year Book, Inc.

Shin Y, Chang JH, Liu J, Williford R, Shin YK, Exarhos GJ. Hybrid nanogels for sustainable positive thermosensitive drug release. J Controlled Release. 2001;73:1-6.

Sorensen J. A physiologic model of glucose metabolism in man and its use to design and assess improved insulin therapies for diabetes. PhD thesis. Dept. of Chemical Engineering, MIT, 1985.

Staples M, Daniel K, Cima M, Langer R. Application of micro- and nano-electromechanical devices to drug delivery. Pharmaceut Res. 2006;23(5):847-863.

Steil GM, Panteleon AE, Rebrin K. Closed-loop insulin delivery—the path to physiological glucose control. Adv Drug Deliver Rev, 2004;56:125-144.

Stewart KM, Wilson MF, Rider JM. Insulin delivery devices. Journal of Pharmacy Practice. 2004;17(1):20-28.

Tiwari AK, Rao JM. Diabetes mellitus and multiple therapeutic approaches of phytochemicals: present status and future prospects. Current Science. 2002;83(1):30-38.

Tofade TS, Liles EA. Intentional Overdose With Insulin Glargine and Insulin Aspart. Pharmacotherapy 2004;24(10):1412-1418.

Tu Y, Lin Y, Ren ZF. Nanoelectrode arrays based on low density aligned carbon nanotubes. Nano Letters. 2003;3(1):107-109.

Vainshtein. Three-dimensional structure of the enzyme catalase. Nature. 1981;293:411-412.

Van De Graaff KM, Fox SI, LaFleur KM. Synopsis of human anatomy & physiology. Dubuque, IA: Wm. C. Brown Publishers, 1997.

Vinter R. Optimal control. Boston: Birkhöuser, 2000.

Webster J. Medical instrumentation: application and design (3rd edition), New York: John Wiley & Sons, Inc., 1998.

White JR, Campbell RK. Insulin in the treatment of type 2 diabetes mellitus. Am J Health-Syst Pharm. 2003;60:1145-1152.

Whitney E, Rolfes SR. Understanding nutrition (10th edition), Belmont, CA: West Group, 2005.

Woodruff, E., Gulaya, S. & Northrop, R. (1988). The Closed-Loop Regulation of Blood Glucose in Diabetes. Proc. of the 14th Annual Northeast Bioengineering Conference, pp. 54-57.

Yao SJ, Li VWT, Dokko Y, Krupper MA, Wolfson Jr SK. Electrochemical detection of glucose at low potentials. Proceeding IEEE/NSF Symposium on Biosensors. 1984:75-77.

Yang H, Kang SK, Shin DH, Kim H, Kim YT. Microfabricated iridium oxide reference electrode for continuous glucose monitoring sensor. Transducers, Solid-State Sensors, Actuators and Microsystems. 12th Innational Conference. 2003;1:103–106.

Yipintsol T, Gatewood L, Ackerman E, Spivak P, Molnar G, Rosevear J, Service F. Mathematical analysis of blood glucose and plasma insulin responses to insulin infusion in healthy and diabetic subjects. Comput Biol Med. 1973;3:71-78.

Zeller H, Novak P, Landgraf R. Blood glucose Measurement by IR spectroscopy. Int J Art Org. 1989;12(2):129-134.